UC-34c+d
LBL-16164
c1

Lawrence Berkeley Laboratory
UNIVERSITY OF CALIFORNIA

Physics, Computer Science & Mathematics Division

RECEIVED
LAWRENCE
BERKELEY LABORATORY
JUL 21 1983
LIBRARY AND
DOCUMENTS SECTION

TWO AND QUASI-TWO BODY STRANGE PARTICLE FINAL STATE PRODUCTION IN $\pi^+ p$ INTERACTIONS AT LOW TO INTERMEDIATE ENERGIES

P. Hanson
(Ph.D. Thesis)

October 1982

For Reference
Not to be taken from this room

Prepared for the U.S. Department of Energy under Contract DE-AC03-76SF00098

LBL-16164
c1

DISCLAIMER

This document was prepared as an account of work sponsored by the United States Government. While this document is believed to contain correct information, neither the United States Government nor any agency thereof, nor the Regents of the University of California, nor any of their employees, makes any warranty, express or implied, or assumes any legal responsibility for the accuracy, completeness, or usefulness of any information, apparatus, product, or process disclosed, or represents that its use would not infringe privately owned rights. Reference herein to any specific commercial product, process, or service by its trade name, trademark, manufacturer, or otherwise, does not necessarily constitute or imply its endorsement, recommendation, or favoring by the United States Government or any agency thereof, or the Regents of the University of California. The views and opinions of authors expressed herein do not necessarily state or reflect those of the United States Government or any agency thereof or the Regents of the University of California.

TWO AND QUASI-TWO BODY STRANGE PARTICLE FINAL STATE PRODUCTION IN π^+p INTERACTIONS AT LOW TO INTERMEDIATE ENERGIES[1]

Philip Hanson

Department of Physics

and

Lawrence Berkeley Laboratory

University of California

Berkeley, California 94720

Ph.D. Thesis

October, 1982

[1]Supported in part by the Director, Office of Energy Research, Division of High Energy and Nuclear Physics of the U.S. Department of Energy under contract DE-AC03-76SF00098.

DEDICATION

To my parents and sister.

σκιᾶς ὄναρ ἄνθρωπος

– Πίνδαρ

ACKNOWLEDGMENTS

I wish to thank my research director Professor Robert P. Ely, Jr., for his encouragement, advice, and patience during this work. I also wish to thank the members of my dissertation committee, Professor Robert Tripp and Professor John Rasmussen, for their reading and criticism of the manuscript, and I gratefully acknowledge many valuable and enlightening discussions with Dr. George Gidal, Dr. George Kalmus, Dr. Denyse Chew, Dr. Robert Birge, and Dr. Fredrick Lott. Additionally I thank Wes Weber, Howard White and the Data Handling Group, and Charlotte Scales for their valuable assistance in data reduction. Finally and especially, I gratefully acknowledge the friendship, advice, and encouragement of Dr. William Michael, whose enthusiastic interest in all areas of physics will always be an inspiration.

This work was supported in part by the Director, Office of Energy Research, Division of High Energy and Nuclear Physics of the U.S. Department of Energy under contract DE-AC03-76SF00098.

CONTENTS

Chapter I - Introduction

Chapter II - Experimental Details and Data Reduction

Chapter III- Experimental Results

Chapter IV - Analysis of the Channels $\Sigma K, \Sigma K^*, \Sigma^* K, \Sigma^* K^*$

Chapter V - Summary,Conclusions,Perspective

Appendix - Properties of Density Matrices under Line Reversal,Weak and Strong Exchange Degeneracy

References

Tables I-VI

Two and Quasi-Two Body Strange Particle Final State Production in π^+p Interactions at Low and Intermediate Energies

Philip Russell Hanson

Abstract

The two and quasi-two body final states Σ^+K^+, $\Sigma^+K^*(892)^+$, $\Sigma^*(1385)^+K^+$, $\Sigma^*(1385)^+K^*(892)^+$ produced by neutral strangeness exchange in π^+p interactions are studied using our own 1-3 GeV/c data, comprising the 14 incident momenta of a two million picture bubble chamber experiment, in combination with the world data on the same and related channels. Because low energy resonance formation is not stongly coupled to the Σ,Σ^* production channels, at very modest incident momenta their dominant features are seen to be understandable in terms of high energy hypercharge exchange phenomenology. We find that Regge models fitted to data in the 10 to 20 GeV/c range adequately describe the Σ and Σ^* channels down to within a few hundred MeV/c of threshold and out to large center of mass scattering angles, and that over the range of the available world data weak exchange degeneracy expectations for these reactions are at least qualitatively successful. We observe that the SU(2),SU(3) flavor symmetries successfully describe these hypercharge exchange processes and relate them to charge exchange via sum rules and equalities expressing flavor independence of the strong interaction; in particular, we derive and test on the available world data a mass broken SU(3) sum rule for $\pi^+p \to K^+\Sigma^+$,

$\pi^- p \to K^0 \Lambda$, $K^- p \to \bar{K}^0 n$ and test over a wider range of momenta than before an earlier expression relating Σ^* and Δ production. We also find at least qualitative agreement between quark model predictions for forward hypercharge exchange and the data, and we find that 90° hypercharge exchange cross sections also conform to the expectations of the quark constituent picture for hadrons.

I. Introduction

The two and quasi-two body final states Σ^+K^+, $\Sigma^+K^*(892)^+$, $\Sigma^*(1385)^+K^+$, $\Sigma^*(1385)^+K^*(892)^+$, produced by neutral strangeness exchange in π^+p interactions provide information about their production dynamics not only through the differential cross sections, but also through the decay distributions of the final state mesons and baryons; the strong coupling of Σ^* and K^* production to the $K\pi\Lambda$ and $K\pi\Sigma$ channels provides a relatively clean and unencumbered sample of the quasi-two body states. Because low energy resonance formation is not strongly coupled to the Σ,Σ^* hyperon production channels in π^+p, at even very modest energies their dominant features can often be understood in terms of high energy hypercharge exchange phenomenology. Thus we use our 1-3 GeV/c strange particle production data in combination with the world data on the same and related channels to investigate how close to threshold the energy and angular dependence of the data are adequately portrayed by high energy (e.g., Regge) formalisms. We also examine over the range of available data aspects such as Weak Exchange Degeneracy expectations for the phase behavior of reaction amplitudes, and the $SU(3)_{flavor}$ symmetries which relate hypercharge exchange to charge exchange via sum rules and equalities expressing flavor independence. In particular, we derive and test a new broken $SU(3)$ sum rule relating $\pi^+p \to K^+\Sigma^+$, $\pi^-p \to K^0\Lambda$, $K^-p \to \bar{K}^0n$, and test (over a wider range of momenta than before) an earlier expression relating Σ^* and Δ production; we also investigate how both the large (~90°)- and small (~0°)-angle scattering features of hypercharge exchange processes conform to the expectations of the quark constituent picture of the hadrons.

Although statistics at single energies are often meager, we shall nonetheless see that these channels are dominated by a few rather striking, characteristically high energy features over a span extending from not far above threshold to roughly an order of magnitude higher in incident momentum. The phenomenological formalisms which most concisely describe these features are probably not in themselves fundamental, but the behavior which they succinctly summarize is, and ultimately will have to be explained by a fundamental theory of strong interactions, which it now appears will be quantum chromodynamics.

II. EXPERIMENTAL DETAILS AND DATA REDUCTION

A. General

The 1-3 GeV/c π^+p hypercharge exchange data for this analysis are taken from an exposure of the LBL 25-inch liquid hydrogen bubble chamber to a separated π^+ beam from the Bevatron at nine incident momenta between 1 and 2 GeV/c (three of these were taken in the LBL 72-inch chamber) and five incident momenta between 2 and 3 GeV/c. A total of 923,000 triad frames were taken at the lower momenta (1.28, 1.34, 1.41, 1.43, 1.55, 1.63, 1.68, 1.77, and 1.84 GeV/c) and 1,086,000 at the higher momenta (1.94, 2.15, 2.30, 2.46, and 2.67 GeV/c). The data from the nine lower momenta have already been discussed elsewhere by this author ($\Sigma K\pi, K\pi\Lambda$; ref. 1) and by Kalmus (ΣK; refs. 2,3). Table I shows the exposure sizes and microbarn equivalents (see section IIIA) for all 14 incident momenta.

B. Beam

The layout for the two-spectrometer electrostatically separated π^+ beam is shown in figure II.1. Spectrometer tuning curves at the various momenta show that the proton contamination is typically small, e.g., $<0.5\%$ at the highest momentum, 2.67 GeV/c (ref. 4), and the μ contamination is estimated to be $3\% \pm 2\%$ (ref. 5). The incident momentum bite varied from 0.7% to 1.15%, and a beam destroyer kept the average number of pions per picture at 10-11.

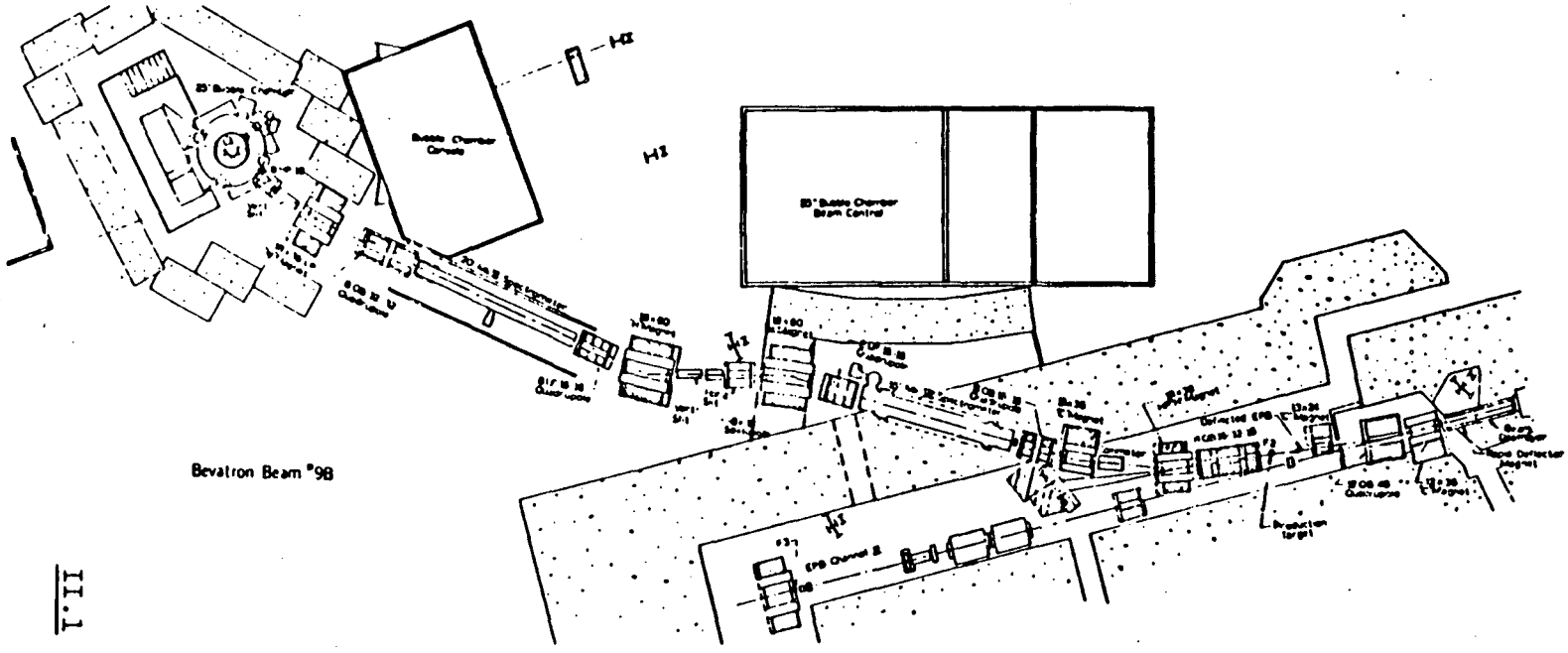

II.1

XBL 6712-6265

C. Data Reduction

All strange particle events at the 14 incident momenta were scanned and measured using the Cobweb system of on-line scan tables and Franckensteins (ref. 6). Scanners searched for all events which had a strange particle decay topology, i.e., one or more kinked tracks and/or associated V^0's, and double scanned every other roll at the 4 highest momenta and every roll at the 10 lower. The measured data from Cobweb were processed by the FOG-CLOUDY-FAIR system of geometric reconstruction and kinematic constraint programs (ref. 7). For this analysis we use only the kinking two prong and two prong V^0 topologies which are dominated by the following reactions (see figure II.2):

$$\pi^+ p \rightarrow \Sigma^+ K^+, \qquad (1)$$
$$\Sigma^+ \rightarrow \pi^+ n \qquad (1i)$$
$$\Sigma^+ \rightarrow p\pi^0 \qquad (1ii)$$

$$\pi^+ p \rightarrow \Sigma^+ K^+ \pi^0, \qquad (2)$$
$$\Sigma^+ \rightarrow \pi^+ n \qquad (2i)$$
$$\Sigma^+ \rightarrow p\pi^0 \qquad (2ii)$$

$$\pi^+ p \rightarrow \Sigma^+ \pi^+ K^0, \qquad (3)$$

$$K^0_S \rightarrow \pi^0\pi^0, \text{ or } K^0_L$$
$$\Sigma^+ \rightarrow \pi^+ n \qquad (3i)$$
$$\Sigma^+ \rightarrow p\pi^0 \qquad (3ii)$$

$$K^0_S \rightarrow \pi^+\pi^-,$$
$$\Sigma^+ \rightarrow \pi^+ n \qquad (3iii)$$
$$\Sigma^+ \rightarrow p\pi^0 \qquad (3iv)$$

$$\pi^+ p \rightarrow K^+ \pi^+ \Lambda \qquad (4)$$
$$\Lambda \rightarrow p\pi^-$$

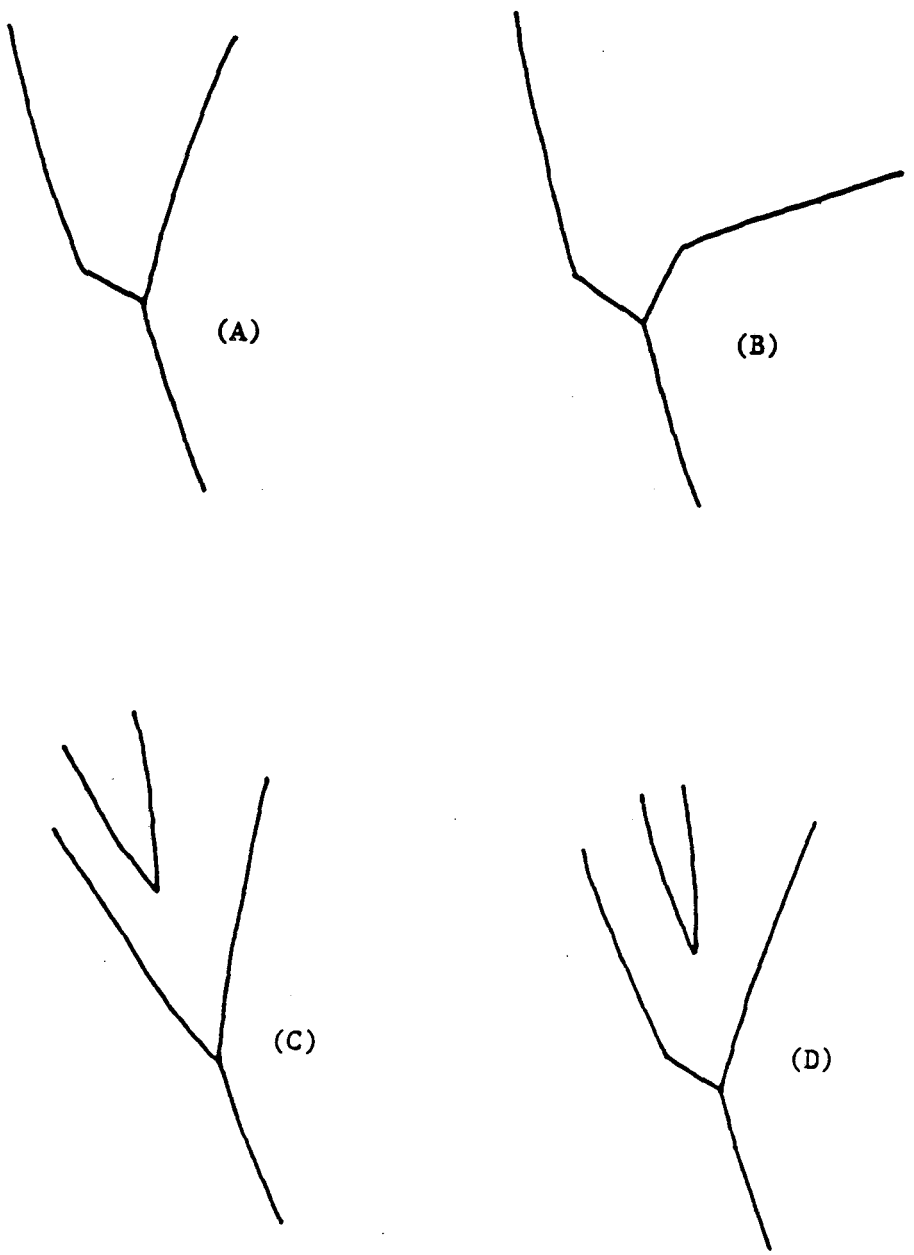

II.2 TOPOLOGIES USED FOR ANALYSIS

The three body final states of reactions 2, 3, and 4 are principally of interest at our incident momenta because they are dominated by the quasi-two body final states:

$$\pi^+ p \rightarrow \Sigma^+ K^{*+}(892), \qquad (5)$$
$$K^{*+}(892) \rightarrow K^+ \pi^0 \qquad (5i)$$
$$K^{*+}(892) \rightarrow K^0 \pi^+ \qquad (5ii)$$

$$\pi^+ p \rightarrow \Sigma^{*+}(1385) K^+, \qquad (6)$$
$$\Sigma^{*+}(1385) \rightarrow \Lambda \pi^+ \qquad (6i)$$

For further discussion of reactions 5 and 6, see Chapters III and IV.

Kinking two prongs were constrained to the Σ^+ reactions 1,2,3i,3ii in a simultaneous 2-vertex (production plus hyperon decay) fit using the Σ^+ measured momentum if $\delta p_\Sigma / p_\Sigma \leq 50\%$, and using only the Σ^+ direction otherwise. About 80% of the events accepted as $\Sigma K(\Sigma K \pi)$ had fits of the 4c(1c) class, and 20% of the 5c(2c) class. Two prong V^0's were constrained to reaction 4 in a simultaneous 2-vertex 7c fit. No charged meson decay vertices were fitted. To investigate overlap of 4 with similar constraint class hypotheses, two prong V^0 events were also fitted as $K^+ \pi^+ \Sigma^0$ and $K^+ p \bar{K}^0$. The beam momentum for each event was constrained to an edited value derived from high statistics samples of 4c nonstrange particle four prong events. At present for these data only events with at most two measured vertices are

available so that reactions 3iii and 3iv are not used for analysis.

D. Selection of Final States and Resolution of Ambiguities

1. General

All events included in final samples were required to have:

(a) successful three view vertex and track reconstruction;

(b) satisfactory kinematic constraint to the appropriate hypothesis, in conjunction with a calculated ionization bubble density (using the fitted momenta) on each track of the event consistent with the ionization as determined on the scan table by a physicist in all three views;

(c) Σ^+ lifetime within the bounds described in the next section for both cross section totals and distributions, and a Λ lifetime within bounds for cross section totals only.

All ionization testing and selection of events was performed on the 3-view multiple magnification scan tables. At the low to moderate energies of these data there was essentially no difficulty distinguishing protons from mesons; the principal source of track ambiguity was $\pi-K$ overlap. The 25 inch chamber was run with a typical bubble size of 0.40 mm and a bubble density at minimum ionization of about 10 bubbles/cm so that there was some residual lacunarity at twice minimum ionization. Thus typically >8 cm (in space) of track was required to differentiate (at the 2σ level for a Poisson distribution) between π and K hypotheses differing in relative ionization by about 20% near minimum, i.e., since most π's were near minimum, K's could, at best, be distinguished up to lab momenta of $\sim$1 GeV/c.

2. Σ^+ Final States

The Σ^+ rest frame decay times (computed from an average of production and decay vertex Σ momenta) for all Σ^+ at the 5 highest momenta are shown in figure II.3a, where the decay times, $c\tau_\Sigma$, are normalized to the mean Σ^+ lifetime $c\tau_0$ from the Particle Data Tables, and the distribution expected from $c\tau_0$ is superimposed (ref. 8). To remove any possible meson contamination, we require $c\tau_\Sigma < 4c\tau_0$ at the 5 upper momenta, and $c\tau_\Sigma < 3c\tau_0$ at the 9 lower (see section IIF on cuts and weights).

At the five upper momenta approximately 5% of the events fitting reaction (1) also fit reactions (2) or (3); as at the lower momenta, these overlap events were assigned to the ΣK hypothesis. The appropriateness of this assignment is illustrated in figure II.4 which shows the missing mass squared (before constraint) recoiling against the charged (π or K) meson track, at 2.3 GeV/c:

$$\pi^+ p \rightarrow K^+[or\ \pi^+] + MM\ .$$

The peak at the sigma mass is clearly visible in the entire sample (figure II.4a) and is gone after the ΣK fits are removed (figure II.4b). As a quantitative check on the purity of the ΣK events, the missing mass squared before constraint recoiling against the K^+, $\pi^+ p \rightarrow K^+ + MM$, was examined for the final ΣK sample and showed, as expected, that the ΣK events are not contaminated by missing-neutral(s) states. For the final $\Sigma K\pi$ event samples, the overall missing mass squared before constraint (the missing energy squared), $\pi^+ p \rightarrow \Sigma^+ + K^{0+} + \pi^{+0} + MM$, was examined and showed no multiple missing neutral contamination.

2.7,2.5,2.3,2.15,1.95 GeV/c

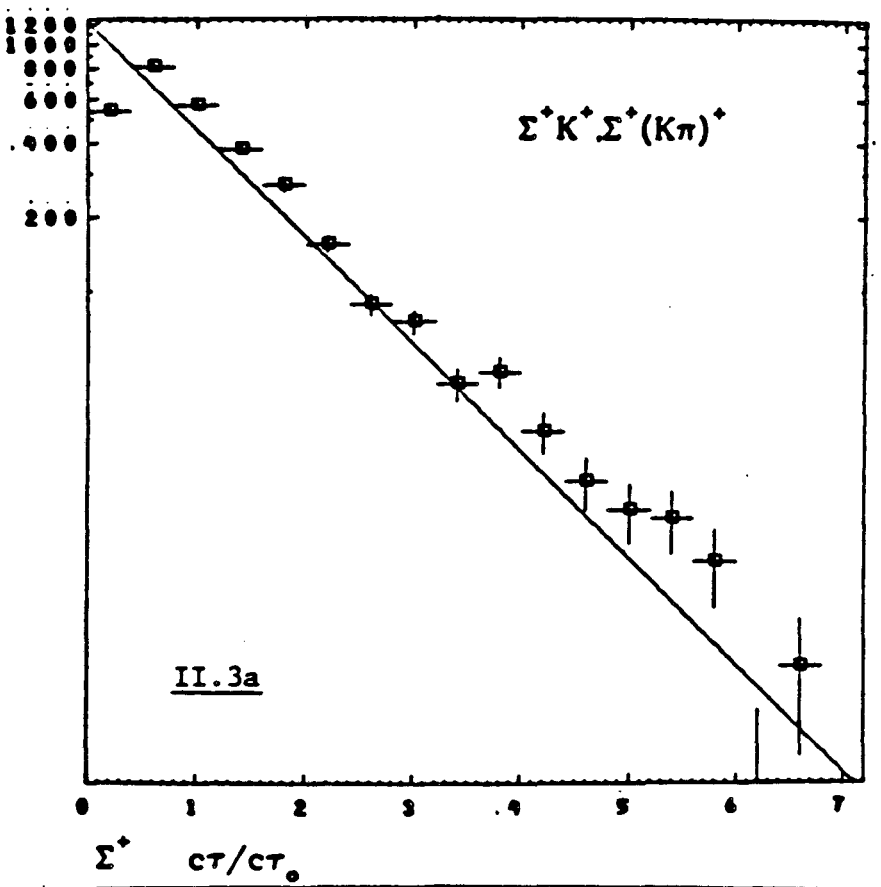

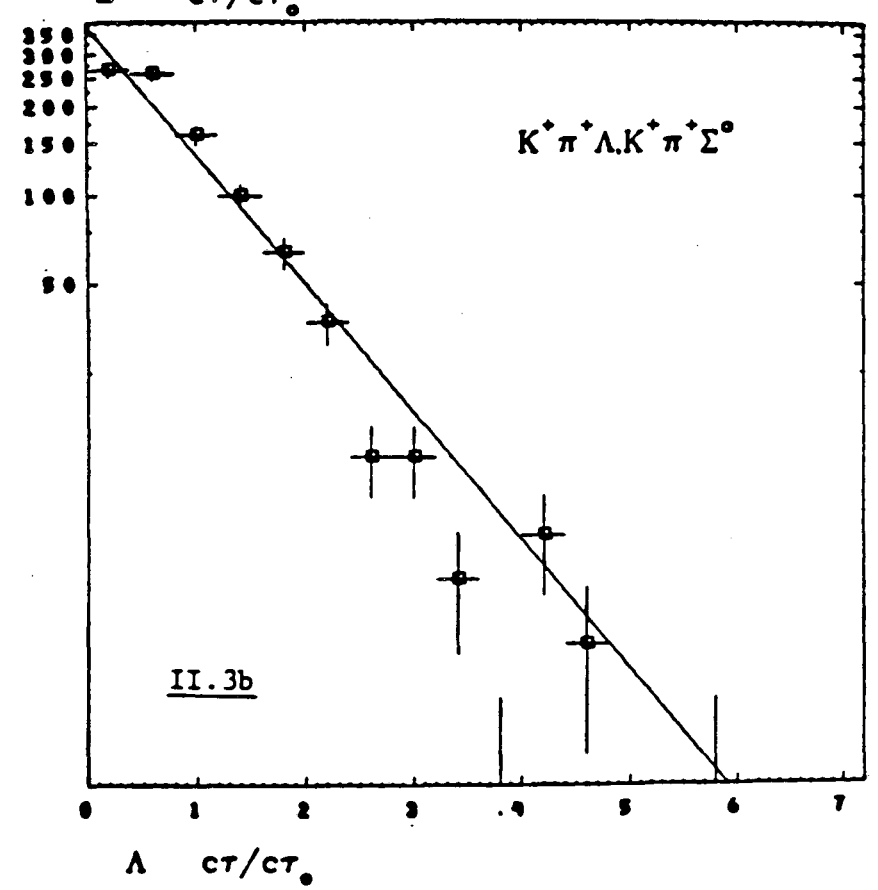

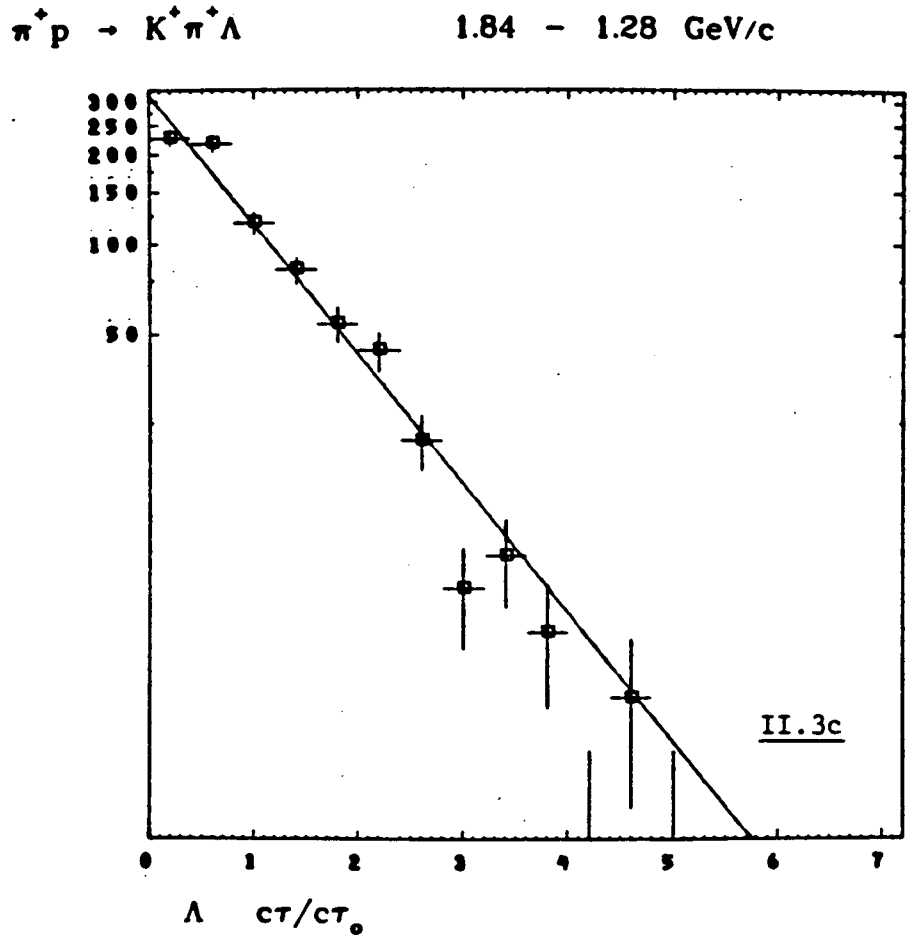
$\pi^+ p \rightarrow K^+ \pi^+ \Lambda$
1.84 - 1.28 GeV/c
300
250
200
150
100
50
0
1
2
3
4
5
6
7
II.3c
Λ $c\tau/c\tau_0$

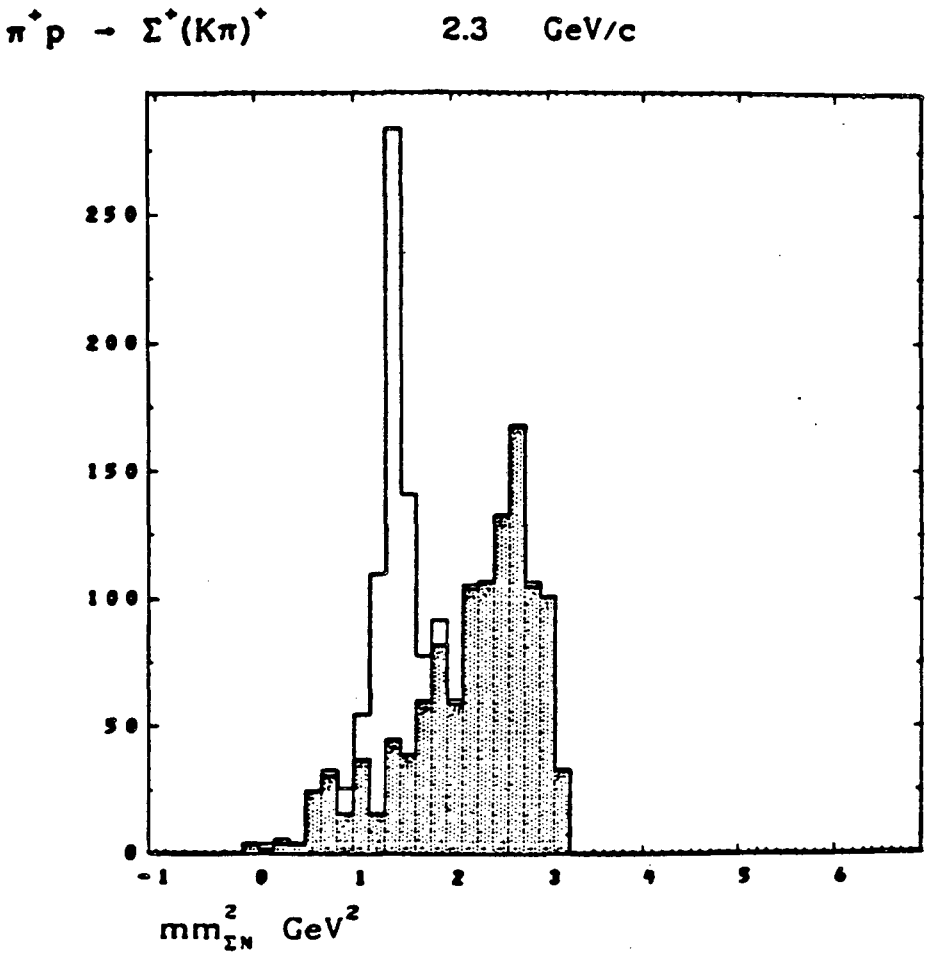

II.4

$\pi^+ p \rightarrow K^+ + MM$

a Unshaded: no cuts

b Shaded: ΣK removed

Approximately 48% of the final $\Sigma K\pi$ events at the five upper momenta were $\pi^+ - K^+$ ambiguous by kinematics alone, but we consider as severely ambiguous (i.e., ambiguous by both kinematics and ionization) those events where the π^+ and K^+ hypothesis ionizations had (see figure II.5):

$$\frac{\delta I}{I} = \frac{|I_K - I_\pi|}{I_\pi} \leq 20\% .$$

These events constitute only 5% of the total $\Sigma K\pi$ sample at the five upper momenta and were resolved event by event by hand in favor of the hypothesis better fitting the observed ionization.

Scatter plots of the lab momenta of the π^{+0} vs. that of the K^{0+} for the final resolved samples of $\Sigma^+K^+\pi^0$ and $\Sigma^+\pi^+K^0$ show that the $\pi - K$ resolution is reasonable and that the K^* mass region, which appears in such plots as diagonal bands from upper left to lower right and corner enhancements, is not strongly dependent on the $\pi - K$ separation, since the K^* bands are roughly orthogonal to the ambiguity region $p_\pi^{LAB} = p_K^{LAB}$ (see figure II.6). The observable enhancements and depletions in figure II.6 agree qualitatively with the expected ΣK^* dominance of the $\Sigma K\pi$ states, with the K^* coupling more strongly to the π^+K^0 charge state. In sections IIIC,D the $\Sigma K\pi$ samples exhibit strong K^* signals over backgrounds generally consistent with phase space, and a careful calculation of the ratio $(K^* \to K^0\pi^+)/(K^* \to K^+\pi^0)$ for the data is consistent with 2. The residual $\Sigma^+K^+\pi^0 - \Sigma^+\pi^+K^0$ overlap in the final samples at the five upper momenta is estimated as ~5%; for the nine lower momenta, the $\pi^+ - K^+$ ambiguity was essentially completely ionization resolvable. The Σ^+ decay mode ambiguity was resolved by ionization.

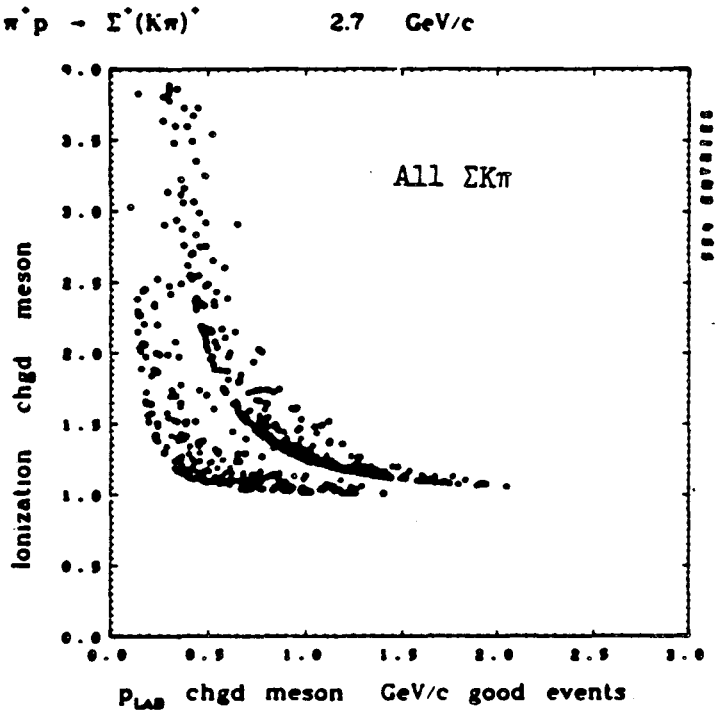
π⁺p → Σ⁺(Kπ)⁺ 2.7 GeV/c
All ΣKπ
Ionization chgd meson
P_LAB chgd meson GeV/c good events

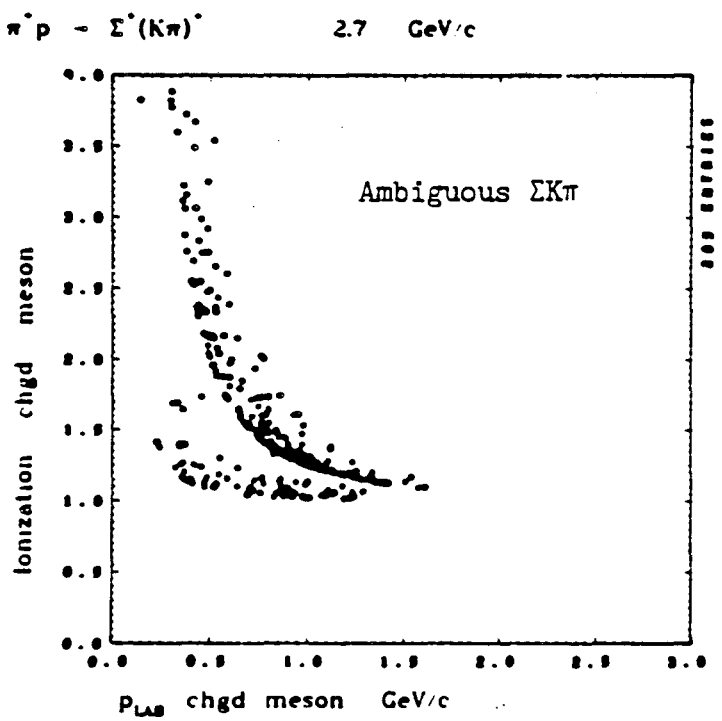
π⁺p → Σ⁺(Kπ)⁺ 2.7 GeV/c
Ambiguous ΣKπ
Ionization chgd meson
P_LAB chgd meson GeV/c

II.5

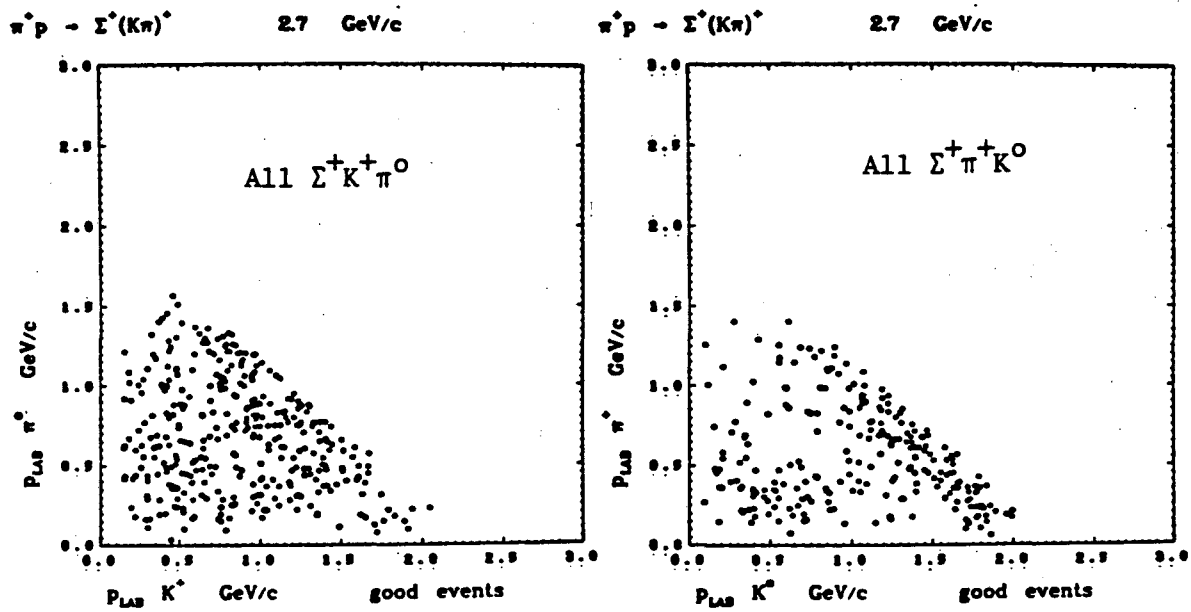
π⁺p → Σ⁺(Kπ)⁺ 2.7 GeV/c
All Σ⁺K⁺π⁰
P_LAB π⁰ GeV/c
P_LAB K⁺ GeV/c good events
π⁺p → Σ⁺(Kπ)⁺ 2.7 GeV/c
All Σ⁺π⁺K⁰
P_LAB π⁺ GeV/c
P_LAB K⁰ GeV/c good events

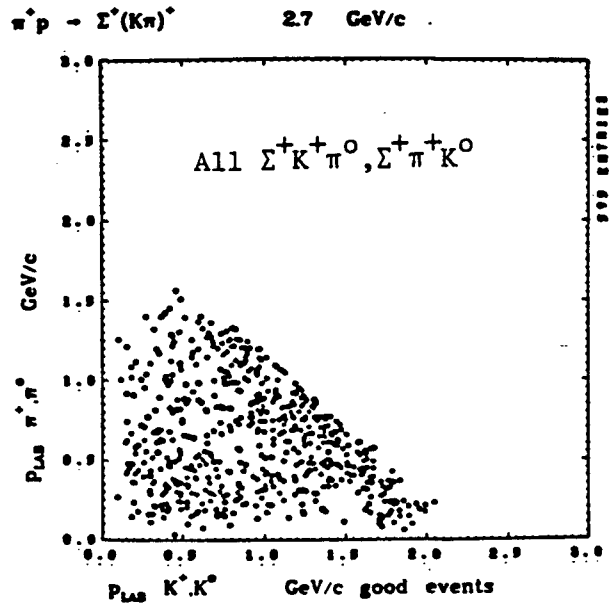
π⁺p → Σ⁺(Kπ)⁺ 2.7 GeV/c
All Σ⁺K⁺π⁰,Σ⁺π⁺K⁰
P_LAB π⁺,π⁰ GeV/c
P_LAB K⁺,K⁰ GeV/c good events

II.6

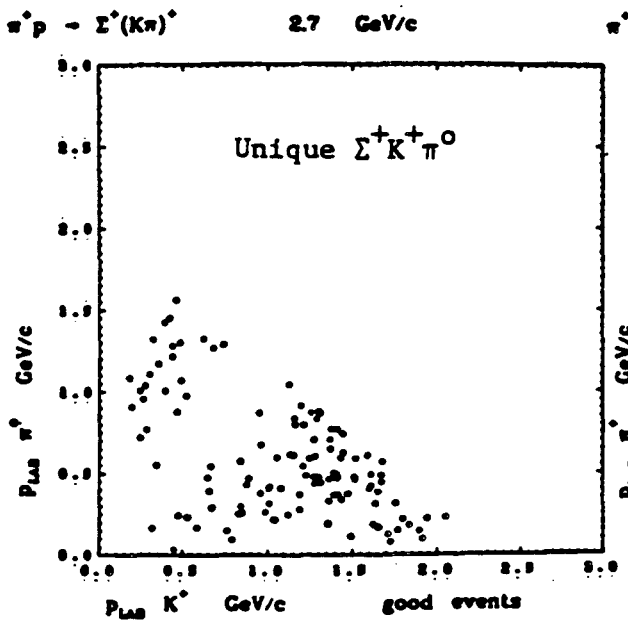
π⁺p → Σ⁺(Kπ)⁺ 2.7 GeV/c
Unique Σ⁺K⁺π⁰
P_LAB π⁺ GeV/c
P_LAB K⁺ GeV/c
good events

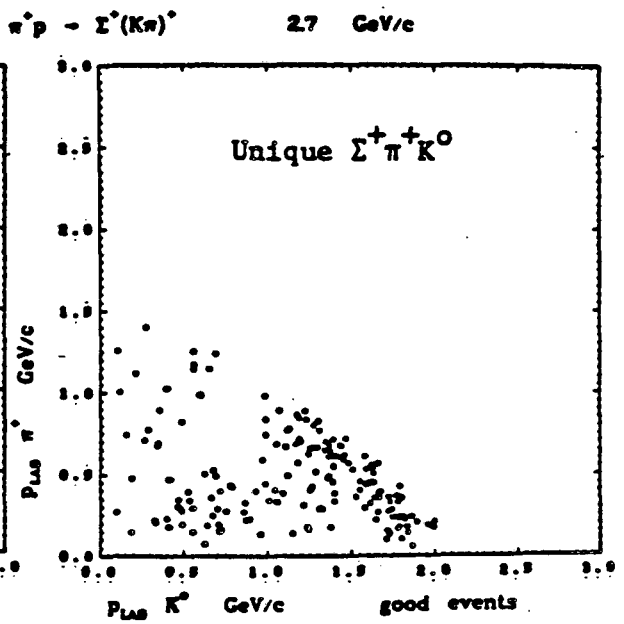
π⁺p → Σ⁺(Kπ)⁺ 2.7 GeV/c
Unique Σ⁺π⁺K⁰
P_LAB π⁺ GeV/c
P_LAB K⁰ GeV/c
good events

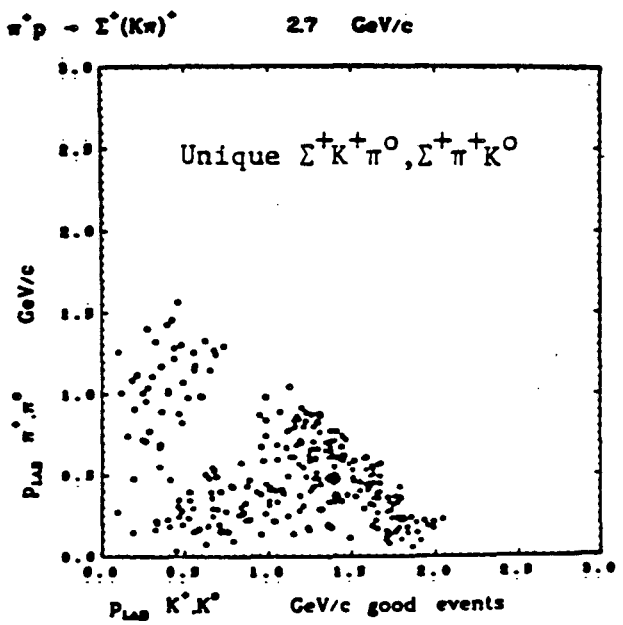
π⁺p → Σ⁺(Kπ)⁺ 2.7 GeV/c
Unique Σ⁺K⁺π⁰,Σ⁺π⁺K⁰
P_LAB π⁺,π⁰ GeV/c
P_LAB K⁺,K⁰ GeV/c
good events

II.6

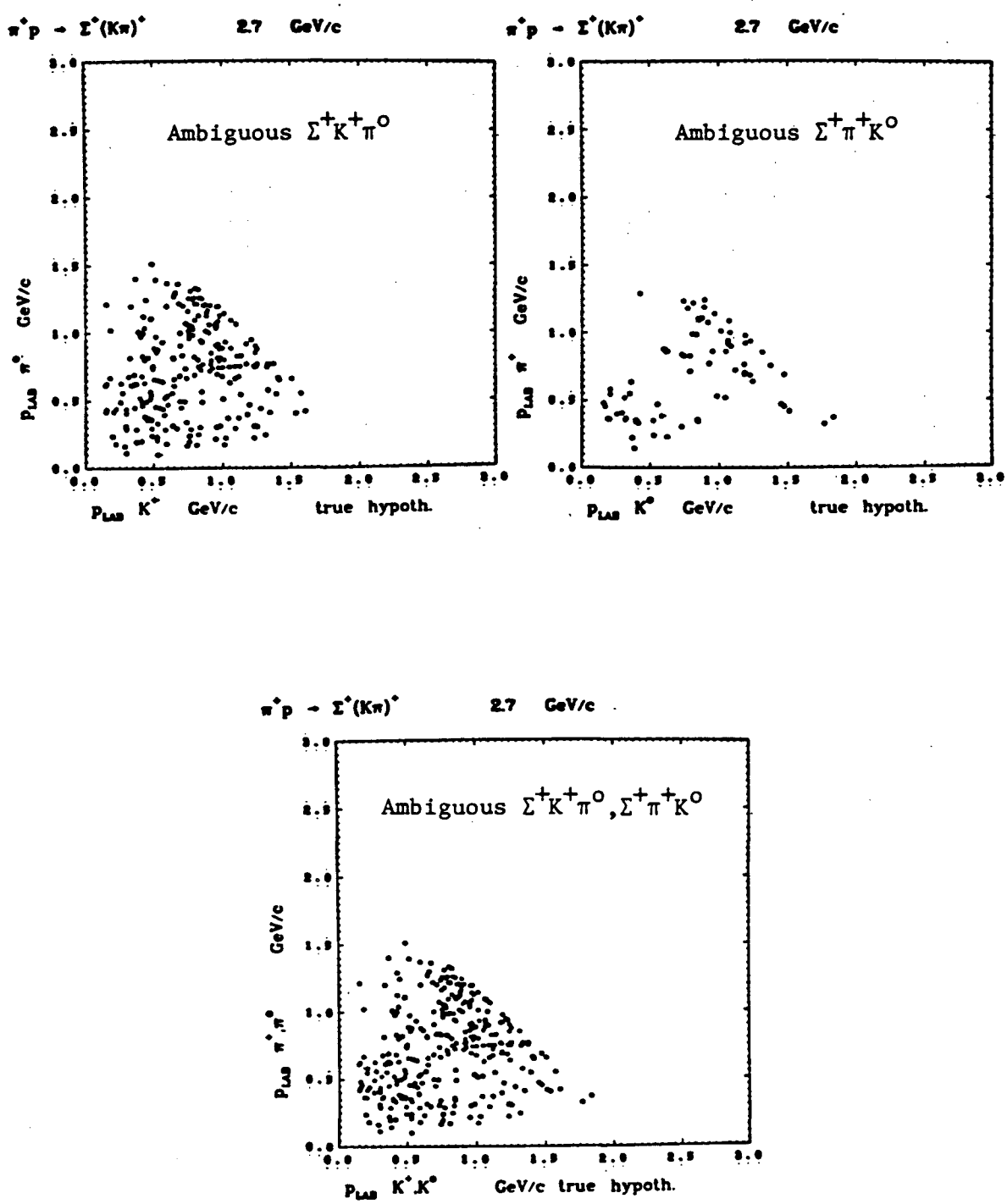
π⁺p → Σ⁺(Kπ)⁺ 2.7 GeV/c
Ambiguous Σ⁺K⁺π⁰
Ambiguous Σ⁺π⁺K⁰
Ambiguous Σ⁺K⁺π⁰,Σ⁺π⁺K⁰
P_LAB π⁺,π⁰ GeV/c
P_LAB K⁺,K⁰ GeV/c true hypoth.

II.6

3. $K\pi\Lambda$ Final States

Figure III.3b shows the distribution of the normalized Λ decay times $c\tau_\Lambda / c\tau_0$ for the final $K\pi\Lambda$ events at the five upper momenta with the Particle Data Tables mean Λ lifetime $c\tau_0$ superimposed. For cross section determination only, we require $c\tau_\Lambda < 4c\tau_0$ at the nine lower momenta and $c\tau_\Lambda < 5c\tau_0$ at the five upper. As with the ΣK events, any candidate which fit $K\pi\Lambda$ was so assigned in preference to any lower constraint class hypothesis. The missing mass squared before constraint recoiling against the $K\pi\Lambda$ state, $\pi^+ p \rightarrow K^+ + \pi^+ + \Lambda + MM$, showed no missing neutral contamination of the final $K\pi\Lambda$ samples.

At the five upper momenta only 2% of the events fitting $K\pi\Lambda$ also fit $Kp\bar{K}^0$; ionization resolved all but one of these in favor of $K\pi\Lambda$. Also at the five upper momenta, 26% of the $K\pi\Lambda$ events had fits to the $K\pi\Sigma^0$ ($\Sigma^0 \rightarrow \Lambda\gamma$) channel, but all except 1% (of the total $K\pi\Lambda$ sample) were assigned to $K\pi\Lambda$. Only when the primary vertex meson track ionizations were inconsistent with all $K\pi\Lambda$ track permutations, but consistent with the $K\pi\Sigma^0$ track identities, were overlap events assigned to $K\pi\Sigma^0$; all other overlap events were assigned to $K\pi\Lambda$. This procedure is justified by the (by now well-known) examination, before and after Λ–Σ^0 separation, of the $\Sigma^0 \rightarrow \Lambda\gamma$ rest frame decay angles with respect to the primary particles of the event, for each of which one expects *a priori* isotropy (see figure II.7). The strong forward peak of figure II.7a indicates spurious fits of $K\pi\Lambda$ events to $K\pi\Sigma^0$ hypotheses manufactured by the fitting program's alignment with the beam momentum of the small additional neutral momentum needed to simulate $\Sigma^0 \rightarrow \Lambda\gamma$, and similar considerations apply to the Σ^0 decay cosines with respect to the other particles of the event.

$\pi^+ p \rightarrow K^+ \pi^+ \Sigma^0$ 2.7,2.5,2.3,2.1 GeV/c

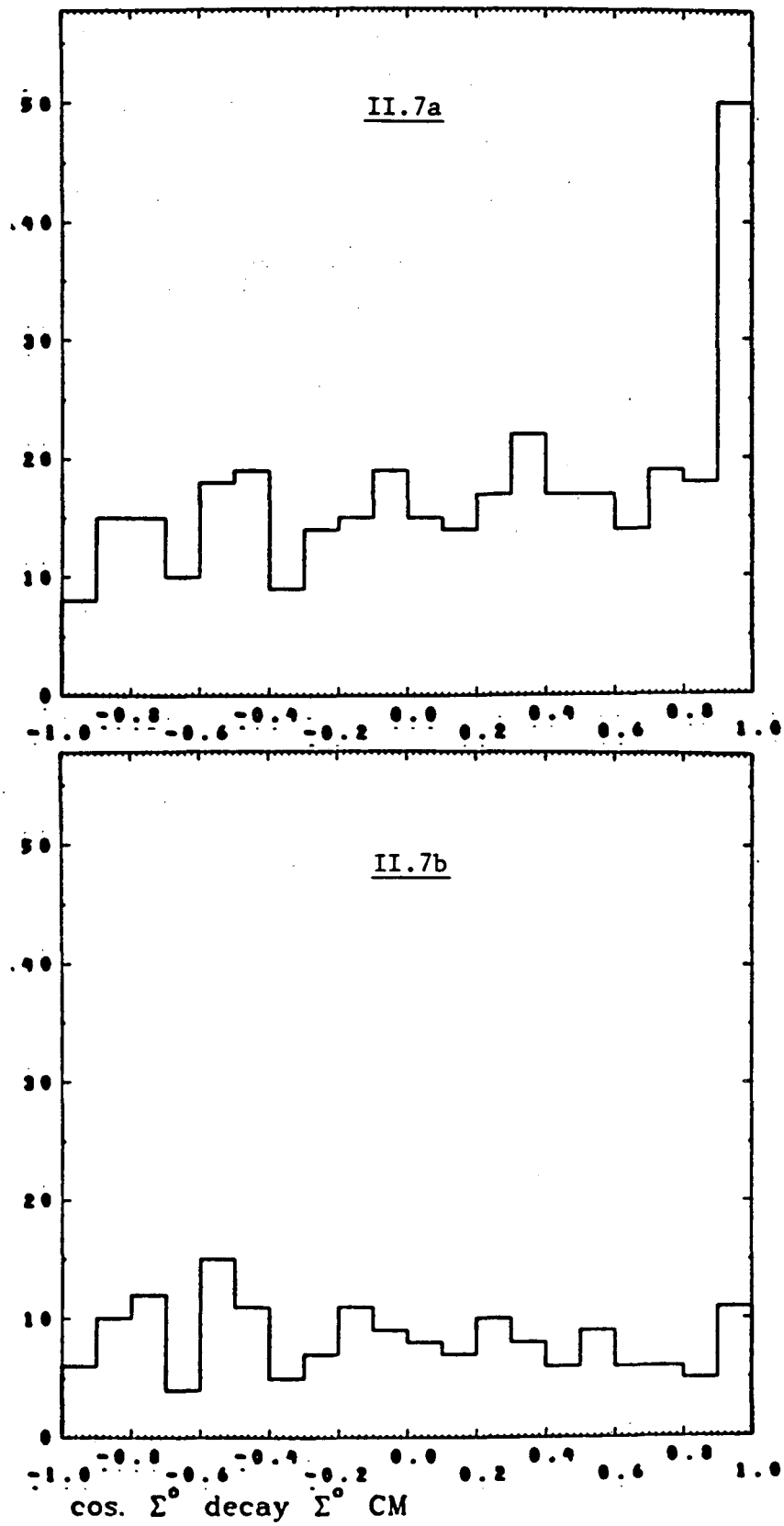

The $\pi-K$ track identity ambiguity which was present in 8% of the final $K\pi\Lambda$ events at the five upper momenta was ionization resolved, as at the nine lower, to within 1% of the total sample, and the $K\pi\Lambda$ data at all momenta ≥ 1.41 GeV/c show a strong $\Sigma^{*+}(1385)$ signal.

E. Throughput Efficiencies

For cross section normalization, the net overall throughput efficiencies for event types used are

$$\varepsilon_T = \varepsilon_S \varepsilon_{MR} \varepsilon_F \varepsilon_B$$

where $\varepsilon_S, \varepsilon_{MR}, \varepsilon_F, \varepsilon_B$ are the scan efficiency, the measure and geometric reconstruction (COBWEB/FOG) efficiency, kinematic fitting and constraining (CLOUDY-FAIR) efficiency, and residual bookkeeping and tape failure event loss efficiency, respectively. The corresponding cross section corrections for these systematic losses are

$$C_T = 1/\varepsilon_T \ , \ C_S = 1/\varepsilon_S \ , \ etc.$$

and the *inefficiency* for the ith category of loss is

$$\delta_i = 1 - \varepsilon_i \ .$$

The scan efficiencies ε_S were calculated for the various topologies from good events only, i.e., for events passing not only scan criteria, but kinematic constraint and ionization selection and final fiducial volume cuts as well. On doubly scanned rolls, events from both scans were accepted for analysis. At the 5 high momenta for kinking 2 prongs which fit $\Sigma^+ \rightarrow \pi^+ n$, the single scan efficiency varied from 89% to >98% and the net efficiency, taking into account the double scan of either all or every other roll, ranged from 95% to

>98%. For 2 prongs with V^0 fitting a Λ, the single scan efficiency varied from 88% to >98%, and the net efficiency ranged from 95% to >98%. For kinking 2 prongs fitting $\Sigma^+ \to p\pi^0$, not used in normalized quantities, efficiencies were somewhat lower.

The measure and geometric reconstruction efficiency ε_{MR} is estimated, for our small statistics, simply and directly for a given topology by

$$1-\delta_{MR} = \varepsilon_{MR} = N_{MR}/N_s$$

where N_{MR} = net total number of events successfully output from measure/reconstruction (MR), and $N_S = N_{MR} + \Delta N$ = net total number of *acceptable* candidates found in scan and input to MR; the ratio

$$\delta_{MR} = \frac{\Delta N}{N_s}$$

represents the MR inefficiency from all causes. The correction is then

$$\frac{1}{C_{MR}} = 1-\delta_{MR} = \varepsilon_{MR} \pm \Delta\varepsilon_{MR} = \frac{N_S - \Delta N}{N_S} \pm \sqrt{\frac{\Delta N(N_S+\Delta N)}{N_S^3}}$$

where the statistical uncertainty $\Delta\varepsilon_{MR}$ is calculated taking N_S and ΔN as (Poisson distributed) independent numbers. For kinking 2 prongs at the 5 high momenta, we find

$$\delta_{MR} = \frac{443}{6376} \approx .069 \pm .03$$

and for 2 prong V^0's,

$$\delta_{MR} = \frac{282}{5073} \approx .056 \pm .03 .$$

Here we have taken .03 as a reasonably conservative estimate of the error in $\delta_{MR}, \varepsilon_{MR}$, since we feel the naive statistical error underestimates the actual uncertainties.

Because the 5 upper momenta are well above threshold for multiple missing neutral final states, not every acceptable candidate which fails to constrain to reactions 1-4 should be regarded as kinematic fitting inefficiency in δ_F, ε_F. Taking into consideration our limited statistics, we estimate ε_F as follows:

(a) $\Sigma^+ \to \pi^+ n$ events

The largest class of Σ^+ events which pass measurement and have acceptable ionization on all tracks but fail to yield an acceptable kinematic fit to reactions 1-3 are those which do attain a constraint to ΣK or $\Sigma K \pi$ but require the CLOUDY-FAIR maximum number of iterations (nine) to achieve the fit; thus, although the solutions for these events have apparently converged, the required 10th iteration to demonstrate their stability is not available. These marginal events are not accepted for analysis; those of them which have a 9 iteration kinematic fit as well as acceptable ionization for the ΣK hypothesis are so assigned (as for the good ΣK events) despite any possible successful fits to a $1c/2c$ $\Sigma K \pi$ hypothesis. In figure II.8 (2 entries/physical event), the unshaded histogram displays the MM^2 (before constraint) recoiling against the outgoing meson track for all kinking 2 prongs at the 5 high momenta ($\pi^+ p \to K^+ + MM$); the shaded histogram is what remains after only the ΣK events accepted for analysis are removed. The residual peak above background at m_Σ^2 consists of the failed fits to ΣK. However, we cannot simply take the ratio of the residual peak to the total Σ signal above background as a measure of $\delta_F = 1 - \varepsilon_F$, because examination of failing ΣK events demonstrated that $\Sigma^+ \to p \pi^0$ constitutes a greater proportion of the residual peak than $\Sigma^+ \to \pi^+ n$, which alone is used for cross sec-

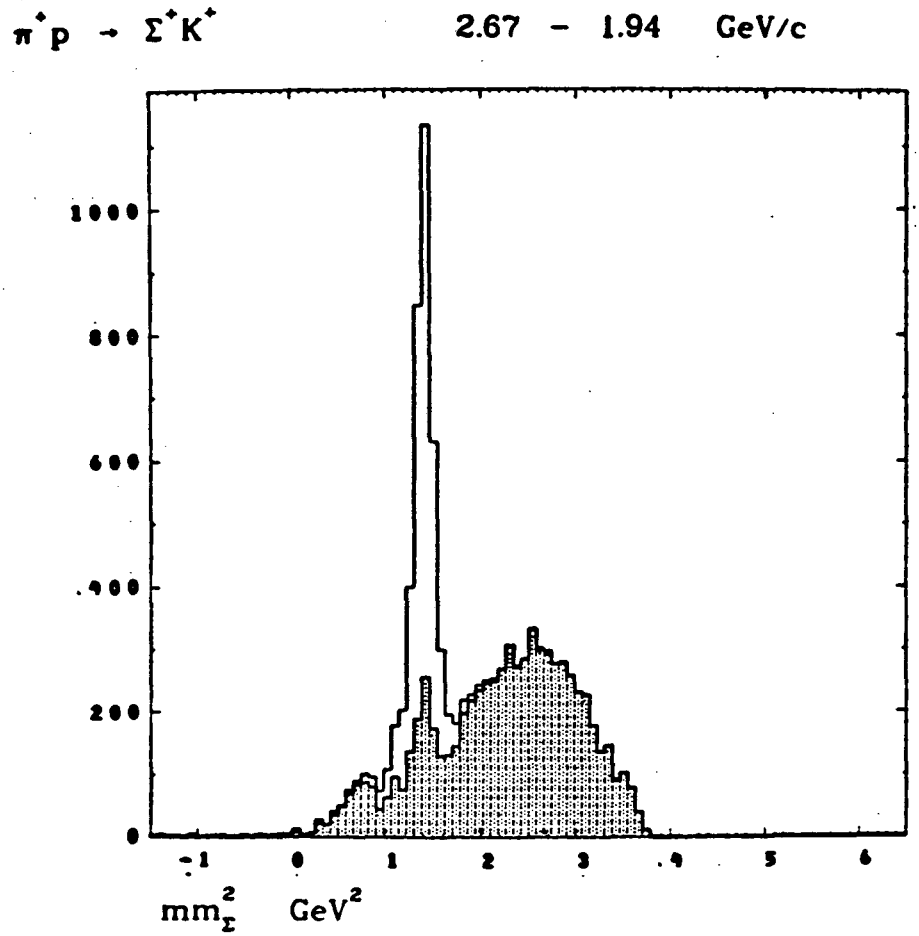
$\pi^+ p \rightarrow \Sigma^+ K^+$
2.67 - 1.94 GeV/c
1000
800
600
400
200
0
-1
0
1
2
3
4
5
6
mm^2_Σ GeV^2

II.8

tions.

When the marginal ΣK events discussed above are removed as well, less than 1% of the original Σ^+ signal remains (in the plot of the same MM^2 in figure II.4b, these marginal events, which, as per above, were not permitted $1c/2c$ $\Sigma K\pi$ assignment, have been thus removed along with the good $4c/5c$ events). Thus these marginal events represent reasonably well the CLOUDY-FAIR ΣK fitting inefficiency (shaded peak in figure II.8), and have been ionization selected and resolved for Σ^+ decay mode along with the good ΣK events. We take the fraction of $\Sigma^+ \to \pi^+ n$ in the residual Σ peak in figure II.8 to be the same as in the rejected marginal ΣK sample. Of the 183 marginal ΣK at the 5 high momenta, 84 are $\Sigma^+ \to \pi^+ n$, and we estimate the shaded residual Σ peak in figure II.8 to be 323 events above background. Of the 1518 accepted ΣK events at the 5 high momenta, 914 are $\Sigma^+ \to \pi^+ n$, and the unshaded Σ^+ peak area in figure II.8 contains 2991 events above background, so we estimate that there are $\left(\frac{914}{1518}\right)(2991) \approx 1801$ $\Sigma^+ \to \pi^+ n$ events in the unshaded Σ peak, and that there are

$$\left(\frac{914+84}{1518+183}\right)(2991+323) = \left(\frac{998}{1701}\right)(3314) \approx 1944\ \Sigma^+ \to \pi^+ n$$

in the total Σ peak. Thus the inefficiency is

$$\delta_F = 1 - \varepsilon_F = \frac{143}{1944} \approx .07 \pm .03\ .$$

Here again, rather than using the naive statistical error in δ_F, we take .03 as a reasonable, conservative estimate of the uncertainty, considering the difficulty of estimating the amounts of signal above background in figure II.8.

We take δ_F to represent also the fitting inefficiency for the $1c/2c$ $\Sigma^+ K^0 \pi^+$, $\Sigma^+ \to \pi^+ n$ events. This is justified in part because the rejected

marginal $\Sigma K\pi$ events bear approximately the same ratio to the good $\Sigma K\pi$ that the marginal ΣK do to the good ΣK sample.

Further, since there is kinematical information on the marginal ΣK events, for $\Sigma^+ \to \pi^+ n$ they have been examined for correlations of the fitting inefficiency with the dynamical variables; it was found that the rejected $\Sigma^+ K^+$, $\Sigma^+ \to \pi^+ n$ events at the 5 upper momenta (~68 total) which passed all primary and decay fiducial volume, angle, and length cuts used for good events were distributed in $\cos\vartheta_{CM}$ the same as the accepted $\Sigma^+ K^+$ events, and were roughly equally divided between forward and backward hemisphere.

(b) Λ events

To estimate the fitting inefficiency for 2 prong V^0 events constrained to $K^+\pi^+\Lambda$ (essentially no Λ events are removed by the iterations cuts), in addition to the simultaneous 2-vertex (7c) kinematic fit plus ionization selection which all accepted events were required to meet, on all $K\pi\Lambda$ candidates independent production (4c) and decay vertex (3c) kinematic fits and ionization selection were performed. Generally any event meeting the simultaneous 2-vertex selection automatically satisfied the independent production and decay vertex requirements, but the converse did not hold. Thus to estimate δ_F we use that sample of $K\pi\Lambda$ candidates which met all selection criteria (including production and decay fiducial volume, angle, and length cuts: see next section on cuts and weights) used for accepted events *except* the simultaneous 2-vertex kinematic fit, but which *did* have the *sum* of the independent production and decay vertex kinematic χ^2's within the acceptance limits used for the simultaneous 2-vertex fits, as well as acceptable

ionization at both vertices. Some of these events fail because of the propensity of Λ's to suffer dissociation of production and decay vertices due to scattering, distortion, etc. Thus, for the 5 high momenta we get for $K\pi\Lambda$

$$\delta_F = 1 - \varepsilon_F = \frac{24}{674} = .036 \pm .02$$

where again we take .02 as a reasonable uncertainty rather than the purely statistical one.

Finally, there is a small residual overall bookkeeping and FOG-CLOUDY-FAIR tape failure event loss inefficiency corrected for in $\varepsilon_B = 1 - \delta_B$; for kinking 2 prongs ($\Sigma K, \Sigma K\pi$) we find $\delta_B \approx 3\% \pm 2\%$ and for 2 prong V^0's ($K\pi\Lambda$), $\delta_B \approx 2\% \pm 1\%$.

F. Decay Angle and Length Cuts and Weights for Σ^+ and Λ

Figures II.9a,b display the Σ^+ rest-frame decay $\cos\vartheta_\Sigma$ and φ_Σ for all $\Sigma^+ \to \pi^+ n$ at the 5 high momenta, where:

$$\cos\vartheta_\Sigma = \hat{p}_\pi \cdot \hat{p}_\Sigma$$

and

$$\varphi_\Sigma = \arccos\left[\frac{\vec{p}_\Sigma^{LAB} \times \vec{p}_\pi^{LAB}}{|\vec{p}_\Sigma^{LAB} \times \vec{p}_\pi^{LAB}|} \cdot \frac{\vec{p}_\Sigma^{LAB} \times \vec{Z}}{|\vec{p}_\Sigma^{LAB} \times \vec{Z}|}\right];$$

$\hat{p}_\Sigma, \hat{p}_\pi$ are unit vectors for the Σ^+, decay π^+ in the Σ^+ rest-frame; $\vec{p}_\Sigma^{LAB}, \vec{p}_\pi^{LAB}$ are their lab momenta; and $\vec{Z}$ is the fixed lab vertical axis (approximately parallel to the camera optical axes). φ_Σ runs from 0° to 180° and is folded so that $\varphi_\Sigma = 0°, 180°$ means the decay plane $[\vec{p}_\Sigma^{LAB} \times \vec{p}_\pi^{LAB}]$ contains $\vec{Z}$. For 100% efficient Σ^+ detection, the $\cos\vartheta_\Sigma$ and φ_Σ distributions should be isotropic.

$\Sigma^+K^+,\Sigma^+(K\pi)^+$ 2.7,2.5,2.3,2.15,1.95 GeV/c

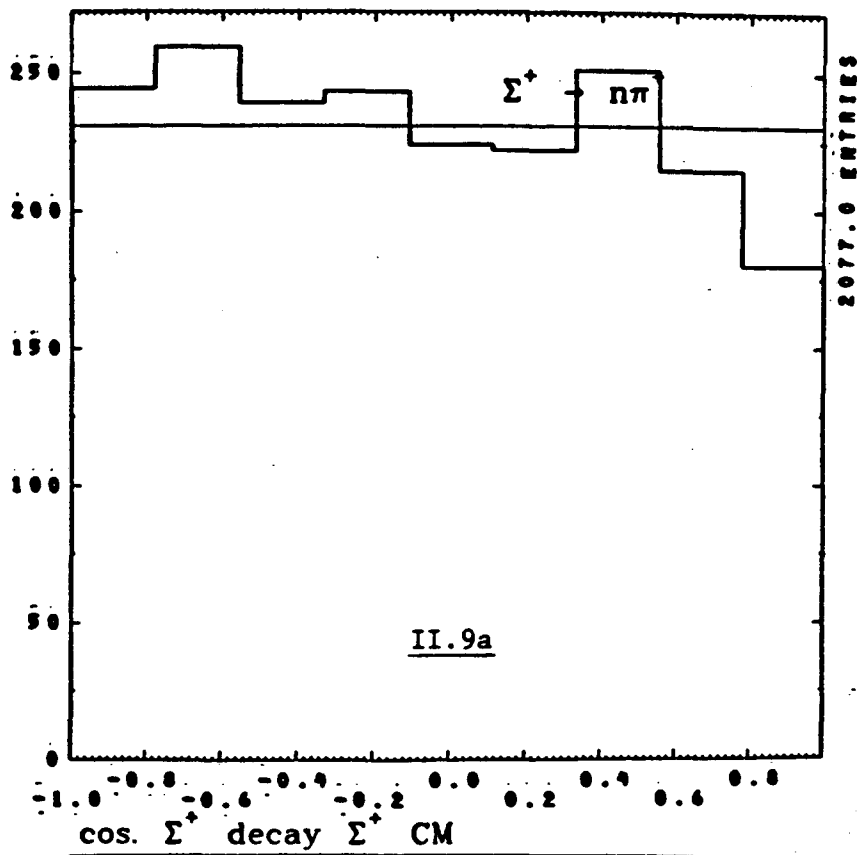

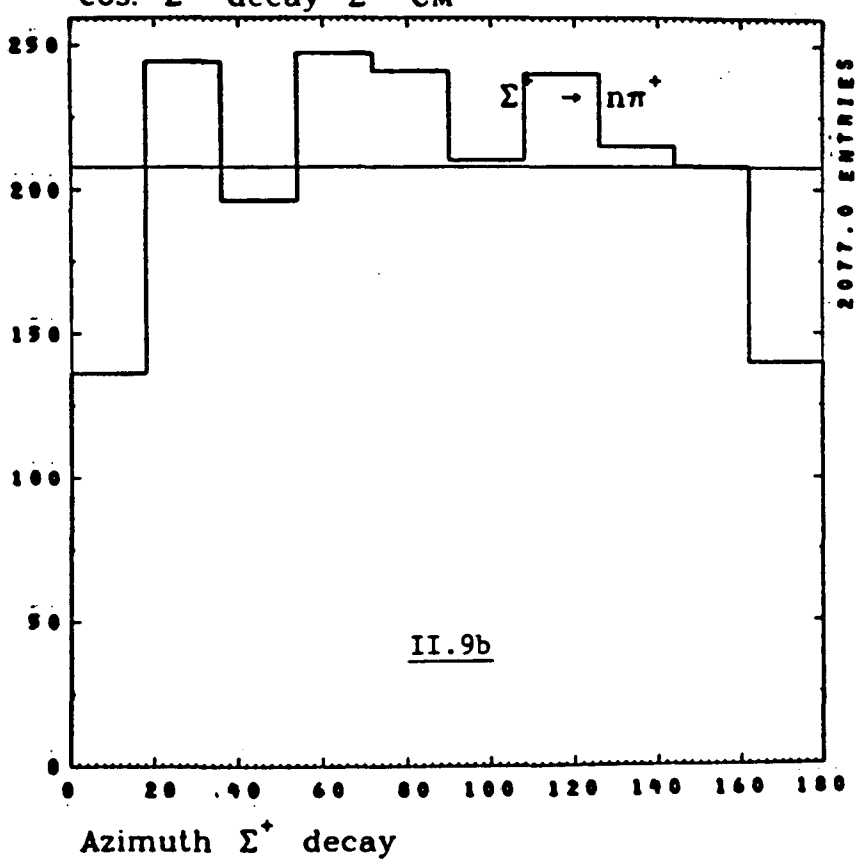

The depletion in II.9a near $\cos\vartheta_\Sigma = +1$ corresponds to small Σ^+ lab decay angles (slight kinks) which are harder to detect. Similarly, II.9b shows losses for φ_Σ near 0° and 180°, where the kink is harder to detect. From the kinematics of $\Sigma^+ \to \pi^+ n$, only for Σ's with $P_\Sigma^{LAB} > p_0 = 1.58\ GeV/c$ do both forward and backward rest-frame decays correspond to small lab angles; for $P_\Sigma^{LAB} < p_0$, backward Σ rest-frame decays are also backwards in the lab (large kinks), so II.9a shows loss mainly for $\cos\vartheta_\Sigma = +1$, since most Σ's in our samples have $P_\Sigma^{LAB} < p_0$. For $\Sigma^+ \to p\pi^0$, not used in normalized quantities, p_0 is only 0.24 GeV/c.

To correct for systematic loss in $\cos\vartheta_\Sigma$, a minimum cut α_c is placed on the Σ lab decay angle α; α_c is typically 4°–5° (10° for 72" data). Each event passing the cut receives a P_Σ^{LAB}-dependent weight W_α equal to the inverse of the probability that its $\cos\vartheta_\Sigma$ fall within the limits $\cos\vartheta_\Sigma^U, \cos\vartheta_\Sigma^L$ determined by α_c:

$$W_\alpha = 2/\left[\cos\vartheta_\Sigma^U(\alpha_c; P_\Sigma^{LAB}) - \cos\vartheta_\Sigma^L(\alpha_c; P_\Sigma^{LAB})\right] .$$

At each of the 5 upper momenta the cuts on α were determined by increasing the value of α_c until the numbers of weighted events became constants within statistics (or maxima; see also ref. 2).

The systematic loss in φ_Σ is approximately independent of P_Σ^{LAB}; thus the fraction lost to this bias in the φ_Σ distributions at each incident momentum was used to calculate a constant correction C_φ for $\Sigma^+ \to \pi^+ n$ events. At the 5 upper momenta, C_φ varied from $1.04 \pm .02$ to $1.11 \pm .03$, comparable to the range of C_φ for the 9 lower energies.

Because of limited bubble chamber spatial resolution, a minimum Σ^+ lab length cut l_c is imposed, and because Σ's might leave the chamber before decay, a lab length cut l_F is also imposed, where l_F = distance from Σ

production vertex to the fixed decay fiducial volume boundary. Also, because there is a slight bias against events with very long, fast Σ's and correspondingly short, slow K's, a direct maximum Σ^+ lab length cut l_{MAX} is imposed. Each Σ^+ accepted has length $l_c < l_\Sigma < l_F, l_{MAX}$ as well as $c\tau_\Sigma < 4c\tau_0$ and receives weight

$$W_l = 1/\left[e^{-(m_\Sigma l_c)/(P_\Sigma^{LAB} c\tau_0)} - e^{-(m_\Sigma l_M)/(P_\Sigma^{LAB} c\tau_0)}\right]$$

where $\frac{m_\Sigma l_M}{P_\Sigma^{LAB}} = \text{minimum}\left[4c\tau_0, \frac{m_\Sigma l_F}{P_\Sigma^{LAB}}, \frac{m_\Sigma l_{MAX}}{P_\Sigma^{LAB}}\right]$. The cut l_c is determined similarly to α_c; for the 5 upper momenta typically $l_c = 4.5\,mm$ and $l_c = 3\,mm$ for the 9 lower energies, and l_{MAX} is typically 16-17 cm. (For $\Sigma K\pi$ distributions such as mass spectra, the l_c cuts were relaxed to 3 mm at the 5 upper momenta.)

For Σ^+K^+ events $\overline{W_a W_l} = 1.36$; for $\Sigma^+K^+\pi^0$ events $\overline{W_a W_l} = 1.33$; and for $\Sigma^+\pi^+K^0$ events $\overline{W_a W_l} = 1.30$.

Figures II.10a,b show the Λ rest-frame decay $\cos\vartheta_\Lambda$ and φ_Λ for $\Lambda \to p\pi^-$ events at the 5 upper momenta, where in analogy to Σ^+ events

$$\cos\vartheta_\Lambda = \hat{p}_p \cdot \hat{p}_\Lambda$$

$$\varphi_\Lambda = \arccos\left[\frac{\vec{P}_\Lambda^{LAB} \times \vec{P}_p^{LAB}}{|\vec{P}_\Lambda^{LAB} \times \vec{P}_p^{LAB}|} \cdot \frac{\vec{P}_\Lambda^{LAB} \times \vec{Z}}{|\vec{P}_\Lambda^{LAB} \times \vec{Z}|}\right]$$

and the ranges and orientations of $\cos\vartheta_\Lambda$ and φ_Λ are as for Σ^+ events. figure II.10a shows depletion for $\cos\vartheta_\Lambda = +1$, corresponding to a backward π^- in the Λ rest-frame, which is a low momentum π^- in the lab; such Λ decays have asymmetric prongs with a short, often stopping or captured π^- which is more difficult to scan and measure. To correct for this systematic loss a cut $P_{\min}$ on the minimum π^- lab momentum is imposed and each accepted event

$\pi^+ p \rightarrow K^+ \pi^+ \Lambda$ 2.67 - 1.94 GeV/c

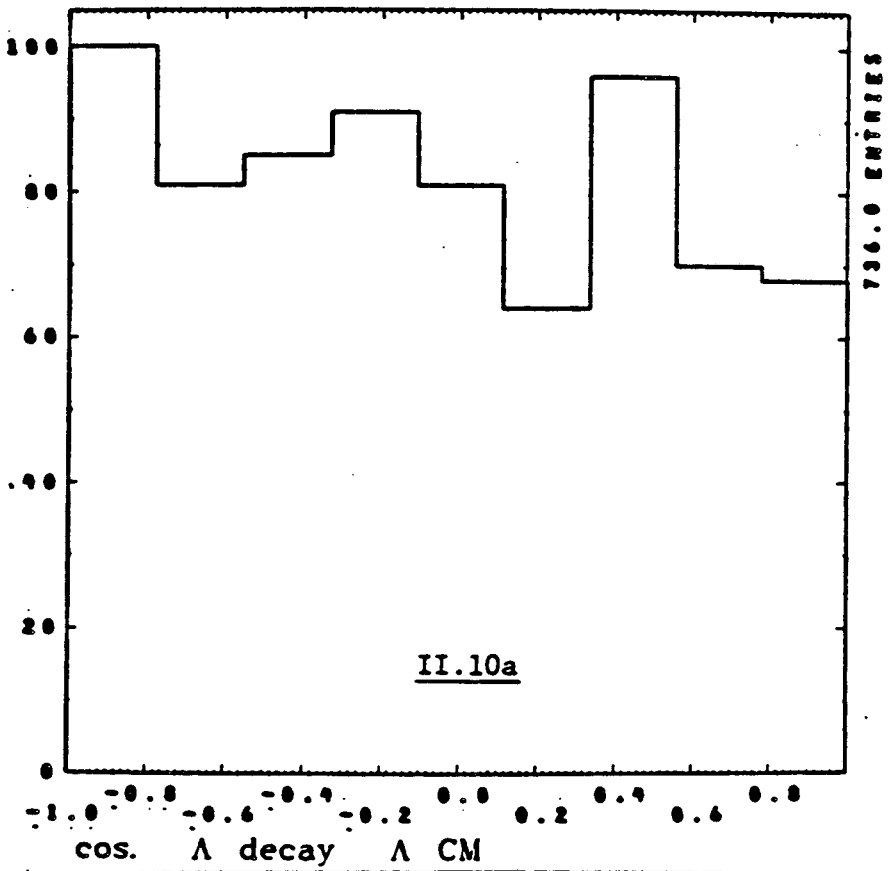

II.10a

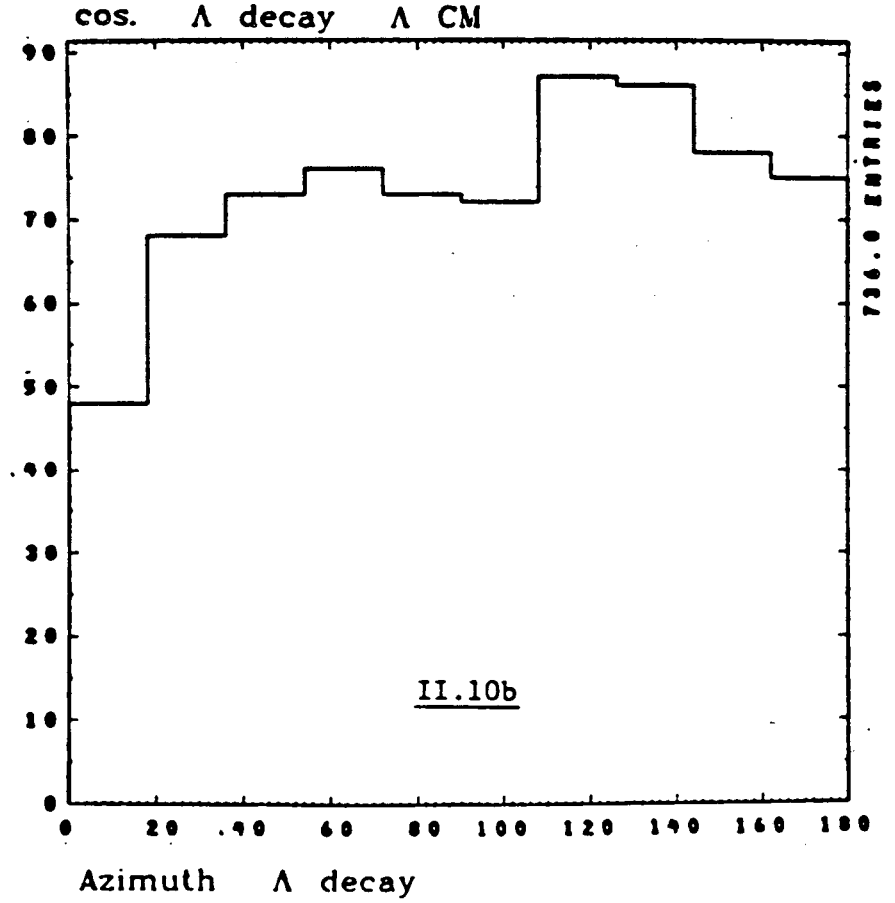

II.10b

receives a P_Λ^{LAB}-dependent weight W_p:

$$W_P = 2/[\ \cos\vartheta_\Lambda(P_{\min};P_\Lambda^{LAB}) - 1\ ]$$

The value of $P_{\min}$ was .04 GeV/c (range $\approx$1.5 cm); no cuts on minimum decay proton lab momentum were used (for our energies, minimum P_p^{LAB} = .2 GeV/c, range $\approx$3.5 cm).

For each incident momentum a constant correction C_φ for $\Lambda \to p\pi^-$ events, determined as with Σ^+ events, was applied to correct for the losses shown in II.10b. C_φ varied from 1.05 $\pm$ .02 to 1.03 $\pm$ .01.

As for Σ^+ events, Λ events required minimum and maximum decay length cuts l_c, l_F and P_Λ^{LAB}-dependent weights W_L:

$$W_L = 1/[\ e^{-(m_\Lambda l_c)/(P_\Lambda^{LAB} c\tau_0)} - e^{-(m_\Lambda l_F)/(P_\Lambda^{LAB} c\tau_0)}\ ]$$

At the 5 upper momenta l_c = 7 mm and at the 9 lower l_c = 8 mm. For distributions such as mass spectra, as opposed to cross sections, the l_c cuts were relaxed to 5 mm. For $K\pi\Lambda$ events $\overline{W_p W_L}$ = 1.33 at the 5 high momenta.

III. EXPERIMENTAL RESULTS

A. Normalization and Microbarn Equivalents

The cross section in microbarns for a given channel at a particular incident momentum is

$$\sigma(\mu b) = \frac{\mu W}{f}$$

where μ is the microbarn/event factor for the channel and momentum, W the number of events weighted as discussed in Chapter II, and f is the fraction of the channel going into the decay mode(s) observed, taken from the Particle Data Group Tables (ref. 8). The microbarn equivalent factor for the channel and incident momentum is given by

$$\mu = \frac{C_\phi C_T}{(\rho_H N_A \; 10^{-30} \; events/\mu b)(L)}$$

where C_T, C_ϕ are as discussed in the last chapter. The density of liquid hydrogen in the chamber, ρ_H, was .0605 gm/cm^3 (see ref. 4), N_A is Avogadro's number, and L is the total beam path length through the production fiducial volume:

$$L = (no.\ frames)\times(average\ no.\ beam\ tracks/frame)\times(length/track).$$

Events counted in cross section totals are required to have a primary vertex whose longitudinal position x, beam entrance lateral position y, and beam entrance azimuthal angle β are within the limits which determine the beam tracks counted in L above. The length per track within the production fiducial volume for each incident momentum is calculated taking curvature into account, and the total is corrected for attenuation by interaction using

the π^+p total cross sections compiled by the Particle Data Group, ref. 10, as well as for μ^+ contamination.

For the 2.46, 2.15, and 1.94 GeV/c data samples the average number of beam tracks per frame was determined, as at the 9 low momenta, by counting at the scan table the tracks within the fiducial volume using a template to define the x, y, and β acceptance. At 1.94 and 2.46 GeV/c, 2 frames every 150 frames were counted for every 4th roll of film; at 2.15, 3 frames every 225 frames were counted for every 4th roll. This sampling averaged over the multiple beam spills per Bevatron pulse, and counted a sufficient number of tracks to determine the number of beam particles at each momentum to within 1.5%. At 2.67 and 2.30 GeV/c we use the similar beam track count performed by Ko (ref. 4), corrected for our slightly different x, y, and β windows.

Finally, for Σ^+ channels at 2.15 GeV/c, the μb equivalents include an additional correction for a FOG-CLOUDY-FAIR processing error which resulted in the loss of approximately 5% of good events for the ΣK channel and 20% of good events for the $\Sigma K\pi$ channels, at that one incident momentum only.

Table I shows the μb equivalents for the 14 incident momenta.

B. Channel Cross Sections

1. Numbers of Events

The numbers of weighted and unweighted events used for cross section calculations for the final states (reactions 1-4) studied at the 14 incident momenta are given in Table II. Since all cross section determinations for

channels with Σ^+ are made from $\Sigma^+ \to \pi^+ n$ events (except $\Sigma K\pi$ channels for $p_\pi \leq 1.84$ GeV/c), no weighted totals of $\Sigma^+ \to p\pi^0$ are given in Table II. Generally the $\Sigma^+ \to p\pi^0$ events for a given channel are ~25-30% fewer than the $\Sigma^+ \to \pi^+ n$ events for $p_\pi \geq 1.68$ GeV/c, reflecting the lower detection efficiencies for the proton decay mode as the incident momentum increases.

2. $\Sigma^+ K^+$

Table III gives the channel cross sections for reaction 1 as determined by this work for the 5 higher momenta, and as determined by refs. 2 and 3 for the 9 lower momenta. Only $\Sigma^+ \to \pi^+ n$ events are used, and the cross sections have been corrected using the branching fractions published in the Particle Data Group (PDG) tables. Errors include both statistical uncertainties and uncertainties in all systematic effects (uncertainties in systematic effects are all included in the errors of the μb equivalent factors).

Figures III.1a,b display plots of the 14 ΣK channel cross sections $\sigma_{\Sigma K}$ as a function of laboratory incident π^+ momentum p_π, as well as the total available world data for this channel taken from the PDG compilations ref. 12, and from refs. 13,15,16,19,20, and 22. Only hydrogen bubble chamber (HBC) or deuterium bubble chamber (DBC) data with 4π steradian acceptance are included, with the exception of the integrated cross section data at 7.5 and 11.5 GeV/c from the spectrometer-bubble chamber experiment of the SLAC SHF Collaborations, ref. 16.

In figure III.1 we note that the main features of $\sigma_{\Sigma K}$ are a rise from threshold to a peak at $p_\pi \approx 1.5\ GeV/c$, presumably corresponding partly to formation of the $[I = 3/2]$ $\Delta(1960)$, and a subsequent power law fall in p_π.

$\pi^+ p \rightarrow \Sigma^+ K^+$

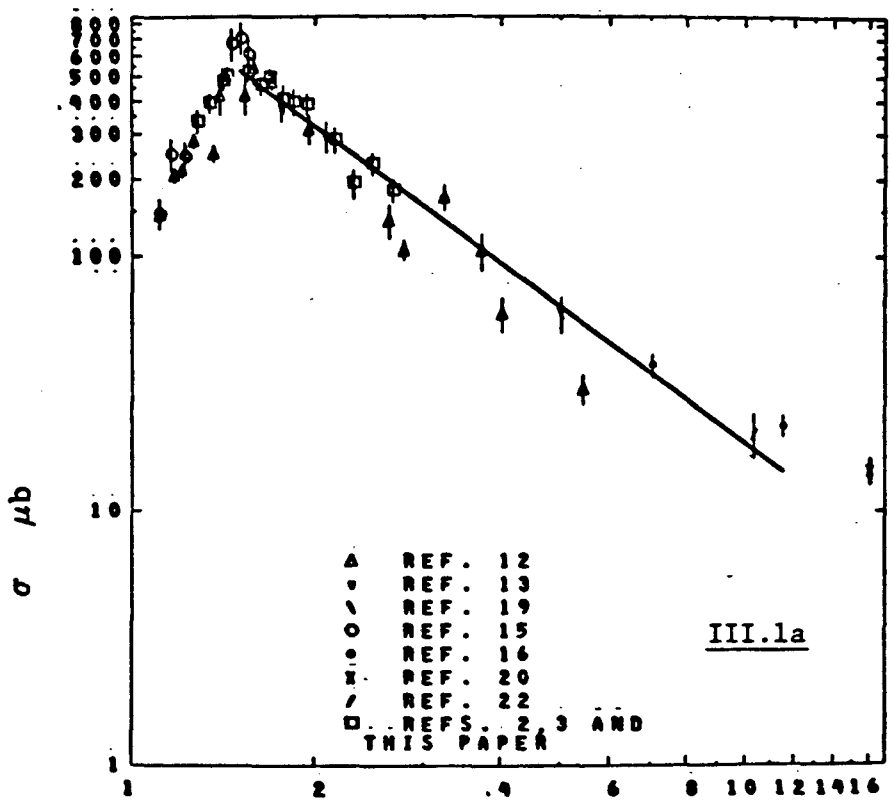

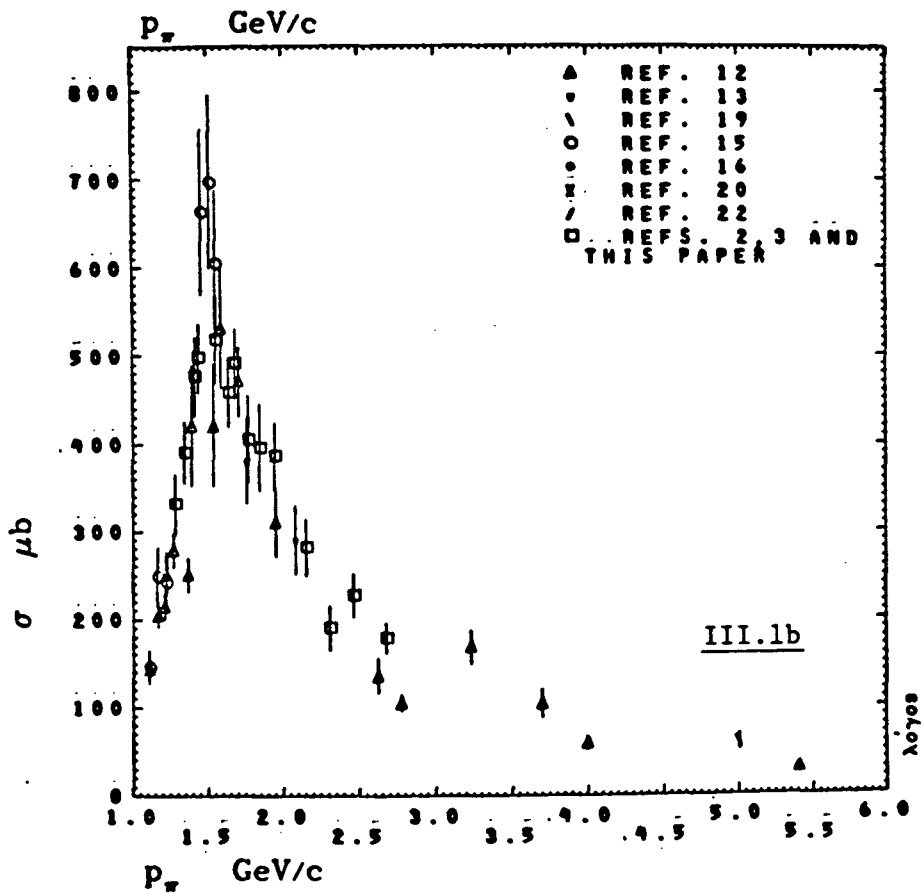

(For branching fraction determination of $\Delta(1960) \to \Sigma K$, see refs. 2 and 3.) Also note that

$$s = (\mathbf{p}_\pi + \mathbf{p}_p)^2 = m_\pi^2 + m_p^2 + 2E_\pi m_p$$
$$\approx m_\pi^2 + m_p^2 + 2m_p p_\pi$$

where $\mathbf{p}_\pi, \mathbf{p}_p$ are the incident π^+ and target p 4-momenta, and E_π, p_π the π^+ lab energy and 3-momentum. Thus s is approximately linear in p_π.

Because $\sigma_{\Sigma K}$ has been extensively measured, the 5 new data points provide a good extrinsic check on the overall experimental normalization of our 5 high momenta.

The slope of the power law fall in p_π obtained by fitting all the data in figure III.1 with $p_\pi \geq 1.5$ GeV/c is given in Table VI (see section III.E).

3. $\Sigma^+K^+\pi^0$ and $\Sigma^+\pi^+K^0$

The values of channel cross sections for $\Sigma^+K^+\pi^0$ for the 5 higher momenta of this work given in Table III are computed from $\Sigma^+ \to \pi^+n$ events using the PDG branching fractions; again, errors include uncertainties in both statistics and systematic effects. At the 9 lower momenta, the $\Sigma^+ \to p\pi^0$ events were sufficiently unbiased so that they were included in cross section computations for $\Sigma K\pi$. The $\Sigma^+\pi^+K^0$ cross sections are similarly calculated, with an additional correction, using PDG branching fractions, to take into account the fact that there is no visible K^0 decay, i.e., all K^0 are $K_s^0 \to \pi^0\pi^0$ or K_L^0.

Figures III.2a,b and III.3a,b show the $\Sigma^+K^+\pi^0$ and $\Sigma^+\pi^+K^0$ channel cross sections as functions of p_π along with the world data (principally HBC or DBC experiments) taken from refs. 12,13,17,18,19, and 22.

$\pi^+ p \rightarrow K^+ \pi^0 \Sigma^+$

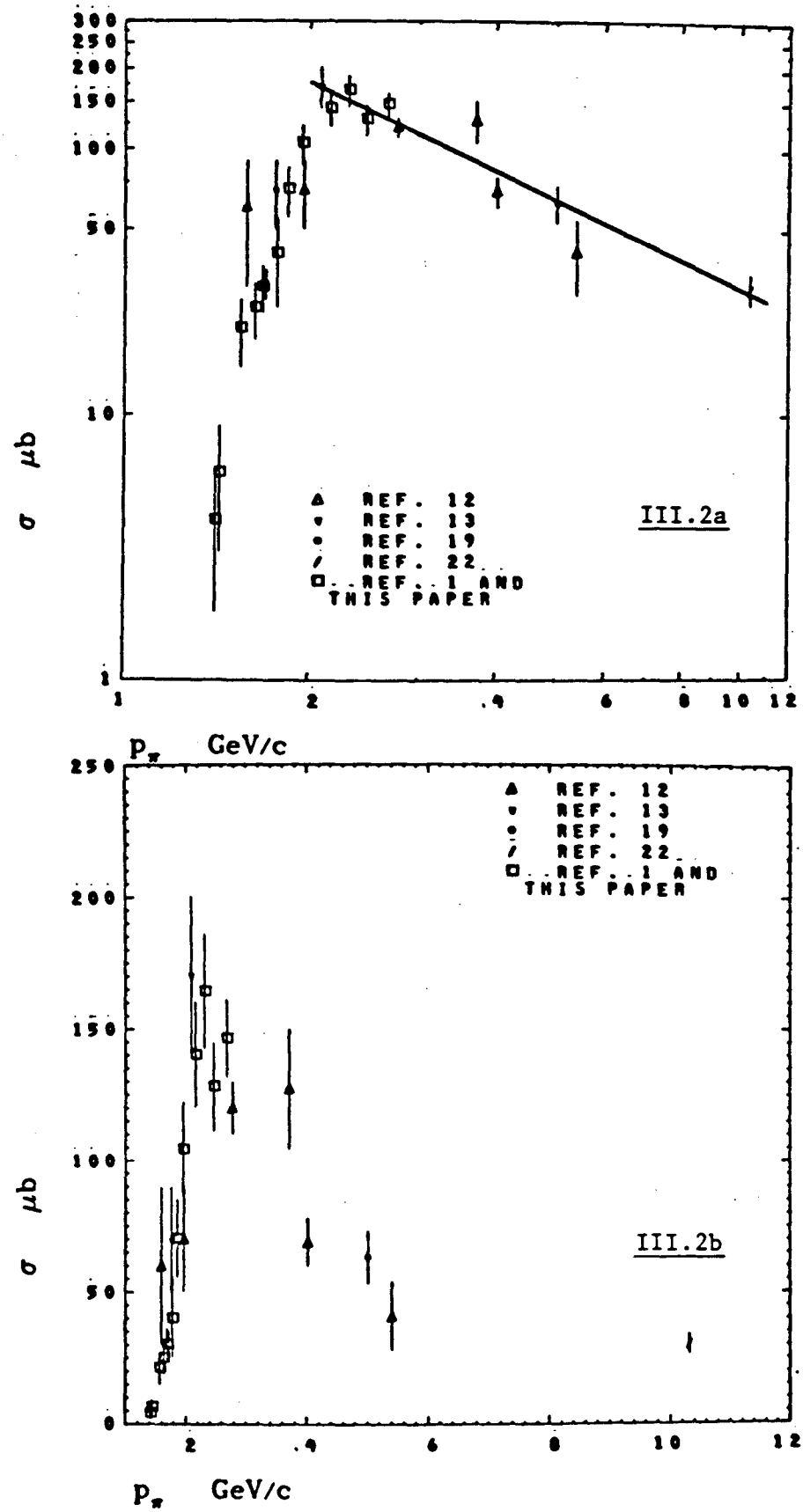

$\pi^+ p \rightarrow K^0 \pi^+ \Sigma^+$

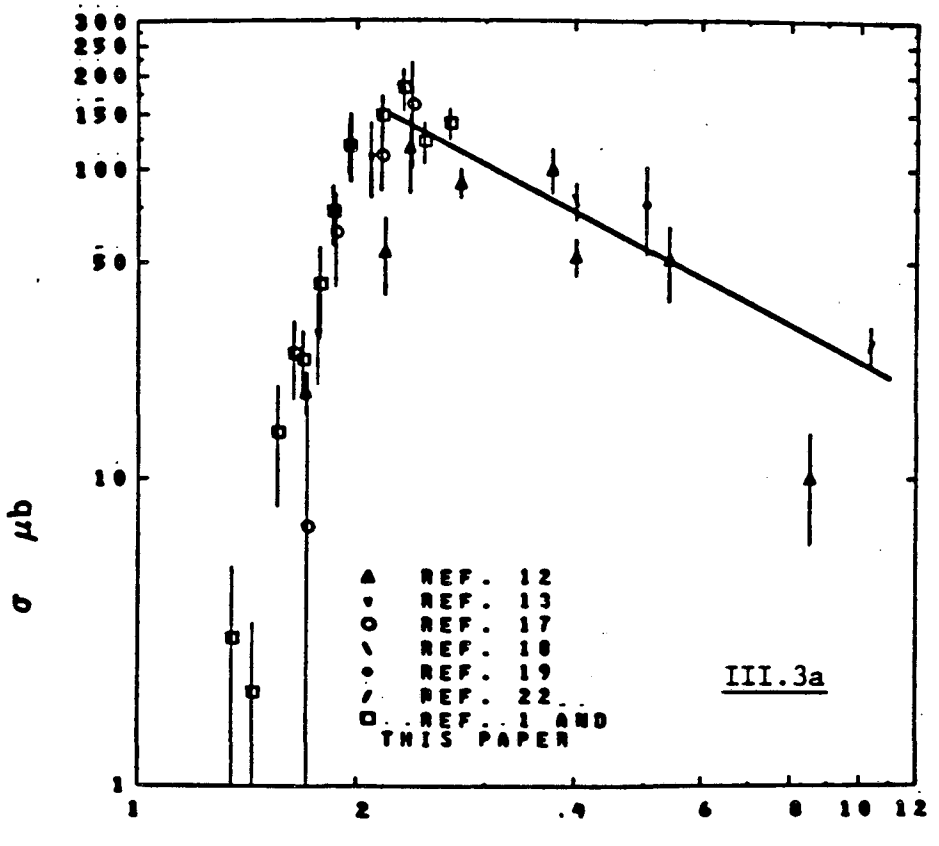

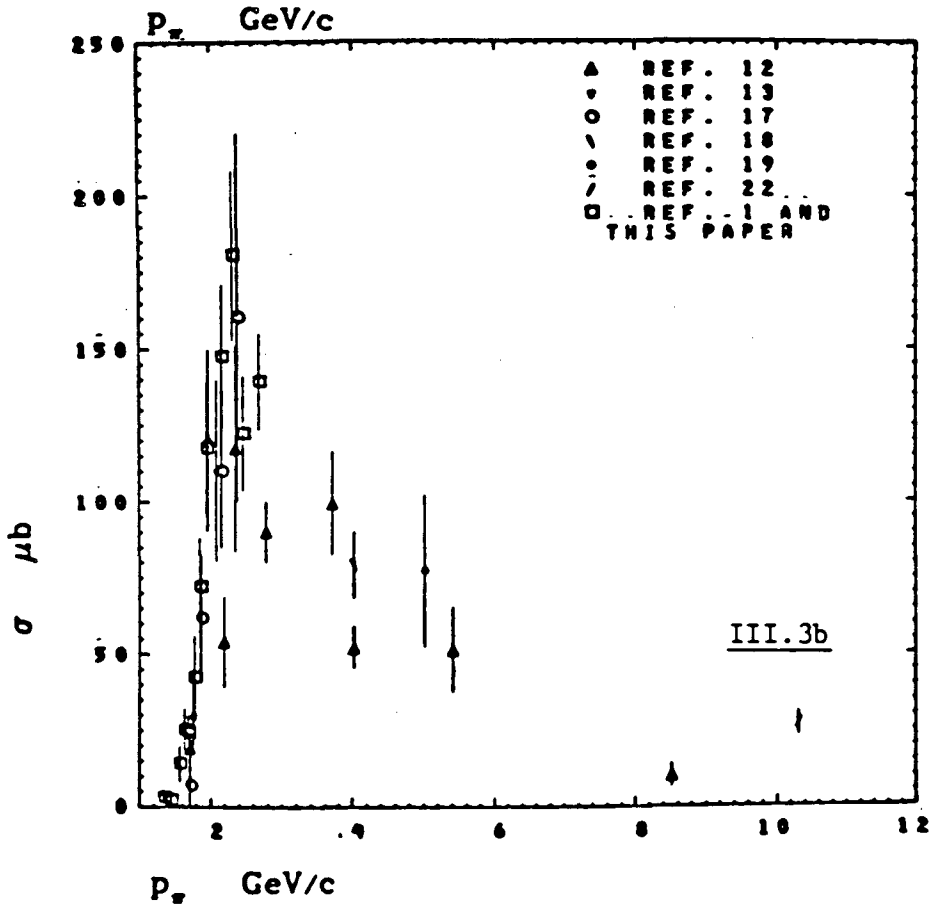

For the $\Sigma^+K^+\pi^0$ channel, the main features are a steep rise to a rather broad maximum in the region ~2.0-2.5 GeV/c and the beginning of a power law decline. The PDG tables list several high spin, rather broad ($\Gamma \sim 400$ MeV), $I = 3/2$ πp resonances corresponding to the region $p_{inc} \sim 2.0$-3.0 GeV/c, but clearly the data is so limited that no useful branching fraction information can be obtained. The resultant slope of a fit to the data of figure III.2 with $p_\pi \geq 2.0$ GeV/c is given in Table VI.

The principal features of the $\Sigma^+\pi^+K^0$ channel total cross sections in figure III.3 are very similar to those of $\Sigma^+K^+\pi^0$. The results of fitting the data of figure III.3 for $p_\pi \geq 2.3$ GeV/c are given in Table VI. (See Section III.E.)

4. $K^+\pi^+\Lambda$

The cross sections for this channel given in Table III and displayed in figure III.4a,b are computed from $\Lambda \rightarrow p\pi^-$ events and corrected using PDG branching fractions for the unseen $\Lambda \rightarrow n\pi^0$ mode. The threshold for this channel is low enough so that $\Delta(1960)$ production may contribute to the peak at $p_\pi \approx 1.75$ GeV/c, to which the cross section rises steeply from threshold. The world data included in figure III.4 are from refs. 12,13,17,18,19,20, and 22. The fitted slope of the data of figure III.4 is given in Table VI. (See Section III.E.)

$\pi^+ p \rightarrow K^+ \pi^+ \Lambda$

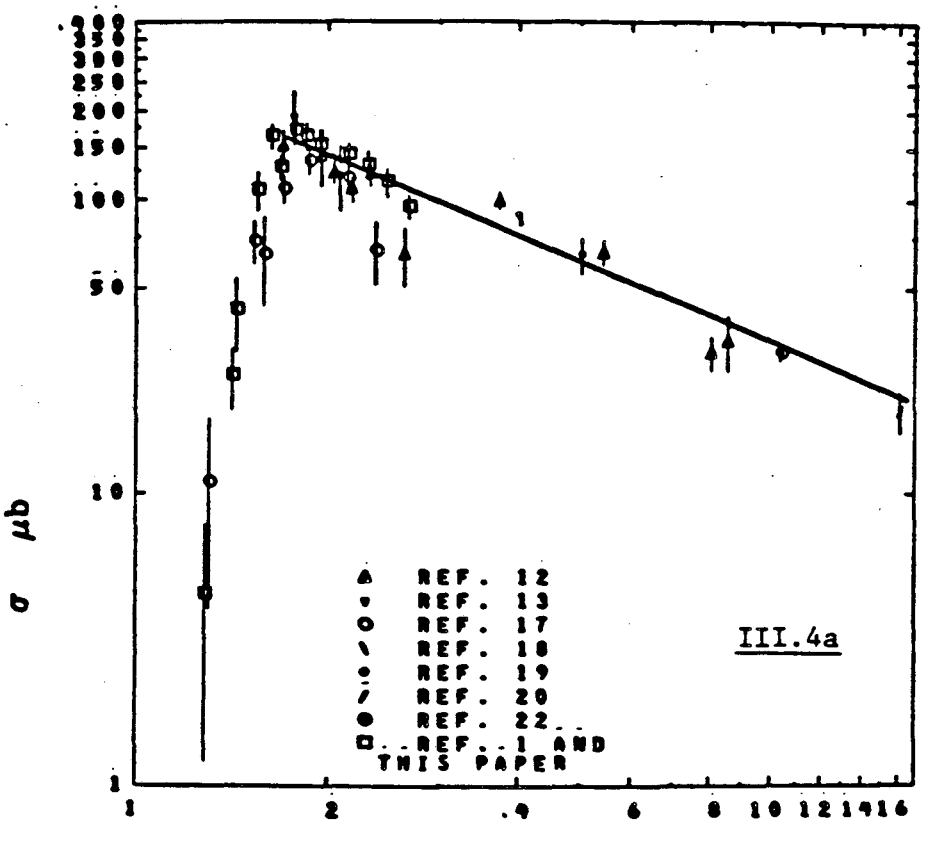

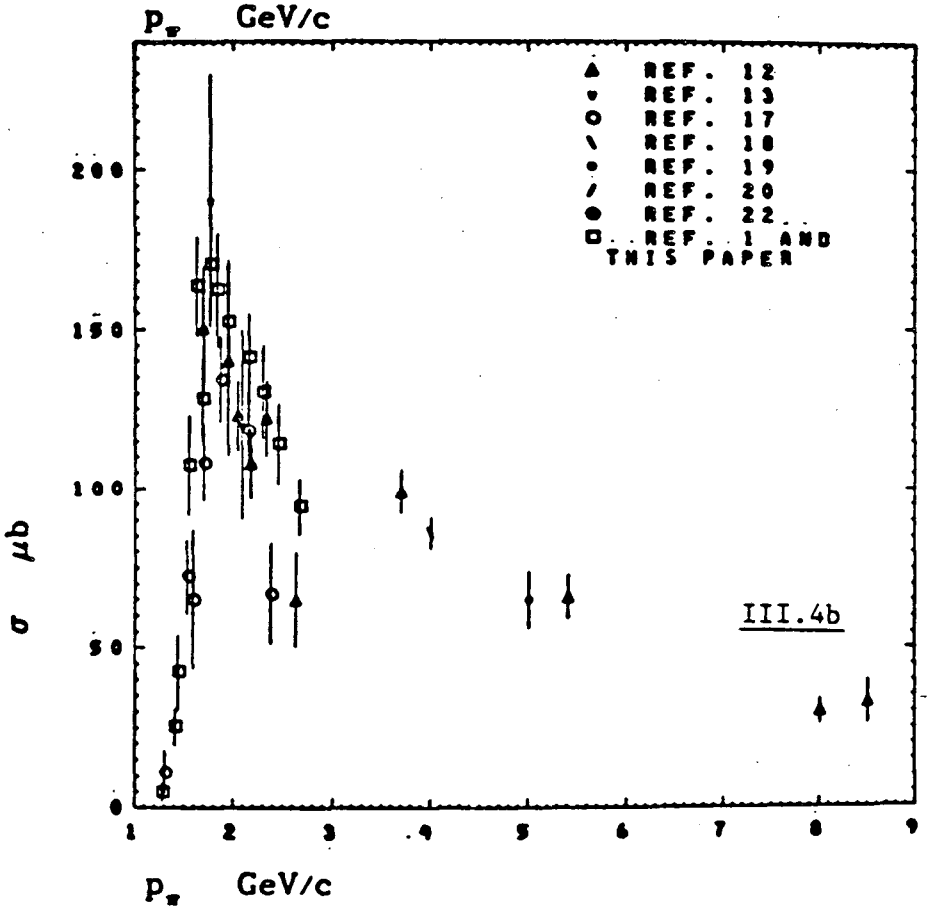

C. General Features of the $K\pi\Sigma, K\pi\Lambda$ Data

This section presents general production features of the final states of reactions 2-4. Fits to $\frac{d\sigma}{dt}$ and determinations of polarizations and density matrix elements are presented in Chapter IV.

1. $\Sigma^+K^+\pi^0$

Dalitz plots of the invariant masses $m^2_{\pi K}$ versus $m^2_{\Sigma\pi}$ for all $\Sigma^+K^+\pi^0$ events at incident momenta 1.55, 1.63, 1.68, 1.77, and 1.84 GeV/c are exhibited in figures III.5 and III.6 (as discussed above and in ref. 1, the $\Sigma^+ \to p\pi^0$ and $\Sigma^+ \to \pi^+n$ events have been combined). In figures III.7 and III.8 are displayed the same Dalitz plots, for $\Sigma^+ \to \pi^+n$ events only, at incident momenta 1.94, 2.15, 2.30, 2.46, and 2.67 GeV/c. Figures III.9 through III.12 present the projected $m^2_{\pi K}$ spectra (with weighted events) for the Dalitz plots of figures III.5-III.8. Finally, figures III.13-III.16 exhibit the Chew-Low plots of invariant momentum transfer squared $t_{p\Sigma}$ versus $m^2_{\pi K}$ for the event samples of figures III.5-III.8, where

$$t_{p\Sigma} \equiv (\mathbf{p}_p - \mathbf{p}_\Sigma)^2$$

and p_p, p_Σ are the 4-momenta of the target proton and Σ^+.

First we note the strong $K^{*+}(892)$ production for the incident momenta $p_\pi \geq 1.94\ GeV/c$, and the general consistency of the mass distributions at the momenta $p_\pi \leq 1.77\ GeV/c$ with phase space. Secondly, the samples at 1.94-2.67 GeV/c do not contain any significant $\Sigma^{*+}(1385) \to \Sigma^+\pi^0$ signal. From the Chew-Low plots shown here (as well as the 5 others at each incident momentum not exhibited) it is clear that the $K^*(892)$ production is forward-

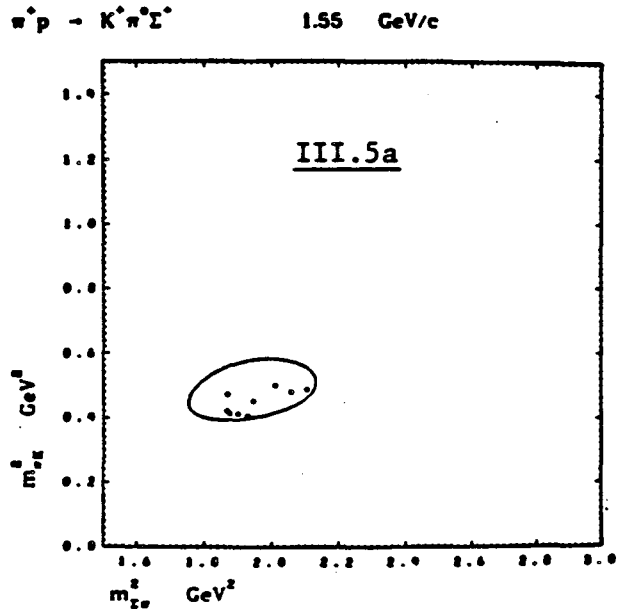
π⁺p → K⁺π⁰Σ⁺
1.55 GeV/c
III.5a
m²πK GeV²
m²Σπ GeV²

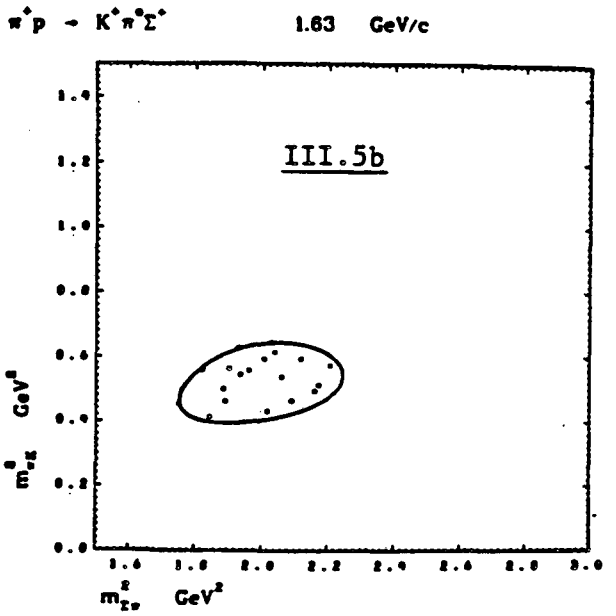
π⁺p → K⁺π⁰Σ⁺
1.63 GeV/c
III.5b
m²πK GeV²
m²Σπ GeV²

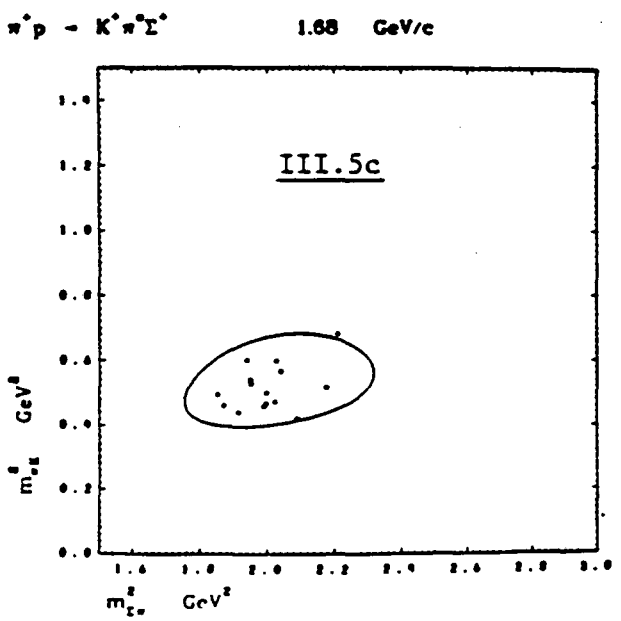
π⁺p → K⁺π⁰Σ⁺
1.68 GeV/c
III.5c
m²πK GeV²
m²Σπ GeV²

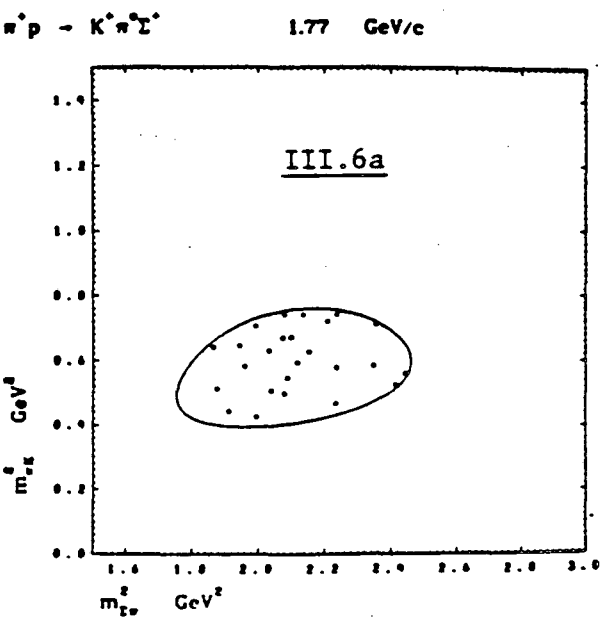
π⁺p → K⁺π⁰Σ⁺
1.77 GeV/c
III.6a
m²πK GeV²
m²Σπ GeV²

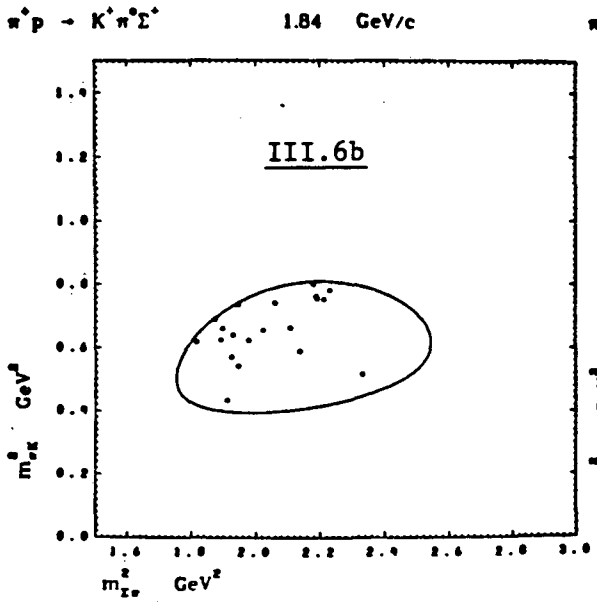
π⁺p → K⁺π⁰Σ⁺
1.84 GeV/c
III.6b
m²πK GeV²
m²Σπ GeV²

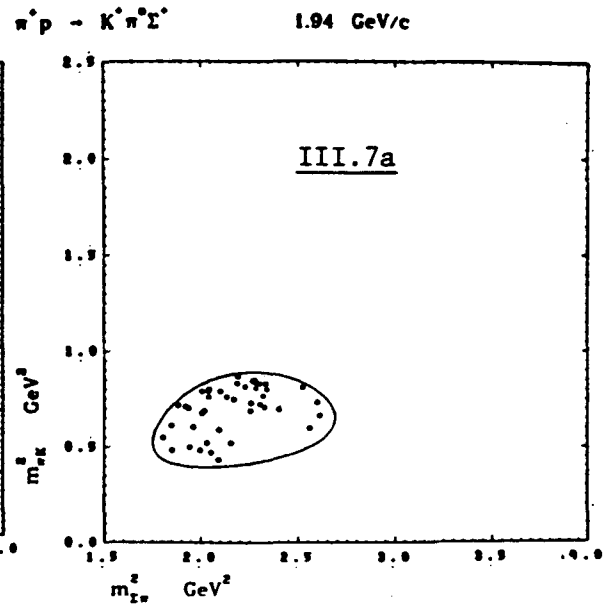
π⁺p → K⁺π⁰Σ⁺
1.94 GeV/c
III.7a
m²πK GeV²
m²Σπ GeV²

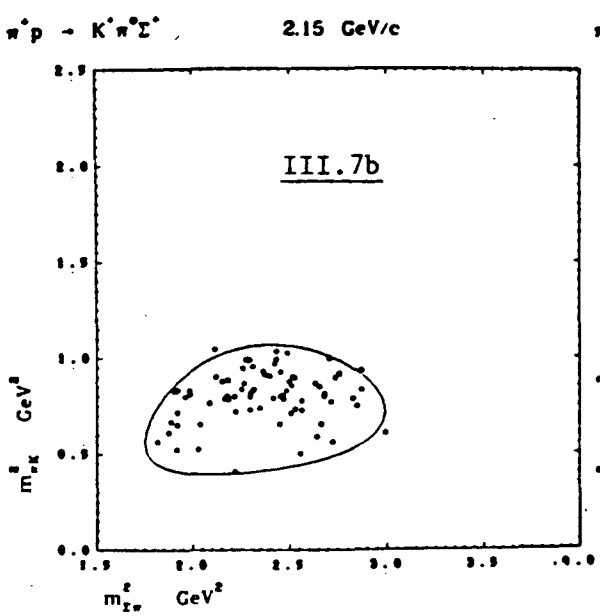
π⁺p → K⁺π⁰Σ⁺
2.15 GeV/c
III.7b
m²πK GeV²
m²Σπ GeV²

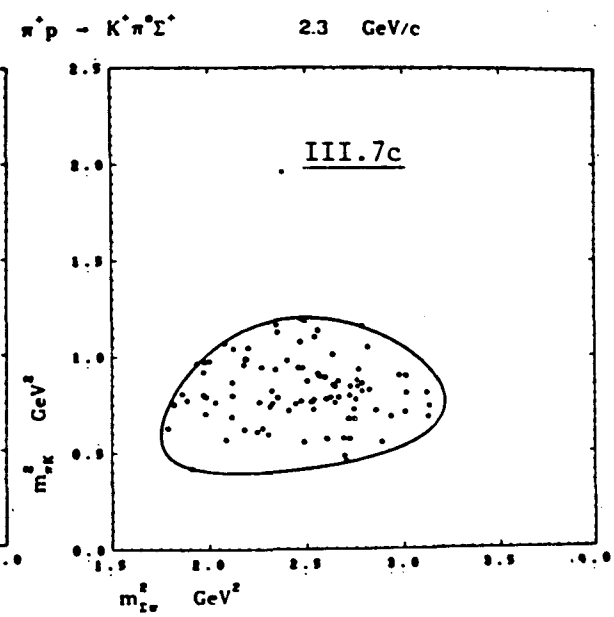
π⁺p → K⁺π⁰Σ⁺
2.3 GeV/c
III.7c
m²πK GeV²
m²Σπ GeV²

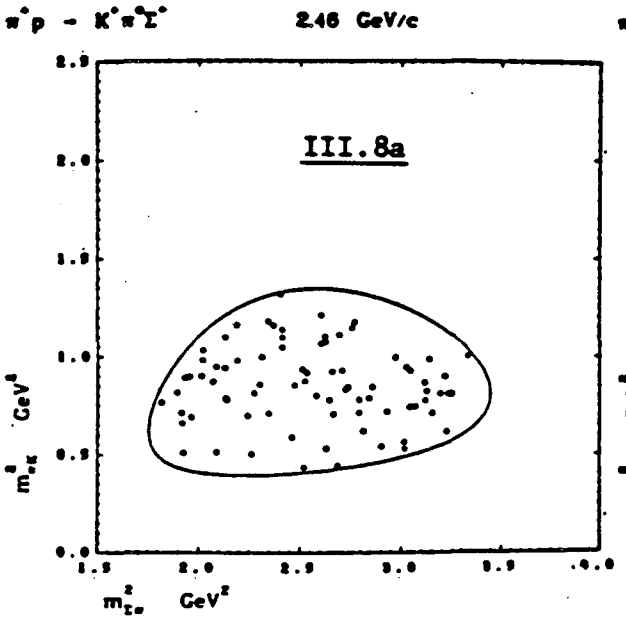
π⁺p → K⁺π⁰Σ⁺
2.46 GeV/c
III.8a
m²πK GeV²
m²Σπ GeV²

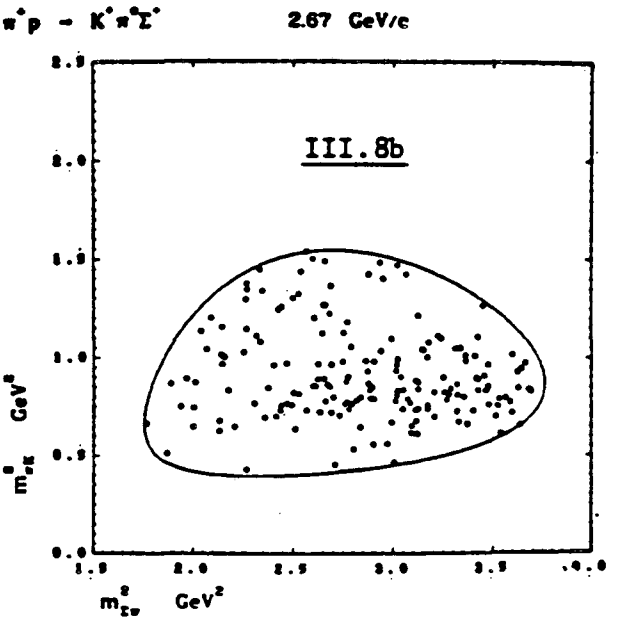
π⁺p → K⁺π⁰Σ⁺
2.67 GeV/c
III.8b
m²πK GeV²
m²Σπ GeV²

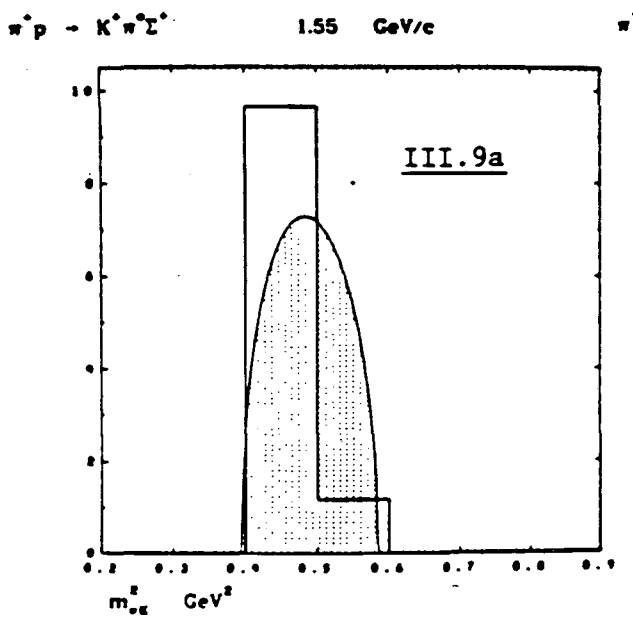
π⁺p → K⁺π⁰Σ⁺
1.55 GeV/c
III.9a
m²πK GeV²

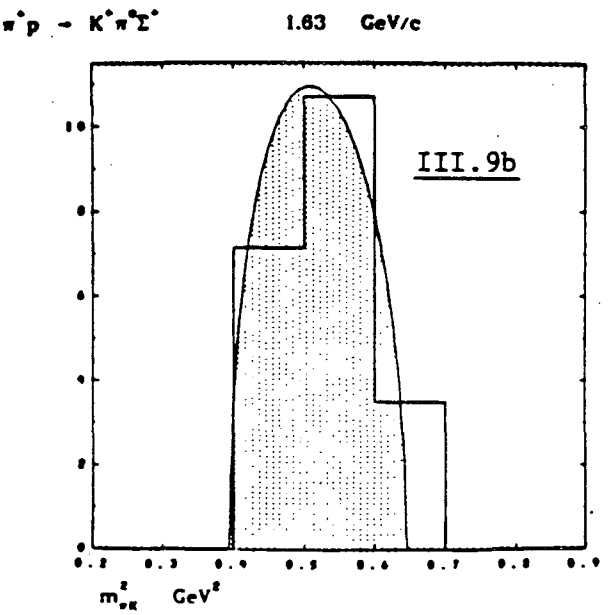
π⁺p → K⁺π⁰Σ⁺
1.63 GeV/c
III.9b
m²πK GeV²

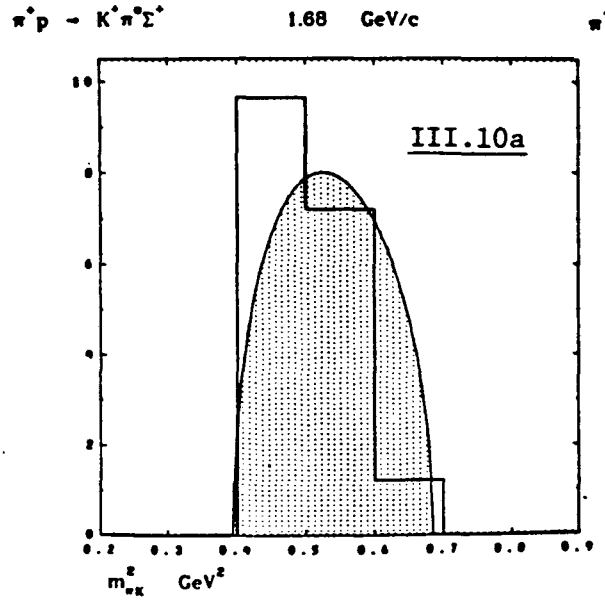
π⁺p → K⁺π⁰Σ⁺
1.68 GeV/c
III.10a
m²πK GeV²

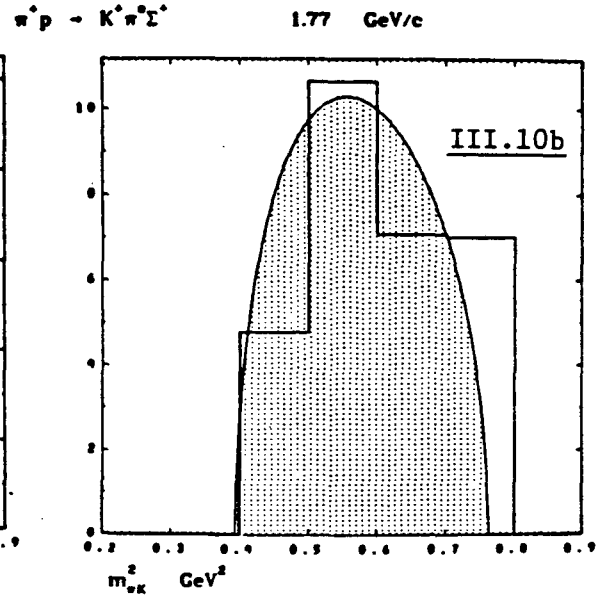
π⁺p → K⁺π⁰Σ⁺
1.77 GeV/c
III.10b
m²πK GeV²

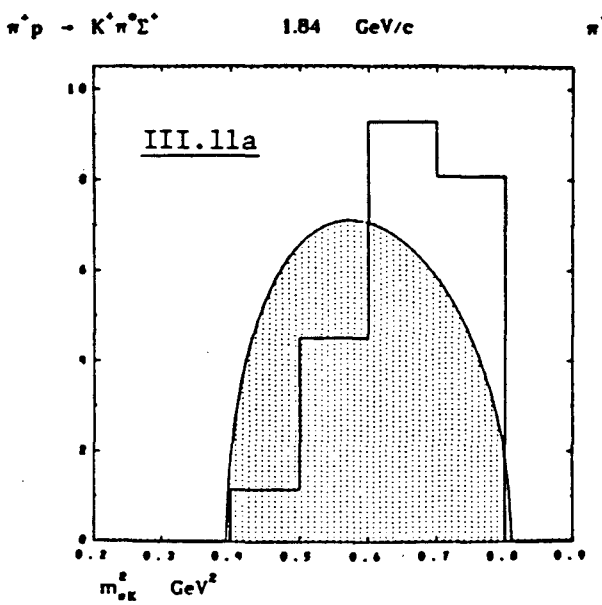
π⁺p → K⁺π⁰Σ⁺
1.84 GeV/c
III.11a
m²πK GeV²

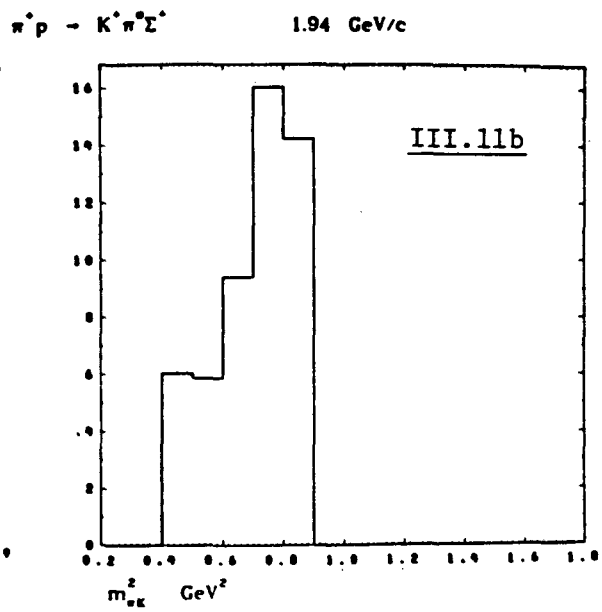
π⁺p → K⁺π⁰Σ⁺
1.94 GeV/c
III.11b
m²πK GeV²

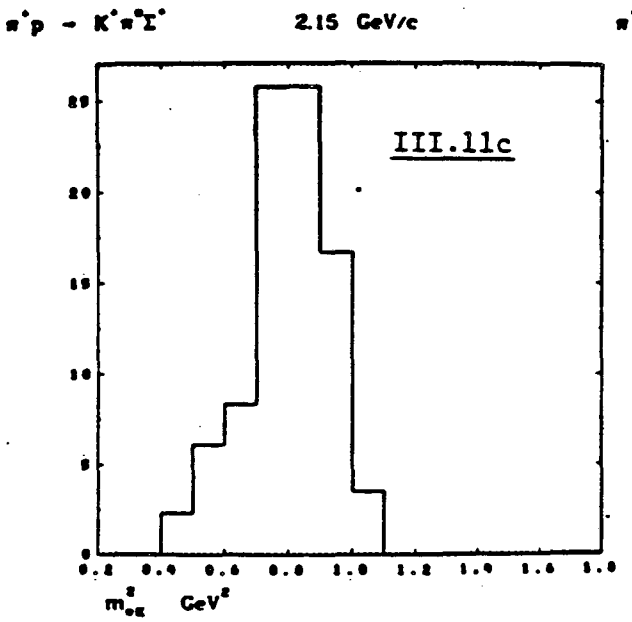
$\pi^+p \to K^+\pi^0\Sigma^+$
2.15 GeV/c
III.11c
$m^2_{\pi K}$ GeV^2

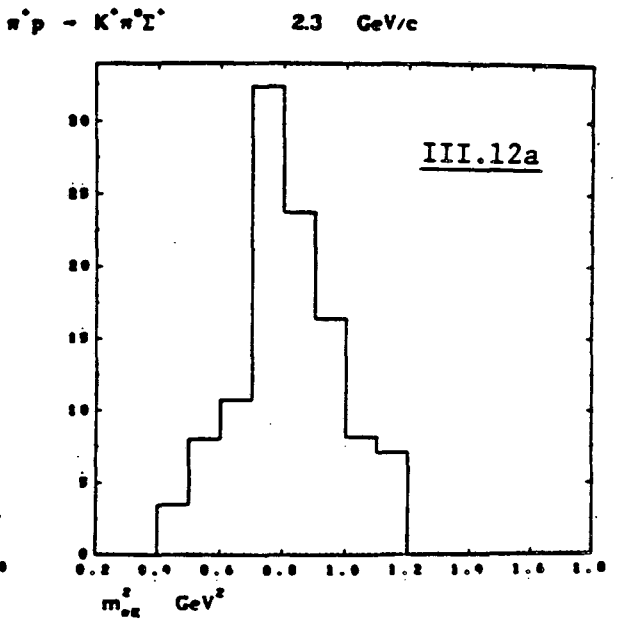
$\pi^+p \to K^+\pi^0\Sigma^+$
2.3 GeV/c
III.12a
$m^2_{\pi K}$ GeV^2

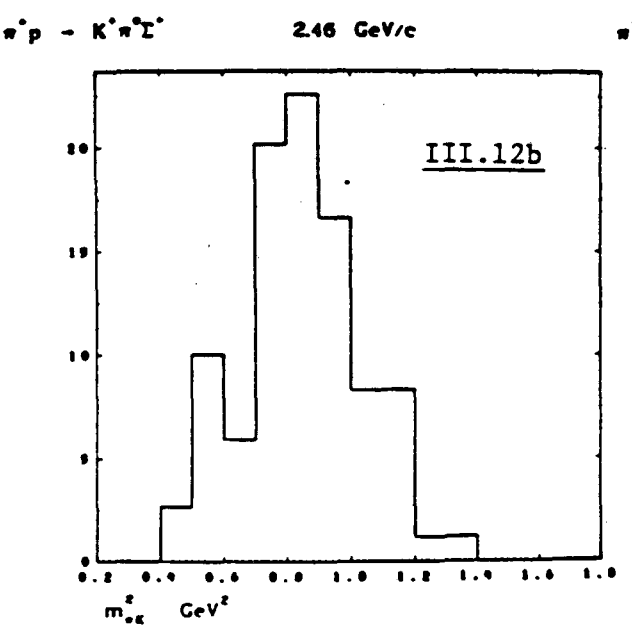
$\pi^+p \to K^+\pi^0\Sigma^+$
2.46 GeV/c
III.12b
$m^2_{\pi K}$ GeV^2

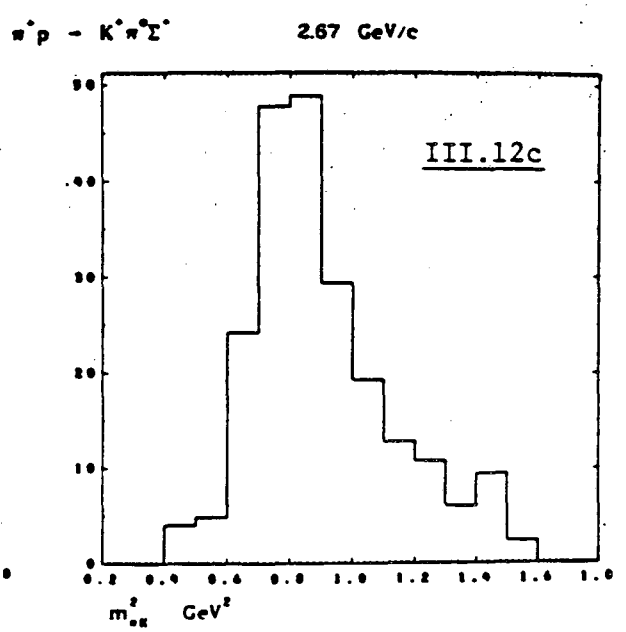
$\pi^+p \to K^+\pi^0\Sigma^+$
2.67 GeV/c
III.12c
$m^2_{\pi K}$ GeV^2

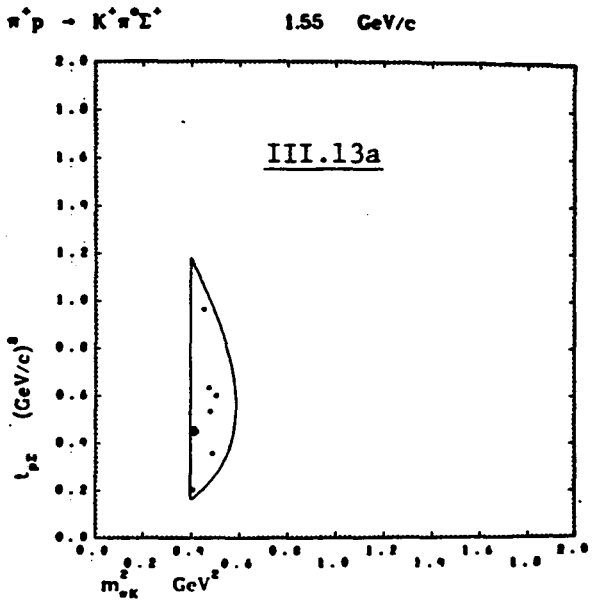
π⁺p → K⁺π⁰Σ⁺
1.55 GeV/c
III.13a
t_pΣ (GeV/c)²
m²_πK GeV²

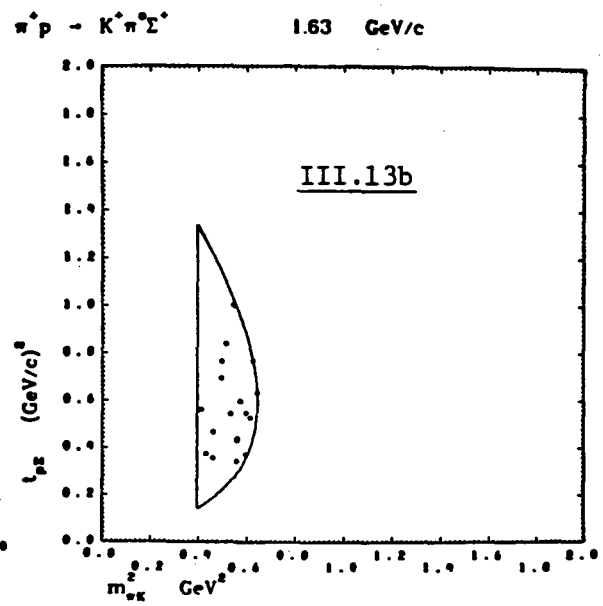
π⁺p → K⁺π⁰Σ⁺
1.63 GeV/c
III.13b
t_pΣ (GeV/c)²
m²_πK GeV²

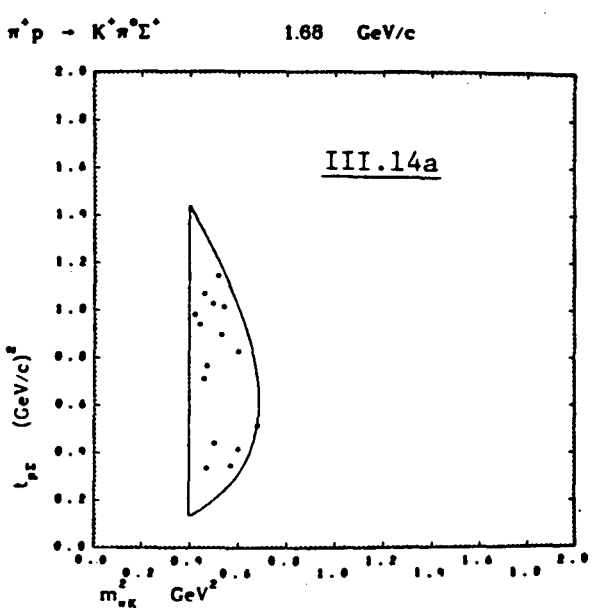
π⁺p → K⁺π⁰Σ⁺
1.68 GeV/c
III.14a
t_pΣ (GeV/c)²
m²_πK GeV²

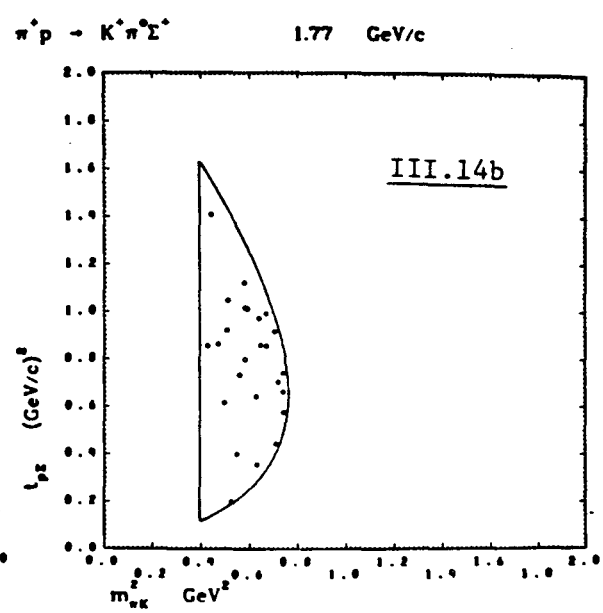
π⁺p → K⁺π⁰Σ⁺
1.77 GeV/c
III.14b
t_pΣ (GeV/c)²
m²_πK GeV²

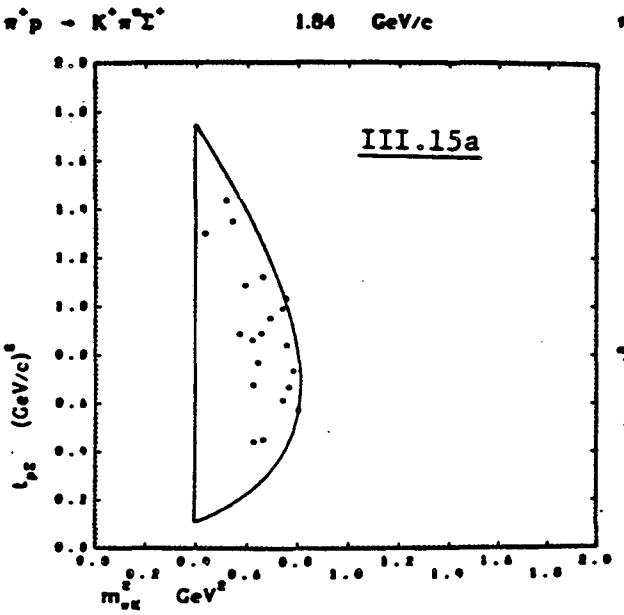
π⁺p → K⁺π⁰Σ⁺
1.84 GeV/c
III.15a
t_pΣ (GeV/c)²
m²_πΣ GeV²

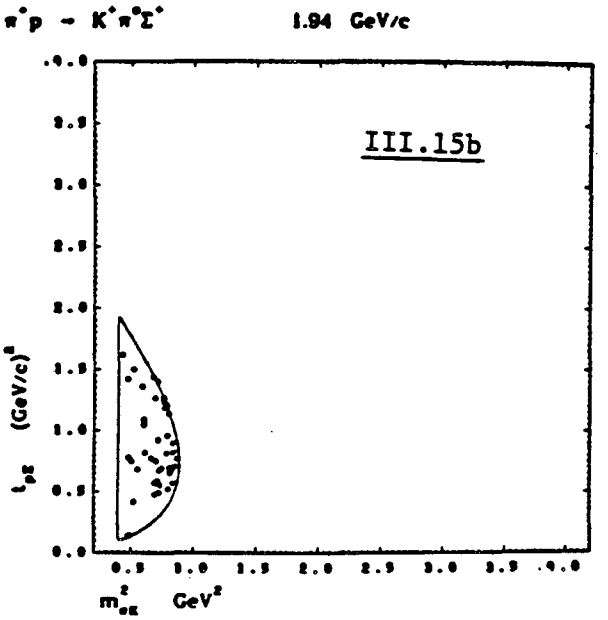
π⁺p → K⁺π⁰Σ⁺
1.94 GeV/c
III.15b
t_pΣ (GeV/c)²
m²_πΣ GeV²

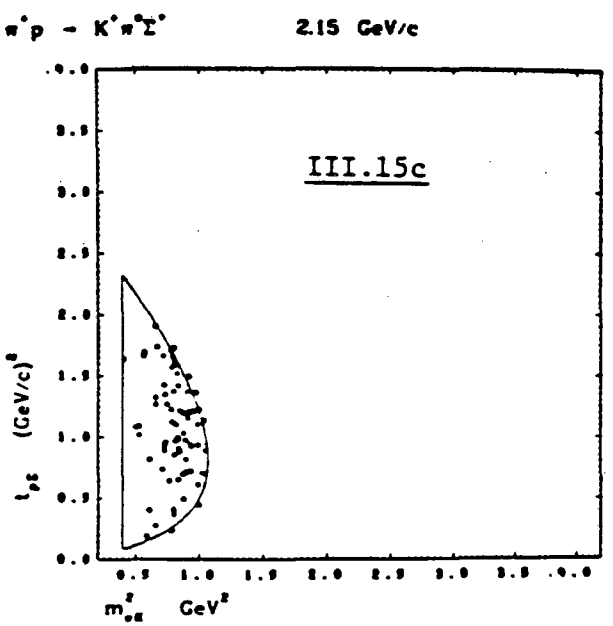
π⁺p → K⁺π⁰Σ⁺
2.15 GeV/c
III.15c
t_pΣ (GeV/c)²
m²_πΣ GeV²

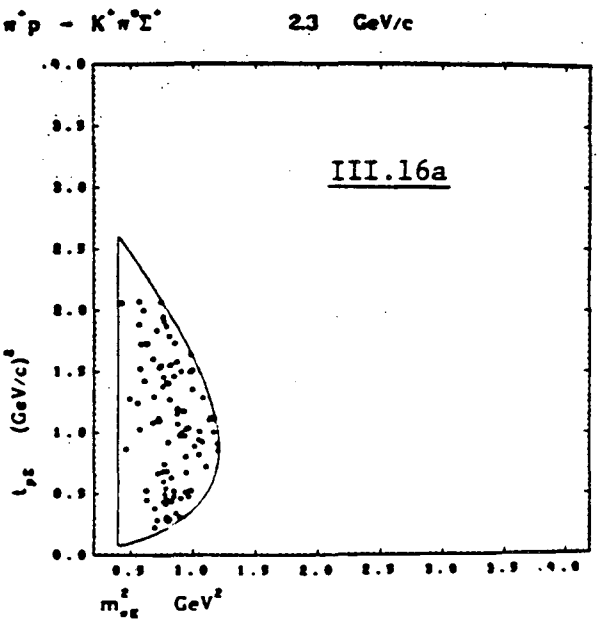
π⁺p → K⁺π⁰Σ⁺
2.3 GeV/c
III.16a
t_pΣ (GeV/c)²
m²_πΣ GeV²

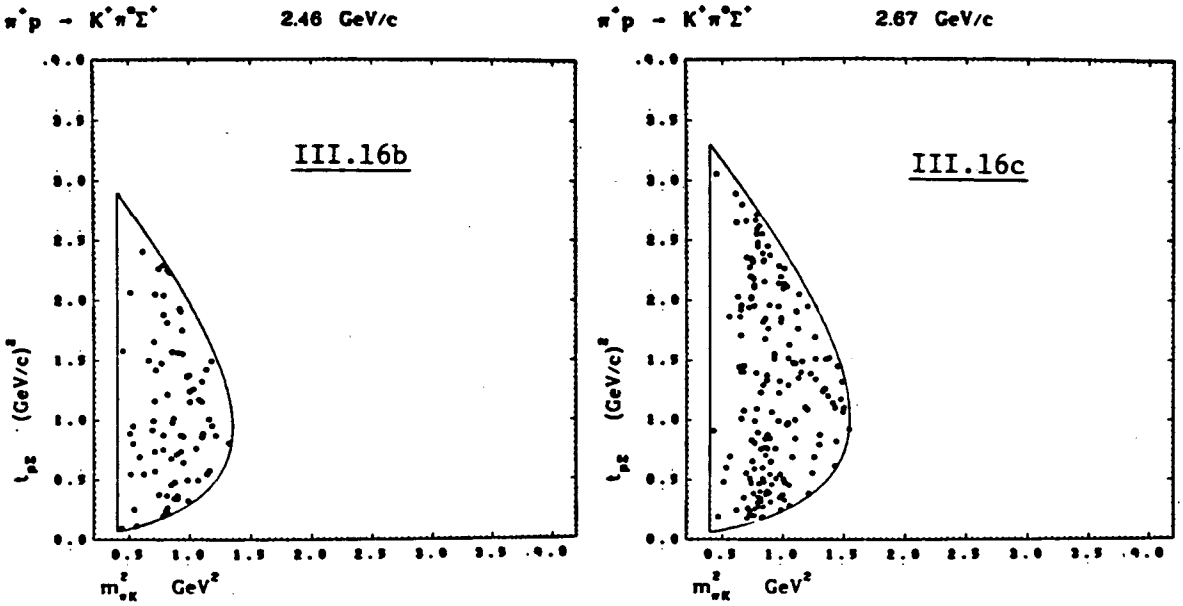
π⁺p → K⁺π⁰Σ⁺
2.46 GeV/c
III.16b
t_pΣ (GeV/c)²
m²_πK GeV²
π⁺p → K⁺π⁰Σ⁺
2.67 GeV/c
III.16c
t_pΣ (GeV/c)²
m²_πK GeV²

backward peaked, cleanly produced, and that the various mass spectra should be free of any kinematical reflections arising from sharp or peculiar invariant momentum transfer dependences. For $p_\pi = 1.84$ GeV/c, phase space limits just barely permit K^* production, and there is a peak at the upper end of the $m^2_{\pi K}$ spectrum.

2. $\Sigma^+ K^0 \pi^+$

Figures III.17-III.28 display for the $\Sigma^+ K^0 \pi^+$ channel the same sequence of Dalitz plots, mass spectra, and Chew-Low plots as figures III.5 through III.16 did for $\Sigma^+ K^+ \pi^0$, with $m^2_{\Sigma K}$ replacing $m^2_{\Sigma\pi}$. Again, the most prominent feature is the strong $K^{*+}(892)$ production for $p_\pi \geq 1.94$ GeV/c, which clearly constitutes a larger fraction of this channel than of $\Sigma^+ K^+ \pi^0$. There is no real evidence of any $N^* \to \Sigma K$ signal; the Chew-Low plots show that the K^* production is strongly forward-backward peaked. Finally, figure III.29 displays the projected $m^2_{\pi K}$ spectrum for $\Sigma^+ \pi^+ K^0$ events with $\Sigma^+ \to p\pi^0$ at 2.67 GeV/c; clearly the shape is similar to that for the $\Sigma^+ \to \pi^+ n$ events.

3. $K^+ \pi^+ \Lambda$

For the channel $K^+ \pi^+ \Lambda$, figures III.30, III.31, and III.32 exhibit plots of $m^2_{\Lambda K}$ versus $m^2_{\Lambda\pi}$; figures III.33, III.34, and III.35 display the $m^2_{\Lambda\pi}$ spectra; and figures III.36, III.37, and III.38 give the $t_{\pi K} \equiv (\mathbf{p}_\pi - \mathbf{p}_K)^2$ versus $m^2_{\Lambda\pi}$ plots for the incident momenta from 1.41 to 2.67 GeV/c. The curves drawn on the $m^2_{\Lambda\pi}$ spectra are phase space normalized to the spectrum well outside the $\Sigma(1385)$ region. The strong $\Sigma^*(1385)$ signal at all momenta is clearly pro-

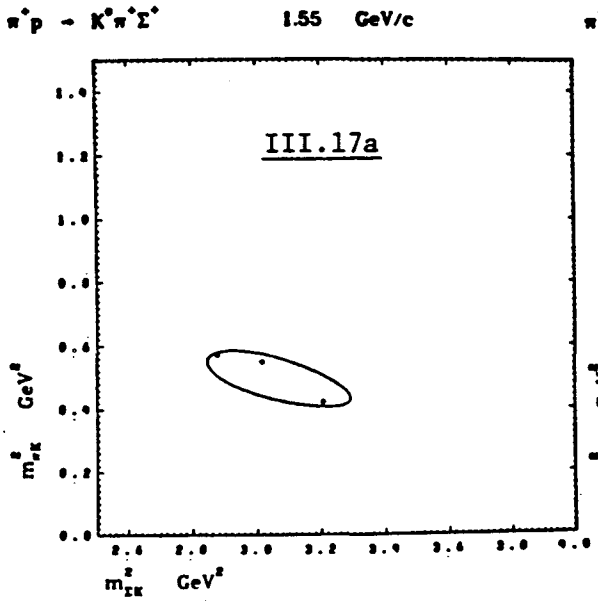
π⁺p → K⁰π⁺Σ⁺
1.55 GeV/c
III.17a
m²πK GeV²
m²ΣK GeV²

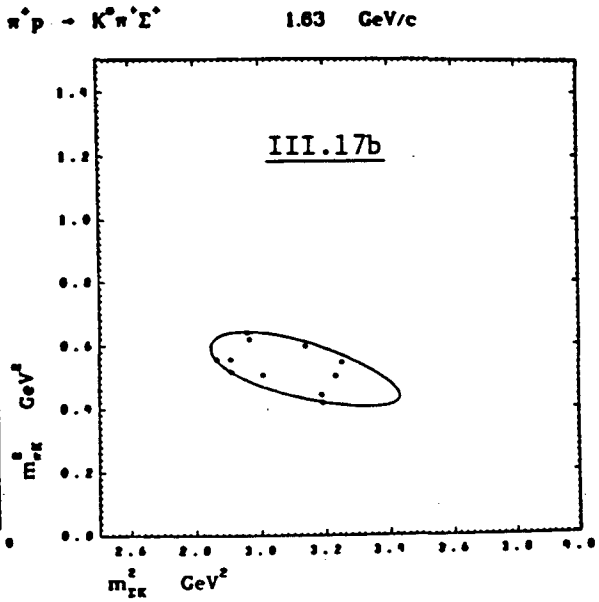
π⁺p → K⁰π⁺Σ⁺
1.63 GeV/c
III.17b
m²πK GeV²
m²ΣK GeV²

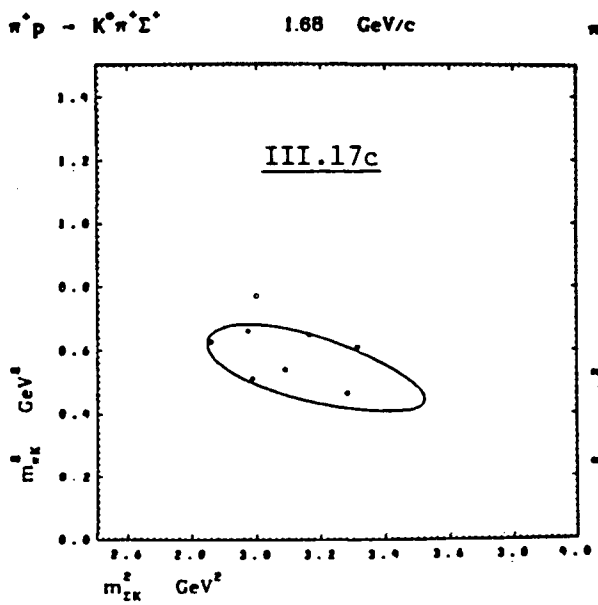
π⁺p → K⁰π⁺Σ⁺
1.68 GeV/c
III.17c
m²πK GeV²
m²ΣK GeV²

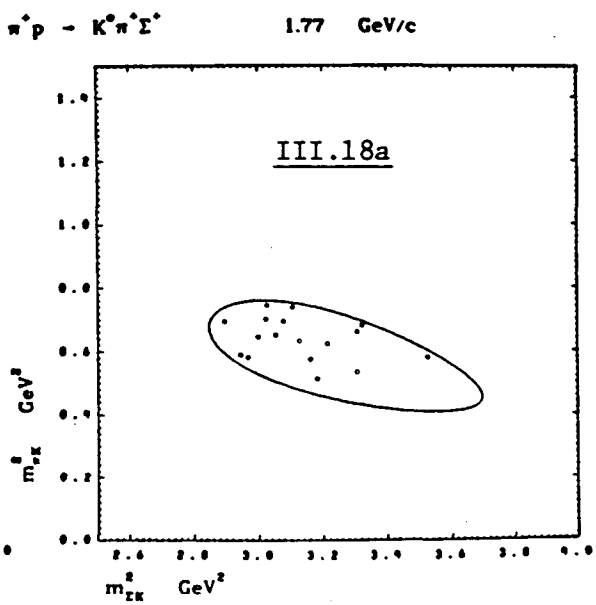
π⁺p → K⁰π⁺Σ⁺
1.77 GeV/c
III.18a
m²πK GeV²
m²ΣK GeV²

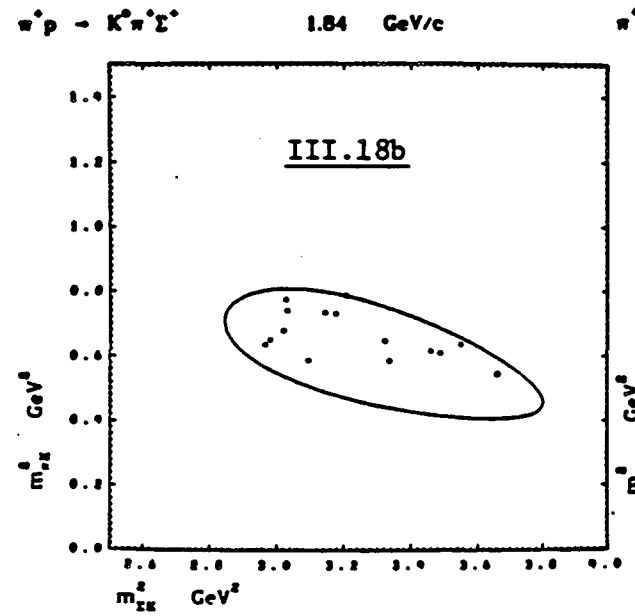
π⁺p → K⁰π⁺Σ⁺
1.84 GeV/c
III.18b
m²πK GeV²
m²ΣK GeV²

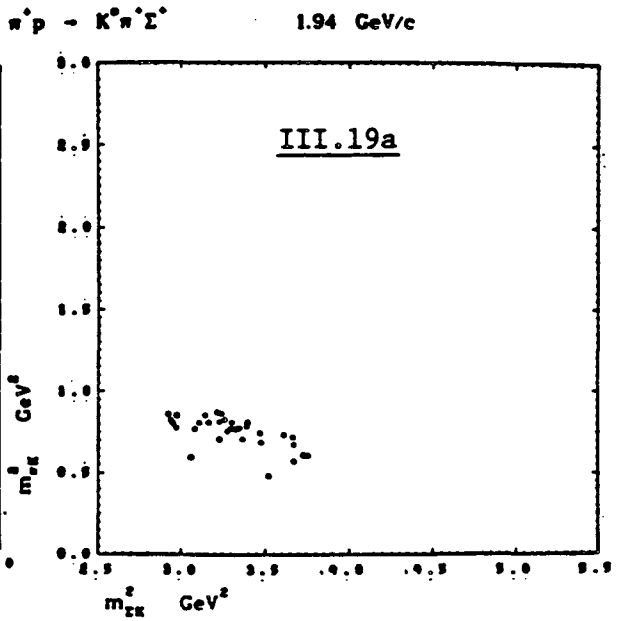
π⁺p → K⁰π⁺Σ⁺
1.94 GeV/c
III.19a
m²πK GeV²
m²ΣK GeV²

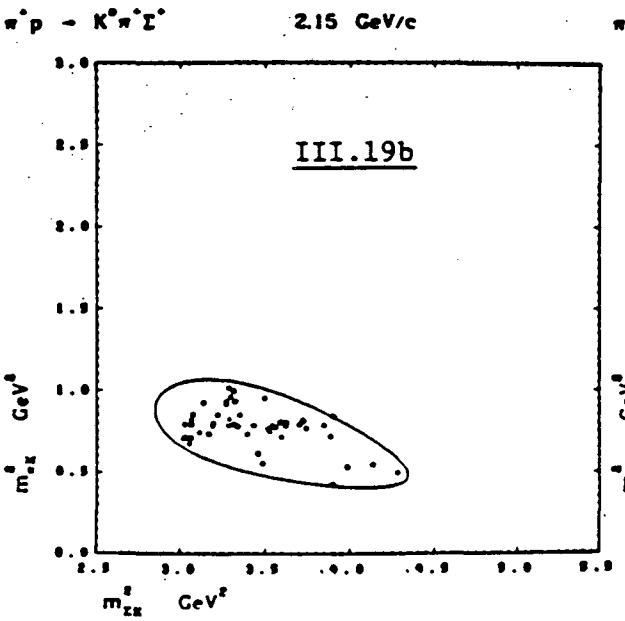
π⁺p → K⁰π⁺Σ⁺
2.15 GeV/c
III.19b
m²πK GeV²
m²ΣK GeV²

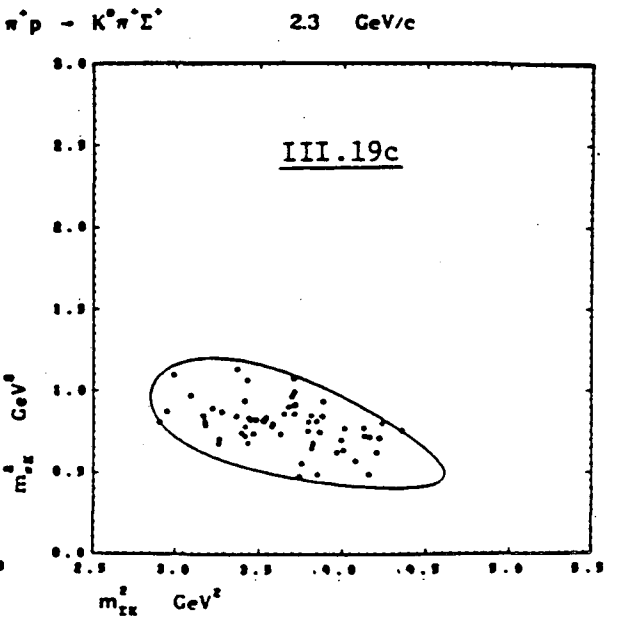
π⁺p → K⁰π⁺Σ⁺
2.3 GeV/c
III.19c
m²πK GeV²
m²ΣK GeV²

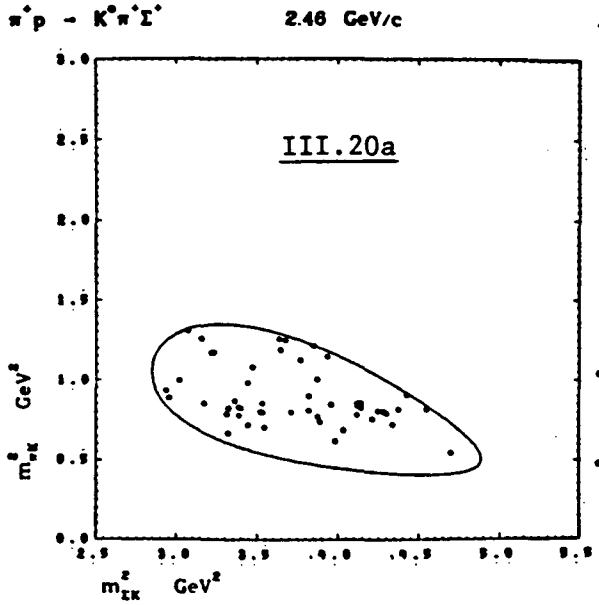
π⁺p → K⁰π⁺Σ⁺
2.46 GeV/c
III.20a
m²ΣK GeV²

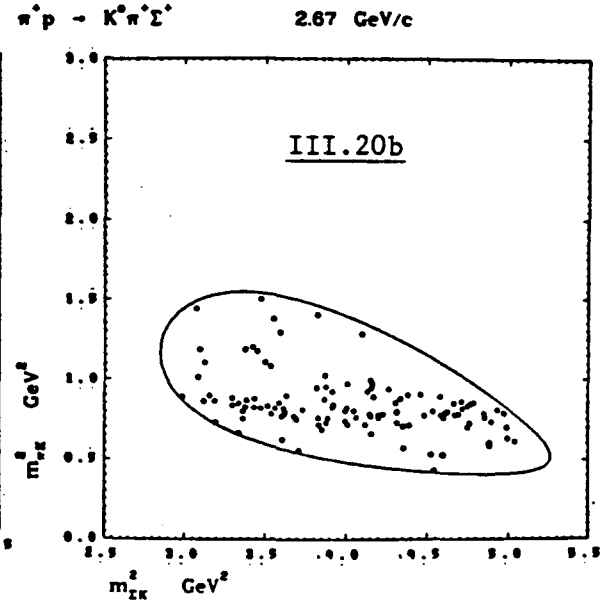
π⁺p → K⁰π⁺Σ⁺
2.67 GeV/c
III.20b
m²ΣK GeV²

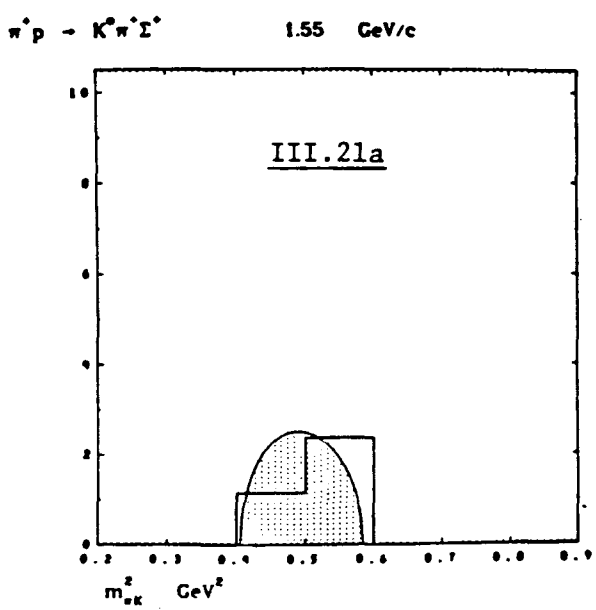
π⁺p → K⁰π⁺Σ⁺
1.55 GeV/c
III.21a
m²πK GeV²

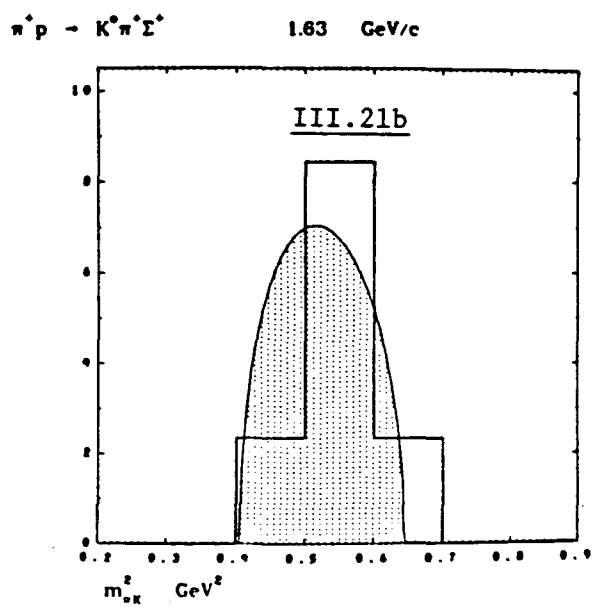
π⁺p → K⁰π⁺Σ⁺
1.63 GeV/c
III.21b
m²πK GeV²

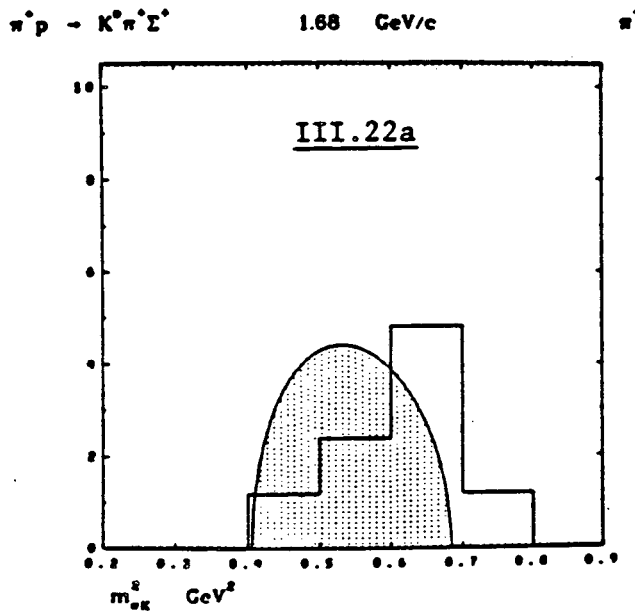
π⁺p → K⁰π⁺Σ⁺
1.68 GeV/c
III.22a
m²πK GeV²

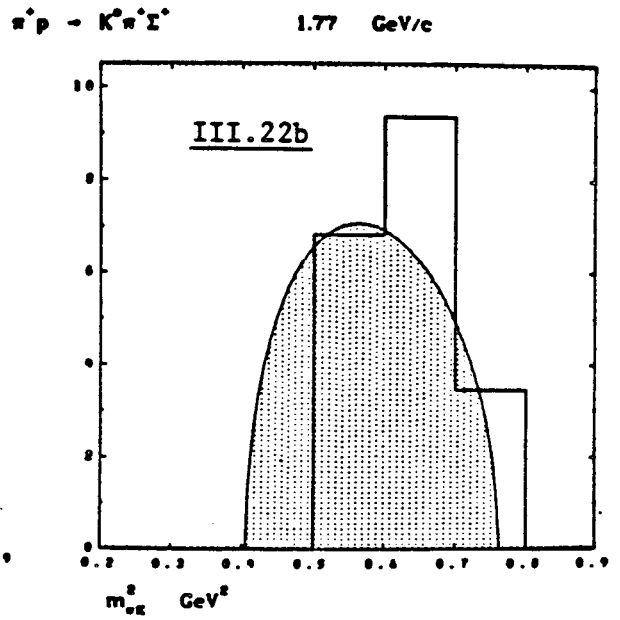
π⁺p → K⁰π⁺Σ⁺
1.77 GeV/c
III.22b
m²πK GeV²

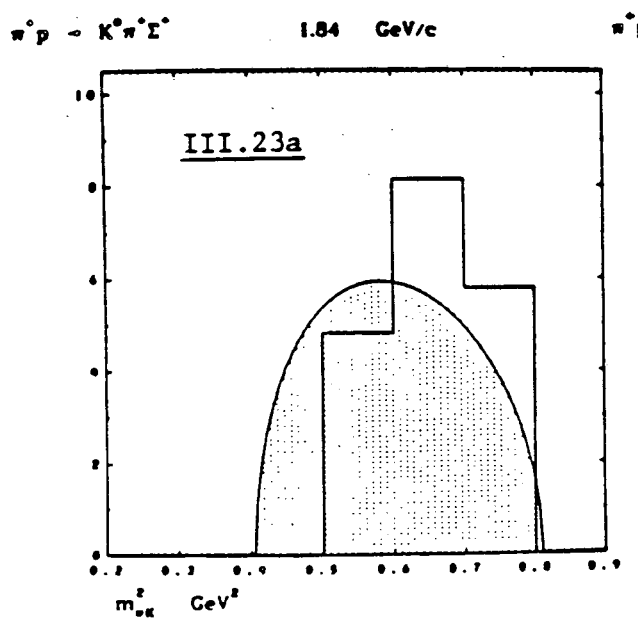
π⁺p → K⁰π⁺Σ⁺
1.84 GeV/c
III.23a
m²πK GeV²

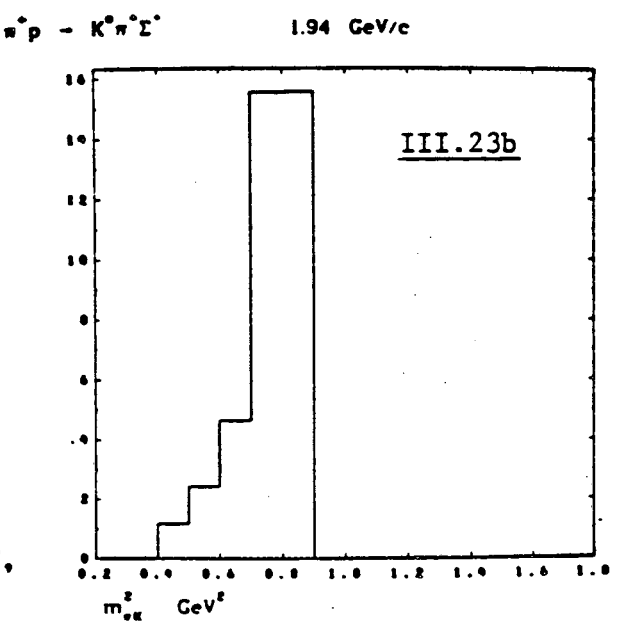
π⁺p → K⁰π⁺Σ⁺
1.94 GeV/c
III.23b
m²πK GeV²

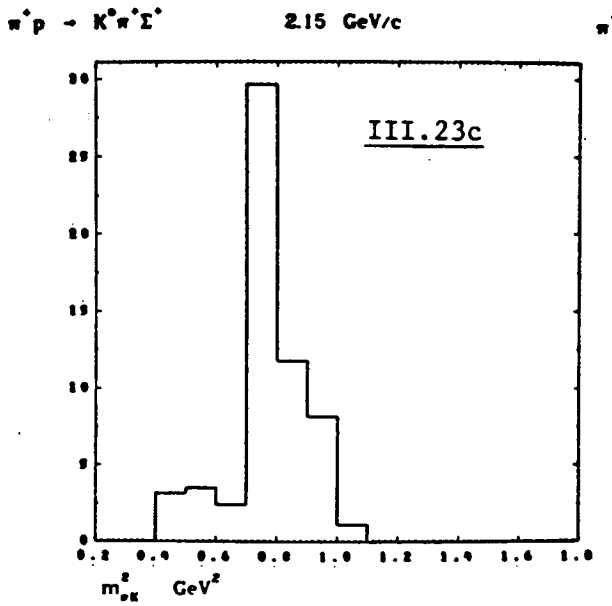
π⁺p → K⁰π⁺Σ⁺
2.15 GeV/c
III.23c
m²πK GeV²

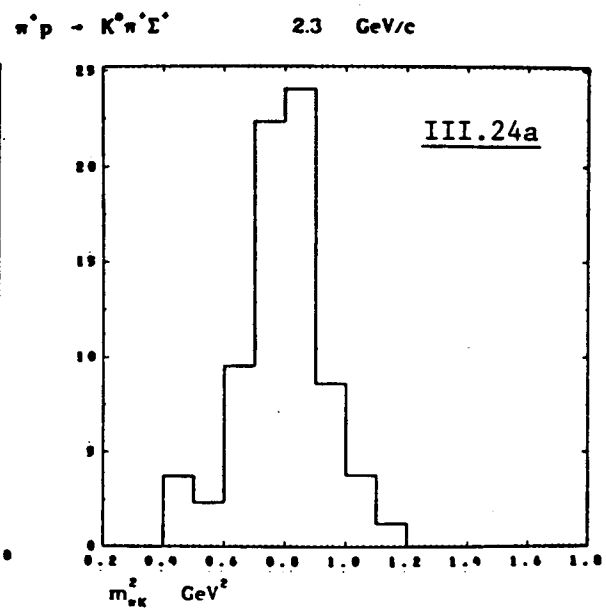
π⁺p → K⁰π⁺Σ⁺
2.3 GeV/c
III.24a
m²πK GeV²

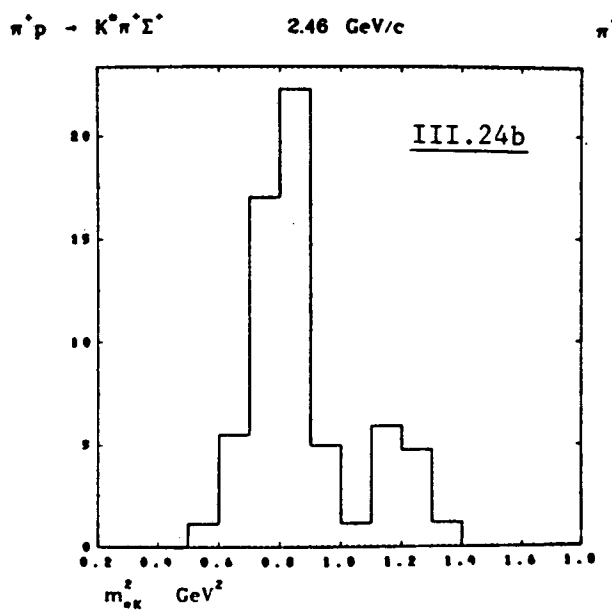
π⁺p → K⁰π⁺Σ⁺
2.46 GeV/c
III.24b
m²πK GeV²

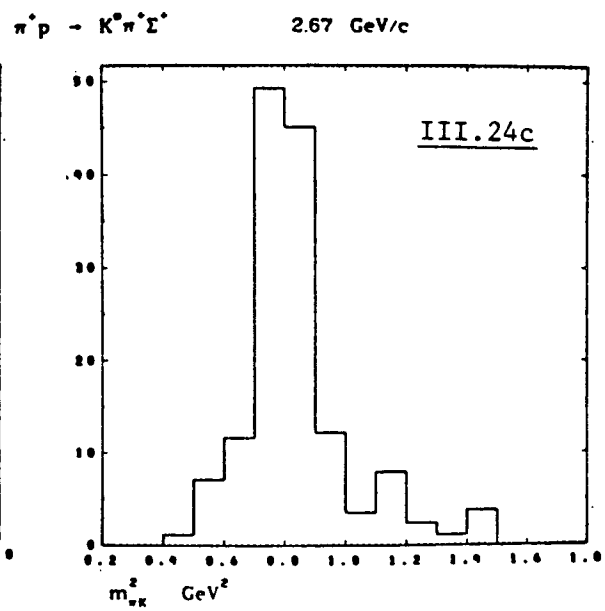
π⁺p → K⁰π⁺Σ⁺
2.67 GeV/c
III.24c
m²πK GeV²

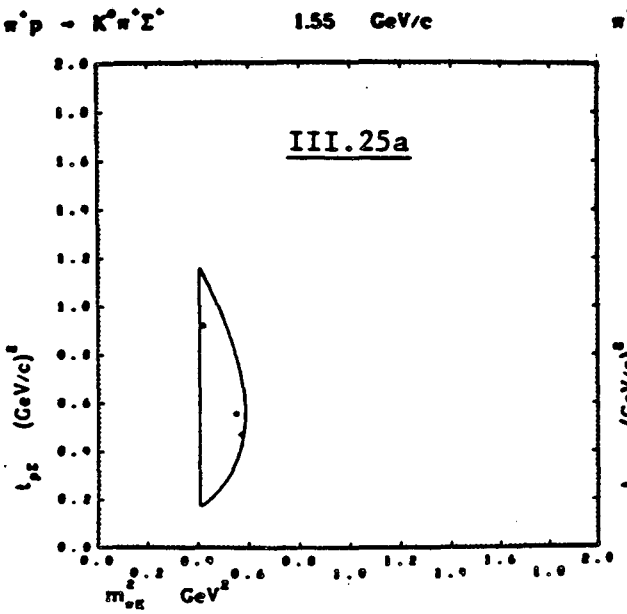
π⁺p → K⁰π⁺Σ⁺
1.55 GeV/c
III.25a
t_pΣ (GeV/c)²
m²_πK GeV²

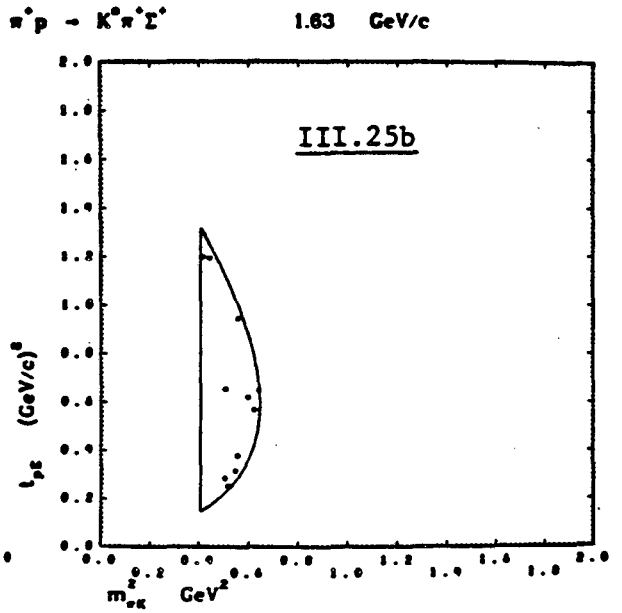
π⁺p → K⁰π⁺Σ⁺
1.63 GeV/c
III.25b
t_pΣ (GeV/c)²
m²_πK GeV²

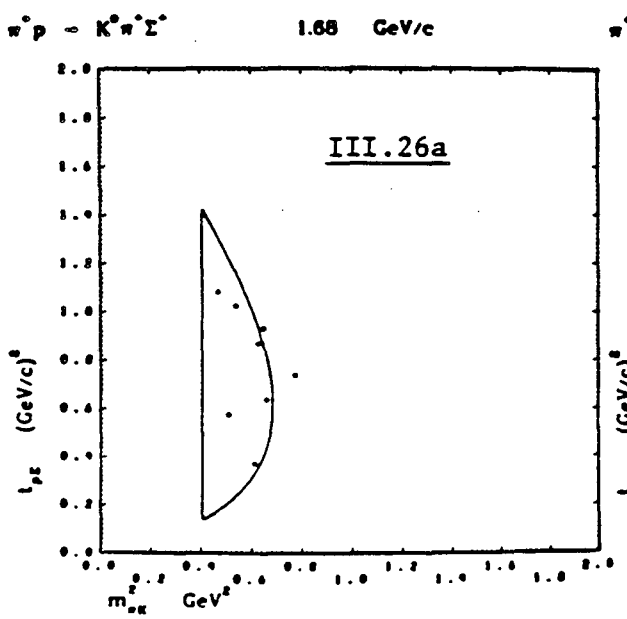
π⁺p → K⁰π⁺Σ⁺
1.68 GeV/c
III.26a
t_pΣ (GeV/c)²
m²_πK GeV²

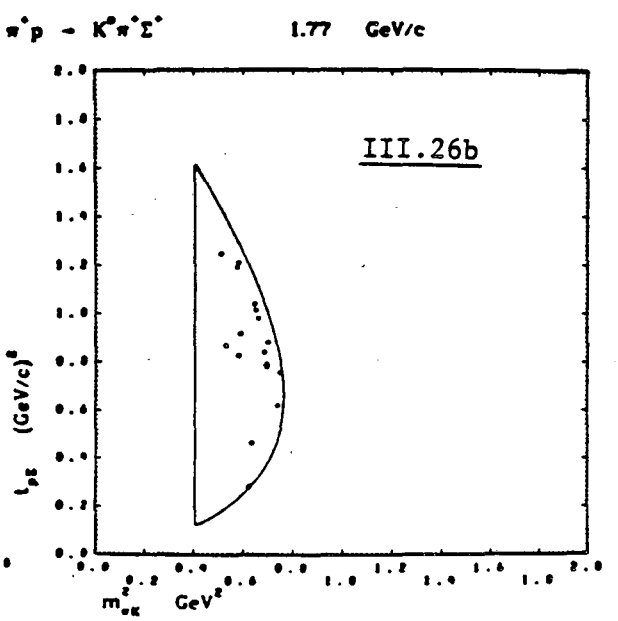
π⁺p → K⁰π⁺Σ⁺
1.77 GeV/c
III.26b
t_pΣ (GeV/c)²
m²_πK GeV²

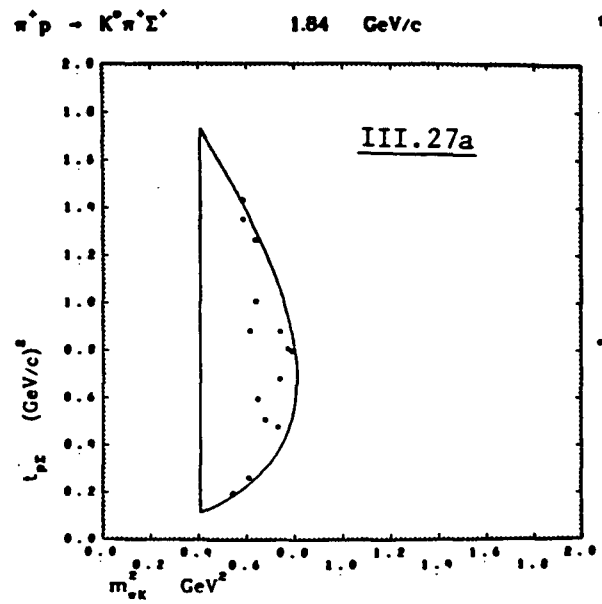
π⁺p → K°π⁺Σ⁺
1.84 GeV/c
III.27a
t_pΣ (GeV/c)²
m²_πK GeV²

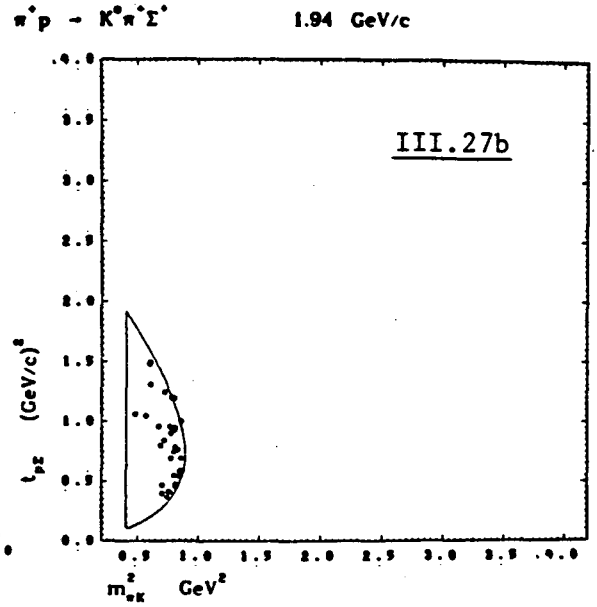
π⁺p → K°π⁺Σ⁺
1.94 GeV/c
III.27b
t_pΣ (GeV/c)²
m²_πK GeV²

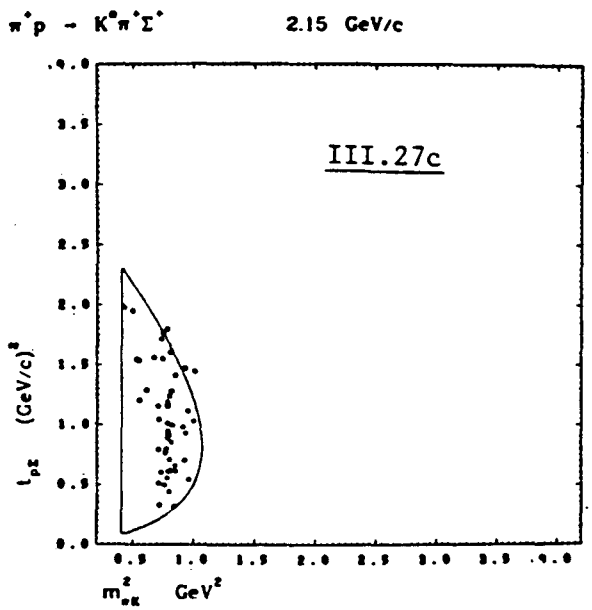
π⁺p → K°π⁺Σ⁺
2.15 GeV/c
III.27c
t_pΣ (GeV/c)²
m²_πK GeV²

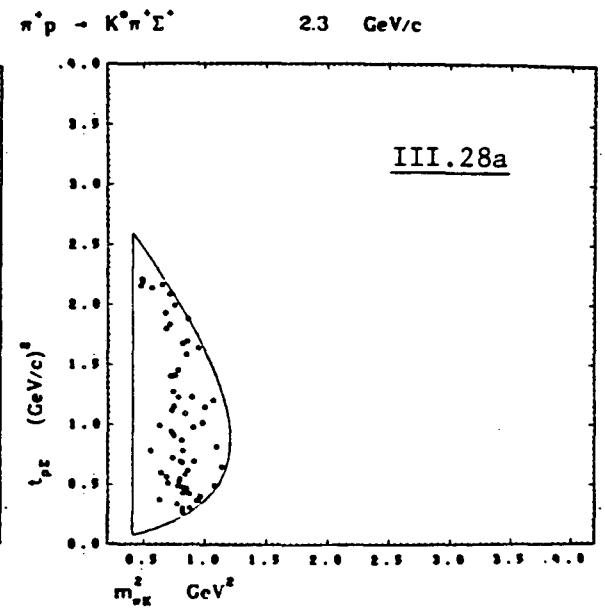
π⁺p → K°π⁺Σ⁺
2.3 GeV/c
III.28a
t_pΣ (GeV/c)²
m²_πK GeV²

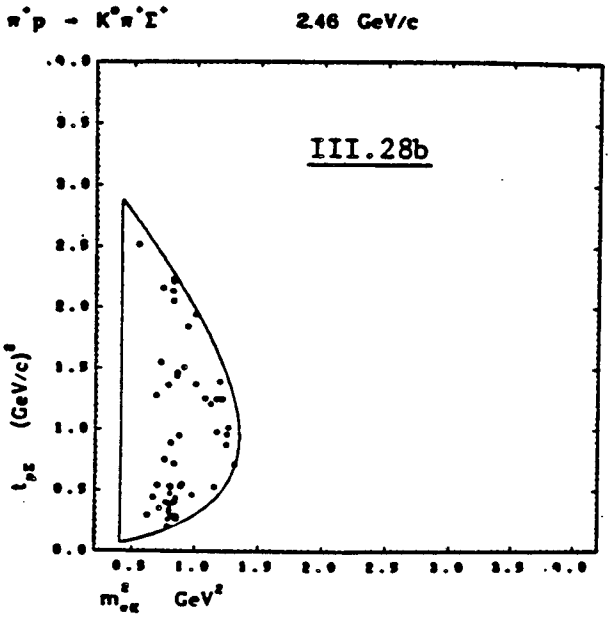
π⁺p → K⁰π⁺Σ⁺
2.46 GeV/c
III.28b
t_pΣ (GeV/c)²
m²_πΣ GeV²

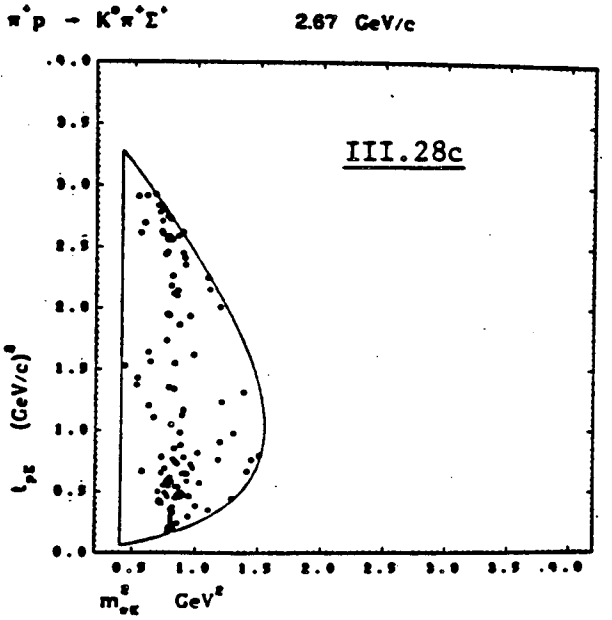
π⁺p → K⁰π⁺Σ⁺
2.67 GeV/c
III.28c
t_pΣ (GeV/c)²
m²_πΣ GeV²

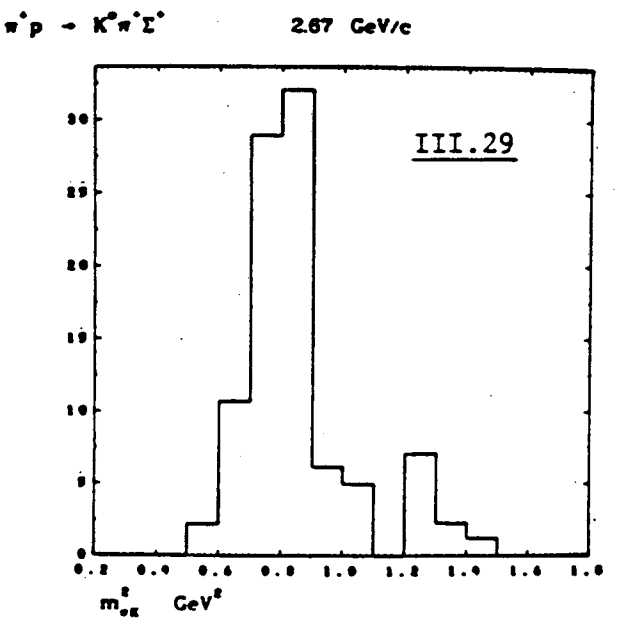
π⁺p → K⁰π⁺Σ⁺
2.67 GeV/c
III.29
m²_πΣ GeV²

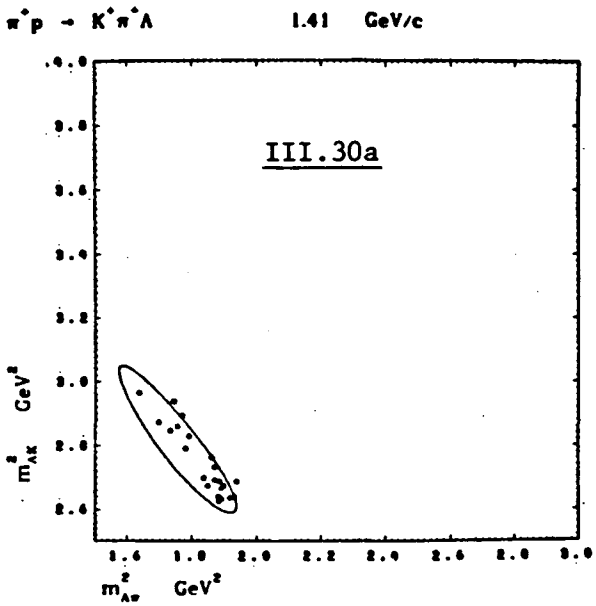
π⁺p → K⁺π⁺Λ 1.41 GeV/c
III.30a
m²ΛK GeV²
m²Aπ GeV²

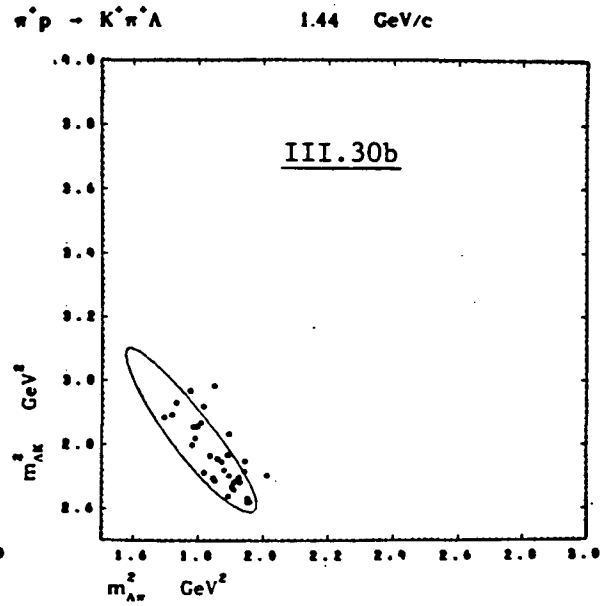
π⁺p → K⁺π⁺Λ 1.44 GeV/c
III.30b
m²ΛK GeV²
m²Aπ GeV²

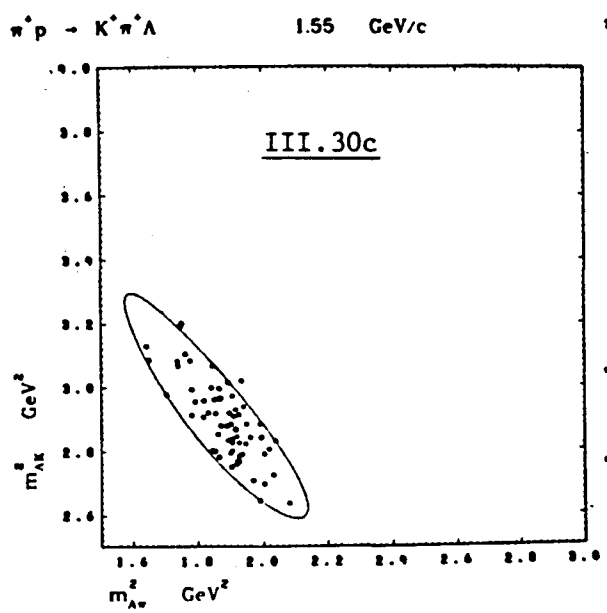
π⁺p → K⁺π⁺Λ 1.55 GeV/c
III.30c
m²ΛK GeV²
m²Aπ GeV²

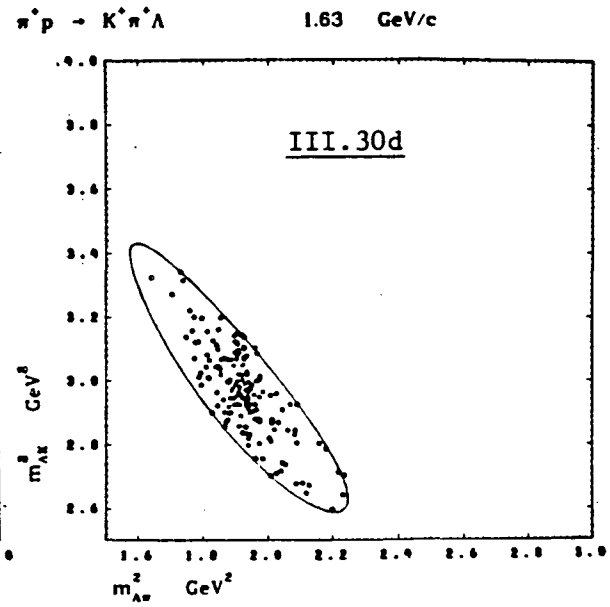
π⁺p → K⁺π⁺Λ 1.63 GeV/c
III.30d
m²ΛK GeV²
m²Aπ GeV²

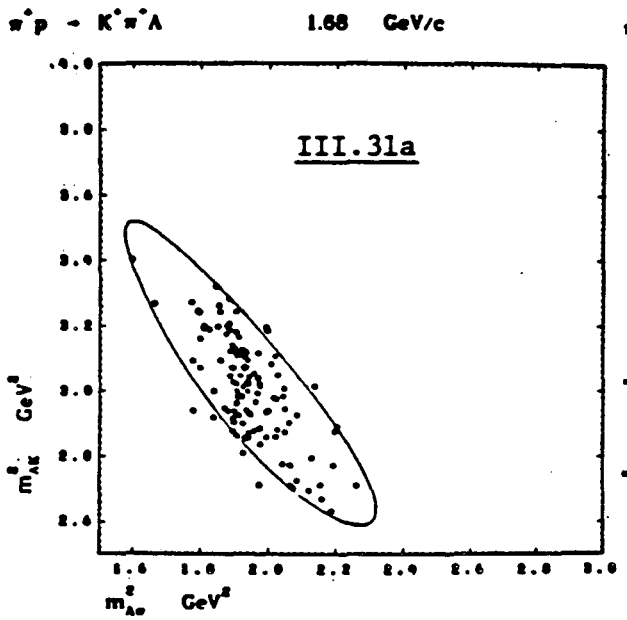
π⁺p → K⁺π⁺Λ
1.68 GeV/c
III.31a
$m^2_{\Lambda K}$ GeV²
$m^2_{\Lambda\pi}$ GeV²

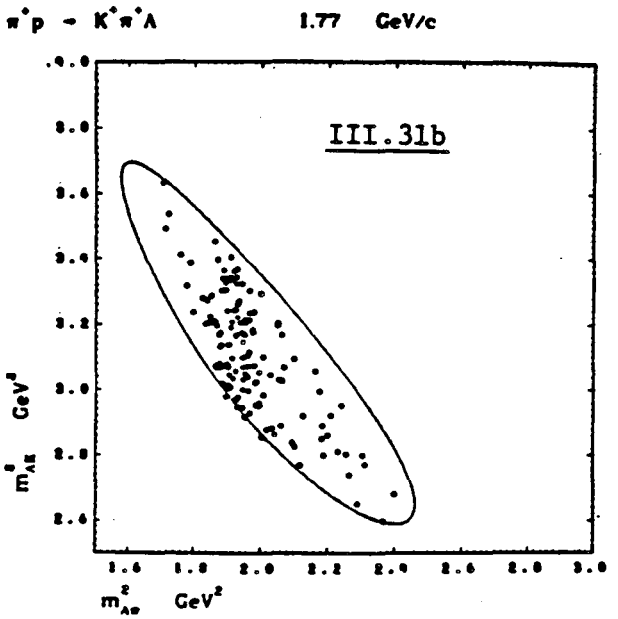
π⁺p → K⁺π⁺Λ
1.77 GeV/c
III.31b
$m^2_{\Lambda K}$ GeV²
$m^2_{\Lambda\pi}$ GeV²

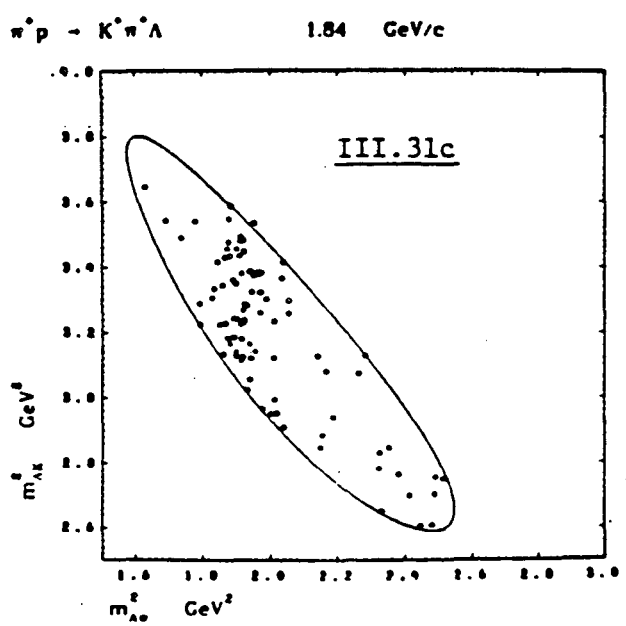
π⁺p → K⁺π⁺Λ
1.84 GeV/c
III.31c
$m^2_{\Lambda K}$ GeV²
$m^2_{\Lambda\pi}$ GeV²

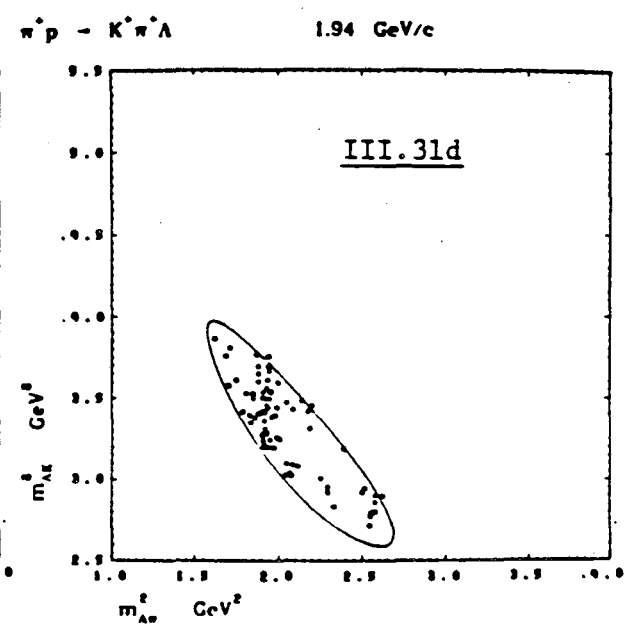
π⁺p → K⁺π⁺Λ
1.94 GeV/c
III.31d
$m^2_{\Lambda K}$ GeV²
$m^2_{\Lambda\pi}$ GeV²

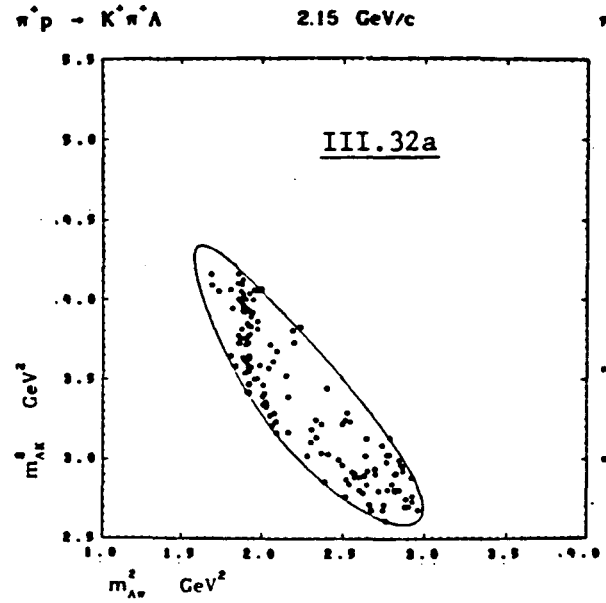
π⁺p → K⁺π⁺Λ
2.15 GeV/c
III.32a
$m^2_{\Lambda K}$ GeV²
$m^2_{\Lambda\pi}$ GeV²

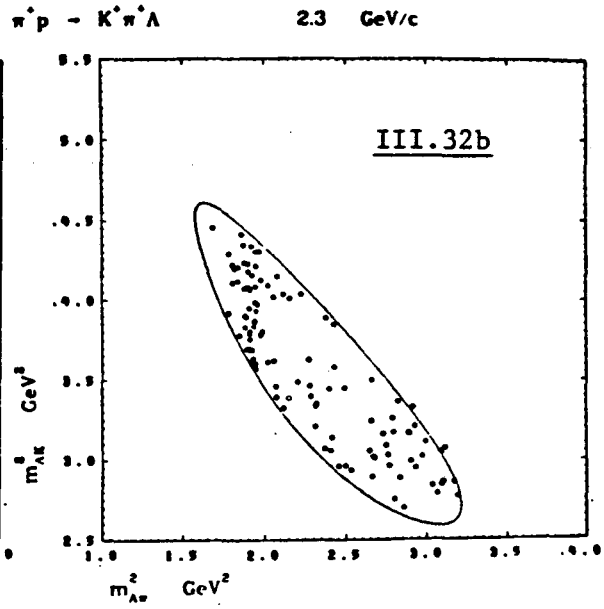
π⁺p → K⁺π⁺Λ
2.3 GeV/c
III.32b
$m^2_{\Lambda K}$ GeV²
$m^2_{\Lambda\pi}$ GeV²

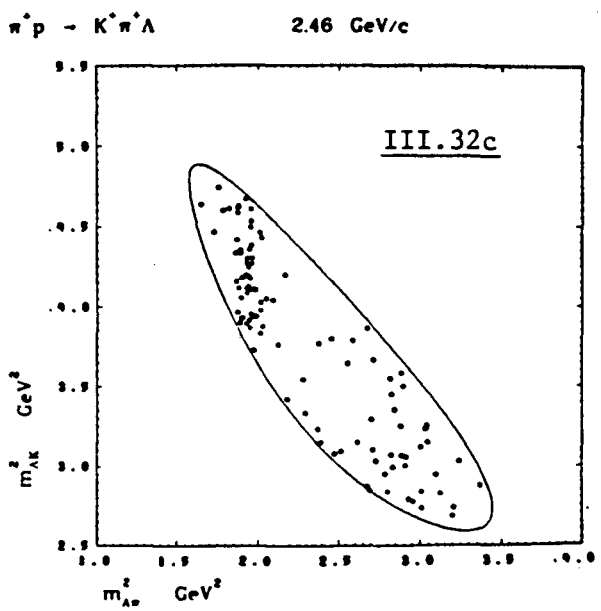
π⁺p → K⁺π⁺Λ
2.46 GeV/c
III.32c
$m^2_{\Lambda K}$ GeV²
$m^2_{\Lambda\pi}$ GeV²

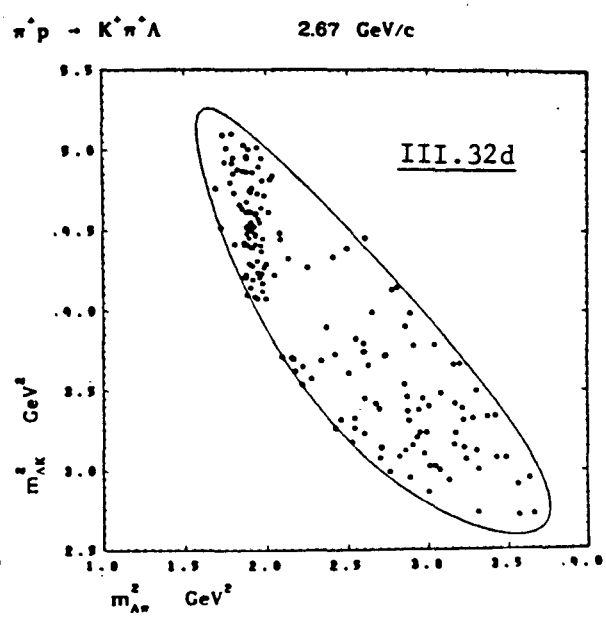
π⁺p → K⁺π⁺Λ
2.67 GeV/c
III.32d
$m^2_{\Lambda K}$ GeV²
$m^2_{\Lambda\pi}$ GeV²

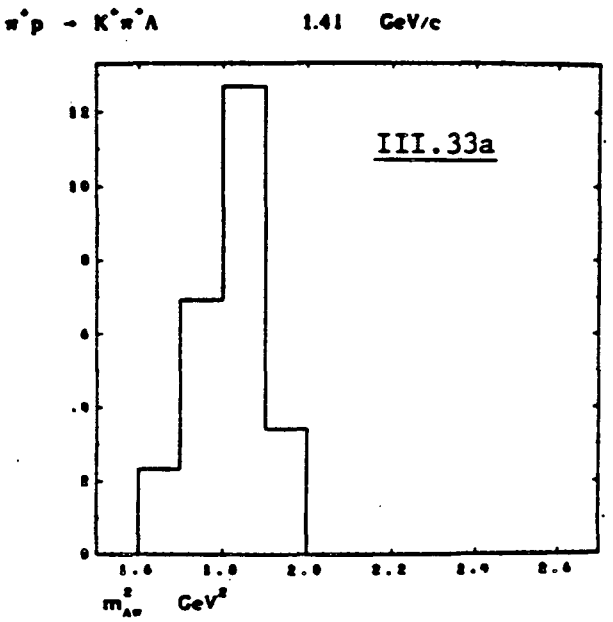
π⁺p → K⁺π⁺Λ 1.41 GeV/c
III.33a
m²Aπ GeV²

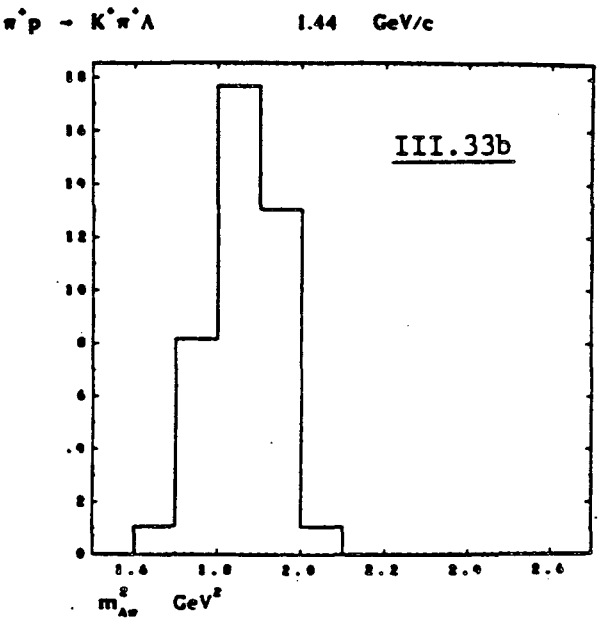
π⁺p → K⁺π⁺Λ 1.44 GeV/c
III.33b
m²Aπ GeV²

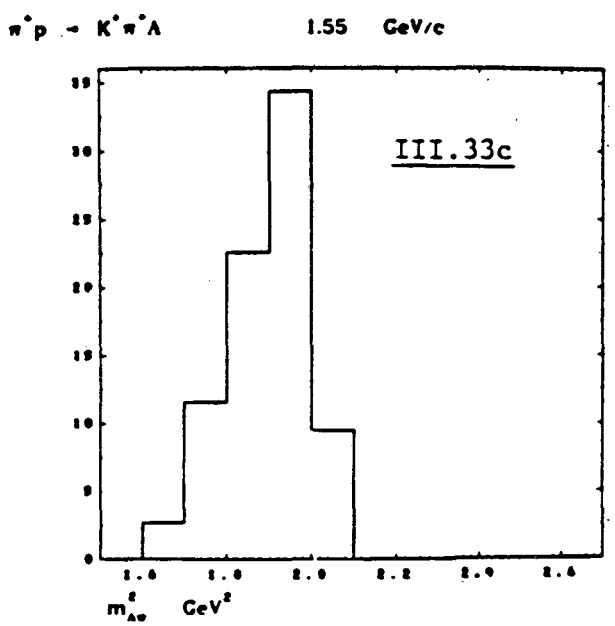
π⁺p → K⁺π⁺Λ 1.55 GeV/c
III.33c
m²Aπ GeV²

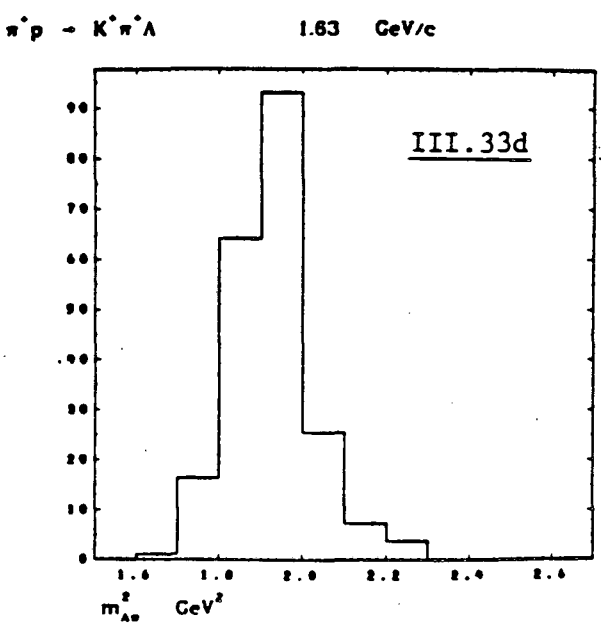
π⁺p → K⁺π⁺Λ 1.63 GeV/c
III.33d
m²Aπ GeV²

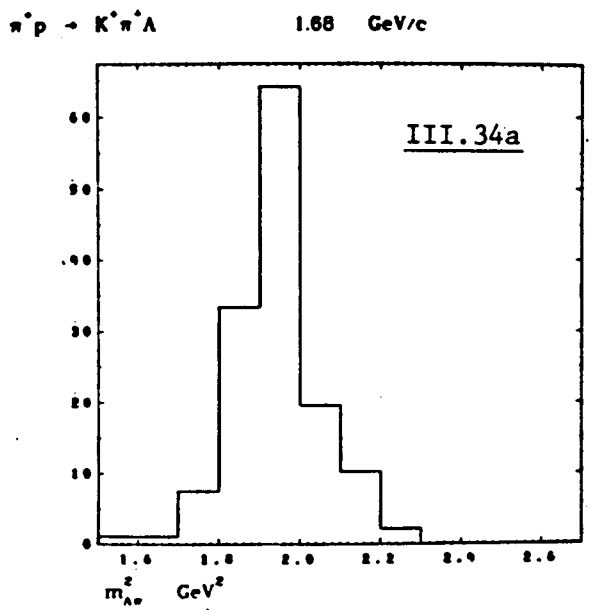
π⁺p → K⁺π⁺Λ
1.68 GeV/c
III.34a
m²Λπ GeV²

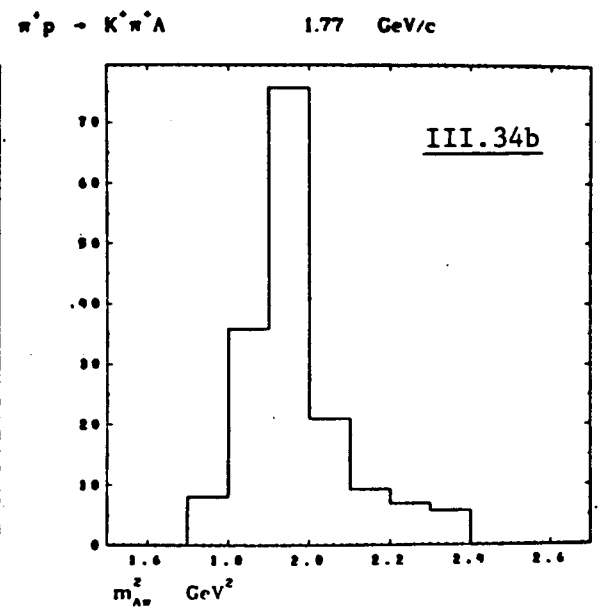
π⁺p → K⁺π⁺Λ
1.77 GeV/c
III.34b
m²Λπ GeV²

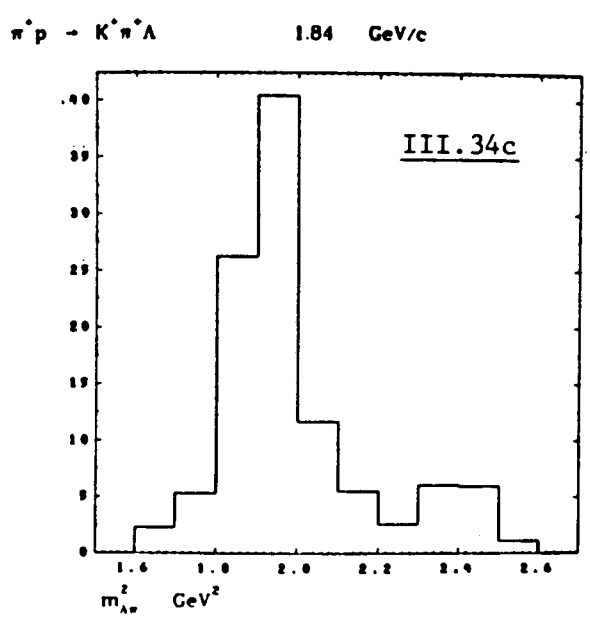
π⁺p → K⁺π⁺Λ
1.84 GeV/c
III.34c
m²Λπ GeV²

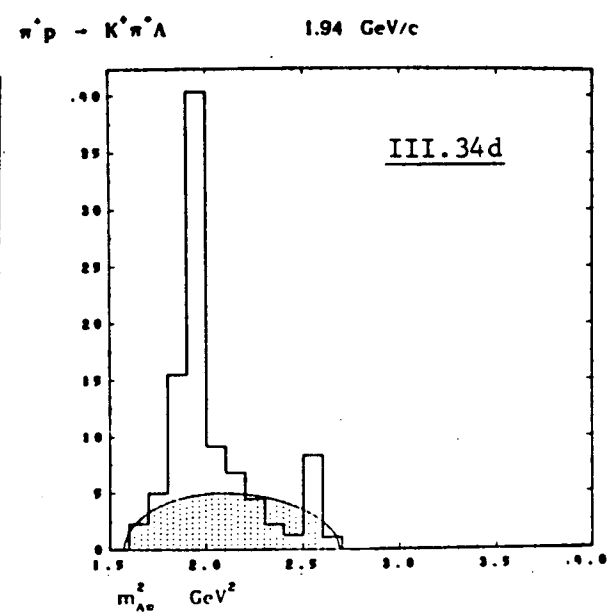
π⁺p → K⁺π⁺Λ
1.94 GeV/c
III.34d
m²Λπ GeV²

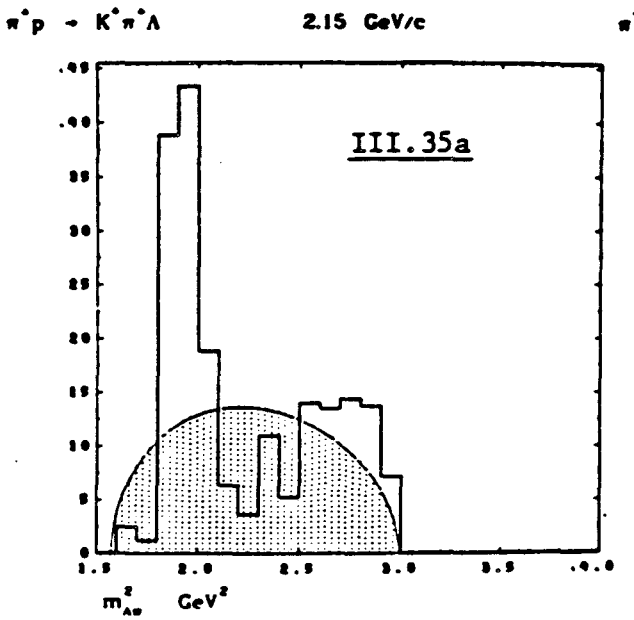
π⁺p → K⁺π⁺Λ
2.15 GeV/c
III.35a
m²Aπ GeV²

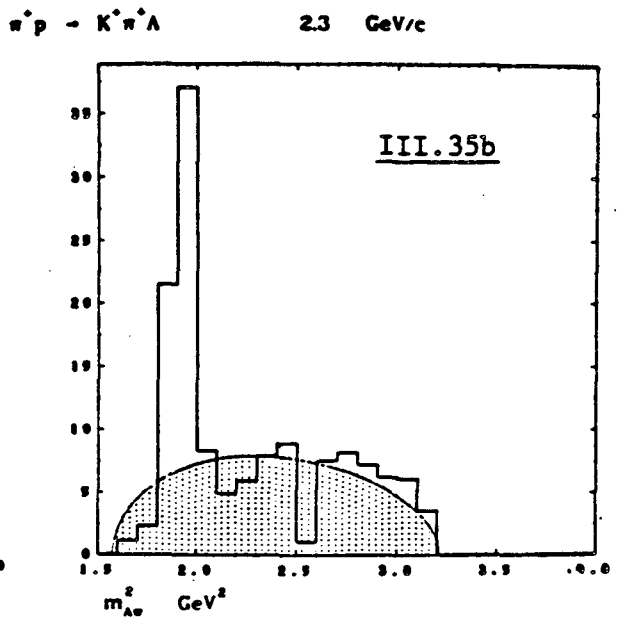
π⁺p → K⁺π⁺Λ
2.3 GeV/c
III.35b
m²Aπ GeV²

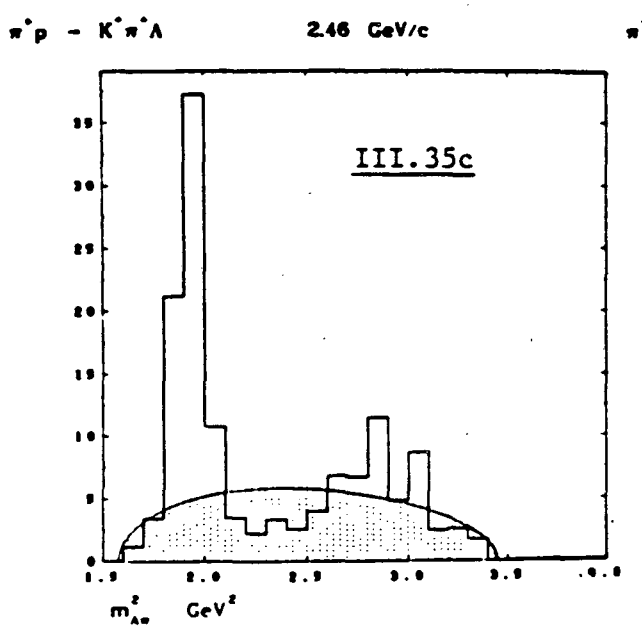
π⁺p → K⁺π⁺Λ
2.46 GeV/c
III.35c
m²Aπ GeV²

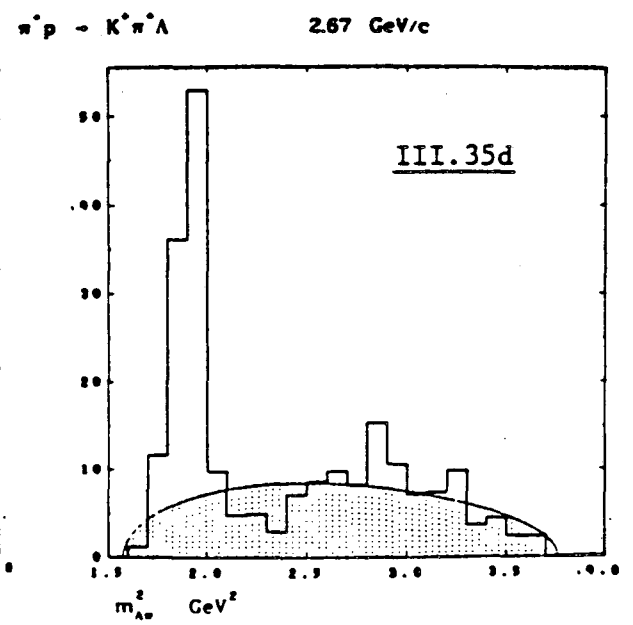
π⁺p → K⁺π⁺Λ
2.67 GeV/c
III.35d
m²Aπ GeV²

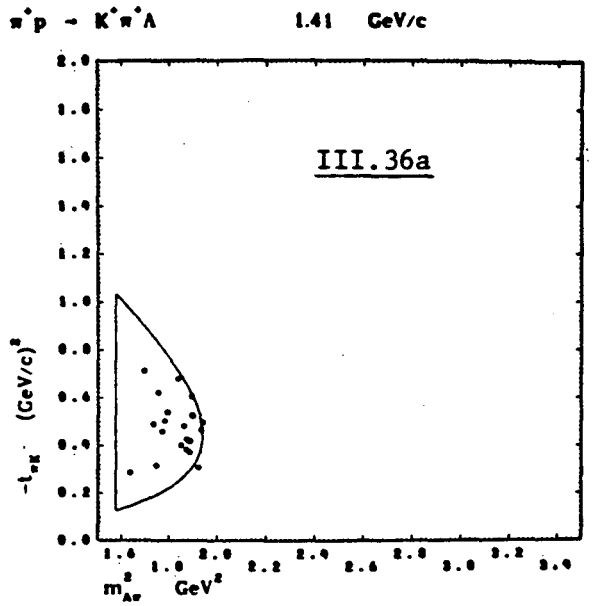
π⁺p → K⁺π⁺Λ
1.41 GeV/c
III.36a
$-t_{\pi K}$ (GeV/c)²
$m^2_{\Lambda\pi}$ GeV²

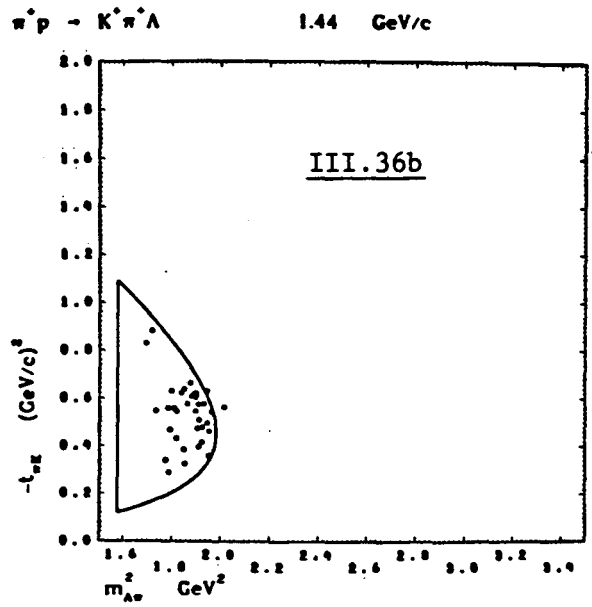
π⁺p → K⁺π⁺Λ
1.44 GeV/c
III.36b
$-t_{\pi K}$ (GeV/c)²
$m^2_{\Lambda\pi}$ GeV²

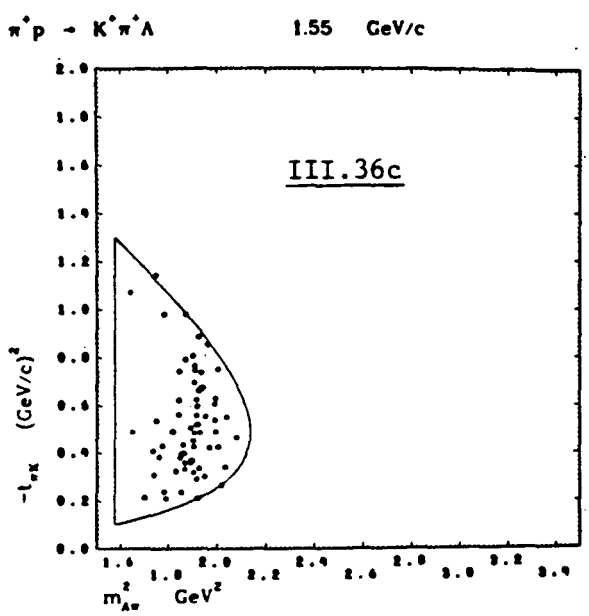
π⁺p → K⁺π⁺Λ
1.55 GeV/c
III.36c
$-t_{\pi K}$ (GeV/c)²
$m^2_{\Lambda\pi}$ GeV²

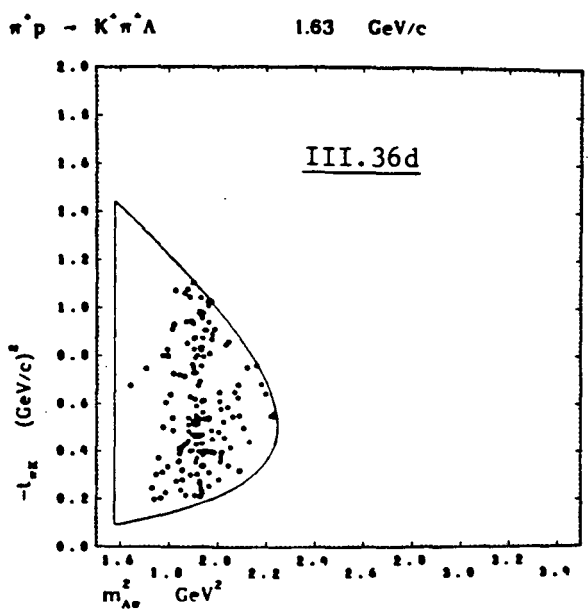
π⁺p → K⁺π⁺Λ
1.63 GeV/c
III.36d
$-t_{\pi K}$ (GeV/c)²
$m^2_{\Lambda\pi}$ GeV²

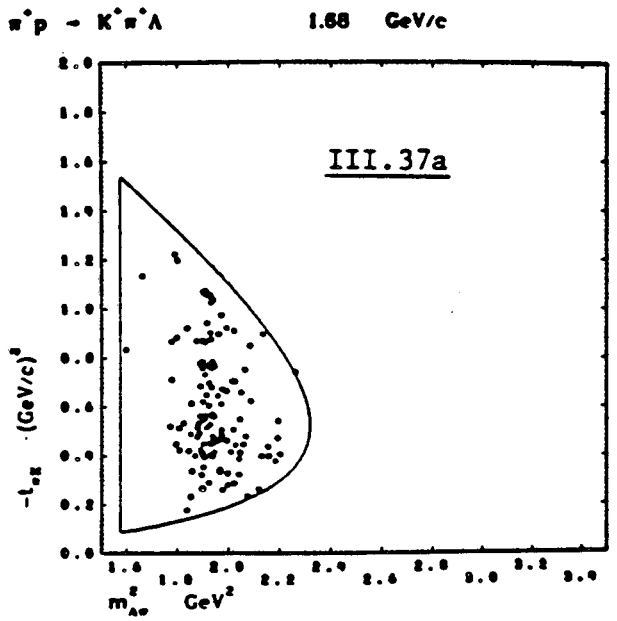
π⁺p → K⁺π⁺Λ 1.68 GeV/c
III.37a
$-t_{\pi K}$ (GeV/c)²
$m^2_{\Lambda\pi}$ GeV²

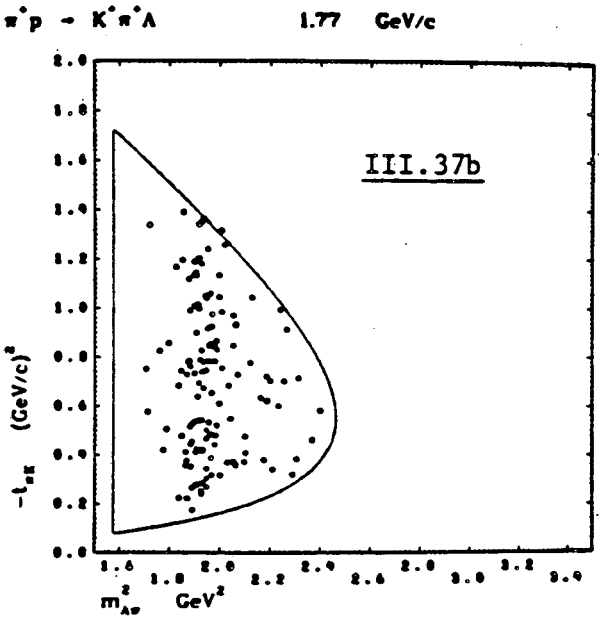
π⁺p → K⁺π⁺Λ 1.77 GeV/c
III.37b
$-t_{\pi K}$ (GeV/c)²
$m^2_{\Lambda\pi}$ GeV²

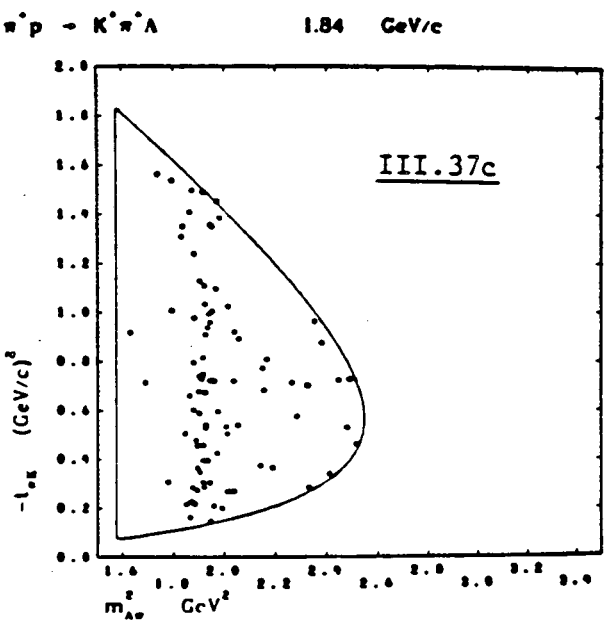
π⁺p → K⁺π⁺Λ 1.84 GeV/c
III.37c
$-t_{\pi K}$ (GeV/c)²
$m^2_{\Lambda\pi}$ GeV²

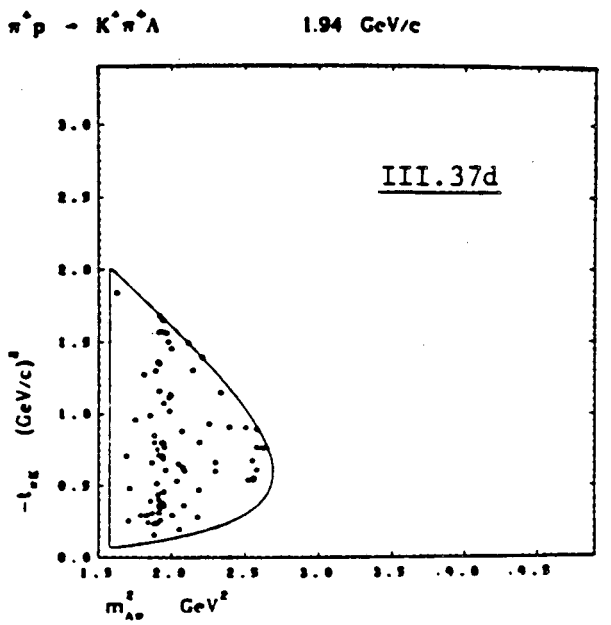
π⁺p → K⁺π⁺Λ 1.94 GeV/c
III.37d
$-t_{\pi K}$ (GeV/c)²
$m^2_{\Lambda\pi}$ GeV²

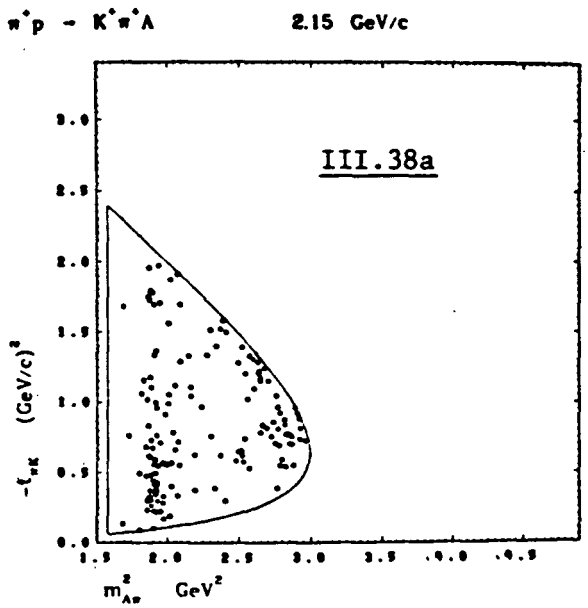
π⁺p → K⁺π⁺Λ
2.15 GeV/c
III.38a
$-t_{\pi K}$ (GeV/c)²
$m^2_{\Lambda\pi}$ GeV²

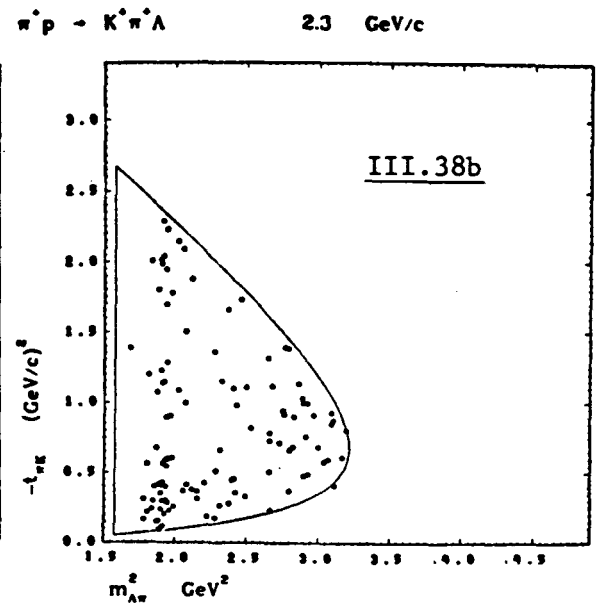
π⁺p → K⁺π⁺Λ
2.3 GeV/c
III.38b
$-t_{\pi K}$ (GeV/c)²
$m^2_{\Lambda\pi}$ GeV²

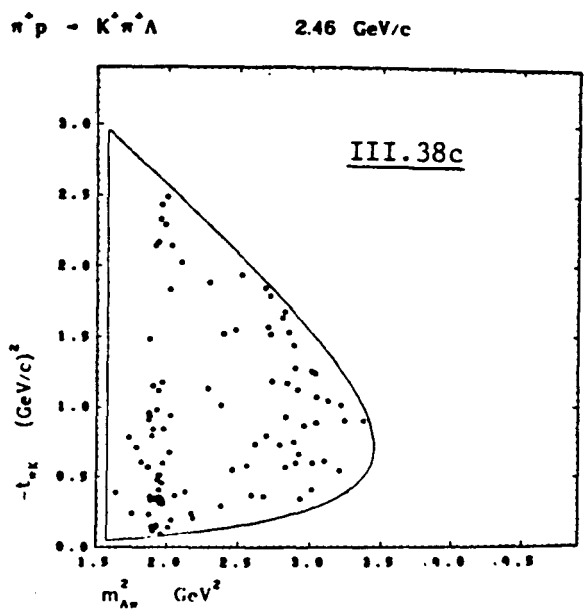
π⁺p → K⁺π⁺Λ
2.46 GeV/c
III.38c
$-t_{\pi K}$ (GeV/c)²
$m^2_{\Lambda\pi}$ GeV²

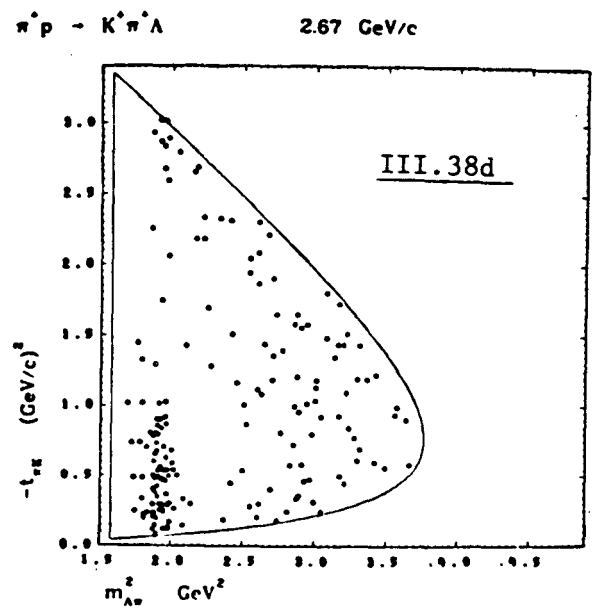
π⁺p → K⁺π⁺Λ
2.67 GeV/c
III.38d
$-t_{\pi K}$ (GeV/c)²
$m^2_{\Lambda\pi}$ GeV²

duced in a progressively more forward-backward preferred $t_{\pi K}$ distribution as the incident momentum increases; furthermore, the background under the $\Sigma(1385)$ signal at the higher momenta is evidently small. There appears to be a broad excess or clustering of events at higher $m^2_{\Lambda\pi}$, which could be due to reflection of a low-mass N^* enhancement in $m^2_{\Lambda K}$, or to production of a $\Lambda\pi$ enhancement in the $m_{\Lambda\pi} \sim 1670-1700$ MeV region, such as the $\Sigma(1670)$ of ref. 8. However, the $\Sigma(1670)$ width is given as 35-70 MeV, which is much narrower than the region of excess in the $m^2_{\Lambda\pi}$ spectra. As will be seen in the next section, the Dalitz plot distributions are statistically consistent with $\Sigma(1385)$ plus phase space background. The clustering or enhancement in the region $m_{\Lambda\pi} \approx 1700$ MeV is visible in other published data, such as that of Butler et al. (ref. 21) at 3.7 GeV/c and Goddard et al. (ref. 22) at 10.3 GeV/c.

D. $\Sigma^+K^{*+}(892)$ and $\Sigma^{*+}(1385)K^+$ Final States

1. Quasi Two Body States

A three body final state:

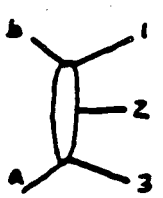

$$a + b \to 1 + 2 + 3:$$

dominated by a single quasi-two body resonance (say 1^*, in the 1-2 diparticle system) production state

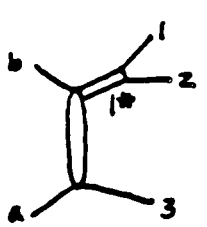

$$a + b \to 1^* + 3 \to 1 + 2 + 3:$$

is described by the variables

$$m^2_{12} \equiv (\mathbf{p}_1 + \mathbf{p}_2)^2 \text{ and } t = t_{a3} \equiv (\mathbf{p}_3 - \mathbf{p}_a)^2$$

along with the decay angles $\Omega = (\vartheta, \varphi)$ of the 1^* state in the 1-2 center of mass, where $\mathbf{p}_i$ is the 4-momentum of the ith particle. The Dalitz plot

densities for our data are adequately described with the phenomenological form for P-wave 1^* resonance production (see, e.g., refs. 23,24):

$$\frac{d^2N}{dm_{12}^2 dm_{23}^2} = \alpha + \beta B(m_{12}^2)[1 + \gamma\cos^2\vartheta_H(m_{12}^2, m_{23}^2)] \qquad \text{(III.D.1)}$$

where α,β,γ are constants, $B(m_{12}^2)$ is a Breit-Wigner function of m_{12}^2, and $\cos\vartheta_H$ is the helicity cosine of the $1^* \to 1 + 2$ decay: $\cos\vartheta_H = \hat{p}_2 \cdot \hat{p}_3$ in the 1-2 center of mass $\cos\vartheta_H$ is completely specified by m_{12}^2 and m_{23}^2.

This form ignores interference between resonance and background, ignores resonance production in m_{23}^2 or m_{13}^2 (as well as its reflection in m_{12}^2), and assumes there should be no significant reflections in m_{12}^2 from sharp or peculiar dependence on the various invariant momentum transfers. Initial fits to the data showed, as expected from the limited statistics, that despite the strong Σ^* and K^* production the $\Sigma K\pi$ and $K\pi\Lambda$ Dalitz plots were adequately fitted with

$$\frac{d^2N}{dm_{12}^2 dm_{23}^2} = \alpha + \beta B(m_{12}^2) \qquad \text{(III.D.2)}$$

where the form of the P-wave Breit Wigner B (with no barrier factors) is that in Jackson, ref. 25:

$$B(m_{12}^2) = \frac{m_{12}}{p} \frac{\Gamma(m_{12}^2)}{(m_{12}^2 - m_0^2)^2 + m_0^2\Gamma^2(m_{12}^2)} \qquad \text{(III.D.3)}$$

and

$$\Gamma(m_{12}^2) = \Gamma_0 \left(\frac{p}{p_0}\right)^3 \left(\frac{p_0^2 + z^2}{p^2 + z^2}\right). \qquad \text{(III.D.4)}$$

m_0, Γ_0 are the mass and width of the $\Sigma^*(1385)$ or $K^*(892)$, $p = p(m_{12}^2)$ is the magnitude of the 3-momentum of 1 (or 2) in the 1-2 center of mass, and $p_0 = p(m_{12}^2 = m_0^2)$; z is a parameter on the order of m_π^{-1} which was fixed at

0.1 GeV/c. Because of the statistics m_0, Γ_0 were fixed at the PDG table values. The fitting was not sensitive to the value of z, and was not sensitive to the form of $B(m_{12}^2)$ either, with a simple non-relativistic S-wave fitting as well as (III.D.3) above.

2. $\Sigma^+K^{*+}(892)$

Table IV displays the fractions of $\Sigma^+K^{*+}(892)$ production present in the $\Sigma^+K^+\pi^0$ and $\Sigma^+\pi^+K^0$ final states at each of the 5 high momenta, and Table V presents the cross sections for $\pi^+p \to \Sigma^+K^{*+} \to \Sigma^+K^+\pi^0, \Sigma^+\pi^+K^0$. The values of f were determined by fitting the functional form in Equation (III.D.2) to the $\Sigma^+K^+\pi^0$ and $\Sigma^+\pi^+K^0$ data by χ^2 minimization; in all cases a satisfactory fit was considered to have been attained when $\chi^2/(NO.\ OF\ DEGREES\ OF\ FREEDOM) \leq 1$. All cross sections in Table V have been corrected for unobserved final hyperon and/or K^0 decay modes using the PDG branching fractions, and the values of cross sections for $\pi^+p \to \Sigma^+K^{*+}$, $K^* \to K^+\pi^0 + \pi^+K^0$ are simply the sums of σ's for the $K^+\pi^0$ and $K^0\pi^+$ decay modes. (As we saw in Chapter II, the K^* mass band is roughly orthogonal to the $\pi-K$ ambiguity region; the summed K^* cross sections should not have a $\pi-K$ misidentification bias.) Finally, the last column of Table V exhibits the ratios

$$R \equiv \sigma(\Sigma K^*;\ K^* \to K^0\pi^+)/\sigma(\Sigma K^*;\ K^* \to K^+\pi^0)$$

From isospin we expect $R = 2$, and at all momenta the values are consistent with this ratio; moreover, the quantity

$$R_{TOT} \equiv \sum_{p_{inc}} (K^* \to K^0\pi^+)/\sum_{p_{inc}} (K^* \to K^+\pi^0)$$

$\pi^+ p \rightarrow \Sigma^+ K^*(892)^+$

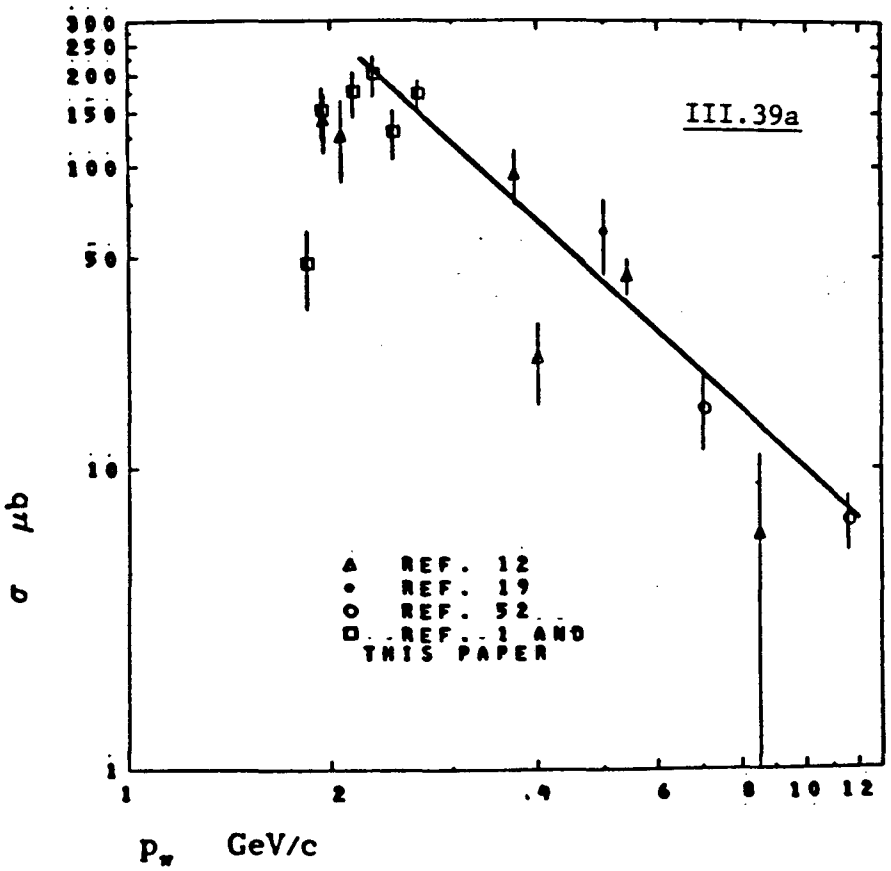

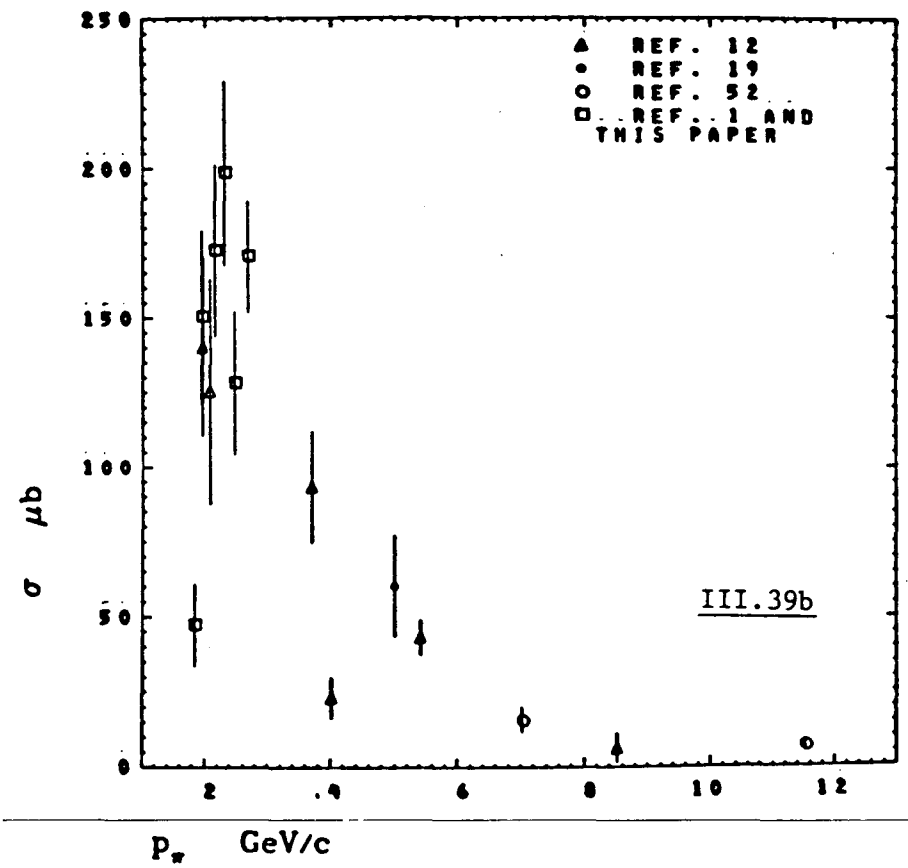

which uses all K^* events at the 5 high momenta has a value of 1.8 ± 0.2. The errors on the cross sections in Table V include uncertainties from both the $\Sigma K\pi$ channel cross sections and the fitted fractions f.

Figure III.39 presents the 5 ΣK^* channel cross sections from this data, as well as the world data for this channel, where data from sources using only one K^* decay mode have been corrected using $R = 2$ and ignoring the negligible branching of K^* into $K\pi\pi$, etc. Also included is the point from fitting our 1.84 GeV/c $\Sigma K\pi$ data (using all Σ^+ decay modes). The slope from a fit to the data in figure III.39 is given in Table VI. For the analysis in Chapter IV the ΣK^* final state is defined as all events within a π–K mass cut of .817 GeV $\leq m_{\pi K} \leq$ .967 GeV, which corresponds to a K^* band $m_0 \pm 1.5\Gamma_0 = .892 \pm .075$ GeV. Integration of the of the fitted mass distribution of Equation (III.D.2) over this $m_{\pi K}$ band yields a background of ~12% for the $\Sigma^+\pi^+K^0$ K^* band, and a background of ~35% for the $\Sigma^+K^+\pi^0$ K^* region. For both $\Sigma^+\pi^+K^0$ and $\Sigma^+K^+\pi^0$ events in the K^* band, the average weight/event is the same as for all events of those channels.

3. $\Sigma^{*+}(1385)K^+$

The fractions f of $\Sigma^{*+}(1385)K^+$ production present in the $K^+\pi^+\Lambda$ final state at each of the 5 high momenta are given in Table IV, and Table V presents the channel cross sections for $\pi^+p \rightarrow \Sigma^{*+}(1385)K^+ \rightarrow \Lambda\pi^+K^+$ for all 12 momenta with $p_\pi \geq 1.41$ GeV/c. For the 5 high momenta the values of f were determined, as for ΣK^*, by fitting the functional form of Equation (III.D.2) to the $\Lambda\pi^+K^+$ data by χ^2 minimization which was considered satisfactory when $\chi^2/(NO.\ OF\ DEGREES\ OF\ FREEDOM) \leq 1$, and successful fits were attained

using only the $\Sigma^*(1385)$ plus incoherent phase space background. For the 7 momenta of ref. 1 with $p_\pi \leq 1.84$ GeV/c, the fraction of $\Sigma^*(1385)K$ present was determined both by fitting the mass distributions and by simply counting the numbers of events in the $\Sigma^*(1385)$ signal above the phase space background (whose normalization was determined well outside the $\Sigma^*(1385)$ region); both these methods were found to be in excellent agreement. The $\Sigma^*(1385)K$ channel cross sections are corrected for the unseen Λ decay mode using PDG table branching fractions, and the errors include uncertainties from both the $K\pi\Lambda$ cross sections and the fitted fractions f.

Figure III.40 displays the 12 $\Sigma^{*+}(1385)K^+$ channel cross sections of this work, as well as the world data, where data from other sources has been corrected where necessary with PDG branching fractions to represent only the $\Sigma^* \rightarrow \Lambda\pi$ mode; Table VI gives the slope from a fit to the data of figure III.40. In Chapter IV Σ^*K events are defined by the mass cut $m_{\Lambda\pi}$: $1.382 \pm .050\ GeV \approx m_0 \pm 1.5\ \Lambda_0$. Integration of the fitted Equation (III.D.2) over this cut yields a background fraction of ~12-14% for the 5 higher momenta. Events in the $\Sigma^*(1385)$ band had the same average weight/event as the complete $K\pi\Lambda$ samples.

4. $\Sigma^*(1385)^+K^*(892)^+$

Although we do not extract $\Sigma^*(1385)^+K^*(892)^+$ cross sections from our own data, we have compiled for comparison (and also for later use of the p_{inc} power law scaling) the total available world data on this channel cross section from refs. 12,19,20,21,22,47,52, which is exhibited in figure III.41; a previous compilation by Goddard (ref. 22) did not include the very recent points of

$\pi^+ p \rightarrow K^+ \Sigma^*(1385)^+ \qquad \Sigma^{*+} \rightarrow \Lambda\pi^+$

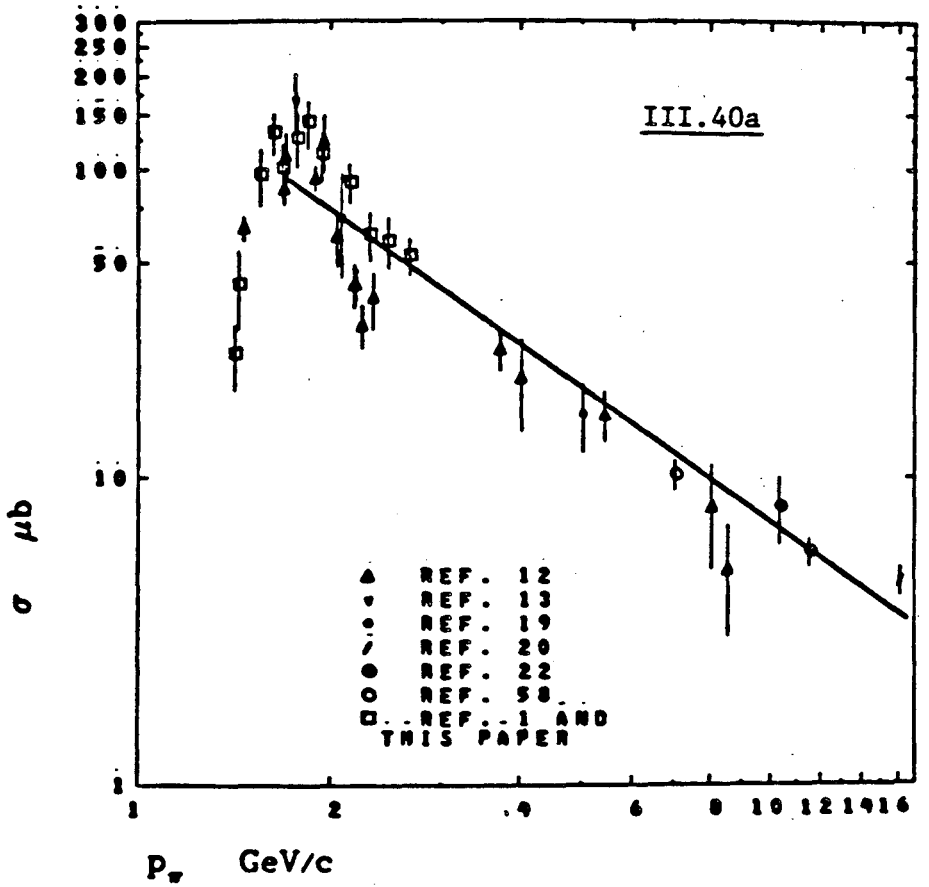

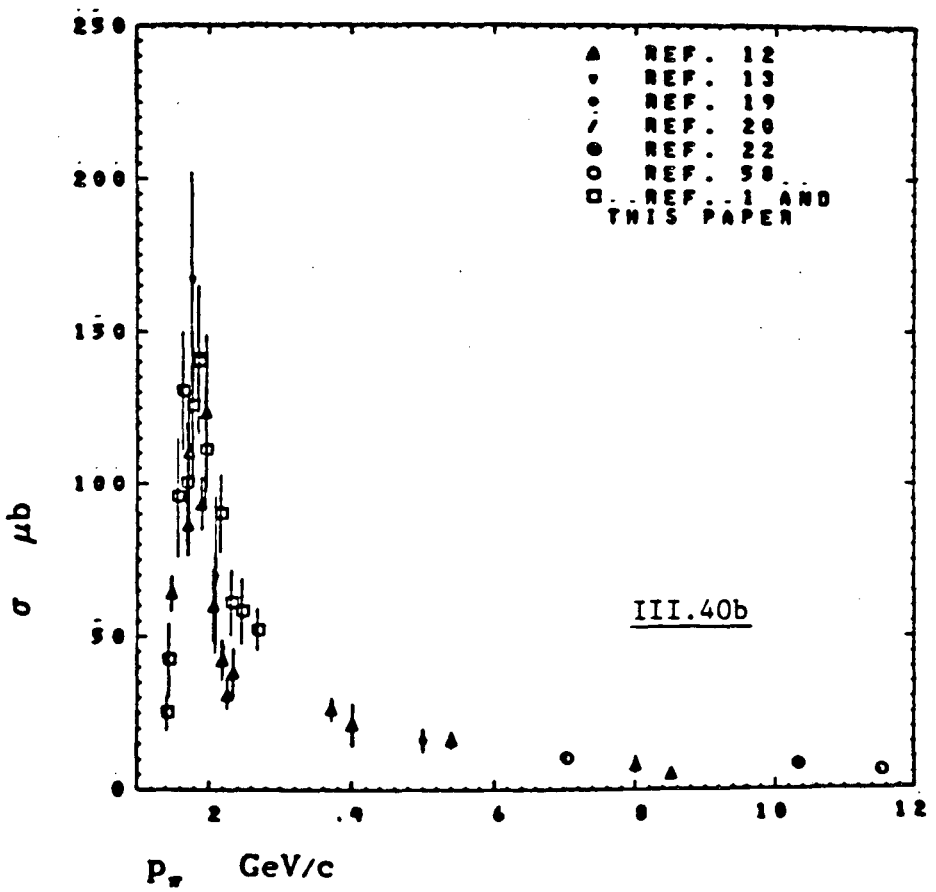

$\pi^+ p \rightarrow K^*(892)^+ \Sigma^*(1385)^+$

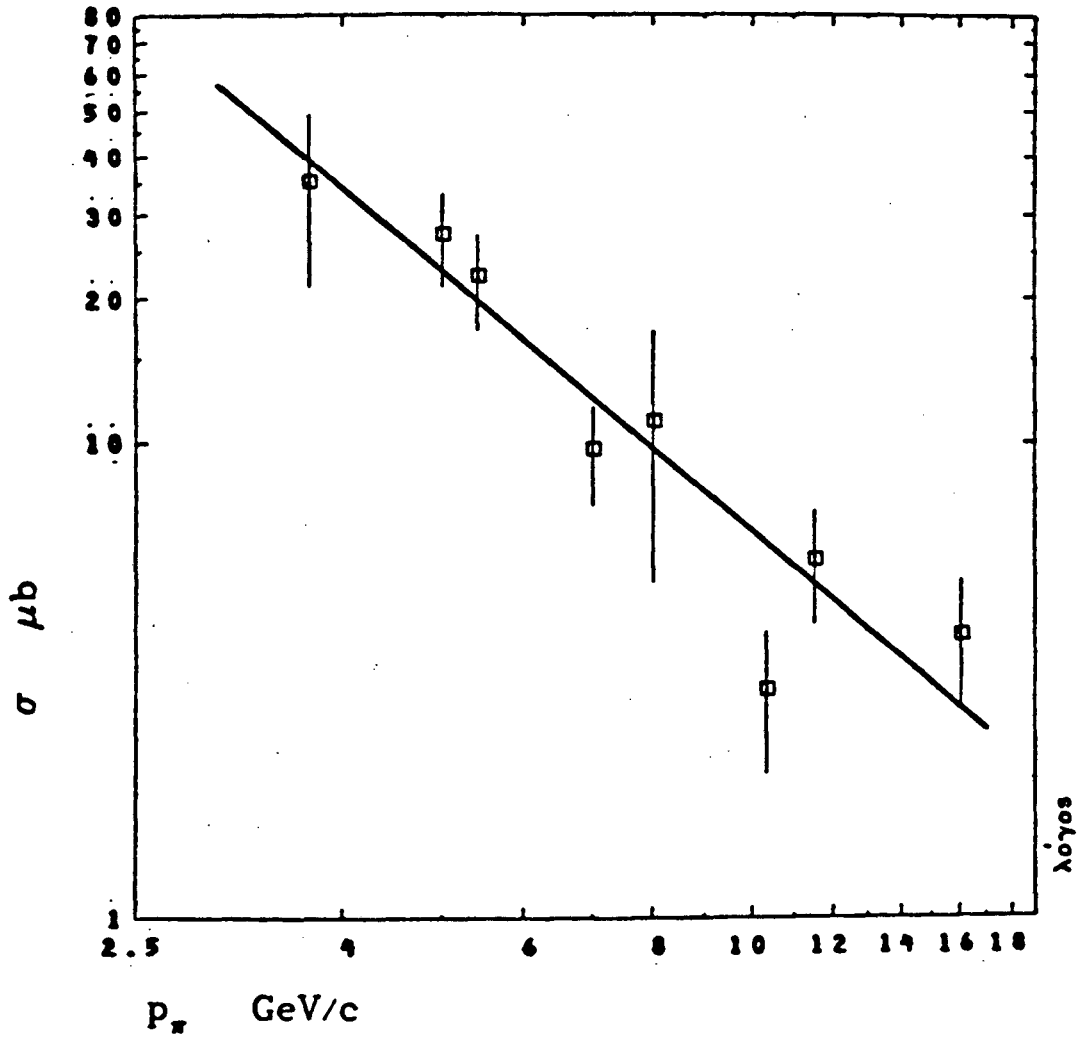

III.41

refs. 20 and 52 at 7, 11.5, and 16 GeV/c. Quite clearly this channel is well described by a power law in p_{inc}.

E. Comparison of Channel Cross Sections for $\Sigma K, \Sigma K^*$, $\Sigma^* K$, $\Sigma^* K^*$; $K\pi\Lambda$ and $K\pi\Sigma$

1. $\Sigma K, \Sigma K^*, \Sigma^* K, \Sigma^* K^*$

The cross sections for the 2-body and quasi-2-body channels ΣK, ΣK^*, $\Sigma^* K$, $\Sigma^* K^*$ displayed in figures III.1,39,40,41 exhibit rough power law behavior in p_π for $p_\pi > 2\ GeV/c$, whose fitted values are given in Table VI. For the ΣK and $\Sigma^* K$ data, the maxima at 1.5 and 1.7 GeV/c presumably represent in part $\Delta \to \Sigma K, \Sigma^* K$, and the fall off immediately beyond the peaks in figures III.1,39 appears steeper than that of the higher lying points. Because of their limited extent in p_π, inclusion of these steeper points in the fits affects mainly the intercepts and not the slopes, which clearly represent well the general trend of the higher p_π points. The threshold for the ΣK^* channel is above the low lying Δ's, and thus it is not surprising that the cross section is closer to a pure power law immediately beyond the maximum.

For the channels $\Sigma K, \Sigma K^*, \Sigma^* K$, $\Sigma^* K^*$ most of the events lie in forward peaks near $\cos\vartheta_{CM} = 1$ (or $t \equiv t_{\pi K} = t_{min}$) as p_π increases, and for these channels in the forward direction the dominant exchanged quantum numbers are those of the $K^*(892)$ and $K^{**}(1430)$ (see Chapter IV for detailed comment).

From simple Regge phenomenology, one expects that for all these channels at higher s (see, e.g., Irving and Worden, ref. 69):

$$\frac{d\sigma}{dt} \propto s^{2\alpha_{eff}(t)-2} \approx s^{2(\alpha_0+\alpha_1 t)-2} \qquad (\alpha_0, \alpha_1 \text{ constants}),$$

where $\alpha_{eff} \approx \alpha_0 + \alpha_1 t$ is the effective trajectory of the (weak exchange degenerate) K^* and K^{**}. Thus one expects (or may simply take as an established empirical result; see Chapter IV) that for all these channels $\frac{d\sigma}{dt}$ has an exponential forward peak which shrinks with increasing p_π or s as (ignoring turnovers, dips, and kinematic zeroes):

$$\frac{d\sigma}{dt} \propto s^{a+bt} \qquad (a, b \text{ constants}),$$

and since most of the channel cross section is contained in the forward peak between $t_0 \equiv t_{\min}$ and some value t_1 for which $\frac{d\sigma}{dt} \approx 0$, one gets the result extensively discussed in the classic treatment of Morrison, ref. (30), or more recently in Barger and Cline, ref. (31):

$$\sigma = \int_{t_1}^{t_0} \frac{d\sigma}{dt} dt = (const) s^{a+bt_0} = (const) s^q = (const)(2m_p p_\pi)^q$$

where a,b,q are constants dependent only upon the exchanged quantum numbers. For hypercharge via K^*, K^{**} one expects from high energy $\frac{d\sigma}{dt}$ data that roughly $q \approx -1.7$ (see ref. 31 and Chapter IV).

As can be seen from the values in Table VI, the powers for $\Sigma K, \Sigma K^*, \Sigma^* K$ are all roughly in agreement with each other as well as with the value $q = -1.7$. The $\Sigma^* K^*$ channel's value of $q = -1.81 \pm 0.24$ is also in good agreement with this expectation.

2. $K^+\pi^+\Lambda, K^+\pi^0\Sigma^+$, and $K^0\pi^+\Sigma^+$

For the 3-body channels the situation is not so simple as for the 2-body cases which are adequately represented as dominated by a single exchange process. However, for $K^+\pi^+\Lambda$, $K^+\pi^0\Sigma^+$, and $K^0\pi^+\Sigma^+$ the various processes which contribute all have couplings, quantum numbers, and kinematics sufficiently similar so that one expects the cross sections all to fall at roughly the same power. Additionally, low lying resonance formation is not strongly apparent in figures III.2,III.3,III.4 and a simple power law represents the data fairly well from the maxima onward. From Table VI evidently all three channels have powers consistent with $q = -1$.

IV. ANALYSIS OF THE CHANNELS $\Sigma K, \Sigma K^*, \Sigma^* K, \Sigma^* K^*$

A. ΣK

1. $\frac{d\sigma}{dt}, P_\Sigma$

Figures IV.1-IV.3 display $\frac{d\sigma}{dt}$ for $\pi^+ p \to \Sigma^+ K^+$ at all 14 incident momenta; here as usual $t \equiv (\mathbf{p}_K - \mathbf{p}_\pi)^2 = (\mathbf{p}_\Sigma - \mathbf{p}_p)^2$, and also $t' \equiv t - t_{\min}$, where $|t_{\min}|$ is the minimum value of $|t|$. The data for the 9 lower momenta only have been obtained by transformation of $\frac{dN}{d\cos\vartheta_{C.M.}}$ into $\frac{d\sigma}{dt}$, which because of Δp_{inc}, results in a very slight sharpening of the peaking in $\frac{d\sigma}{dt}$. Figures IV.4-IV.6 exhibit the Σ^+ polarization P_Σ versus t for all 14 momenta. Curves superimposed on the data are predictions from hypercharge exchange (HYCEX) amplitude analysis models discussed below. Only $\Sigma^+ \to \pi^+ n$ events are used for $\frac{d\sigma}{dt}$; because the asymmetry parameter α for the $\Sigma^+ \to \pi^+ n$ decay is only .07, only $\Sigma^+ \to p\pi^0$ events are used for P_Σ.

Because the strong interaction conserves parity, for $\pi^+ p \to \Sigma^+ K^+$, $\vec{P}_\Sigma$ must be parallel to the production normal $\hat{n} \equiv \hat{p}_{\pi C.M.} \times \hat{p}_{KC.M.} = \hat{p}_{p'C.M.} \times \hat{p}_{\Sigma C.M.}$ (p' is initial state proton). Since the decay $\Sigma^+ \to p\pi^0$ is parity violating, the Σ^+ rest frame decay distribution has the form (see Gasiorowicz, ref. 33):

$$\frac{dN}{d\cos\vartheta} = \frac{1}{2}(1 + \alpha P_\Sigma \cos\vartheta) \qquad \text{(IV.A.1)}$$

where α is the $\Sigma^+ \to p\pi^0$ asymmetry parameter and ϑ is the angle in the Σ^+ rest frame between the decay proton and the axis with respect to which P_Σ is

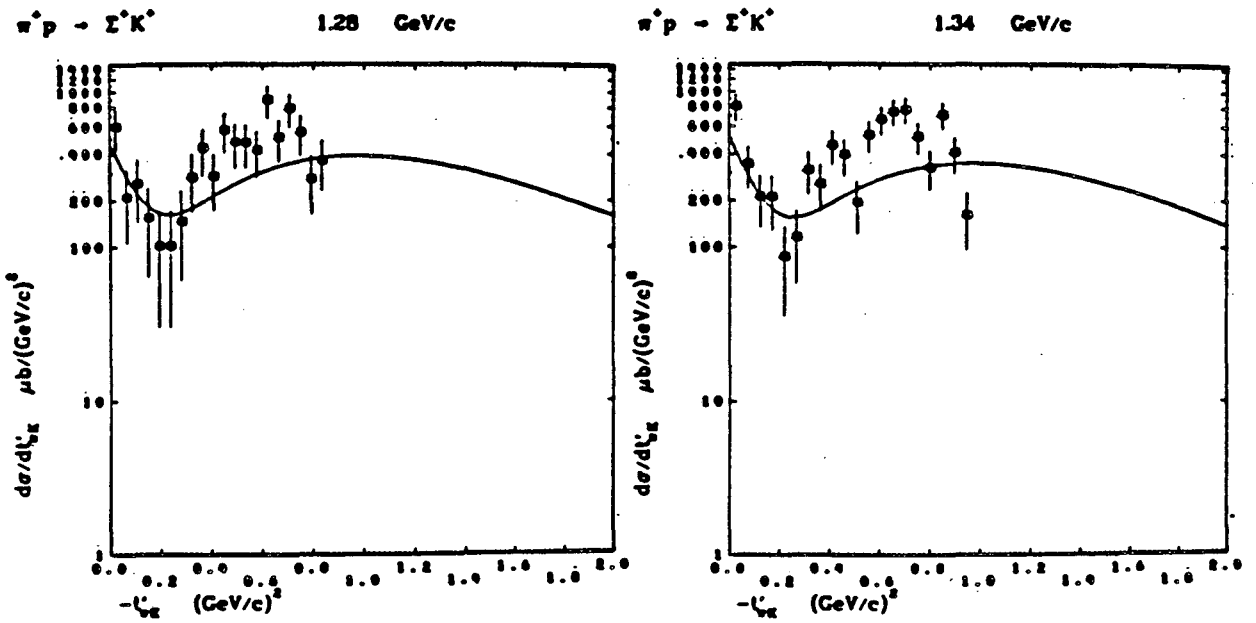
π⁺p → Σ⁺K⁺
1.28 GeV/c
π⁺p → Σ⁺K⁺
1.34 GeV/c
dσ/dt'_πK μb/(GeV/c)²
-t'_πK (GeV/c)²

IV.1a

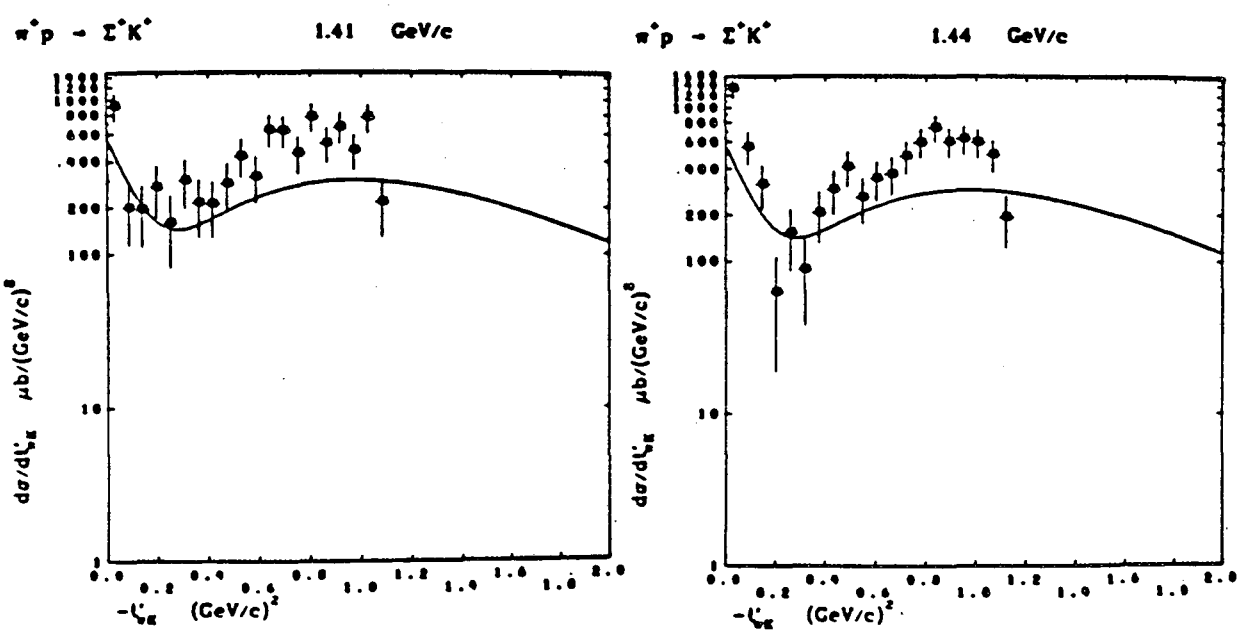
π⁺p → Σ⁺K⁺
1.41 GeV/c
π⁺p → Σ⁺K⁺
1.44 GeV/c
dσ/dt'_πK μb/(GeV/c)²
-t'_πK (GeV/c)²

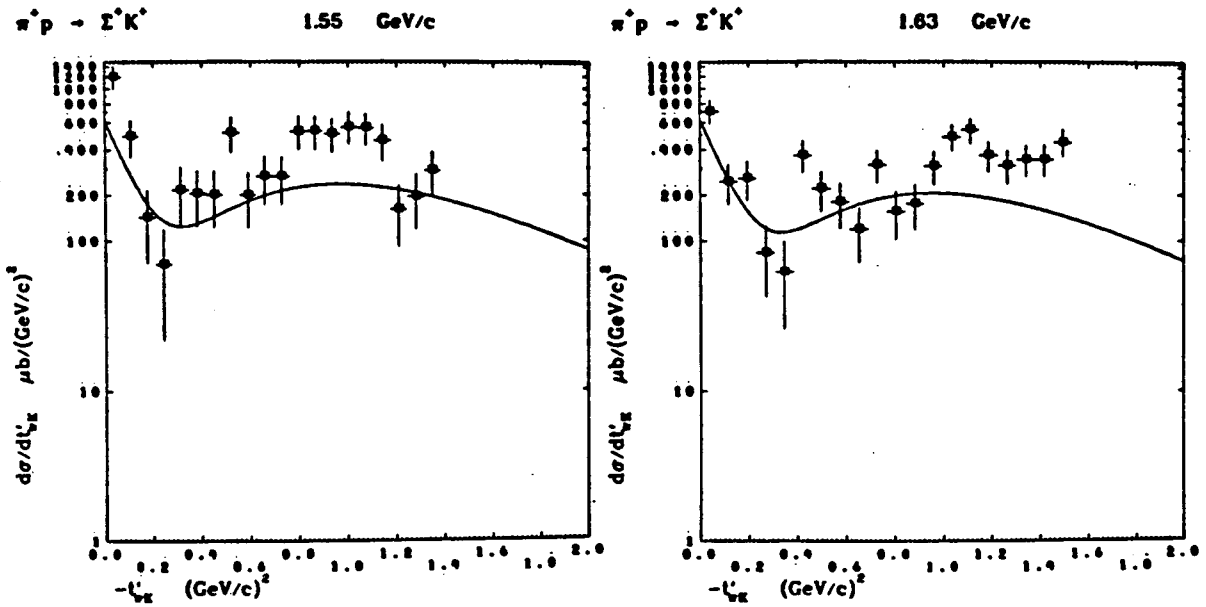
π⁺p → Σ⁺K⁺
1.55 GeV/c
π⁺p → Σ⁺K⁺
1.63 GeV/c
dσ/dt'πK μb/(GeV/c)²
-t'πK (GeV/c)²

IV.1b

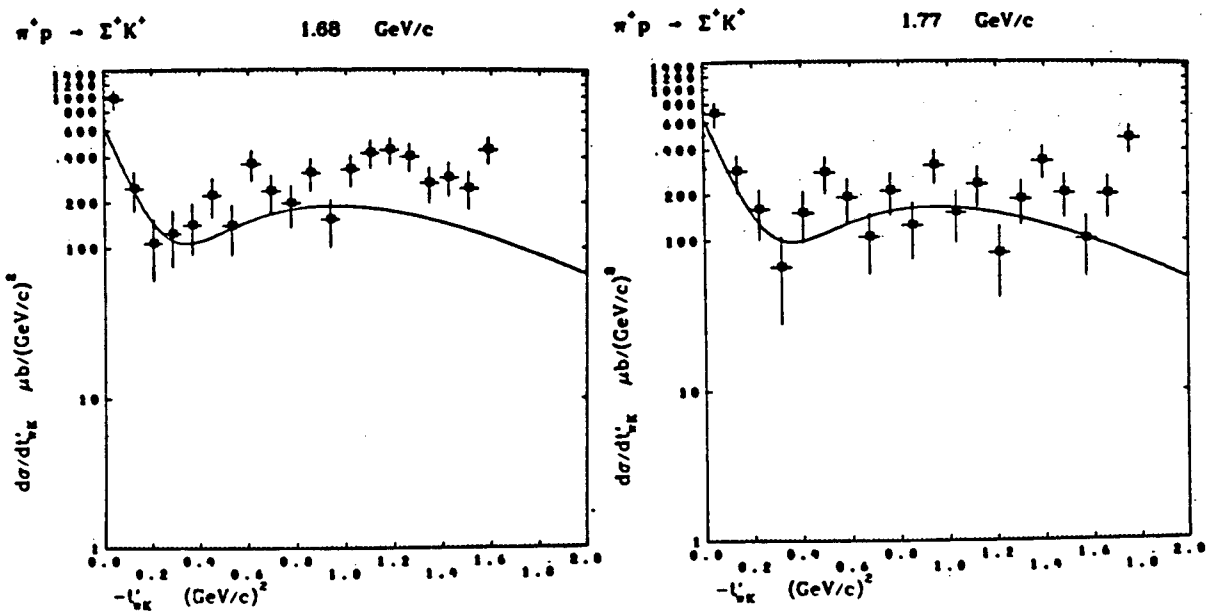
π⁺p → Σ⁺K⁺
1.68 GeV/c
π⁺p → Σ⁺K⁺
1.77 GeV/c
dσ/dt'πK μb/(GeV/c)²
-t'πK (GeV/c)²

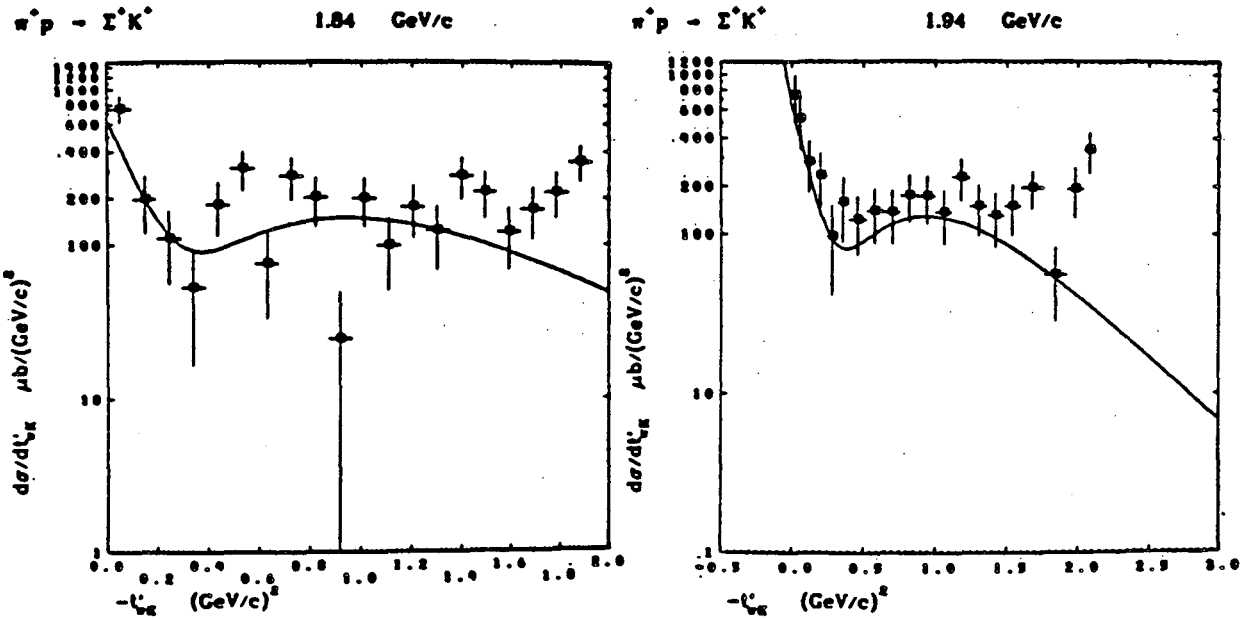
π⁺p → Σ⁺K⁺
1.84 GeV/c
1.94 GeV/c
dσ/dt'_πK μb/(GeV/c)²
-t'_πK (GeV/c)²

IV.2a

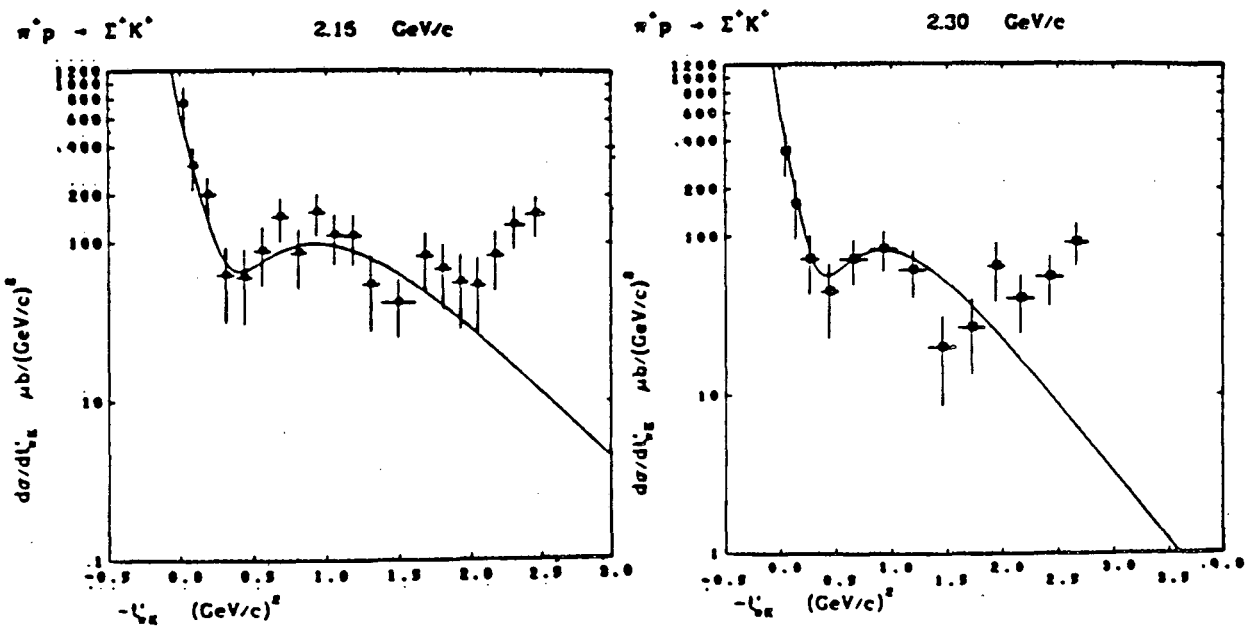
π⁺p → Σ⁺K⁺
2.15 GeV/c
2.30 GeV/c
dσ/dt'_πK μb/(GeV/c)²
-t'_πK (GeV/c)²

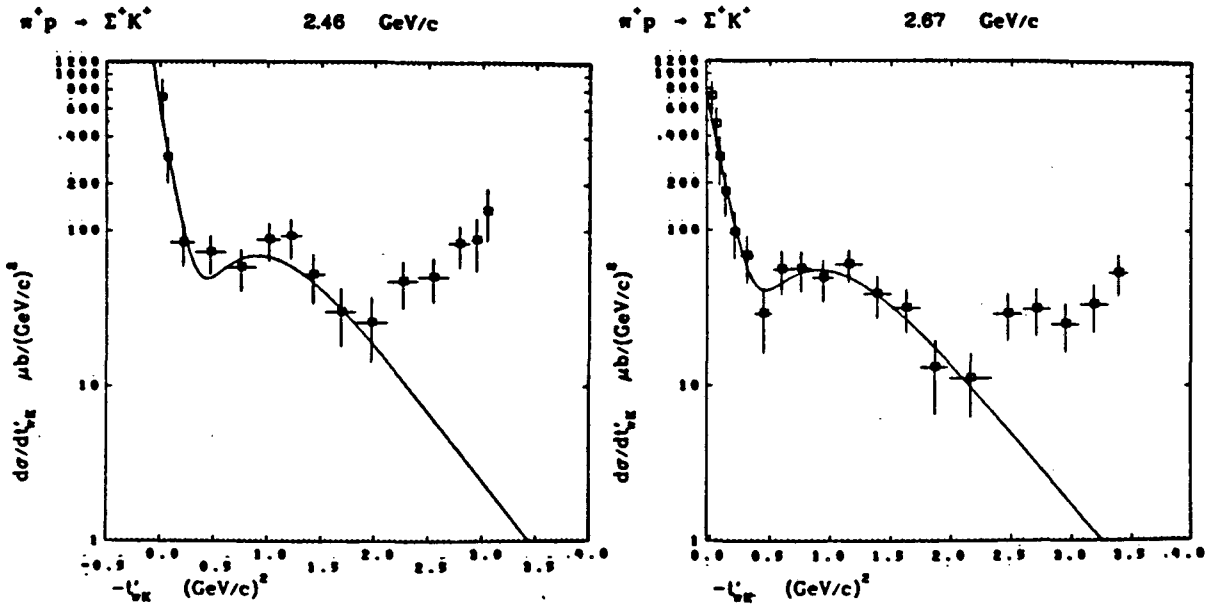
π⁺p → Σ⁺K⁺
2.46 GeV/c
2.67 GeV/c
dσ/dt'πK μb/(GeV/c)²
-t'πK (GeV/c)²

IV.2b

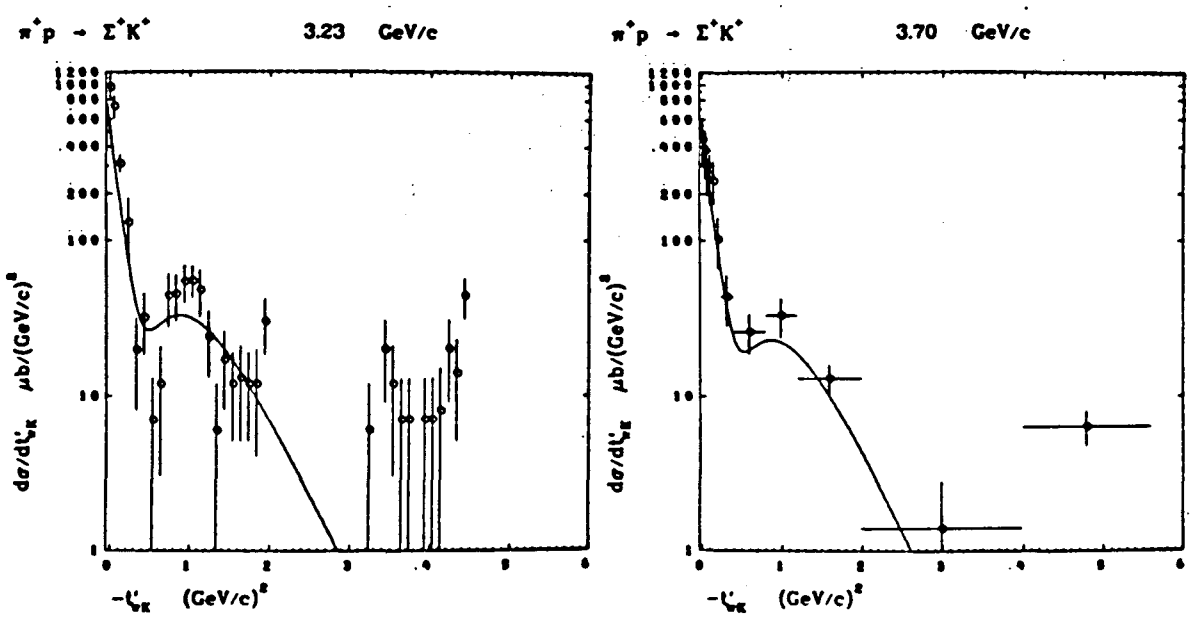
π⁺p → Σ⁺K⁺
3.23 GeV/c
3.70 GeV/c
dσ/dt'πK μb/(GeV/c)²
-t'πK (GeV/c)²

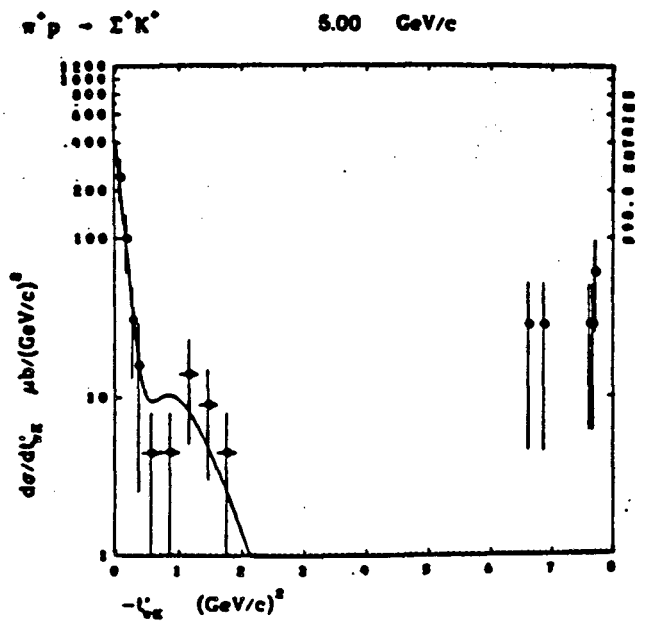

IV.3

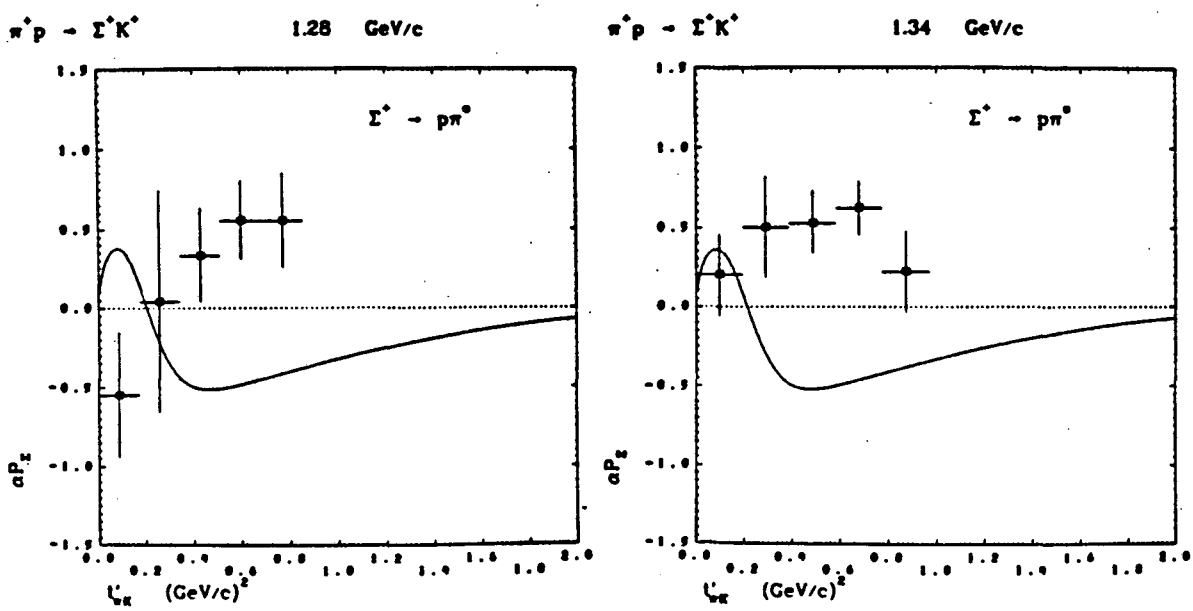
π⁺p → Σ⁺K⁺
1.28 GeV/c
Σ⁺ → pπ⁰
αP_Σ
t'_πK (GeV/c)²
π⁺p → Σ⁺K⁺
1.34 GeV/c
Σ⁺ → pπ⁰
αP_Σ
t'_πK (GeV/c)²

IV.4a

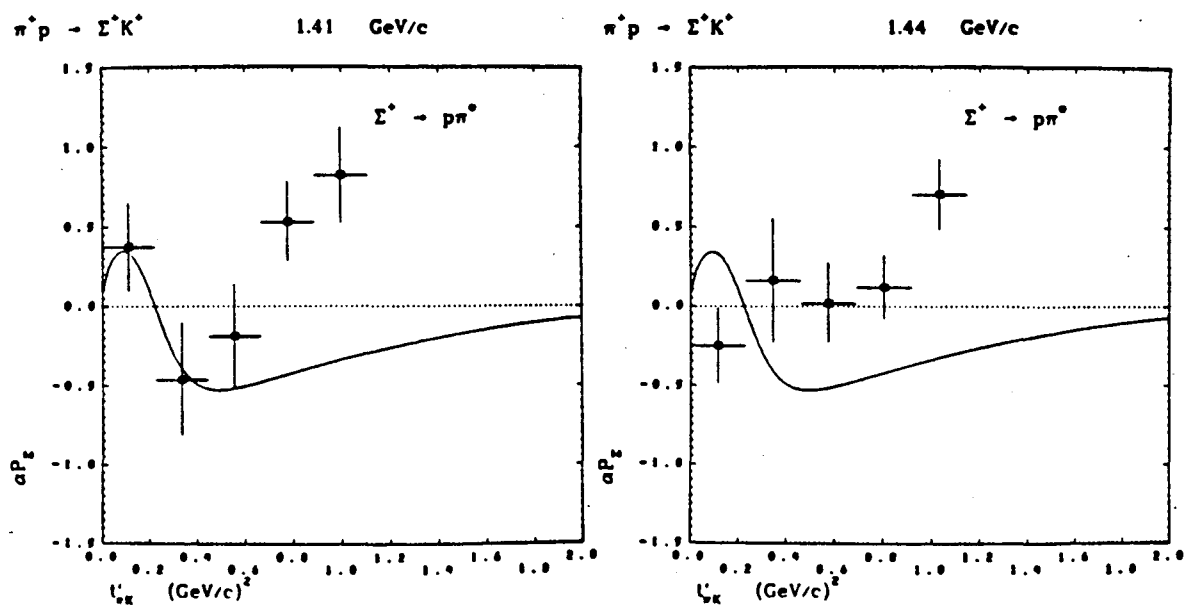
π⁺p → Σ⁺K⁺
1.41 GeV/c
Σ⁺ → pπ⁰
αP_Σ
t'_πK (GeV/c)²
π⁺p → Σ⁺K⁺
1.44 GeV/c
Σ⁺ → pπ⁰
αP_Σ
t'_πK (GeV/c)²

IV.4b

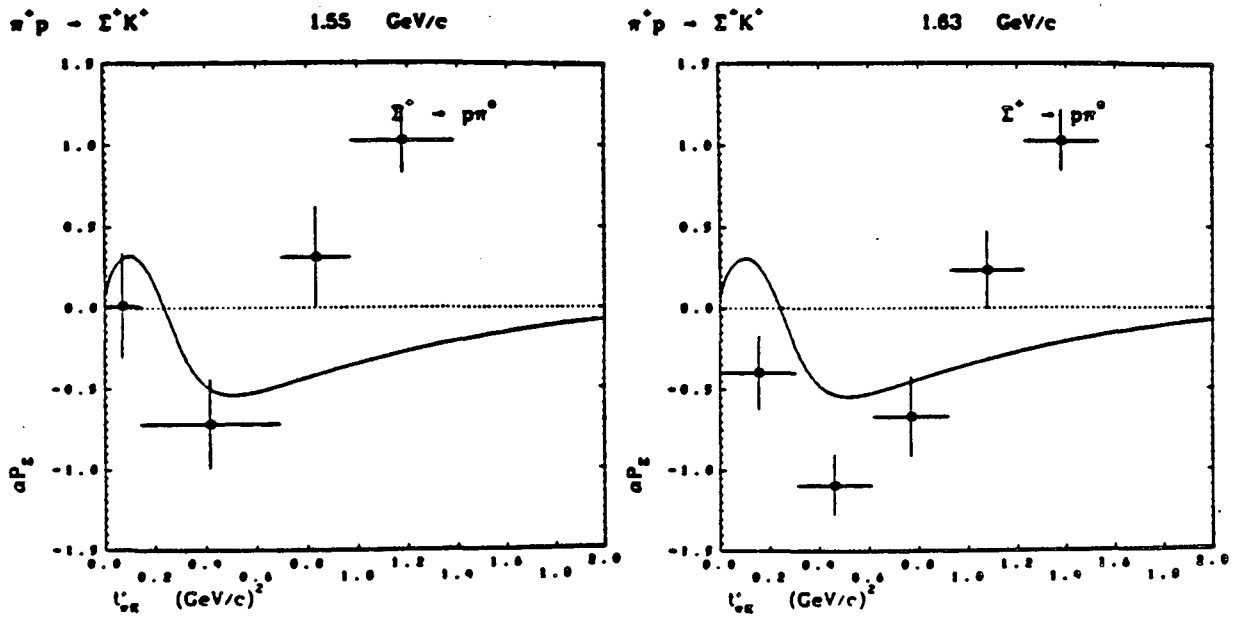
π⁺p → Σ⁺K⁺
1.55 GeV/c
Σ⁺ → pπ⁰
αP_Σ
t'_Σπ (GeV/c)²
π⁺p → Σ⁺K⁺
1.63 GeV/c
Σ⁺ → pπ⁰
αP_Σ
t'_Σπ (GeV/c)²

IV.5a

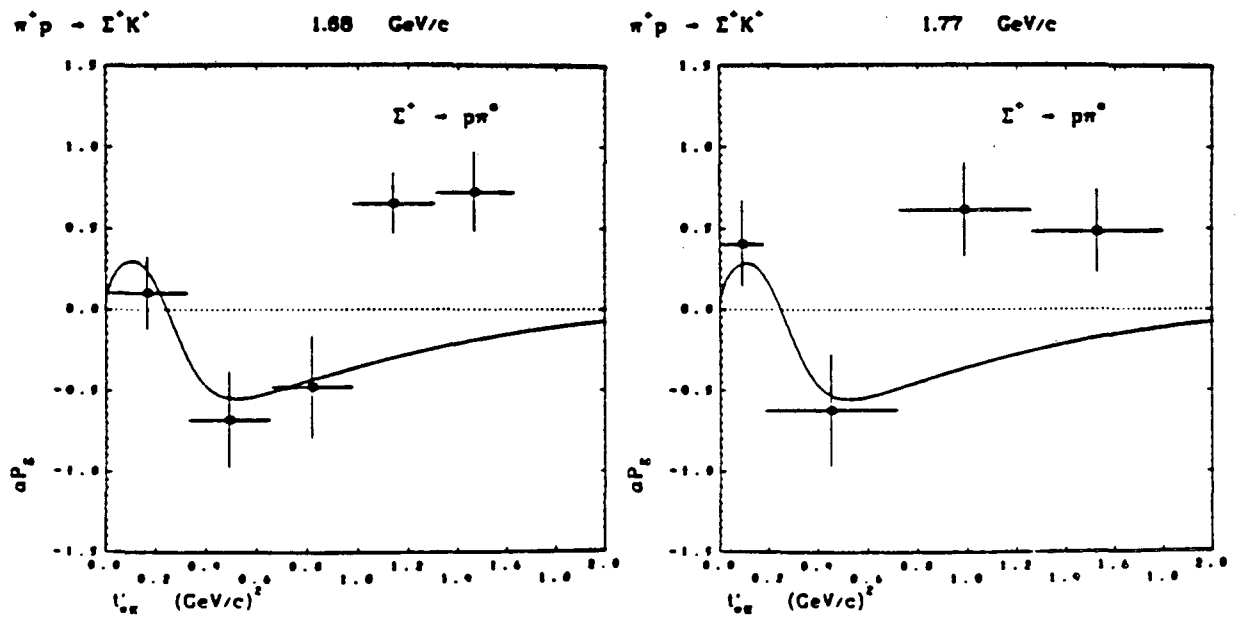
π⁺p → Σ⁺K⁺
1.68 GeV/c
Σ⁺ → pπ⁰
αP_Σ
t'_Σπ (GeV/c)²
π⁺p → Σ⁺K⁺
1.77 GeV/c
Σ⁺ → pπ⁰
αP_Σ
t'_Σπ (GeV/c)²

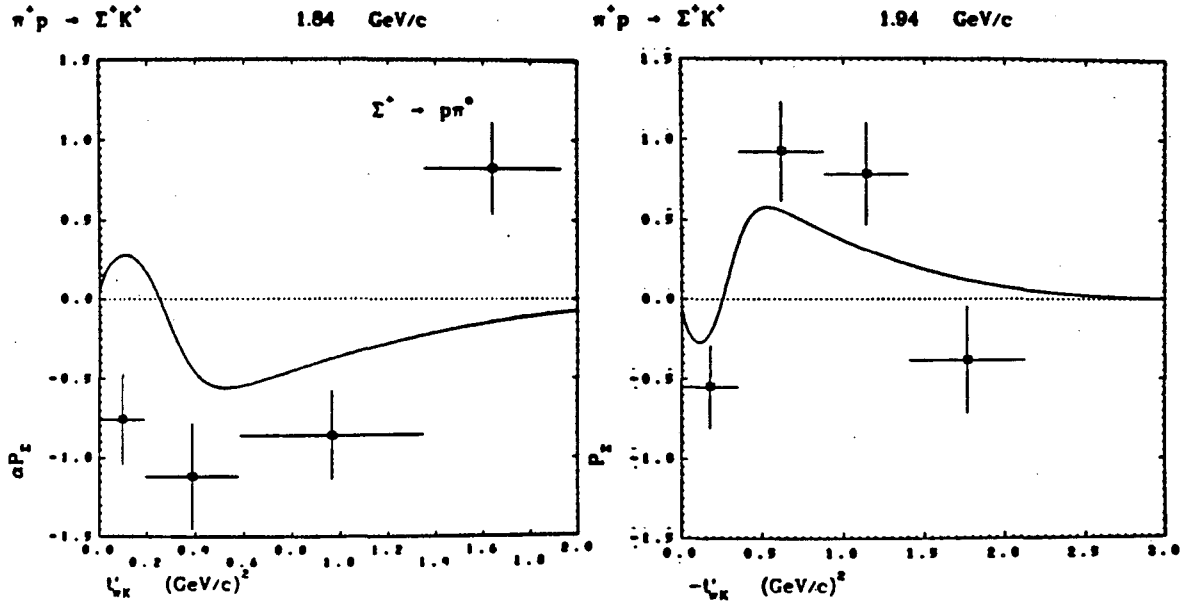
π⁺p → Σ⁺K⁺
1.84 GeV/c
Σ⁺ → pπ⁰
αP_Σ
t'_πK (GeV/c)²
π⁺p → Σ⁺K⁺
1.94 GeV/c
P_Σ
-t'_πK (GeV/c)²

IV.5b

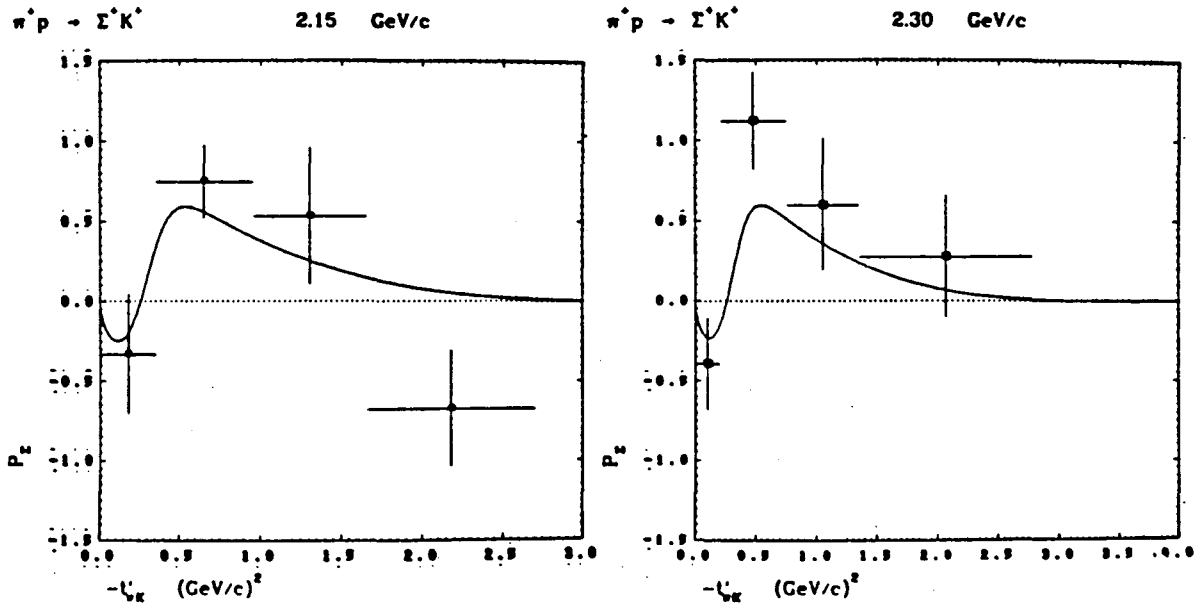
π⁺p → Σ⁺K⁺
2.15 GeV/c
P_Σ
-t'_πK (GeV/c)²
π⁺p → Σ⁺K⁺
2.30 GeV/c
P_Σ
-t'_πK (GeV/c)²

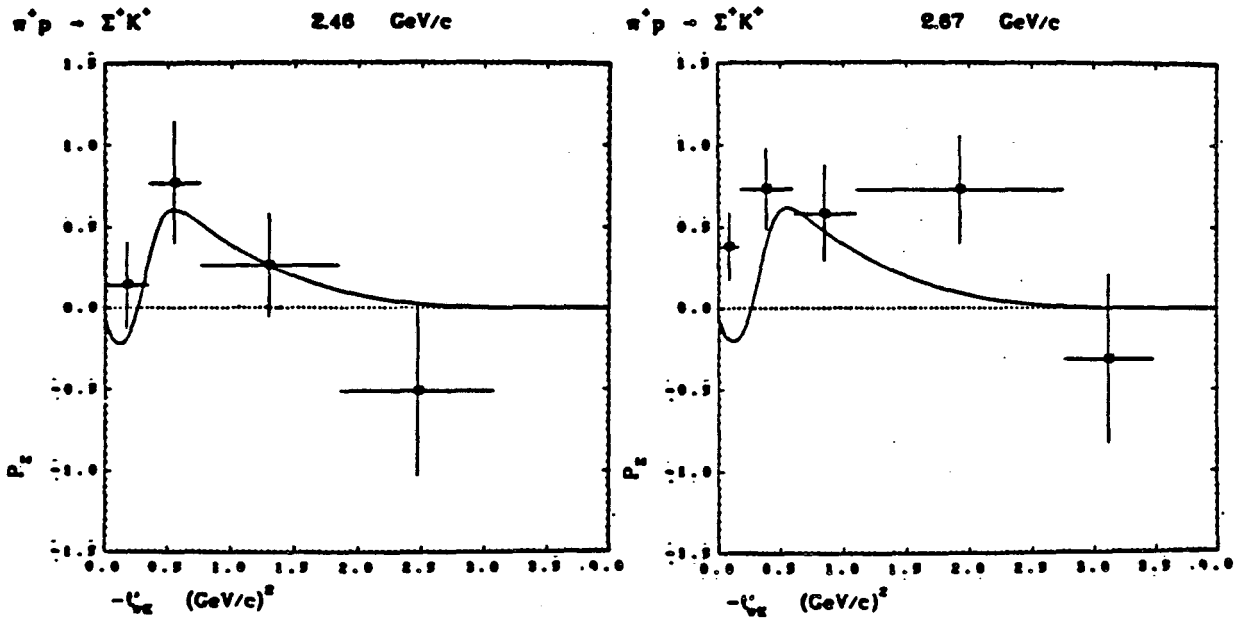

IV.6

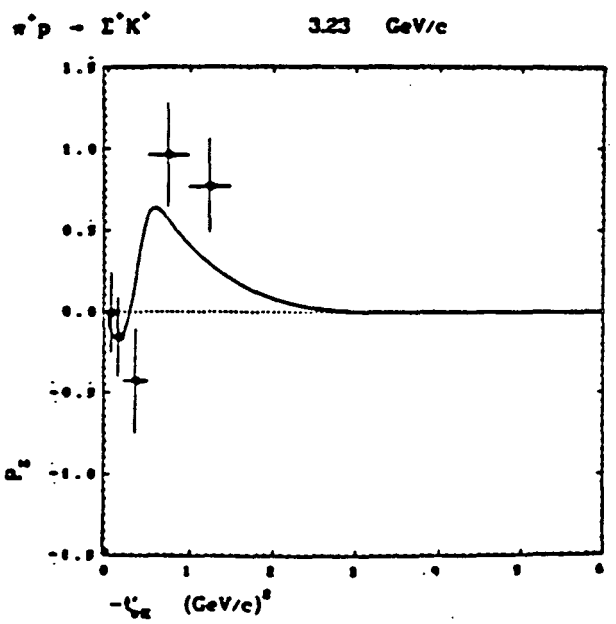

measured.

For $\cos\vartheta = \hat{n}\cdot\hat{p}_p$, with $\hat{p}_p$ in the Σ^+ rest frame ($\hat{n}$ is invariant under transformation from the overall C.M. to the Σ^+ rest frame), the simplest moment estimator of P_Σ is (see Solmitz, ref. 34):

$$P_\Sigma = \frac{1}{\alpha} 3 \langle\cos\vartheta\rangle = \frac{1}{\alpha}\frac{3}{N}\sum_i \cos\vartheta_i \qquad \text{(IV.A.2)}$$

where the sum is over all events in the given sample, $N = \sum_i$. Kofler et al. (ref. 35) observed that since detection efficiency for $\Sigma^+ \to p\pi^0$ is very low in the region $\hat{p}_\Sigma\cdot\hat{p}_p \approx 1$, i.e., $\hat{n}\cdot\hat{p}_p = (\hat{p}_{p'}\times\hat{p}_\Sigma)\cdot\hat{p}_p \approx 0$, for the 1st moment estimator the numerator $\sum_i \cos\vartheta_i = \sum_i (\hat{n}\cdot\hat{p}_p)_i$ is not greatly different from its value for 100% $\Sigma^+ \to p\pi^0$ detection efficiency, but the denominator $N = \sum_i$ *is* biased by loss of events. Bangerter (ref. 36) has shown that a simple remedy is to use the ratio-of-moments (r.o.m.) estimator:

$$P_\Sigma = \frac{1}{\alpha}\frac{\langle\cos\vartheta\rangle}{\langle\cos^2\vartheta\rangle} = \frac{1}{\alpha}\frac{\sum_i \cos\vartheta_i}{\sum_i \cos^2\vartheta_i} \qquad \text{(IV.A.3)}$$

since $\langle\cos^2\vartheta\rangle = \frac{1}{3}$ will be formally valid provided the detection bias is an even function of $\cos\vartheta$. At the 5 higher momenta we have compared the 1st moment estimator with the r.o.m. estimator, and found no significant differences; we use the r.o.m. estimator because it is no more difficult to compute. All P_Σ values at the 9 lower momenta are 1st moment estimates, and all P_Σ values at the 5 high momenta are r.o.m. estimates. All errors shown on $\frac{d\sigma}{dt}$ and P_Σ are statistical.

The principal features of $\frac{d\sigma}{dt}$ are: a strong forward peak for all p_{inc}; a minimum or break at $|t| \approx 0.4\ (GeV/c)^2$ at all $p_{inc} > 1.5\ GeV/c$; and a

pronounced backward peak for $p_{inc} > 1.5\ GeV/c$. Near $p_{inc} \approx 1.55$, which corresponds to the formation energy for the $\Delta(1950)$, the central regions have a complicated dip and peak structure, but for $p_{inc} \geq 2\ GeV/c$ the central regions are highly suppressed with simple fixed-t (or fixed-u) features. For comparison figure IV.3 also displays the 3.23 GeV/c Σ^+K^+ data of Kofler (ref. 35), the 3.7 data of Butler (ref. 21), and the 5 GeV/c data of Toet et al. (ref. 19). The main features of their data appear also in ours for $p_{inc} \geq 2\ GeV/c$.

For $p_{inc} > 1.4$, P_Σ is generally small or negative in the forward region near $t \approx t_{min}$, large and positive in the middle region, and small or negative in the backward direction; generally there is a crossover in the forward region at $|t| \approx 0.4\ (GeV/c)^2$, corresponding to the dip in $\frac{d\sigma}{dt}$. The forward features of P_Σ are seen at higher energies such as in refs. 16,67, while the backward behavior is similar to that in the 3.5 GeV/c P_Σ data of Bradamante et al., ref. 37.

The slopes b and intercepts A from fits to the forward peaks in $\frac{d\sigma}{dt}$ of form

$$\frac{d\sigma}{dt} = Ae^{bt} \ ,$$

are shown in figures IV.7,8 which display our values of $A = \left.\frac{d\sigma}{dt}\right|_0$ and b along with the available world data from the PDG compilation (ref. 12), and refs. 16, 19, and 67. $\left.\frac{d\sigma}{dt}\right|_0$ peaks approximately at the $\Delta(1950)$ and falls sharply to $p_{inc} \approx 2\ GeV/c$, and then declines roughly in a power-law, which one would expect of Regge behavior; b also shows a peak at the $\Delta(1950)$ and then a possible slow rise in p_{inc} or s. Again, if ΣK is Regge-like at higher p_{inc}, one would

$\pi^+ p \rightarrow \Sigma^+ K^+$

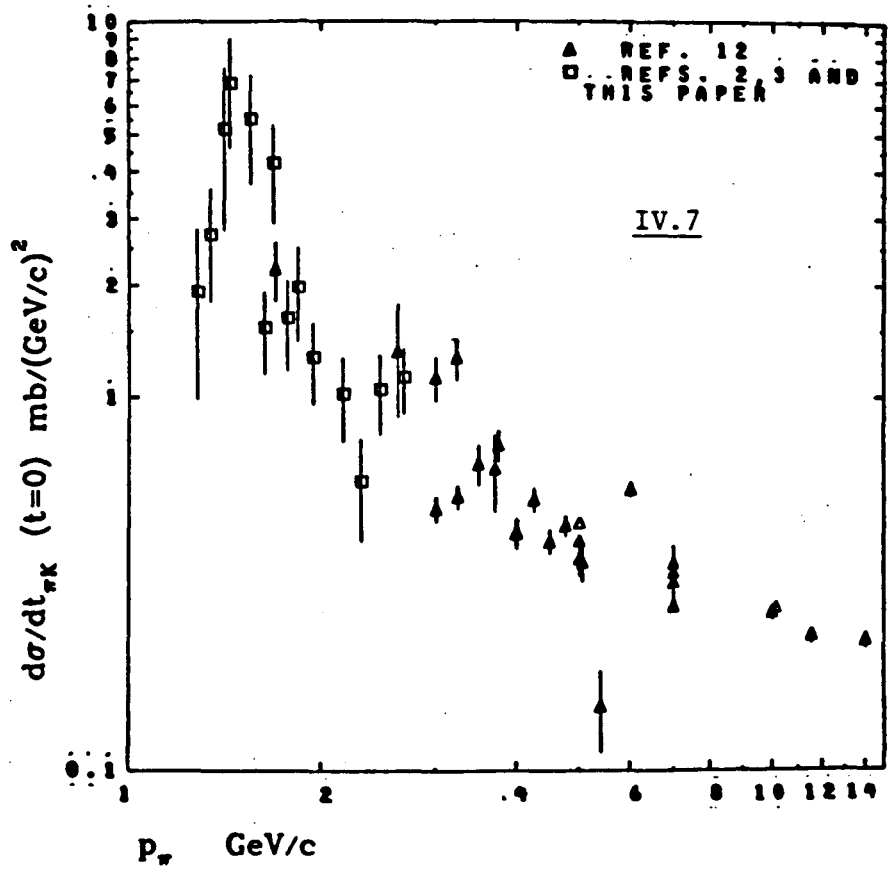

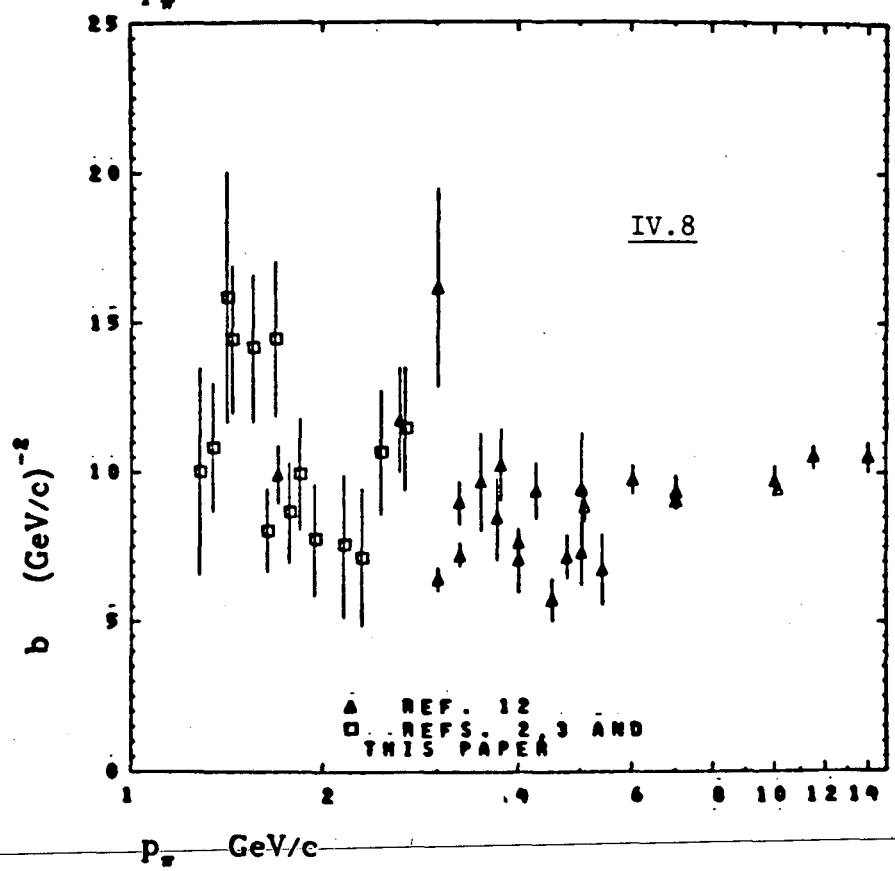

expect an $\ln s$ rise in b (Regge shrinkage).

For a $0^-\frac{1}{2}^+ \to 0^-\frac{1}{2}^+$ process like $\pi^+p \to \Sigma^+K^+$, after taking parity conservation into account, there are two independent Lorentz invariant (s- or t-channel) helicity amplitudes H_{++} and H_{+-}, where the subscripts denote the initial and final baryon helicities $\pm\frac{1}{2}$. In terms of H_{++} and H_{+-} (see, e.g., Barger and Cline, ref. 31) the observables $\frac{d\sigma}{dt}$ and P are given by the well-known relations:

$$\frac{d\sigma}{dt} = |H_{++}|^2 + |H_{+-}|^2 \qquad \text{(IV.A.4)}$$

and

$$P\,\frac{d\sigma}{dt} = -2\,\mathrm{Im}(H_{++}H_{+-}^*) \qquad \text{(IV.A.5)}$$

Angular momentum conservation requires as $t \to t_{min}$, $H_{+-} \to 0$ (again, see ref. 31) so that in the very forward direction, only H_{++} contributes to $\frac{d\sigma}{dt}$; the sharp forward peaks of the Σ^+K^+ data indicate the channel is dominated by H_{++} near t_{min}. This behavior is typical of the channel at much higher energies (cf. refs. 12,16,67) and persists down into the low and intermediate energies of these data. May et al., ref. 59, see the same forward region behavior at the highest momenta yet available, the 35, 70, and 140 GeV/c FNAL data. The dip or break at $-t = 0.4$ in particular is a constant feature over the entire range from our momenta to that of May et al.

2. Comparisons with $\pi^- p \to K^0\Sigma^0, K^+\Sigma^-$

In the forward and backward regions the reaction

$$\pi^+ p \to \Sigma^+ K^+ \tag{IV.A.6}$$

is related by isospin of the t- and u-channel exchanges to the reactions

$$\pi^- p \to K^0\Sigma^0 \tag{IV.A.7}$$

$$\pi^- p \to K^+\Sigma^- . \tag{IV.A.8}$$

For (IV.A.6) and (IV.A.7) in the forward region both $I = \frac{1}{2}$ and $\frac{3}{2}$ exchanges are possible, whereas for (IV.A.8) the exchange must be $I = \frac{3}{2}$. If only $SU(3)$ octet quantum numbers are exchanged (no exotic exchange), then $I = \frac{3}{2}$ exchange cannot occur as a single process, but must proceed through multiple exchanges (such as cut contributions). The high energy data of Akerlof, Bashian (ref. 38) show that forward $\pi^- p \to K^+\Sigma^-$ scattering is small, so that $I = \frac{3}{2}$ exchange is negligible. If only $I = \frac{1}{2}$ exchange occurs, t-channel isospin yields for forward cross-sections the well-known relation:

$$\frac{d\sigma}{dt}(\pi^+ p \to \Sigma^+ K^+) = 2\,\frac{d\sigma}{dt}(\pi^- p \to K^0\Sigma^0) \tag{IV.A.9}$$

For (IV.A.6) and (IV.A.8) in the backward region, $I = 0$ and 1 exchange is possible, while for (IV.A.7) only $I = 1$ can occur. The data of Dahl (ref. 39) for $\pi^- p \to K^0\Sigma^0$ show very small backward cross sections for $p_{inc} > 2\ GeV/c$, so that presumably u-channel HYCEX is mainly $I = 0$.

The relationship (IV.A.9) has been found to hold well at higher energies by Ward (5 GeV/c), ref. 40, and Berglund (7 GeV/c), ref. 67. Figure IV.9 shows our 1.77, 1.84, 1.94, 2.15, 2.3, 2.46, 2.67 GeV/c Σ^+K^+ data along with the 3.0

GeV/c $K^0\Sigma^0$ data of Ward (ref. 40), the $K^+\Sigma^-$ data of Dahl (ref. 39), and the $K^0\Sigma^0$ data of Hart (ref. 40). We also compare the data of Butler (ref. 21), 3.7 GeV/c, with the 4 GeV/c Σ^0K^0 data of Ward, and the new 3.95 GeV/c Σ^0K^0 data of Loverre, ref. 32. The 3.0 GeV/c data of Ward has been scaled to 2.67 GeV/c by fitting their 3, 4, 5, 6, 8, 10.7, 15.7 GeV/c $K^0\Sigma^0$ integrated peripheral cross section compilation to a power law in p_{inc}, and all $K^0\Sigma^0$ data has been multiplied by 2. The low energy Σ^0K^0 data of Hart have been similarly scaled to our momenta where necessary using a fit to the low momenta Σ^0K^0 cross sections, the 3.95 and 4 Σ^0K^0 data have been scaled to 3.7, and all $K^+\Sigma^-$ data of Dahl have been scaled where appropriate using their fit to a world data compilation. Clearly at all momenta $I = \frac{1}{2}$-only t-channel exchange seems to hold well even at these modest energies. At 2.67 GeV/c the backward Σ^+K^+ and Σ^-K^+ cross sections are in excellent agreement, and the 2.6 Σ^0K^0 data of Dahl (not shown) has a negligible backward hemisphere cross section of $\sim 3\mu b$, all of which agrees with I = 0-only u-channel HYCEX. By 1.77, 1.84, however, the backward Σ^0K^0 and Σ^-K^+ cross sections are comparable and smaller than Σ^+K^+.

In figure IV.10, we display the backward hemisphere ($\cos\vartheta_{CM} \leq 0$) integrated cross sections σ_B for $\pi^+p \to \Sigma^+K^+$ from our data and the data of Kofler, Butler, Toet, and Cooper (refs. 35,21,19,47); the line drawn on figure IV.10 represents a fit of form $\sigma_B = Ap_\pi^{-b}$. We find that $b \approx 4$ as expected for baryon Regge exchange processes. In particular we note that Dahl (ref. 39) finds that the channel cross section for $\pi^-p \to \Sigma^-K^+$ (which is nearly all backward hemisphere) follows a p_π^{-4} power law.

$\pi^+ p \rightarrow \Sigma^+ K^+$

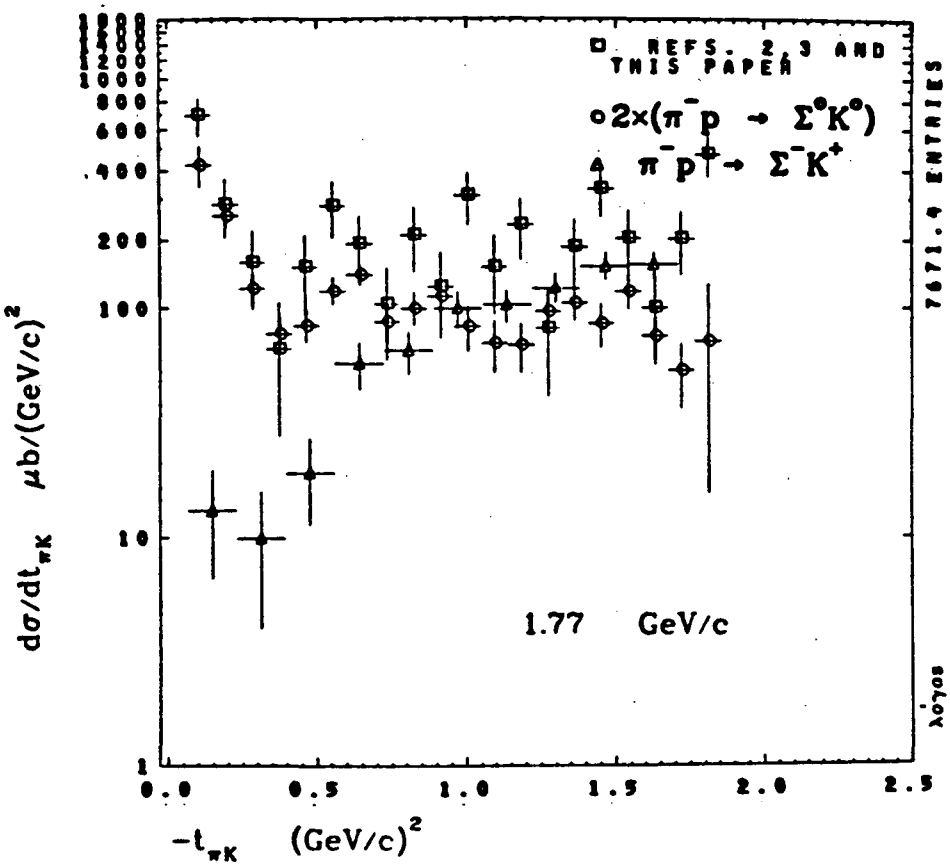

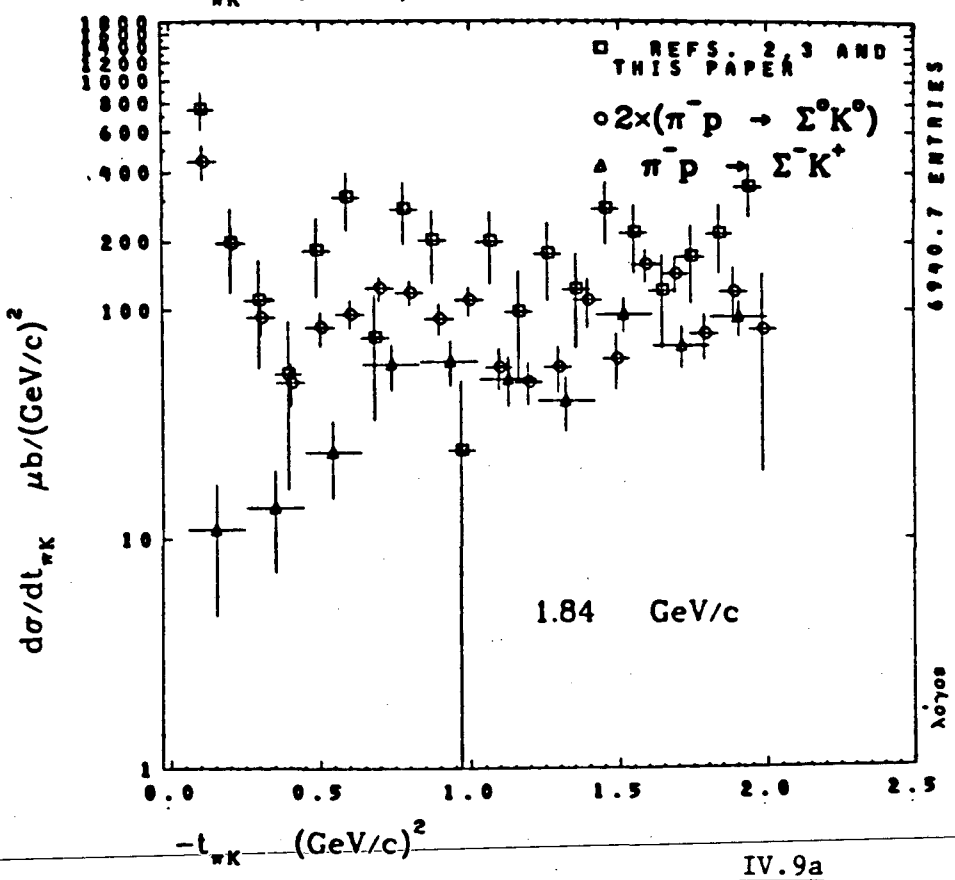

IV.9a

$\pi^+ p \rightarrow \Sigma^+ K^+$

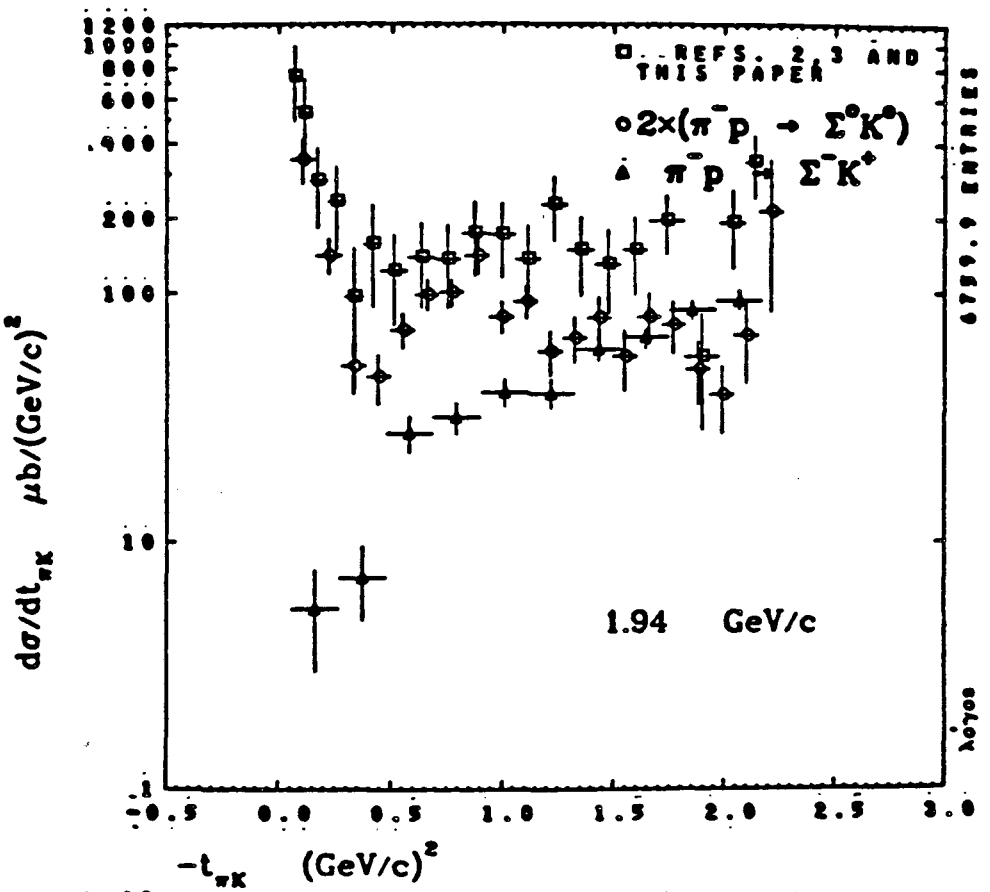

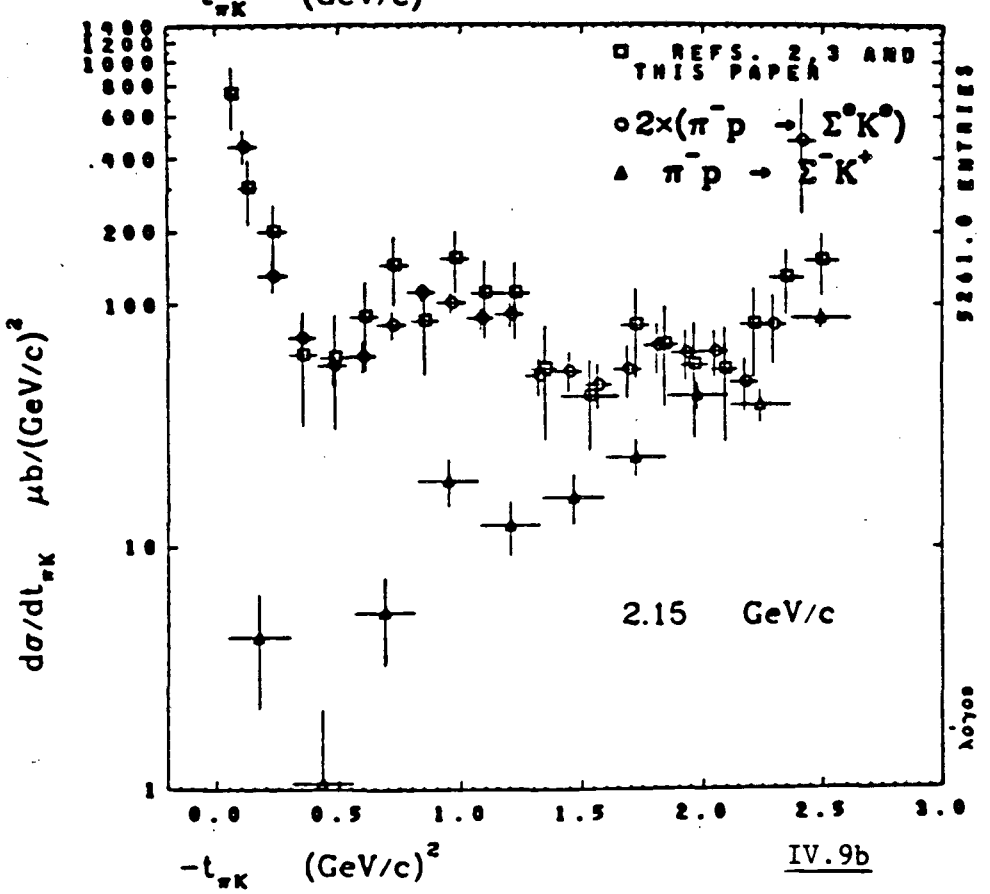

IV.9b

$\pi^+ p \rightarrow \Sigma^+ K^+$

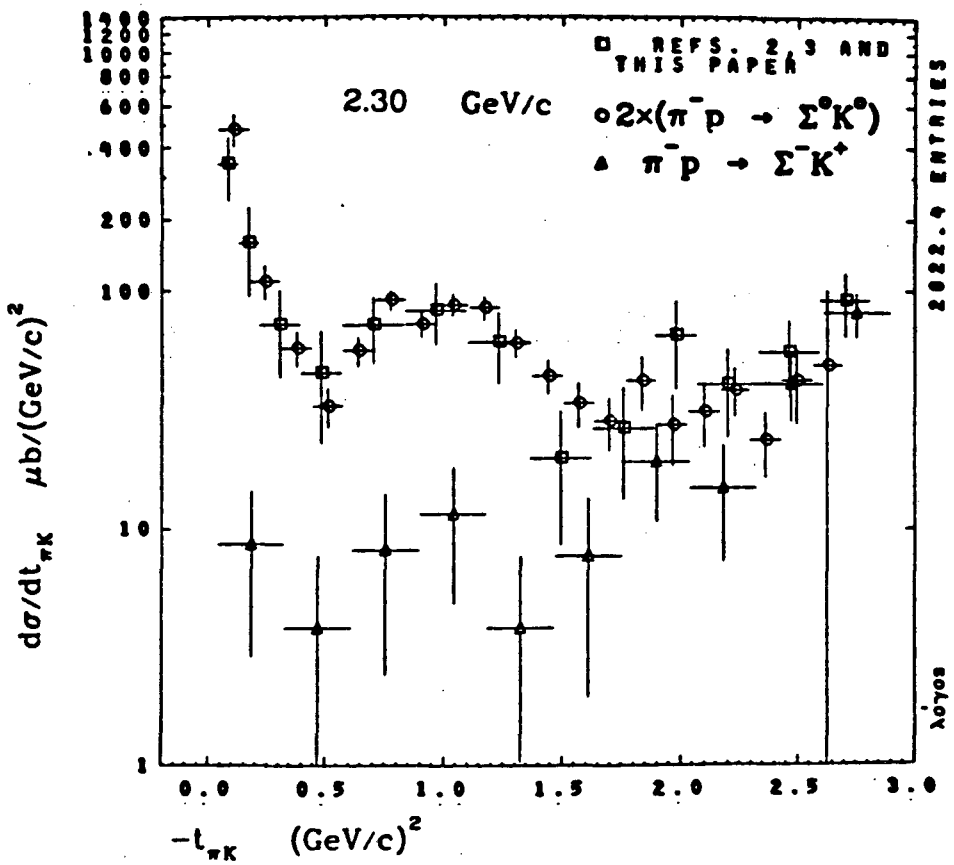

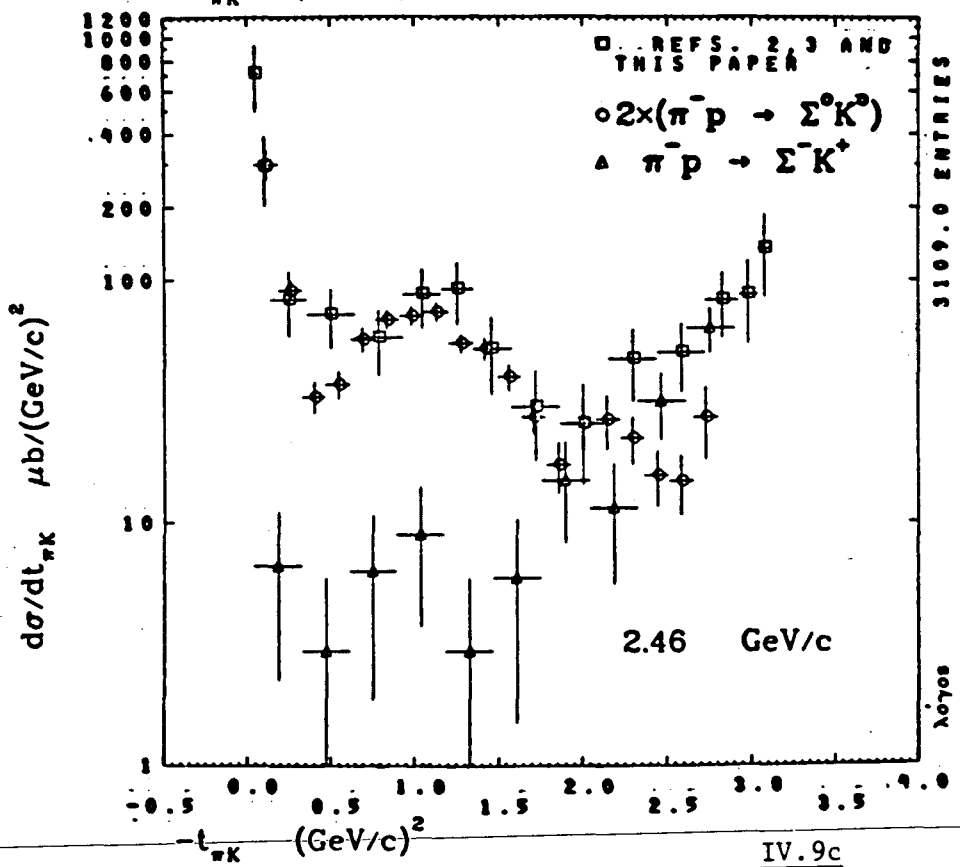

IV.9c

$\pi^+ p \rightarrow \Sigma^+ K^+$

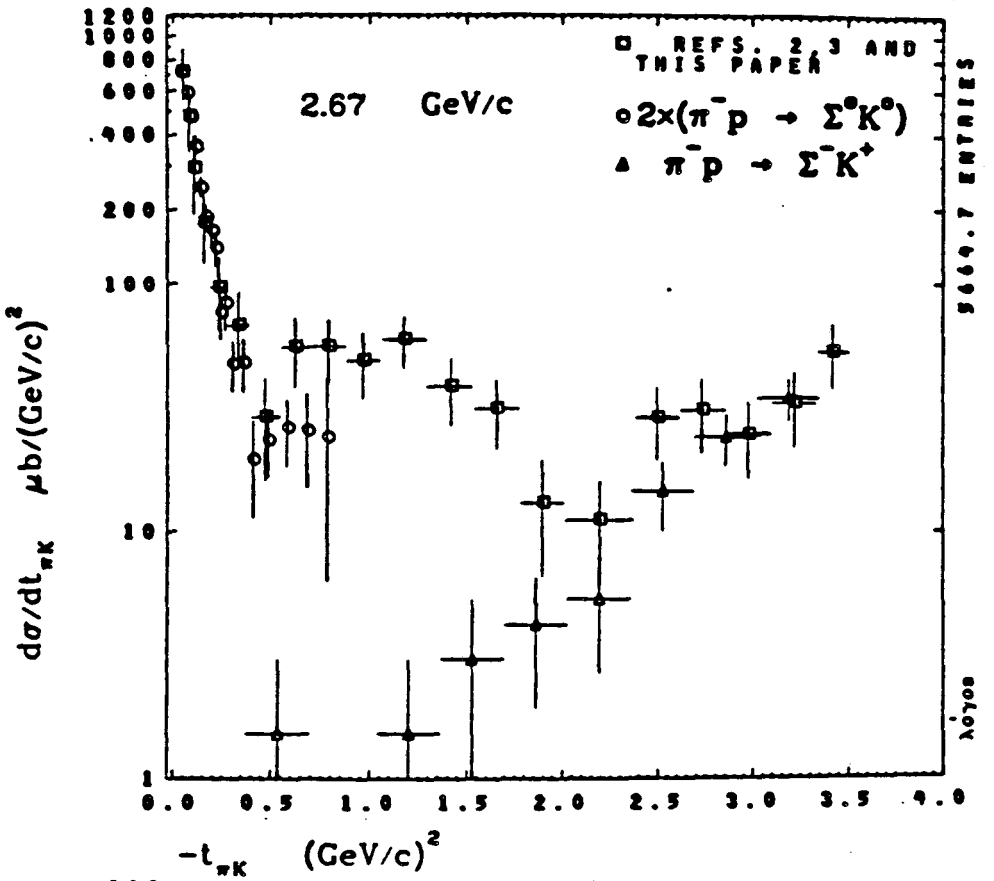

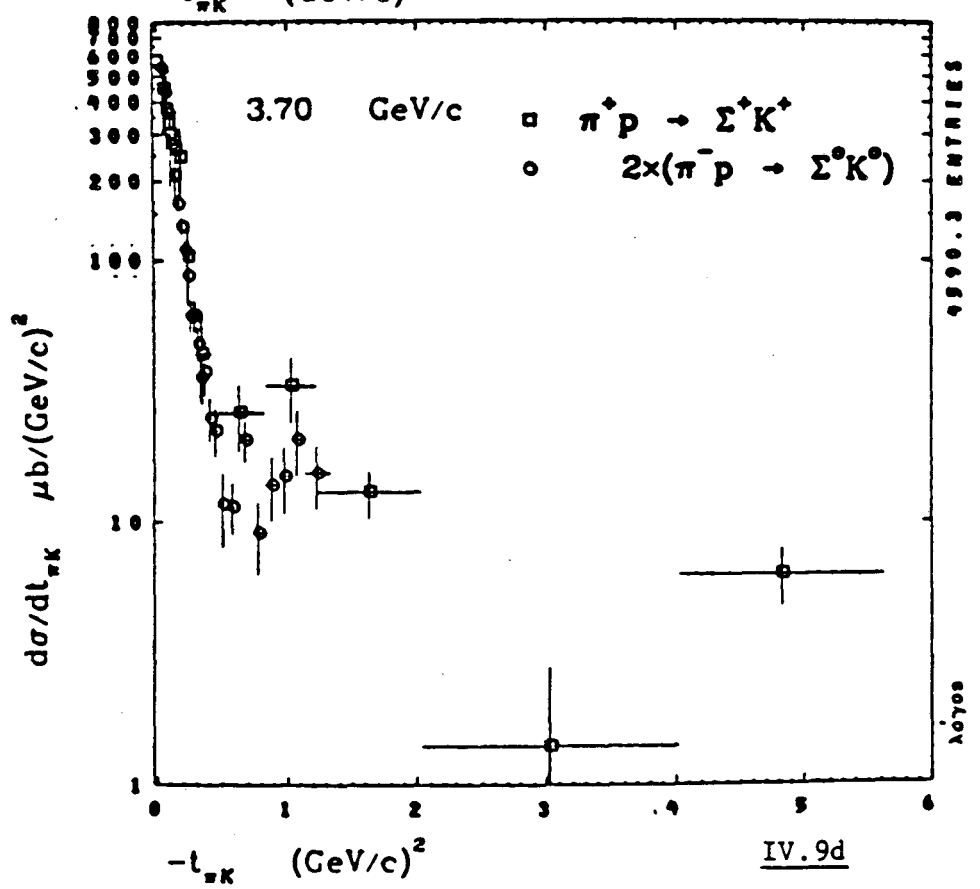

IV.9d

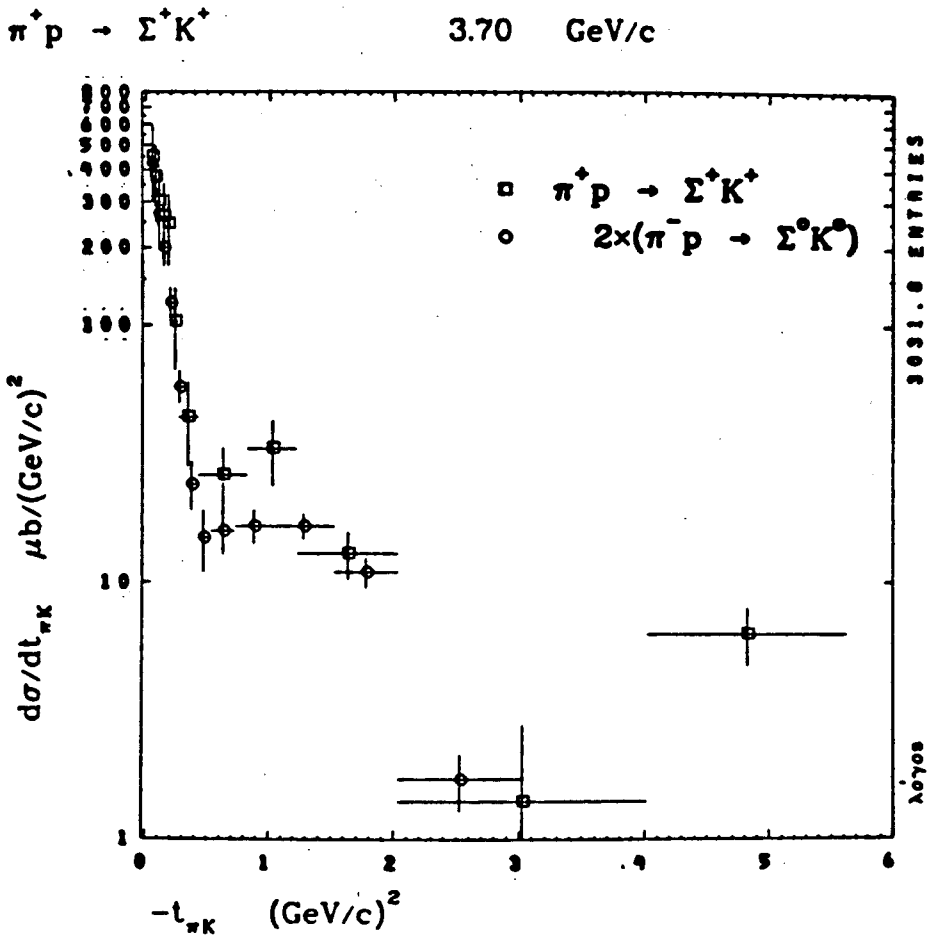
π⁺p → Σ⁺K⁺
3.70 GeV/c
π⁺p → Σ⁺K⁺
2×(π⁻p → Σ⁰K⁰)
dσ/dt_πK μb/(GeV/c)²
−t_πK (GeV/c)²
3031.0 ENTRIES
λόγος

IV.9e

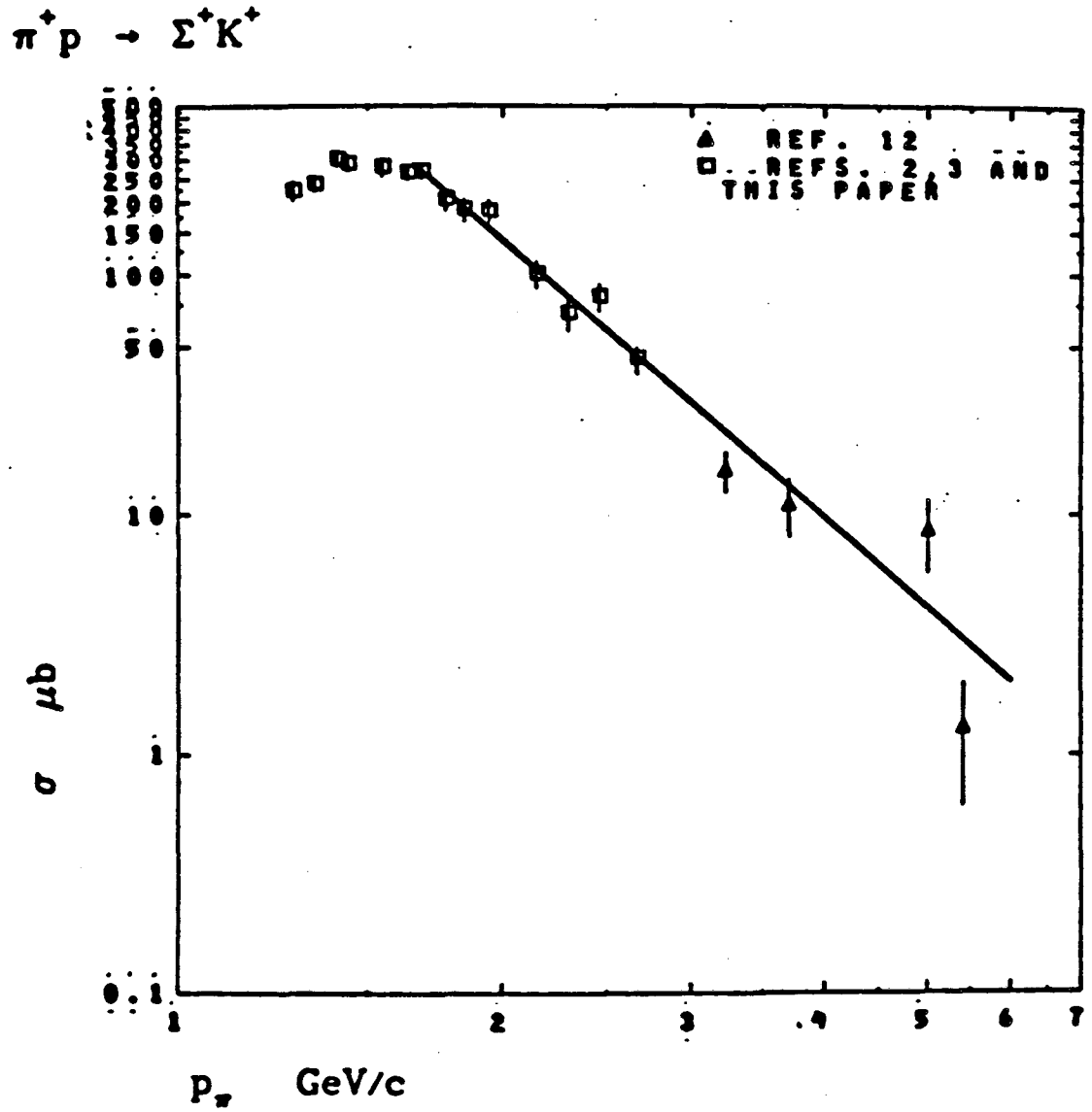
$\pi^+ p \rightarrow \Sigma^+ K^+$
▲ REF. 12
□ REFS. 2, 3 AND THIS PAPER
σ μb
p_π GeV/c

IV.10

3. Amplitude Analysis Models for HYCEX and Weak Exchange Degeneracy

For $\pi^+p \to \Sigma^+K^+$, Regge phenomenology describes the amplitudes at high energy in the forward region as a sum of Regge pole exchanges, each of which contributes to H_{++}, H_{+-} terms (see Barger and Cline, ref. 31) of form (we ignore for now absorptive and cut contributions):

$$K_{++} = f_{++}(t)[\tau + e^{-i\pi\alpha(t)}]\left(\frac{s}{s_0}\right)^{\alpha(t)}$$
$$K_{+-} = \sqrt{-t'}\, f_{+-}(t)[\tau + e^{-i\pi\alpha(t)}]\left(\frac{s}{s_0}\right)^{\alpha(t)} \qquad \text{(IV.A.10)}$$

Here $\alpha(t)$ is the exchanged trajectory, $f_{++}(t), f_{+-}(t)$ the residues of the particular exchange, and τ, the signature factor, = +1 (-1) for even (odd) signature exchanges; s_0 is a scale parameter. For the vector K^*, $\tau = -1$; $\tau = +1$ for the tensor K^{**}. The phase is entirely specified by $(\tau + e^{-i\pi\alpha(t)})$, and the energy dependence is in the $s^{\alpha(t)}$ factor (except for a $\frac{1}{p_{CM}\sqrt{s}} \approx \frac{1}{s}$ dependence of f_{++}, f_{+-}). Thus we expect, since for this process unnatural J^P exchange (in particular, pseudoscalar K) is forbidden, and ignoring non-pole terms, the amplitudes are:

$$H(\pi N \to \Sigma K) = K^* + K^{**}$$

where K^*, K^{**} each have the form (IV.A.10) above. The line reversed process $(K^-p \to \pi^-\Sigma^+)$ in the forward region has, similarly:

$$H(\bar{K}N \to \Sigma\pi) = -K^* + K^{**}$$

since the odd signature K^* changes sign under line reversal (see Appendix A).

The K^* and K^{**} are strong exchange degenerate (EXD) if $f_{K^*} = f_{K^{**}}$ and $\alpha_{K^*} = \alpha_{K^{**}}$, and one gets the predictions for the forward region:

$$\frac{d\sigma}{dt}(\pi N \to \Sigma K) = \frac{d\sigma}{dt}(\bar{K}N \to \Sigma\pi)$$

and (IV.A.11)

$$P(\pi N \to \Sigma K) = P(\bar{K}N \to \Sigma\pi) = 0\,.$$

Weak exchange degeneracy (WEXD) holds if $\alpha_{K^*} = \alpha_{K^{**}}$ but $f_{K^*} \neq f_{K^{**}}$, whence:

$$\frac{d\sigma}{dt}(\pi N \to \Sigma K) = \frac{d\sigma}{dt}(\bar{K}N \to \Sigma\pi)$$

and (IV.A.12)

$$P(\pi N \to \Sigma K) = -P(\bar{K}N \to \Sigma\pi)\,.$$

Under line reversal alone, without assuming WEXD or EXD (i.e., $\alpha_{K^*} \neq \alpha_{K^{**}}$ and $f_{K^*} \neq f_{K^{**}}$), one predicts only:

$$P(\pi N \to \Sigma K)P(\bar{K}N \to \Sigma\pi) < 0 \;\text{ or }\; P(\Sigma K)\,\frac{d\sigma}{dt} = -P(\Sigma\pi)\,\frac{d\sigma}{dt}\,. \quad \text{(IV.A.13)}$$

Thus the mere fact of opposite signs for P in πN and $\bar{K}N$ channels does not imply WEXD, since (IV.A.13) follows from line reversal alone; this consideration does not seem to be sufficiently appreciated in the literature. For WEXD, we must have $P(\pi N) = -P(\bar{K}N)$. (For a detailed review of all the preceding, see Appendix A.)

Since at all incident momenta, $P_\Sigma \neq 0$, we *can* conclude that EXD does not hold. Recent measurements of $\pi N \to \Sigma K$ and $\bar{K}N \to \Sigma\pi$ in the same detector by Baker et al. (7,11.5 GeV/c), ref. 16, and Berglund et al. (7,10.1 GeV/c), ref. 67, indicate that WEXD (IV.A.12) holds well at high energy. WEXD seems to be violated at $p_{inc} \leq 4\ GeV/c$ (see the reviews of Navelet and Stevens, ref. 41, and Ward, ref. 42). The P_Σ data of refs. 16,67 do show the expected mirror symmetry of WEXD. May et al. (70 GeV/c) find some WEXD breaking at the highest momentum yet studied.

Navelet and Stevens (NS), ref. 41, formulated a typical Regge model for HYCEX amplitudes of the form:

$$H_{++} = K^{*}_{++} + K^{**}_{++} + K^{*}_{c} + K^{**}_{c}$$
$$H_{+-} = K^{*}_{+-} + K^{**}_{+-} \qquad \text{(IV.A.14)}$$

where K^{*}, K^{**} are basically WEXD pole amplitudes like (IV.A.10), and K^{*}_{c}, K^{**}_{c} are effective cut terms necessary in H_{++} to parameterize the absorptive and Regge cut contributions which lead, among other things, to WEXD breaking; K^{*}_{c}, K^{**}_{c} have the form of pole amplitudes, but with a trajectory of smaller intercept and slope than $\alpha_{K^{*}, K^{**}}$. At high energies, NS note, cut and absorptive corrections have long been known to be significant mainly for the non-flip amplitude, while the flip amplitudes seem to be closer to pure Regge poles. Navelet and Stevens determined the model parameters (residues and trajectories) by fitting most then available (1976) data for $\pi N \to \Sigma K$, $\pi N \to \Lambda K$, $\bar{K}N \to \Sigma\pi$, $\bar{K}N \to \Lambda\pi$ from $p_{inc} = 4\ GeV/c$ to $p_{inc} = 16\ GeV/c$ and $-t \approx 0-1.5(GeV/c)^2$. The curves drawn on $\frac{d\sigma}{dt}$ and P_{Σ} in figures IV.1-IV.6 are the (absolute) predictions of the NS amplitudes for ΣK, and we observe that their high energy formalism fits the data well, down even into the $\Delta(1950)$ region. Specifically:

(a) For $p_{inc} > 1.7\ GeV/c$ NS describe the forward peak well, though the data slopes are slightly steeper; not surprisingly, for $p_{inc} < 1.7$ the slopes are increasingly steeper than the model as one approaches the $\Delta(1950)$; the dip at $-t \approx 0.4$, which corresponds to the wrong-signature-nonsense-zero (WSNZ) of the amplitudes, where $\alpha_{K^{*}} \approx \alpha_{K^{**}} \approx 0$, is described well at all p_{inc}.

(b) For $p_{inc} > 2\ GeV/c$ the central region of $\frac{d\sigma}{dt}$ is well described even out beyond 90° in the C.M.; for $p_{inc} < 2\ GeV/c$ the model describes the *average* behavior of $\frac{d\sigma}{dt}$ nearly out to the backward peak, in accord with duality expectations for high energy amplitudes extrapolated to low energies.

(c) For P_Σ the NS predictions are qualitatively good for $p_{inc} > 1.5$ – the crossover at $t \sim 0.3-0.4(GeV/c)^2$, corresponding to the WSNZ, appears at most momenta, and away from $t \approx t_{min}$, P_Σ is positive, although larger than the NS prediction.

We thus conclude that forward $\pi^+p \to \Sigma^+K^+$ is Regge-like down to within a few hundred MeV/c of the $\Delta(1950)$, as one might expect from the weak coupling of s-channel Δ formation to ΣK; NS also describe the 3.23, 3.7, and 5.0 data well, on which the NS model had not been previously tested.

Further, we have examined the NS predictions for WEXD breaking at our energies; in figures IV.11,IV.12 we show our 2.46, 2.30, 2.15, 1.94, 1.84, 1.77 Σ^+K^+ data with the $K^-p \to \Sigma^+\pi^-$ data of De Bellefon and Berthon, ref. 43, at 2.516, 2.331, 2.135, 1.934, 1.842, 1.741 GeV/c, as well as NS predictions for both channels. We also show the NS predictions for P_Σ at 2.3 GeV/c. Clearly, WEXD is violated, but the NS model describes the breaking in $\frac{d\sigma}{dt}$ very well even at the lower p_{inc}. The NS model has also been tested on very recent ΣK data by Loverre (ref. 32), 3.95 GeV/c, Baker (ref. 16), 7,11.5 GeV/c, and Berglund (ref. 67), 7,10.1 GeV/c; at all these momenta, the NS amplitudes give an excellent qualitative description of both the ΣK data and the WEXD breaking in the $\bar{K}N$ data, although most authors refitted the NS parameters to get

$\pi^+ p \rightarrow \Sigma^+ K^+$

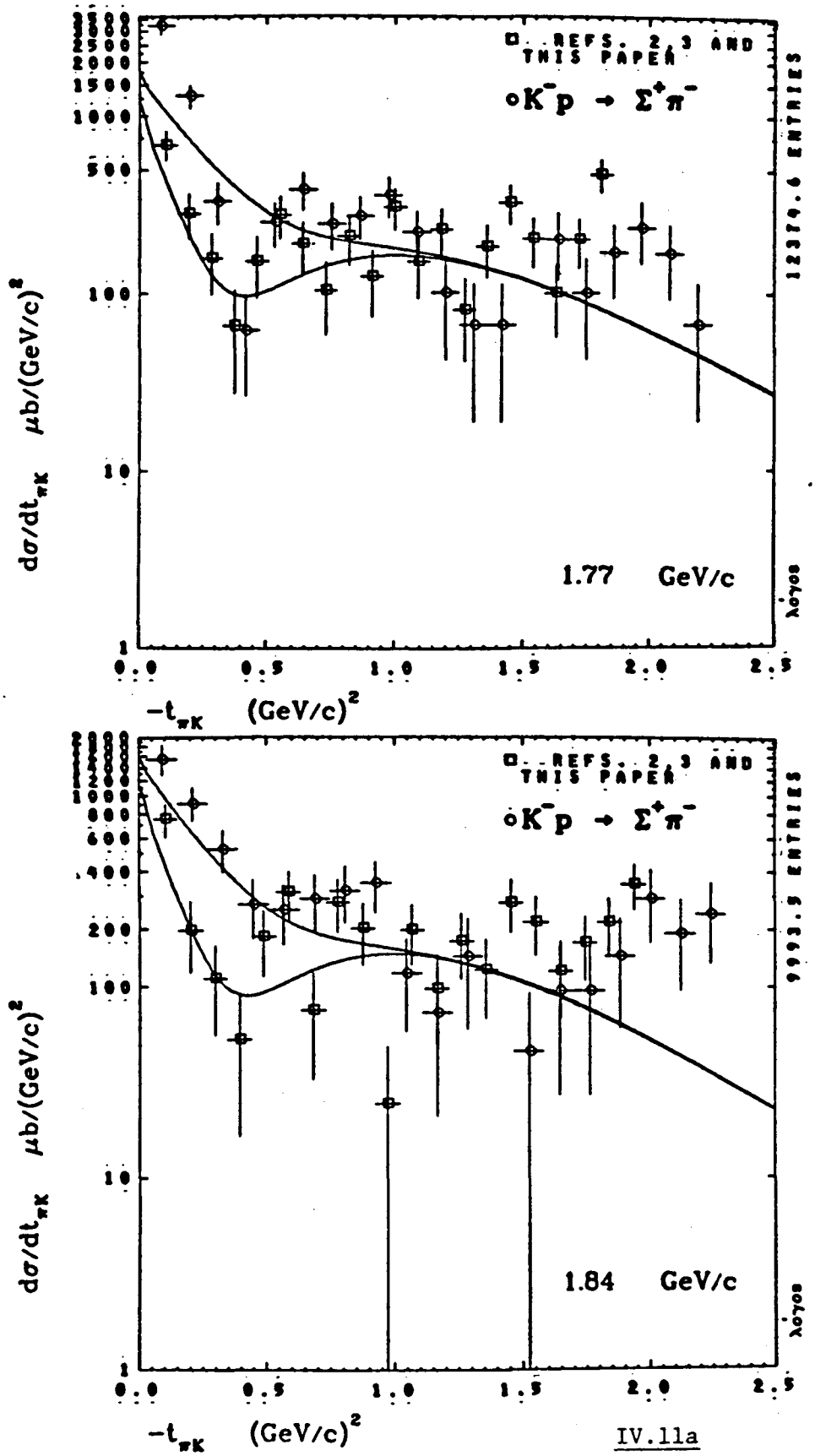

IV.11a

$\pi^+ p \rightarrow \Sigma^+ K^+$

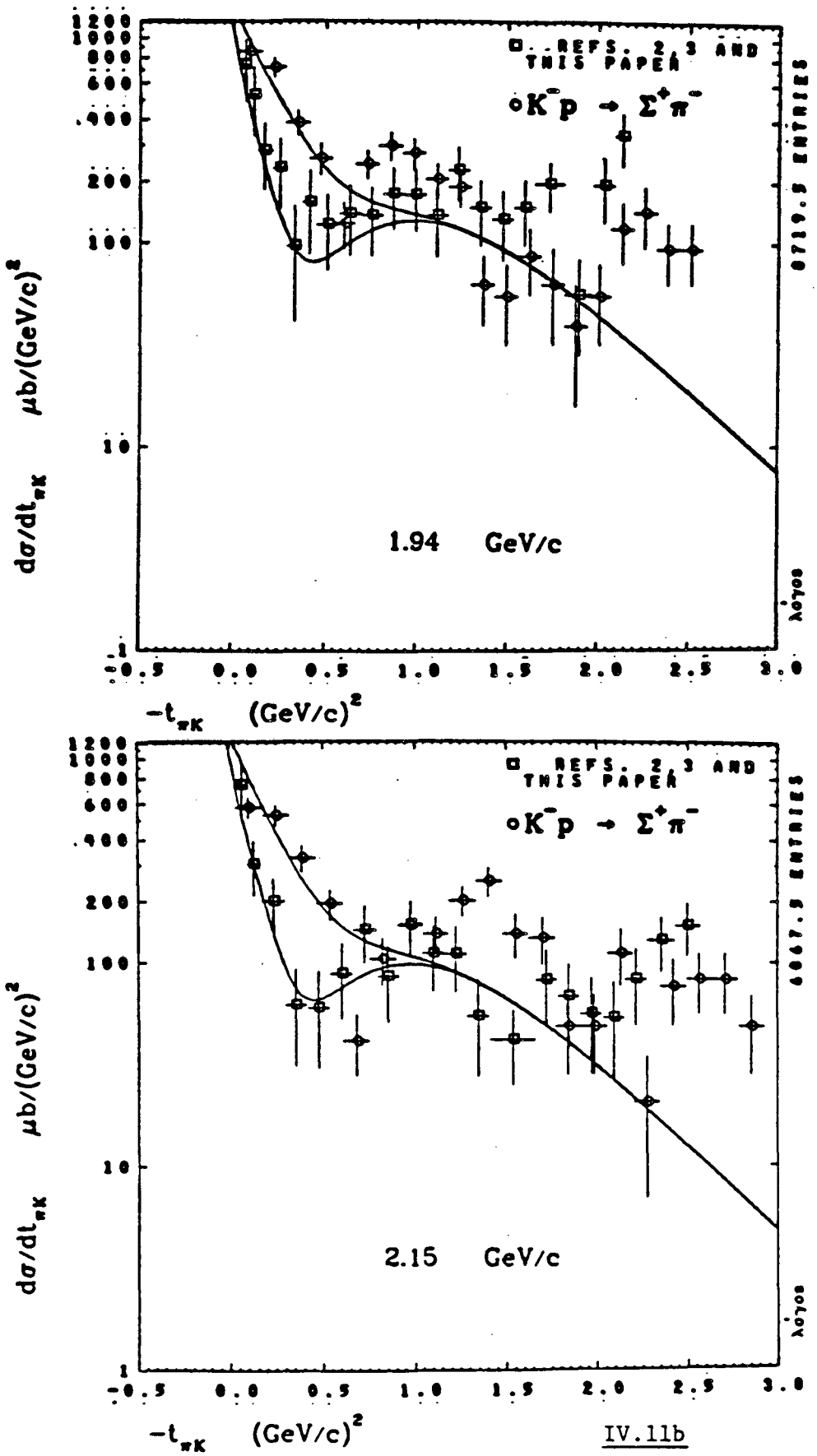

IV.11b

$\pi^+ p \rightarrow \Sigma^+ K^+$

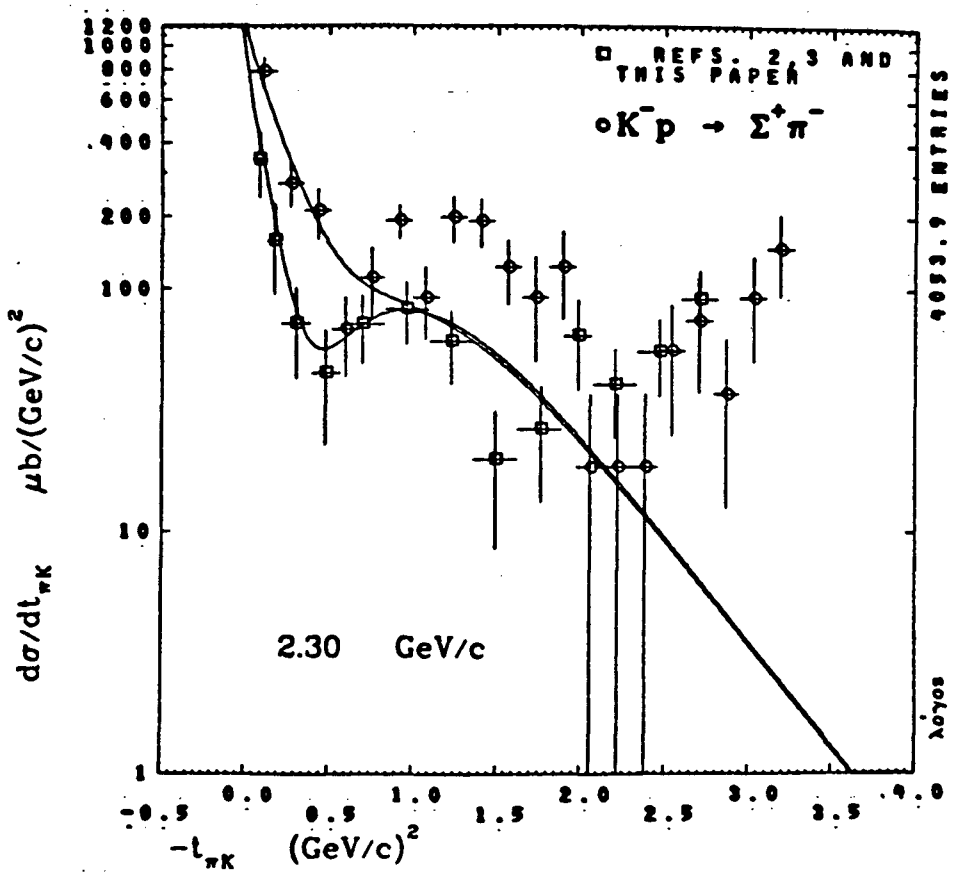

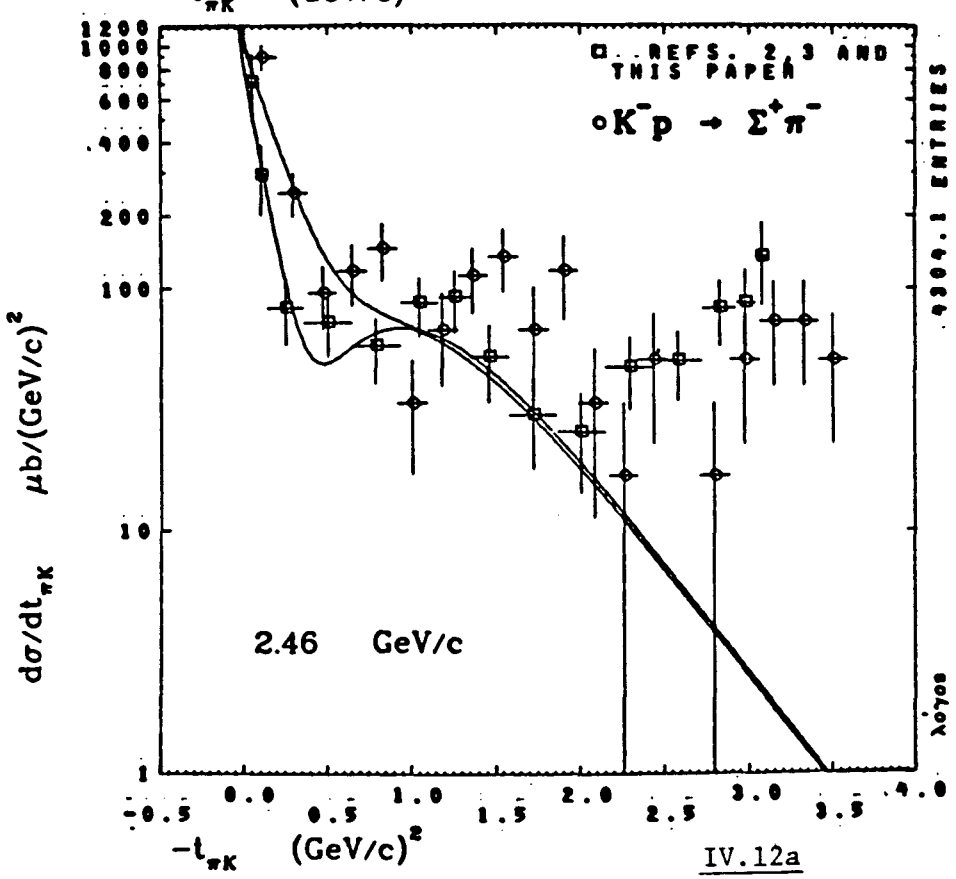

IV.12a

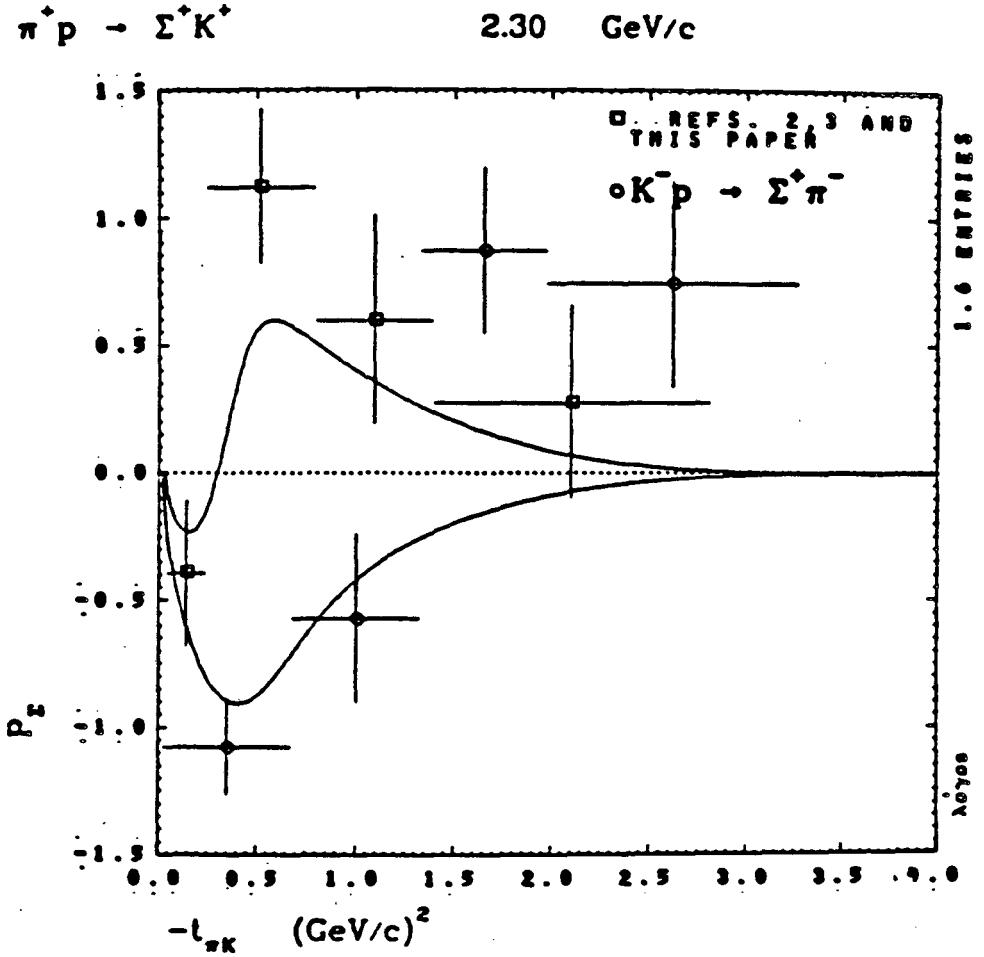
$\pi^+ p \to \Sigma^+ K^+$
2.30 GeV/c
□ REFS. 2,3 AND THIS PAPER
○ $K^- p \to \Sigma^+ \pi^-$
1.6 ENTRIES
SCALY
P^Σ
$-t_{\pi K}$ $(GeV/c)^2$

IV.12b

even better agreement with their data, which yielded slightly different residues and α's.

Finally, we observe that the opposite signs of P_Σ in figure IV.12b are in agreement with pole dominance of the $\pi p, \bar{K}p\Sigma^+$ poduction channels, although the poles are evidently not exactly WEXD (see Appendix).

We have compared $\frac{d\sigma}{dt}(\pi N \to \Sigma K)$ with $\frac{d\sigma}{dt}(\bar{K}N \to \Sigma\pi)$ at the same p_{inc}; at very high energy this is clearly appropriate. The energy dependence of a pure Regge pole $\frac{d\sigma}{dt}$ for $t \approx 0$ is

$$\frac{d\sigma}{dt} \sim \frac{1}{p_{CM}^2 s} s^{2\alpha(0)}$$

where p_{CM} is the C.M. momentum of the initial state. Thus with $\alpha(0) \approx .35$ for HYCEX, $\frac{d\sigma}{dt} \sim (p_{CM})^{-2}(\sqrt{s})^{-0.6}$. In our p_{inc} range, with $p_{inc}(\pi N) \approx p_{inc}(\bar{K}N)$, typically $p_{CM}(\bar{K}N) \approx .97\, p_{CM}(\pi N)$ and $\sqrt{s_{KN}} \approx 1.03\sqrt{s_{\pi N}}$, so that for a pure pole model we expect kinematics alone to yield EXD breaking of order

$$\frac{d\sigma}{dt}(\bar{K}N) \approx (.97)^{-2}(1.03)^{-0.6}\frac{d\sigma}{dt}(\pi N) \approx 1.04\,\frac{d\sigma}{dt}(\pi N)\,,$$

i.e., ~4% of the breaking is purely kinematic, which is much smaller than the observed (and predicted) breaking, as well as the statistical precision, and which justifies ignoring small differences in $\sqrt{s}$ when comparing at the same p_{inc}. NS parameterize f_{++}, f_{+-} in the usual way, $f \sim \frac{\gamma}{p_{CM}\sqrt{s}}$ where γ is the reduced residue; the model describes all $\pi N \to \Sigma K, \Lambda K$ and $\bar{K}N \to \Sigma\pi, \Lambda\pi$ HYCEX processes with 8 distinct γ's: one for each helicity (++,+-) for each exchange (K^*, K^{**}) for each hyperon (Λ, Σ).

Finally, NS observe that their K^*-K^{**} trajectories and amplitudes for HYCEX are very similar to results of $\rho-A_2$ analysis of πN and KN charge

exchange (CEX) except for the trajectory intercepts; NS find $\alpha_{K^*} = 0.375 + 0.678t$, $\alpha_{K^{**}} = 0.322 + 0.678t$, which is typical of HYCEX analyses (see next section on broken $SU(3)$ and flavor independence).

We note that NS have used the extreme asymptotic Regge dependence $s^{\alpha(t)}$ in their amplitudes; if we take Regge formalism as a serious theory rather than as a convenient high energy phenomenological parameterization, then partial wave expansion in the t-channel leads to asymptotic Regge s-dependence in eqs. (IV.A.10) of:

$$H(s,t) \sim (z_t)^{\alpha(t)} \sim \left(\frac{s-u}{2}\right)^{\alpha(t)} = \left(s + \frac{t-\Sigma m^2}{2}\right)^{\alpha(t)}$$

where $u \equiv (p_\pi - p_\Sigma)^2$, $s+t+u = m_\pi^2 + m_K^2 + m_p^2 + m_\Sigma^2 \equiv \Sigma m^2$, and z_t is the t-channel C.M. scattering angle (see section IV.B.2 for z_t as a function of s,t). The NS parameterization of the cut terms as s^{α_C} rather than the usual $\frac{s^{\alpha_C}}{(a+b\ln s)}$ is also ad hoc, so that we regard the NS model merely as an extremely successful phenomenological representation of HYCEX processes whose high energy features adequately characterize $\pi N \to \Sigma K$ and $\bar{K}N \to \Sigma\pi$, as well as WEXD breaking, down into the low and intermediate energy region.

The fact that Regge formalisms work well at relatively large t can be related to a constituent scattering picture for hadron interactions; see the review of Sivers, Brodsky, and Blankenbecler (ref. 46).

4. t-Channel $SU(3)$ and HYCEX,CEX Flavor Independence

The long- and well-known similarities between CEX and HYCEX support the view that they are different manifestations of the same dominant vector and tensor octet exchange processes (basically light-quark flavor independence of the strong interaction as embodied in $SU(3)_{flavor}$ symmetry for the t-channel exchanges in 2-body scattering). Thus the helicity amplitudes for forward $K^-p \to \bar{K}^0 n$ (CEX) and $\pi^+p \to K^+\Sigma^+$, $\pi^-p \to K^0\Lambda$ (HYCEX) are, using $SU(3)$ for the t-channel and following Martin, Michael, and Phillips (MMP), ref. 45:

$$\begin{aligned} H(K^-p \to \bar{K}^0 n) &= -(T+V) \\ H(\pi^+p \to K^+\Sigma^+) &= -\lambda(2F-1)(T+V) \\ H(\pi^-p \to K^0\Lambda) &= -\frac{1}{\sqrt{6}}\lambda(2F+1)(T+V) \end{aligned} \qquad \text{(IV.A.15)}$$

$$(\textit{helicities suppressed})$$

where V,T are the vector and tensor exchanges ρ, A_2, and K^*,K^{**}; F is the fraction of F-type $SU(3)$ meson-baryon octet coupling. H,F,T,V all carry helicity subscripts ++ or +−. The new addition in IV.A.15 to the standard $SU(3)$ relations between CEX,HYCEX amplitudes (which were long known to be violated by typically factors of 3, at least) is the λ factor: for exact $SU(3)$ we would have $|\lambda| = 1$, but empirically $|\lambda|$ is very different from unity. MMP use exact $SU(3)$ for vertices in IV.A.15 and attribute all the $SU(3)$ breaking to λ, which they take to be of Regge dynamical form:

$$|\lambda| = \left(\frac{s}{s_0}\right)^{-\Delta\alpha} \qquad \text{(IV.A.16)}$$

where $\Delta\alpha = \alpha(\rho,A_2) - \alpha(K^*,K^{**}) \approx m_{K^*}^2 - m_\rho^2 \approx 0.2$, and s_0 is a scale parameter. Thus IV.A.16 effectively ascribes all the $SU(3)$ breaking to the non-

strange/strange mass splitting, which is a consequence of non-degeneracy of the (p,n) and λ quark masses. *No* assumptions about the explicit forms of V,T are made, and IV.A.15 contains the following limited EXD assumptions:

(a) λ is the same for V,T;

(b) F is the same for V,T within each helicity amplitude. Also as a further simplifying assumption, we take the F's to be t-independent (see below), and in IV.A.16, $|\lambda|$ and $\Delta\alpha$ are taken as t-independent.

$SU(3)$ relations for $0^-\frac{1}{2}^+ \to 0^-\frac{1}{2}^+$ CEX only (no λ involved) have been used to derive CEX cross section sum rules such as the famous, successful Barger-Cline relation (see ref. 31); similar expressions for HYCEX only (again, no λ) lead to sum rules at the level of HYCEX cross sections which work fairly well, but expressions like IV.A.15, which relate CEX to HYCEX, have been used thus far (by MMP) only to derive sum rules at the level of ***amplitudes***, which lead to ***inequalities*** at the level of cross sections. This is because such inequalities (which are difficult to test empirically) allow the elimination of the F's from the expression: the magnitudes and t-dependence of the F's have not always been well known. However, by now many amplitude analyses have been performed (such as the *NS* fit, ref. 41) and all agree that $F_{++} \approx \frac{3}{2}$ and $F_{+-} \approx \frac{1}{4}$. Also F_{++}, F_{+-} are approximately t-independent. Thus we now use IV.A.15 to derive a new (F ratio-dependent) broken $SU(3)$ sum rule for CEX and HYCEX cross sections. We write for brevity

$$H_+ \equiv H_{++} = V_{++} + T_{++} \ , \ H_- \equiv H_{+-} = V_{+-} + T_{+-} \ , \ F_+ \equiv F_{++} \ , \ F_- \equiv F_{+-}$$

so that IV.A.15 gives

$$\frac{d\sigma}{dt}(\bar{K}^0 n) = |H_+|^2 + |H_-|^2$$

$$\frac{d\sigma}{dt}(\Sigma^+ K^+) = |\lambda|^2 (2F_+ - 1)^2 |H_+|^2 + |\lambda|^2 (2F_- - 1)^2 |H_-|^2 \qquad \text{(IV.A.17)}$$

$$\frac{d\sigma}{dt}(K^0 \Lambda) = \frac{|\lambda|^2}{6}(2F_+ + 1)^2 |H_+|^2 + \frac{|\lambda|^2}{6}(2F_- + 1)^2 |H_-|^2 .$$

Eliminating the $|H_+|^2, |H_-|^2$ we get the broken $SU(3)$ sum rule for cross sections:

$$\frac{d\sigma}{dt}(\Sigma^+ K^+) = 6\left(\frac{a-b}{c-d}\right) \frac{d\sigma}{dt}(K^0 \Lambda) + |\lambda|^2 \left(\frac{bc-ad}{c-d}\right) \frac{d\sigma}{dt}(\bar{K}^0 n) \qquad \text{(IV.A.18)}$$

where

$$a \equiv (2F_+ - 1)^2 \qquad b \equiv (2F_- - 1)^2$$

$$c \equiv (2F_+ + 1)^2 \qquad d \equiv (2F_- + 1)^2 \qquad |\lambda|^2 = \left(\frac{s}{s_0}\right)^{-2\Delta\alpha}$$

We use for F_+, F_- the average values that MMP in ref. 45 found from their amplitude analysis fit to HYCEX $\frac{d\sigma}{dt}$ and P data at 4 GeV/c:

$$F_+ = 1.42 \qquad F_- = .275$$

(These are quite comparable to the NS results of ref. 41: the NS fit allowed $F_+(V), F_-(V)$ to be independent of $F_+(T), F_-(T)$ respectively, but their fit yielded $F_+(V) = 1.42$, $F_+(T) = 1.51$, and $F_-(V) = .204$, $F_-(T) = .237$, so taking $F(V) = F(T)$ is also not unreasonable.)

By comparing $\left.\frac{d\sigma}{dt}\right|_0$ for CEX and HYCEX, MMP found at 4 GeV/c that the average value of $|\lambda|^2$ was 0.285, which implies

$$s_0 = 0.37 \text{ GeV}^2 .$$

Thus to test IV.A.18 we take as given the 4 GeV/c average fitted values of F_+, F_-, s_0 of MMP, and we take $\Delta\alpha = 0.2$. We cast IV.A.18 into its particular form because there now exists abundant $K^0\Lambda$ and $\bar{K}^0 n$ data not only at the

same energies, but from the same detectors in compatible bins. We test IV.A.18 at 3, 4, 5, 6, and 10.7 GeV/c using: our 2.67 ΣK scaled to the 3 GeV/c $\bar{K}^0 n, K^0\Lambda$ Argonne spectrometer data of Ward et al., Ambats et al., ref. 40; the 4,5,6 GeV/c ΣK data of Bashian et al., Pruss et al., ref. 44, and 4,5,6 $\bar{K}^0 n, K^0\Lambda$ data of Ward, Ambats; the 10.1 GeV/c data of Berglund, ref. 67, scaled to the 10.7 $\bar{K}^0 n, K^0\Lambda$ Brookhaven spectrometer data of Foley, ref. 40. Figure IV.13 displays $\frac{d\sigma}{dt}(\Sigma K)$ (squares) and $6\left(\frac{a-b}{c-d}\right)\frac{d\sigma}{dt}(K^0\Lambda) + |\lambda|^2\left(\frac{bc-ad}{c-d}\right)\frac{d\sigma}{dt}(\bar{K}^0 n)$ (circles), where we have combined $K^0\Lambda$ and $\bar{K}^0 n$ data at equal t. We see that at all momenta the agreement is excellent at least out to the dip or break at $-t = 0.4-0.5$, and that the shapes of the left and right hand sides of IV.A.18 are remarkably similar.

At 3 GeV/c, the $\bar{K}^0 n$ term in the right hand side of IV.A.18 is ~30% of the $K^0\Lambda$ term, while at 10.7 GeV/c, the $\bar{K}^0 n$ term is ~20% of the $K^0\Lambda$ term. As $s \to \infty$, $|\lambda|^2 \to 0$, and since there is a minimum ~10% systematic uncertainty in the spectrometer data normalization, at very much higher energies than 10 GeV/c the $\bar{K}^0 n$ contribution to IV.A.18 shrinks to the order of the measurement precision; IV.A.18 at very high energies will become merely an $SU(3)$ relation between the HYCEX processes. At all momenta from 3 to 10 GeV/c, $\frac{d\sigma}{dt}(\bar{K}^0 n)$ is ~3 times greater than $\frac{d\sigma}{dt}(K^0\Lambda)$, $\frac{d\sigma}{dt}(\Sigma^+ K^+)$ so that IV.A.18 is a significant test of the form of $|\lambda|$ and the values of $F_+, F_-, s_0, \Delta\alpha$.

Thus we conclude that when the non-strange/strange mass splitting is taken into account by the remarkably few and simple assumptions going into IV.A.18, the HYCEX and CEX processes considered exhibit light-quark flavor-independence even as low as 3 GeV/c. We conclude that over the s,t range considered, s,t-independence of F_+, F_- is a good approximation, and that the

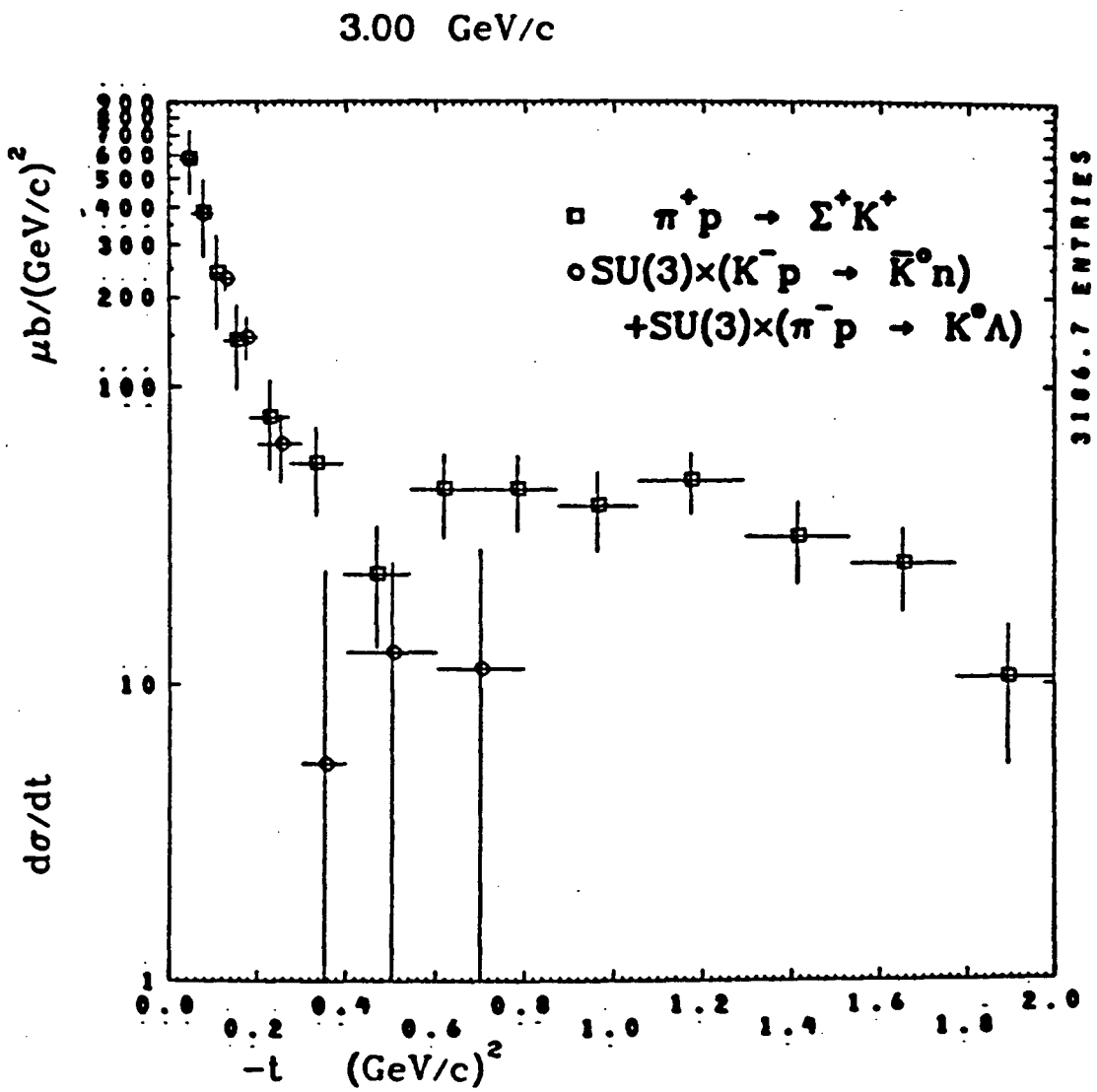
3.00 GeV/c
μb/(GeV/c)²
dσ/dt
□ π⁺p → Σ⁺K⁺
○SU(3)×(K⁻p → K̄⁰n)
+SU(3)×(π⁻p → K⁰Λ)
3186.7 ENTRIES
−t (GeV/c)²

IV.13a

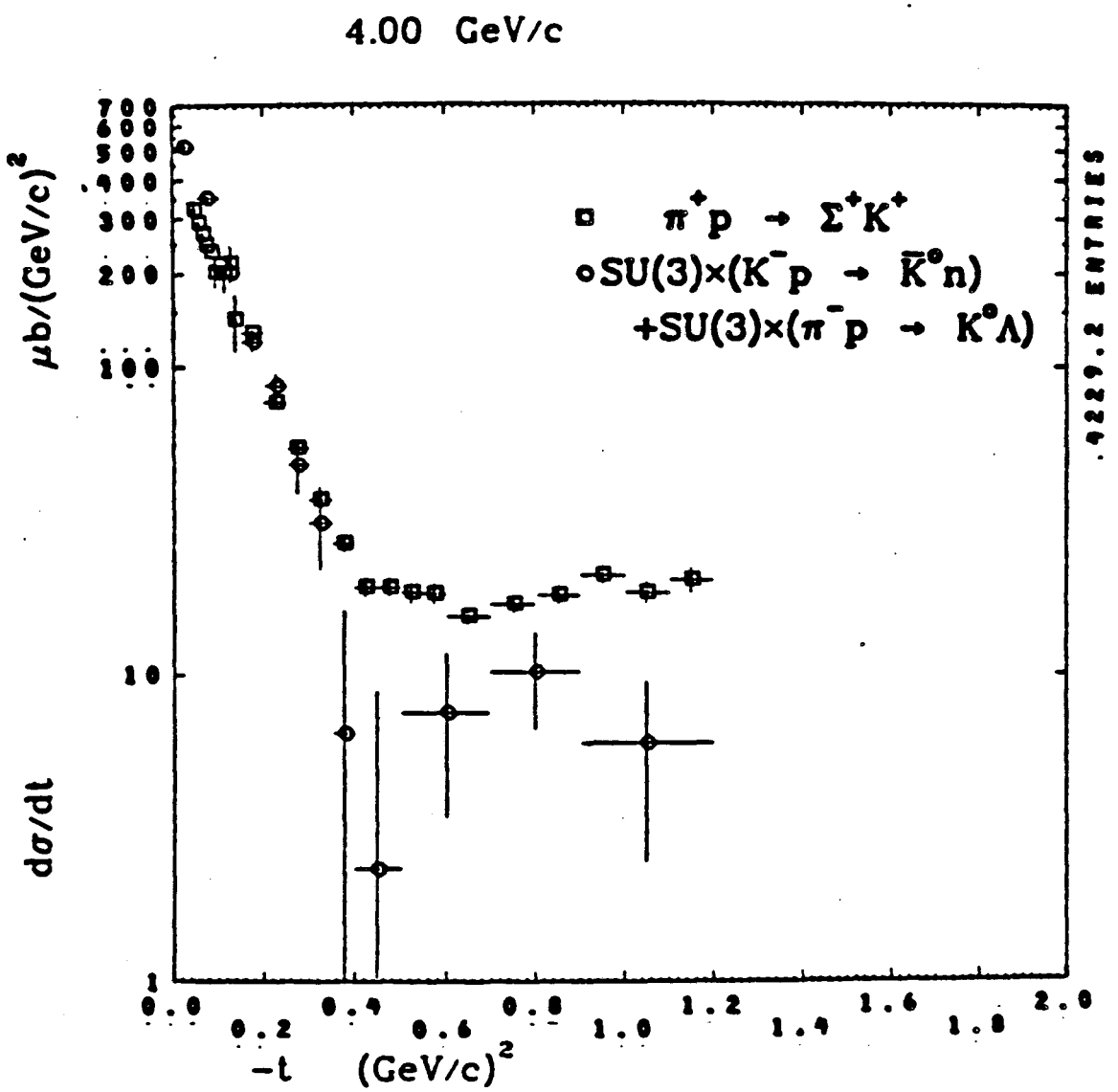
4.00 GeV/c
μb/(GeV/c)²
dσ/dt
700
600
500
400
300
200
100
10
1
0.0
0.2
0.4
0.6
0.8
1.0
1.2
1.4
1.6
1.8
2.0
−t (GeV/c)²
π⁺p → Σ⁺K⁺
SU(3)×(K⁻p → K̄⁰n)
+SU(3)×(π⁻p → K⁰Λ)
4229.2 ENTRIES

IV.13b

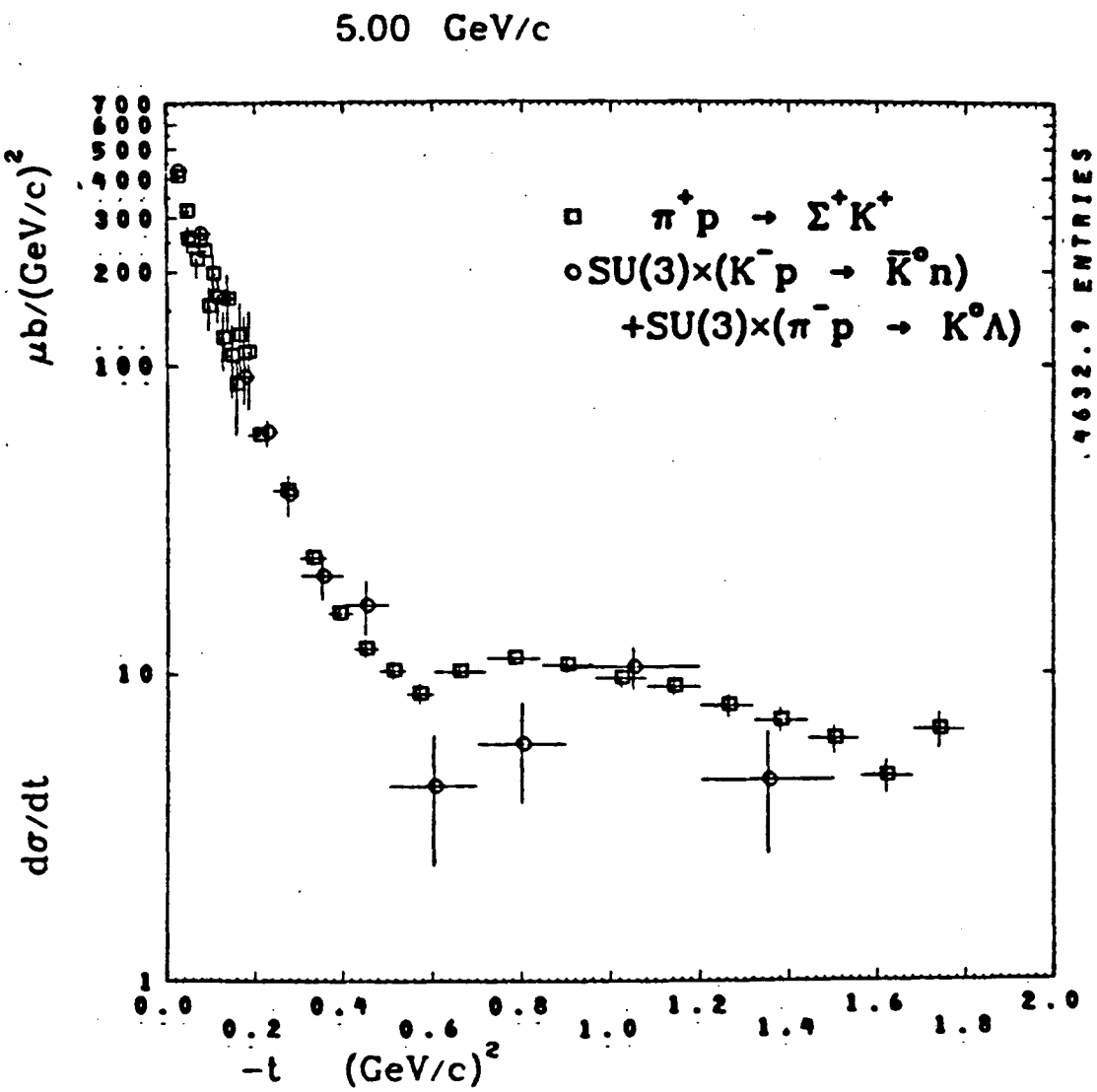
5.00 GeV/c
μb/(GeV/c)²
dσ/dt
700
600
500
400
300
200
100
10
1
0.0
0.2
0.4
0.6
0.8
1.0
1.2
1.4
1.6
1.8
2.0
−t (GeV/c)²
π⁺p → Σ⁺K⁺
SU(3)×(K⁻p → K̄⁰n)
+SU(3)×(π⁻p → K⁰Λ)
4632.9 ENTRIES

IV.13c

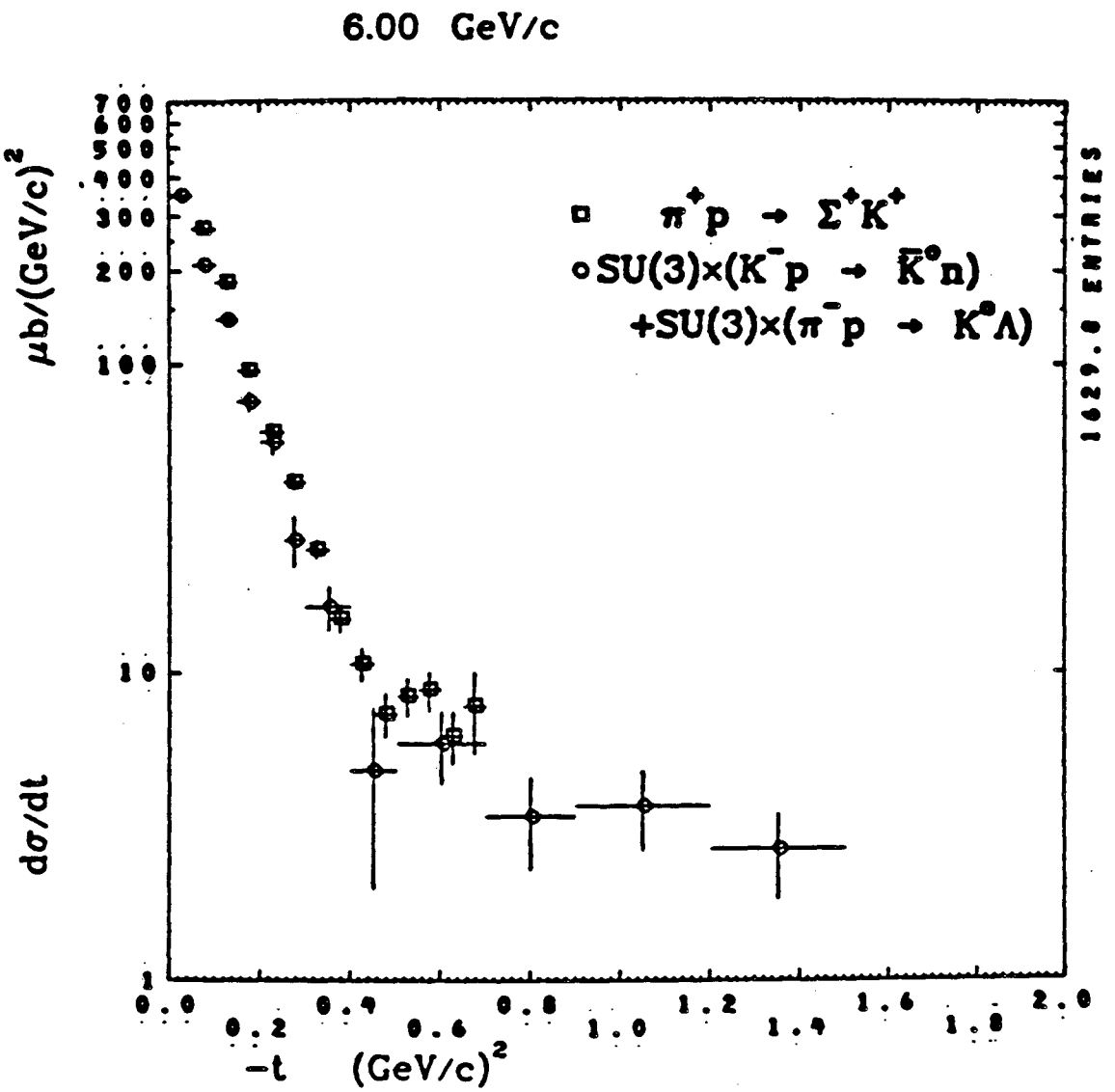
6.00 GeV/c
μb/(GeV/c)²
dσ/dt
700
600
500
400
300
200
100
10
1
0.0
0.2
0.4
0.6
0.8
1.0
1.2
1.4
1.6
1.8
2.0
−t (GeV/c)²
π⁺p → Σ⁺K⁺
SU(3)×(K⁻p → K̄⁰n)
+SU(3)×(π⁻p → K⁰Λ)
1629.0 ENTRIES

IV.13d

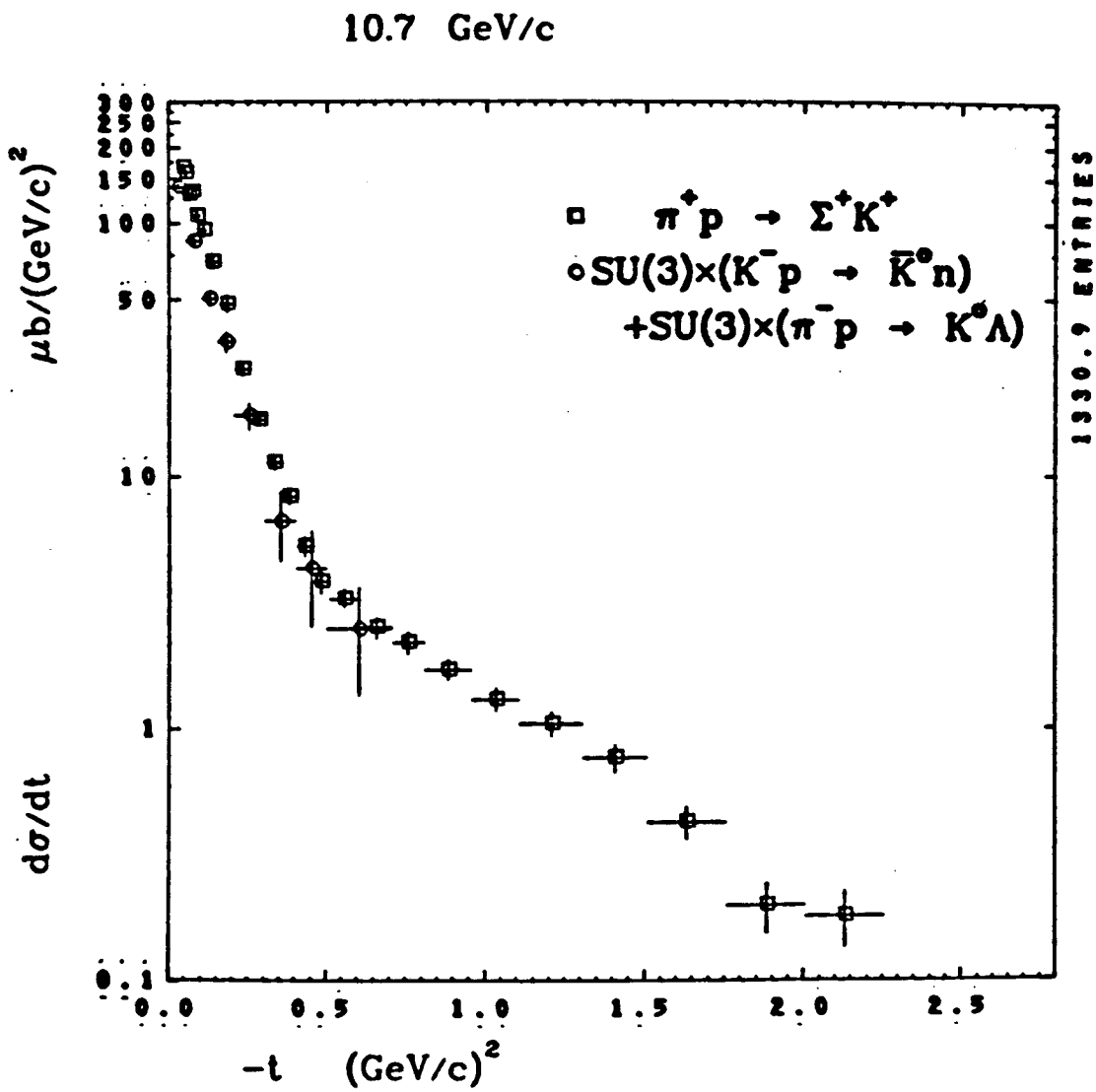
10.7 GeV/c
$\pi^+p \to \Sigma^+K^+$
$SU(3)\times(K^-p \to \bar{K}^0n)$
$+SU(3)\times(\pi^-p \to K^0\Lambda)$
1330.9 ENTRIES
$d\sigma/dt$ $\mu b/(GeV/c)^2$
$-t$ $(GeV/c)^2$
300
250
200
150
100
50
10
1
0.1
0.0
0.5
1.0
1.5
2.0
2.5

IV.13e

EXD-Regge dynamical form of $|\lambda|$ describes the energy dependence of the $SU(3)_{flavor}$ breaking well, reconciling factors of 3 between CEX and HYCEX cross sections.

Equations IV.A.15 also lead to relations for the polarization as given in equation IV.A.5; in ref. 45, MMP derive:

$$P\,\frac{d\sigma}{dt}(K^-p \to \bar{K}^0 n) = C_\Lambda P\,\frac{d\sigma}{dt}(\pi^-p \to K^0\Lambda) = C_\Sigma P\,\frac{d\sigma}{dt}(\pi^+p \to K^+\Sigma^+) \qquad \text{(IV.A.19)}$$

where

$$C_\Lambda = \frac{6}{|\lambda|^2(2F_+ + 1)(2F_- + 1)}\,, \quad C_\Sigma = \frac{1}{|\lambda|^2(2F_+ - 1)(2F_- - 1)}\,.$$

Because $F_+ \approx \frac{3}{2}$, $F_- \approx \frac{1}{4}$, this implies that $P(K^0\Lambda)$ is opposite in sign to $P(\Sigma^+K^+)$. In figure IV.14 we show our $P(\Sigma^+K^+)$ at 1.94, 2.30, 2.67 GeV/c with the $P(K^0\Lambda)$ data of Saxon et al., ref. 40, and we see that within the low precision, generally in the forward regions $P(K^0\Lambda)P(\Sigma^+K^+) < 0$, especially above ~2.3 GeV/c. Ward, ref. 40, compares his 5 GeV/c $P(K^0\Lambda)$ data with $P(\Sigma^+K^+)$, and sees excellent agreement with $P(K^0\Lambda)P(\Sigma^+K^+) < 0$. This further confirms that the F_+, F_- values used in IV.A.18 are reasonable.

5. Quark Counting Rules and Large Angle Scattering

The quark constituent picture for hadrons leads not only to the flavor independence considerations of the previous section and to the Additive Quark Model predictions for *forward* high energy scattering (see sections B,C of this chapter) but also leads one to expect (see Sivers, Brodsky, and Blankenbecler, ref. 46) that for 2-body scattering $\frac{d\sigma}{dt}$ at *large* transverse momenta (C.M. angles near 90°) should fall at a large power of s:

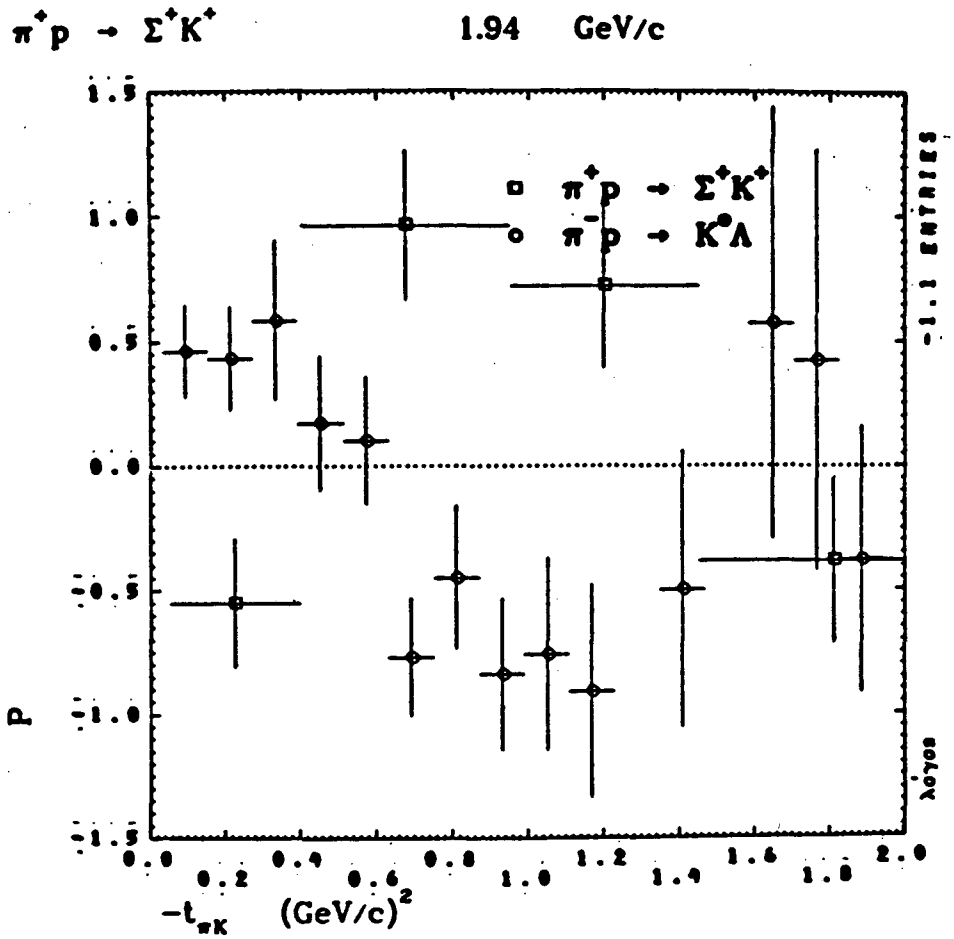
π⁺p → Σ⁺K⁺
1.94 GeV/c
π⁺p → Σ⁺K⁺
π⁻p → K⁰Λ
P
−t_πK (GeV/c)²
-1.1 ENTRIES
1.5
1.0
0.5
0.0
-0.5
-1.0
-1.5
0.0
0.2
0.4
0.6
0.8
1.0
1.2
1.4
1.6
1.8
2.0

IV.14a

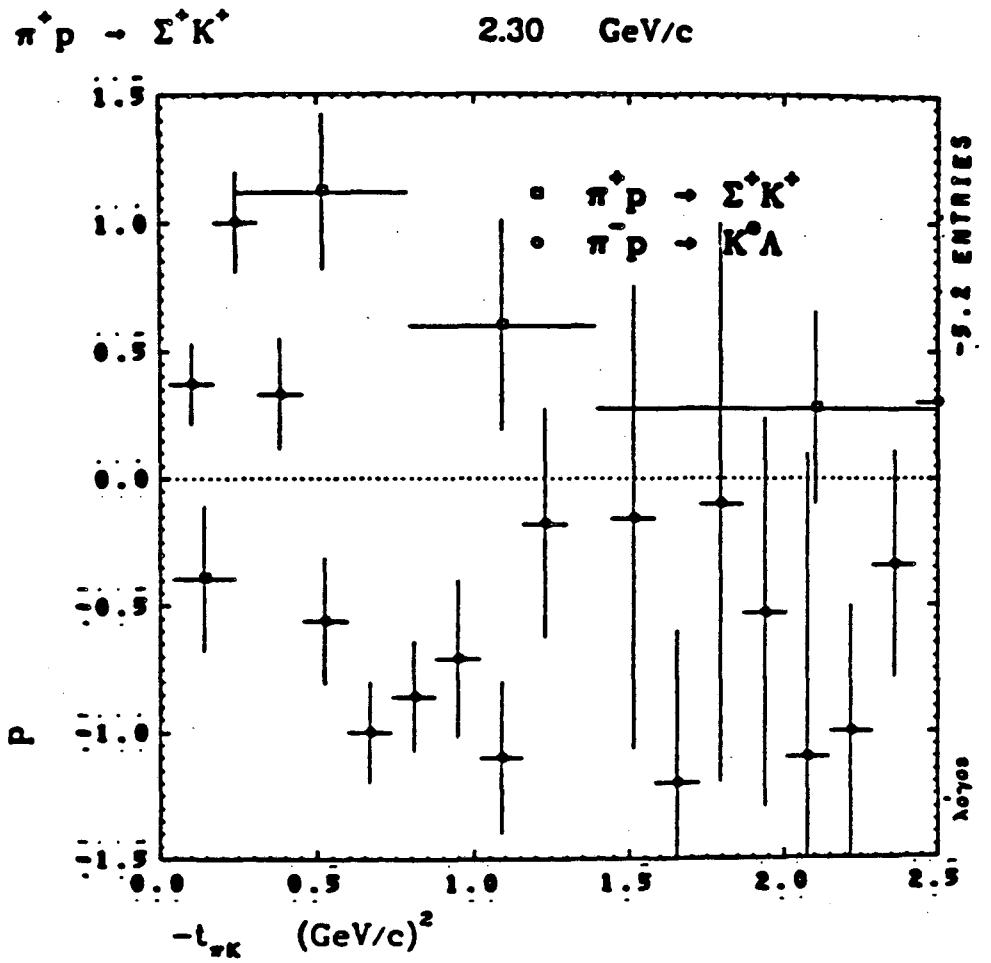
π⁺p → Σ⁺K⁺
2.30 GeV/c
π⁺p → Σ⁺K⁺
π⁻p → K⁰Λ
P
1.5
1.0
0.5
0.0
-0.5
-1.0
-1.5
0.0
0.5
1.0
1.5
2.0
2.5
-t_πK (GeV/c)²
-5.2 ENTRIES
SCALY

IV.14b

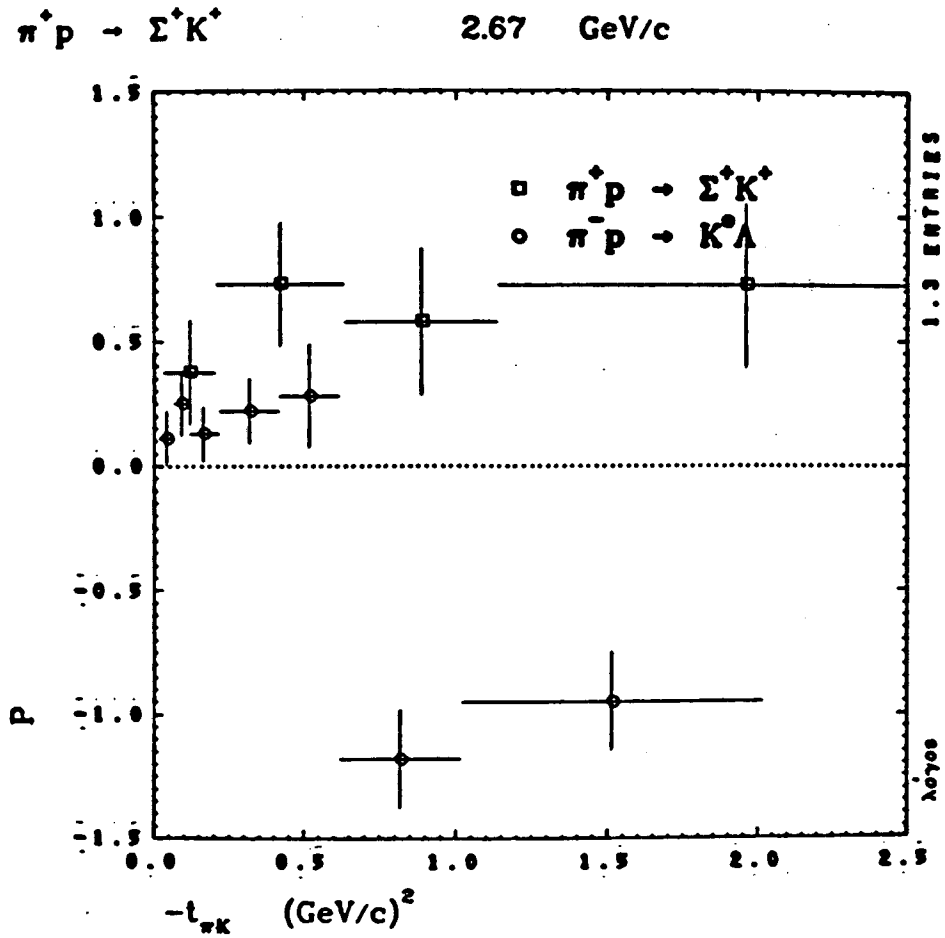
π⁺p → Σ⁺K⁺
2.67 GeV/c
π⁺p → Σ⁺K⁺
π⁻p → K⁰Λ
P
1.5
1.0
0.5
0.0
-0.5
-1.0
-1.5
0.0
0.5
1.0
1.5
2.0
2.5
−t_πK (GeV/c)²
1.3 ENTRIES
SOLOY

IV.14c

$$\frac{d\sigma}{dt}(ab \to cd) = \frac{1}{s^{n_a+n_b+n_c+n_d-2}} f(\cos\vartheta_{CM})$$

where n_a = no. of active fields (or valence quarks) in hadron a, etc. Thus for $\pi p \to \Sigma K$ we expect using the standard $SU(6)$ quark contents for the particles:

$$\frac{d\sigma}{dt} = \frac{1}{s^8} f(\cos\vartheta_{CM}) \,. \qquad \text{(IV.A.20)}$$

Unfortunately the world ΣK large angle data is very limited, but in Fig. IV.15 we display $s^8 \frac{d\sigma}{dt}$ versus $\cos\vartheta_{CM}$ for our 7 highest energies and for data at 3.23 (ref. 35), 3.7 (ref. 21), and 5 GeV/c (ref. 19); this represents a range in s^8 of a factor of $\sim 10^3$. There is a definite narrowing of the envelope of points for $\cos\vartheta_{CM} \approx 0$, but plots of $s^9 \frac{d\sigma}{dt}$ and $s^7 \frac{d\sigma}{dt}$ show this also. Thus one can say the agreement of the ΣK data with (IV.A.20) is qualitatively good; the rapid fall of the large angle cross section is suggestive of composite hadron scattering in HYCEX, as in elastic and CEX reactions. The only other test of relations like IV.A.20 for HYCEX is by Brandenburg et al. (ref. 56), using $\bar{K}^0 p \to \pi^+\Lambda$, $\pi^+\Sigma^0$ data at 90° -- they find $\frac{d\sigma}{dt} \sim \frac{1}{s^7} f(\cos\vartheta_{CM})$. However, we note that their reactions at 90° are not unambiguously HYCEX, since their u-channel exchanges are CEX.

$\pi^+ p \rightarrow \Sigma^+ K^+$

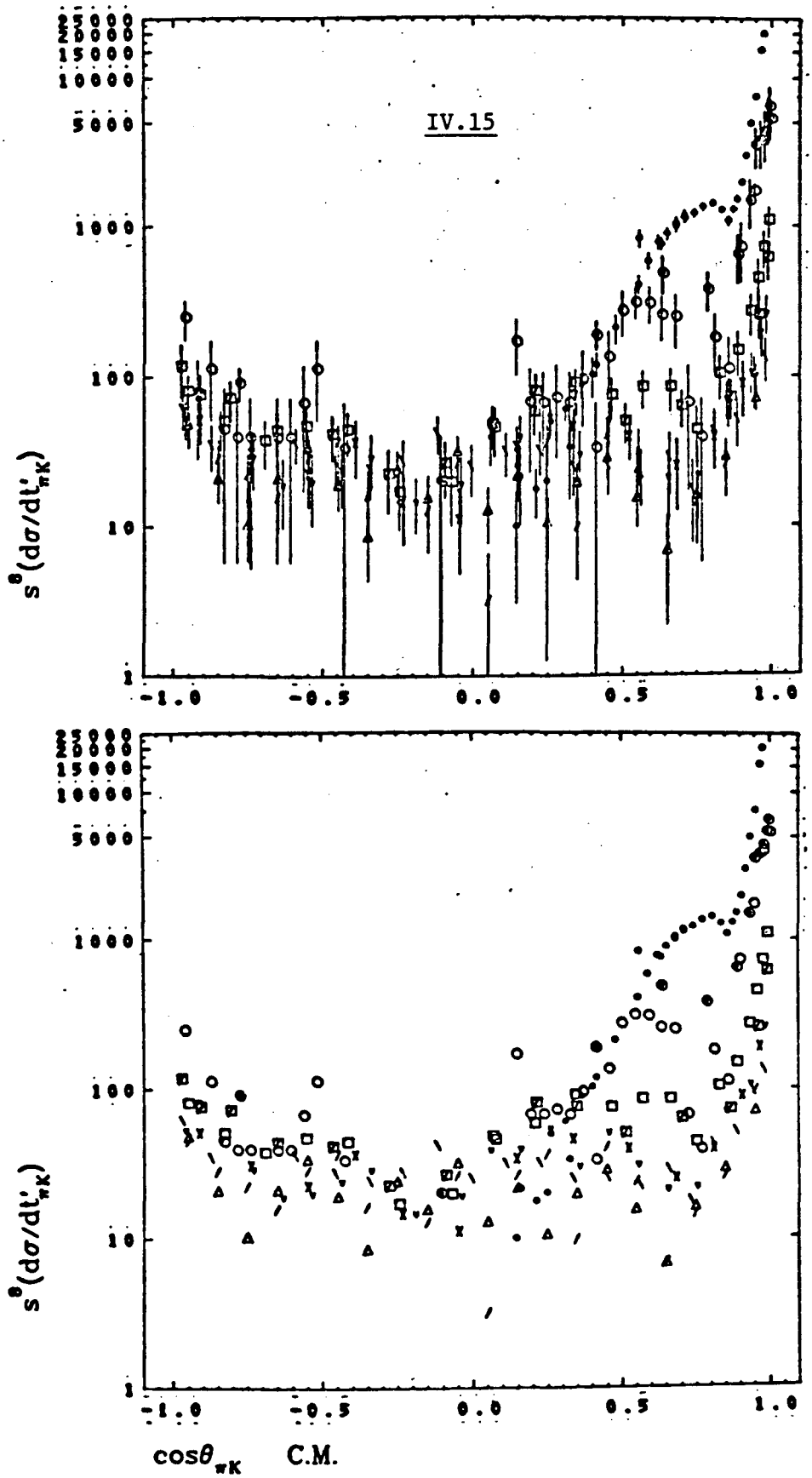

B. ΣK^*

1. $\frac{d\sigma}{dt'}$, $\rho_{ij}(K^*)$, and P_Σ

For $\pi^+p \to \Sigma^+K^*(892)^+$ there are, after taking parity conservation into account, 6 independent invariant helicity amplitudes H, labeled by the K^* helicity $(0,\pm1)$ and the baryon helicity flip/non-flip $(+-,++)$: $H^1_{++}, H^0_{++}, H^{-1}_{++}, H^1_{+-}, H^0_{+-}, H^{-1}_{+-}$, in terms of which (see Doncel, Minnaert, and Michel, ref. 57):

$$\frac{d\sigma}{dt'} = \sum_{helicities} |H|^2 \qquad \text{(IV.B.1)}$$

where as usual $t' \equiv t - t_{min}$, $|t_{min}| = minimum|t|$. The helicity state of the produced K^* is specified by the K^* decay density matrix ρ, where (see Pilkuhn, ref. 23):

$$\rho_{ij} = \frac{\sum_{lm} H^i_{lm} H^{j*}_{lm}}{\sum_{nlm} |H^n_{lm}|^2}. \qquad \text{(IV.B.2)}$$

As in Chapter III, we define the ΣK^* state by a simple mass cut: $m_{K^*} - 1.5\Gamma_0 \le m_{\pi K} \le m_{K^*} + 1.5\Gamma_0$; for the analysis which follows we use only $\Sigma^+K^{*+} \to \Sigma^+K^0\pi^+$ events because fits to $m_{\pi K}$ in Chapter III show events in $\Sigma^+K^+\pi^0$ have ~35% background in the K^* interval; also the $\Sigma^+K^+\pi^0$ data has the possibility of a small $\Sigma^* \to \Sigma\pi$ reflection in $m^2_{\pi K}$. Because of limited statistics and because background in the $K^* \to K^0\pi^+$ events is only ~10%, no t'-dependent background correction is used. We have combined the 1.94 with the 2.15 GeV/c data, and also the 2.30 with the 2.46 GeV/c data, which are referred to as the 2.06 and 2.39 GeV/c samples.

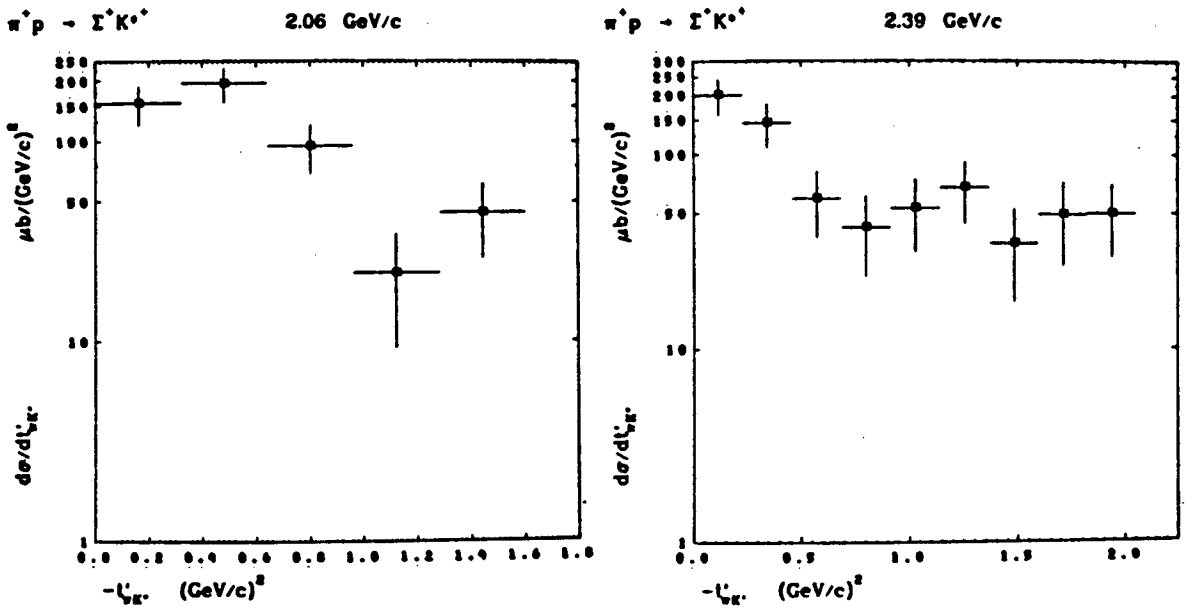
π⁺p → Σ⁺K*⁺
2.06 GeV/c
π⁺p → Σ⁺K*⁺
2.39 GeV/c
μb/(GeV/c)²
dσ/dt'
-t' (GeV/c)²

IV.16a

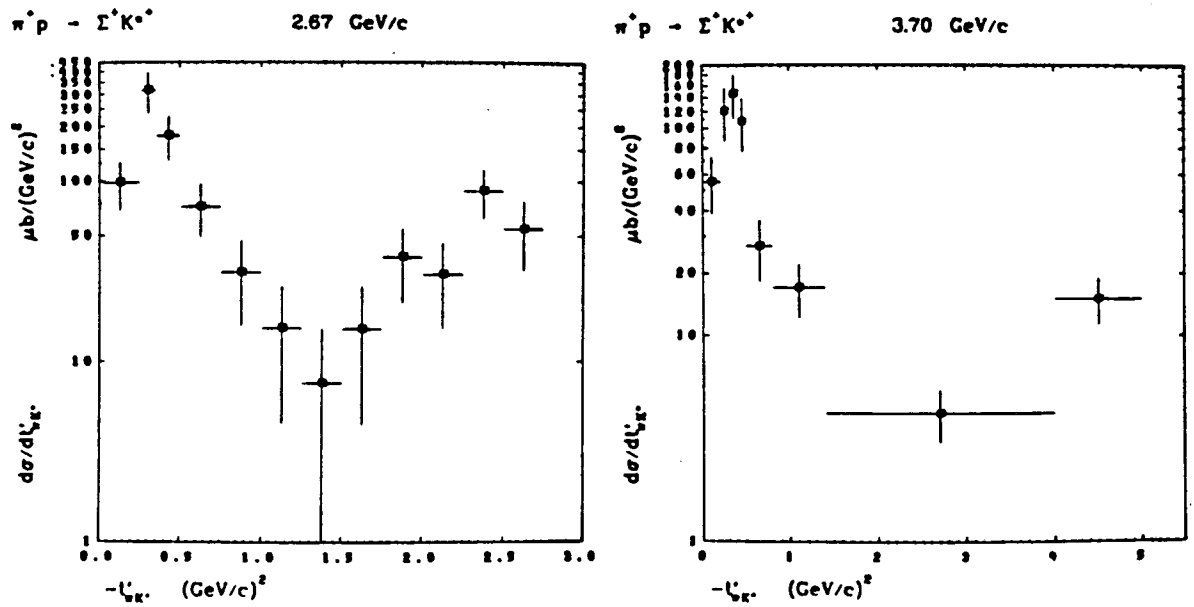
π⁺p → Σ⁺K*⁺
2.67 GeV/c
π⁺p → Σ⁺K*⁺
3.70 GeV/c
μb/(GeV/c)²
dσ/dt'
-t' (GeV/c)²

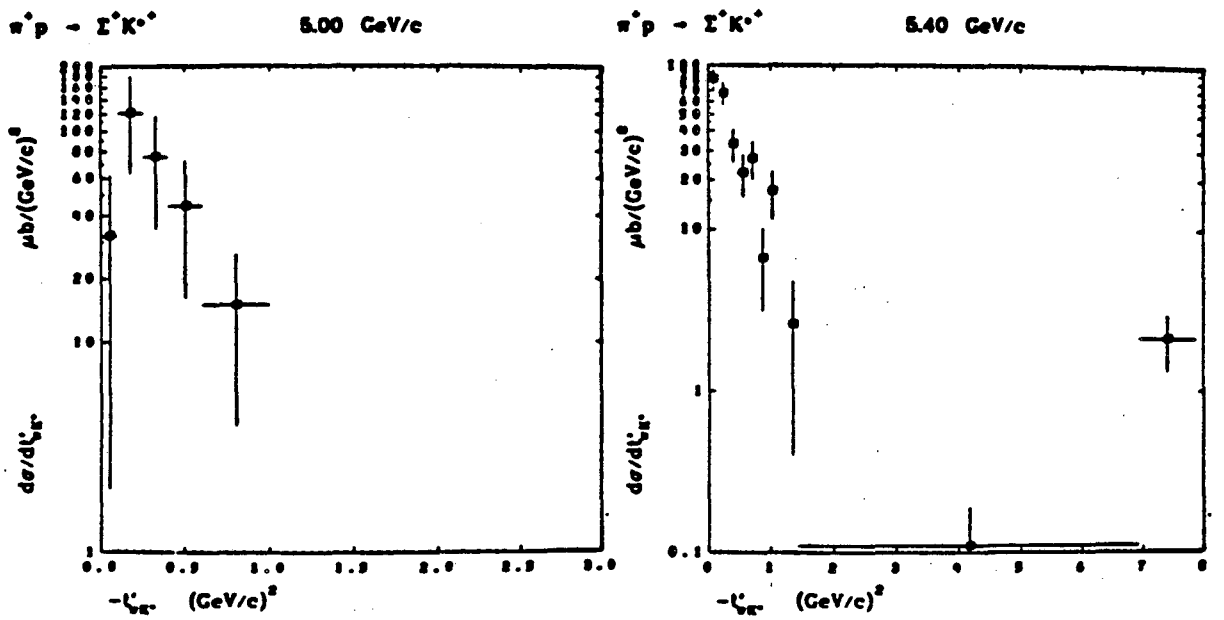
π⁺p → Σ⁺K*⁺
5.00 GeV/c
π⁺p → Σ⁺K*⁺
5.40 GeV/c
μb/(GeV/c)²
dσ/dt'
-t' (GeV/c)²

IV.16b

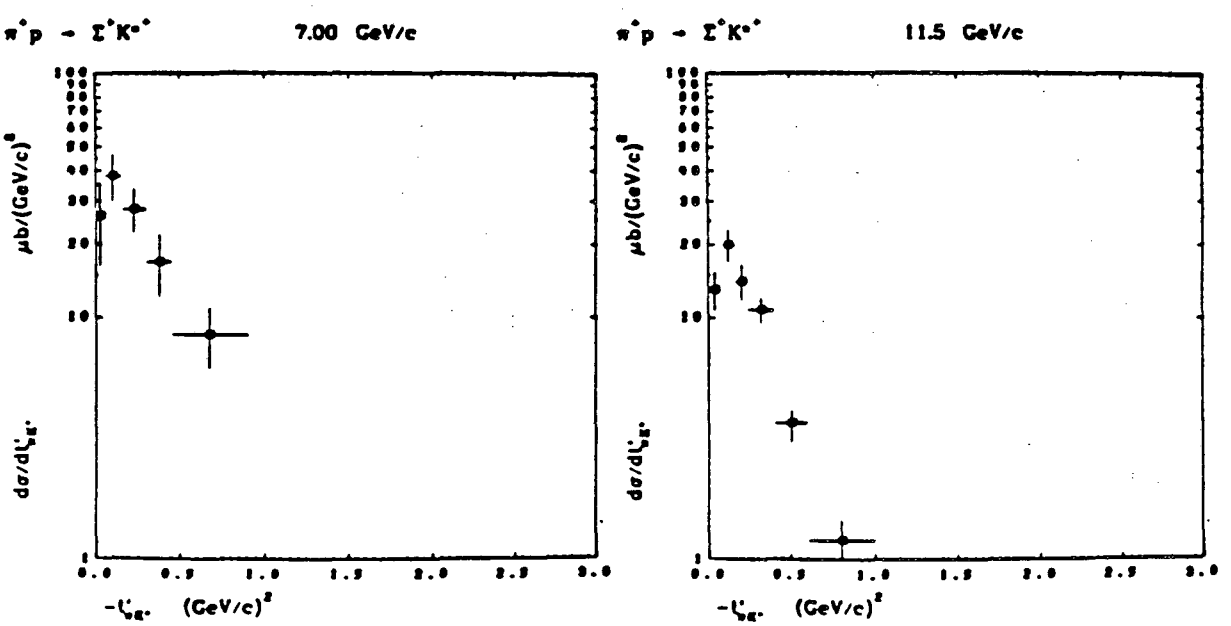
π⁺p → Σ⁺K*⁺
7.00 GeV/c
π⁺p → Σ⁺K*⁺
11.5 GeV/c
μb/(GeV/c)²
dσ/dt'
-t' (GeV/c)²

Figure IV.16 displays $\frac{d\sigma}{dt'}$ (where only $\Sigma^+ \to \pi^+ n$ events are used), and we note generally a strong forward peak, and at 2.06 and 2.67, a lesser backward peaking. Near $t' = 0$ the 2.67 sample has a turnover in the forward direction. Such a turnover indicates the dominance of helicity flip contributions in the forward direction, and is also seen in the data of Butler (3.7 GeV/c), ref. 21, Toet (5.0 GeV/c), ref. 19, and Ballam et al. (7,11.5 GeV/c), ref. 52, but not in the 5.4 GeV/c data of Cooper, ref. 47. At 2.38 there is a slight flattening near $t' = 0$ but no turnover; no turnover is evident in the 2.30 and 2.46 samples taken separately. (For the $K^{*+} \to K^+\pi^0$ data, which have a 1/3 background, no turnover or flattening near $t' = 0$ is seen at any of our 3 momenta.)

To study the K^* decay in its own rest frame, two helicity-type coordinate systems are used for reactions $0^-\frac{1}{2}^+ \to 1^-\frac{1}{2}^+$ (all unit vectors are in the $K^*C.M.$):

$$\begin{aligned} t\text{-channel} \quad & \hat{y}_t \equiv \hat{n} \equiv \hat{p}_\pi \times \hat{p}_{K^*} = \hat{p}_p \times \hat{p}_\Sigma \\ \text{helicity frame:} \quad & \hat{z}_t \equiv \hat{p}_\pi \\ & \hat{x}_t \equiv \hat{y}_t \times \hat{z}_t \end{aligned} \tag{IV.B.3}$$

(π is the initial state pion)

$$\begin{aligned} s\text{-channel} \quad & \hat{y}_s \equiv \hat{n} \equiv \hat{p}_p \times \hat{p}_\Sigma = \hat{y}_t \\ \text{helicity frame:} \quad & \hat{z}_s \equiv \hat{p}_{K^*} = -\hat{p}_\Sigma \\ & \hat{x}_s \equiv \hat{y}_s \times \hat{z}_s \end{aligned} \tag{IV.B.4}$$

We note that the t-channel system of axes is invariant (unrotated) under a Lorentz transformation from the K^* rest frame to the t-channel center of mass (πK^*) frame, and the s-channel axes are invariant under a Lorentz transformation from the K^* rest frame to the s-channel center of mass (πp) frame. With respect to either system of axes the K^* rest frame decay angular distribution is given in terms of the K^* density matrix elements ρ_{ij} as

(see, e.g., H.J. Schreiber, ref. 48):

$$W(\cos\vartheta,\varphi) = \frac{3}{4\pi}[\tfrac{1}{2}(1-\rho_{00}) + \tfrac{1}{2}(3\rho_{00}-1)\cos^2\vartheta - \rho_{1-1}\sin^2\vartheta\cos 2\varphi - \sqrt{2}\,\mathrm{Re}\,\rho_{10}\sin 2\vartheta\cos\varphi] \tag{IV.B.5}$$

and where $tr\rho = 1$ and $\rho_{-m-n} = (-1)^{m-n}\rho_{mn}$ requires $\rho_{11} = \tfrac{1}{2}(1-\rho_{00})$. Because the background in $K^{*+} \to K^0\pi^+$ events is only ~10% we use the method of moment estimators to determine the ρ_{ij} in $W(\cos\vartheta,\varphi)$ (again, see ref. 48):

$$\rho_{00} = \langle \frac{5}{2}\cos^2\vartheta - \tfrac{1}{2} \rangle \tag{IV.B.6a}$$

$$\rho_{1-1} = \langle -\frac{5}{4}\sin^2\vartheta\cos 2\varphi \rangle \tag{IV.B.6b}$$

$$\mathrm{Re}\rho_{10} = \langle -\frac{5\sqrt{2}}{8}\sin 2\vartheta\cos\varphi \rangle \tag{IV.B.6c}$$

$$\rho_{11} = \tfrac{1}{2}(1-\rho_{00}) = \langle -\frac{5}{4}\cos^2\vartheta + \frac{3}{4} \rangle \tag{IV.B.6d}$$

An exchange is said to have natural parity if the particles associated with it have spin J and parity P such that $P = (-1)^J$, and unnatural parity if $P = (-1)^{J+1}$. It has been shown (ref. 49) that to leading order in $\frac{1}{s}$, in either the t- or s-channel frame,

(a) ρ_{00} measures the fraction of meson helicity-non-flip unnatural parity exchange;

(b) $\rho_{11}-\rho_{1-1}$ measures the fraction of meson helicity-flip unnatural parity exchange;

(c) $\rho_{11}+\rho_{1-1}$ measures the fraction of meson helicity-flip natural parity exchange;

(in fact, (a) is always true to all orders in $\frac{1}{s}$ in the t-channel frame). We note that $\rho_{00} + (\rho_{11}+\rho_{1-1}) + (\rho_{11}-\rho_{1-1}) = \rho_{00} + 2\rho_{11} = 1$.

For forward $\pi^+p \to \Sigma^+K^+, \Sigma^{*+}K^+$ J^P conservation at the meson vertex forbids unnatural J^P (in particular, pseudoscalar K) exchange, so that only vector-tensor (K^*, K^{**}) exchanges can occur; for forward $\pi^+p \to \Sigma^+K^{*+}$ the meson vertex is not similarly restricted, and K (and Q) exchange is allowed. Thus K exchange will contribute to ρ_{00}, K^*, K^{**} to $\rho_{11}+\rho_{1-1}$, and any 1^+ Q-type exchanges to $\rho_{11}-\rho_{1-1}$. In figure IV.17 are shown ρ_{00}, ρ_{1-1}, Re ρ_{10}, ρ_{11}, $\rho_{11}+\rho_{1-1}$, $\rho_{11}-\rho_{1-1}$, and P_Σ (with respect to $\hat{n}$) as functions of t' for the ΣK^* samples (for the ρ_{ij}, both $\Sigma^+ \to p\pi^0$ and π^+n events are used; for P_Σ, only $\Sigma^+ \to p\pi^0$ are included); for comparison, figure IV.18 presents the only other data on the $K^{*+}\rho_{ij}$, from the 3.7, 5.0, 5.4, 7, and 11.5 GeV/c experiments (see next section). Clearly at all momenta from 2.06 upward the dominant contribution to forward ($-t<1$) ΣK^* is from helicity flip natural parity exchange, i.e., K^*, K^{**}; this dominance of $\rho_{11}+\rho_{1-1}$ is also seen in $\pi^-p \to \Sigma^0K^{*0}$ data such as that at 4.5, 6.0 GeV/c of Crenell, ref. 50, and at 3.95 GeV/c of Aguilar-Benitez, ref. 51, but not as strongly in $\pi^-p \to \Lambda K^{*0}$ in the same references. Both Aguilar-Benitez and Crenell observe that because one predicts from, e.g., $SU(6)$, that baryon vertex couplings have $g_{KN\Lambda} > g_{KN\Sigma}$, one expects that K exchange is not as important in ΣK^* as in ΛK^*. The turnover in $\frac{d\sigma}{dt'}$ near $t' \to 0$ also indicates that ρ_{00} is small, since ρ_{00} contributes to helicity nonflip; turnovers are similarly seen in Σ^0K^{*0}, but not as strongly in ΛK^{*0}.

The P_Σ data clearly have such large errors that the only useful information provided (with high statistics it would be possible to use $\rho_{ij}(K^*)$, P_Σ, and the joint $K^*-\Sigma$ decay density matrix to obtain the complete helicity amplitudes up to 2 undetermined phases; see ref. 57) is that we can say $P_\Sigma > 0$; in

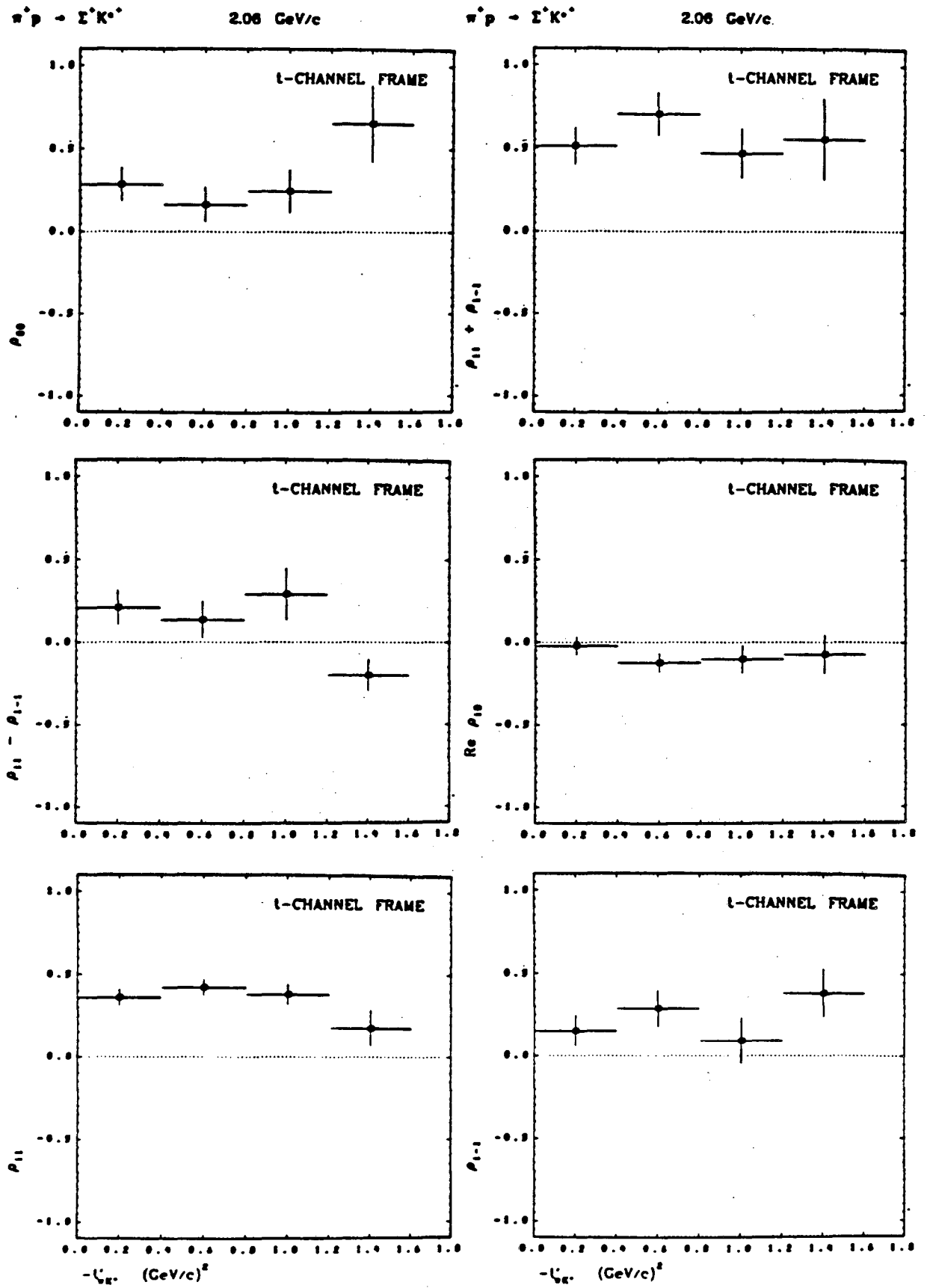
π⁺p → Σ⁺K*⁺
2.06 GeV/c
t-CHANNEL FRAME
ρ00
ρ11 + ρ1-1
ρ11 − ρ1-1
Re ρ10
ρ11
ρ1-1
-t'K* (GeV/c)²

IV.17a

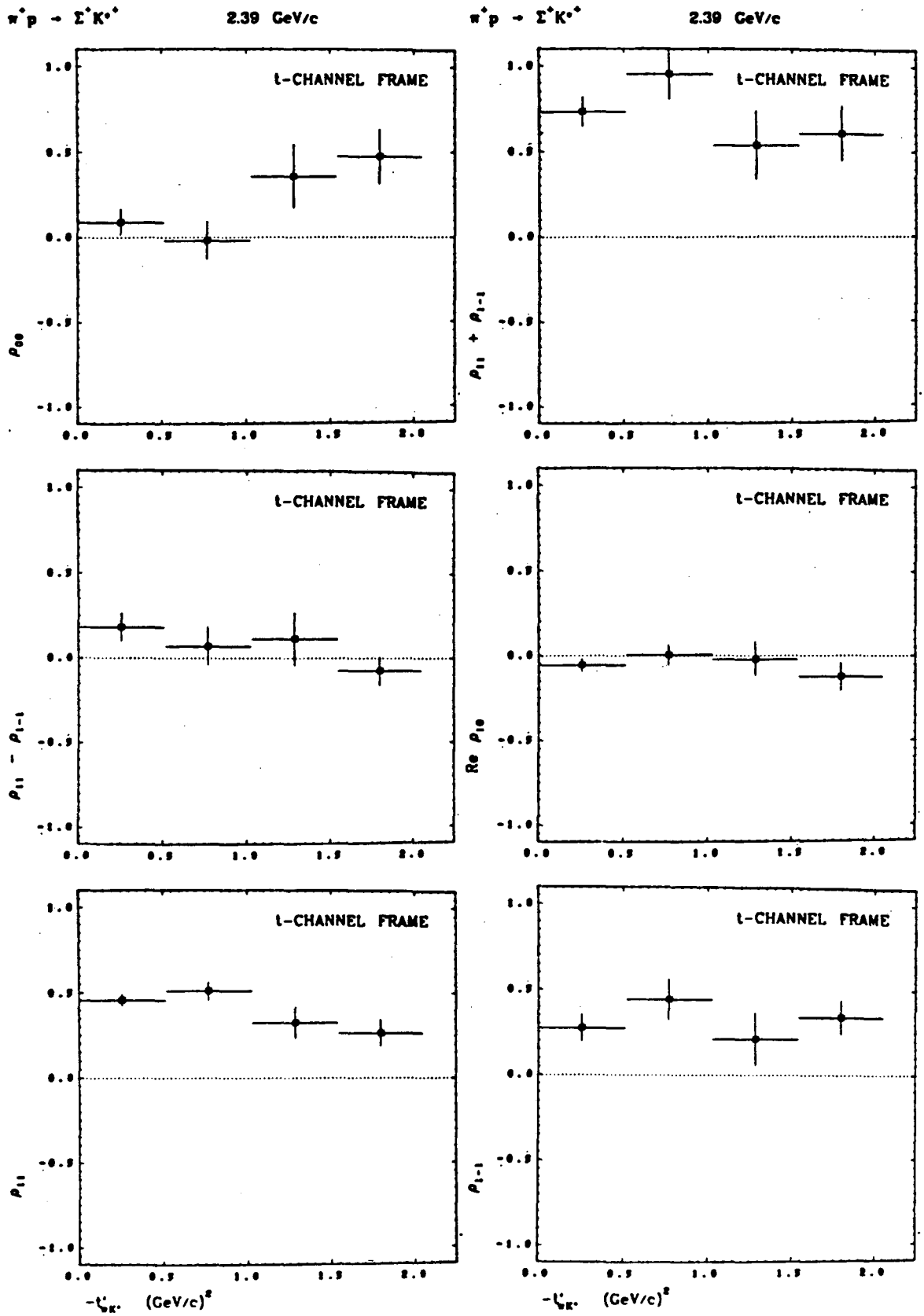
π⁺p → Σ⁺K*⁺
2.39 GeV/c
t-CHANNEL FRAME
ρ00
ρ11 + ρ1-1
ρ11 − ρ1-1
Re ρ10
ρ11
ρ1-1
-t'K* (GeV/c)²

IV.17b

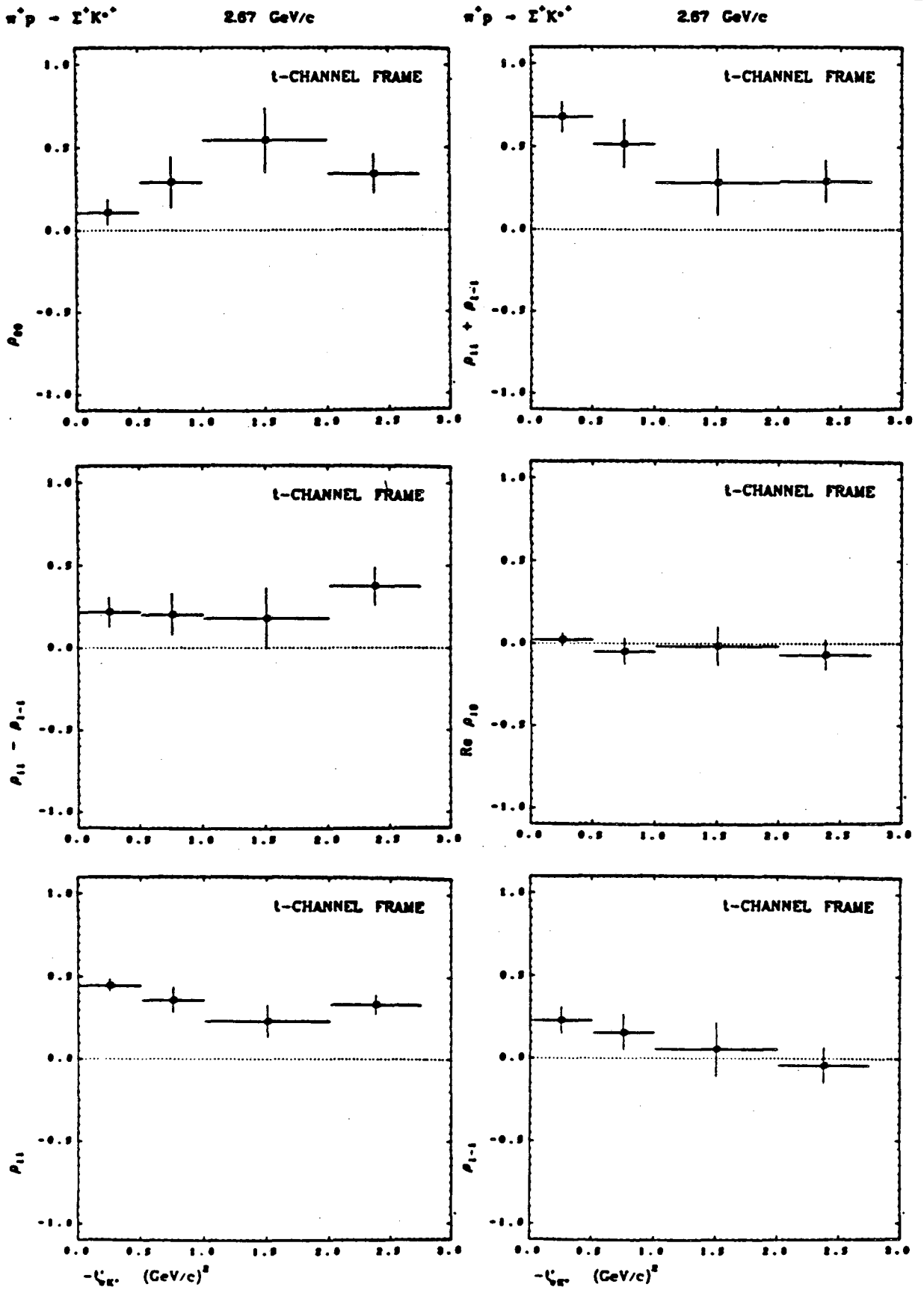
π⁺p → Σ⁺K*⁺
2.67 GeV/c
t-CHANNEL FRAME
ρ00
ρ11 + ρ1-1
ρ11 − ρ1-1
Re ρ10
ρ11
ρ1-1
-t'K* (GeV/c)²

IV.17c

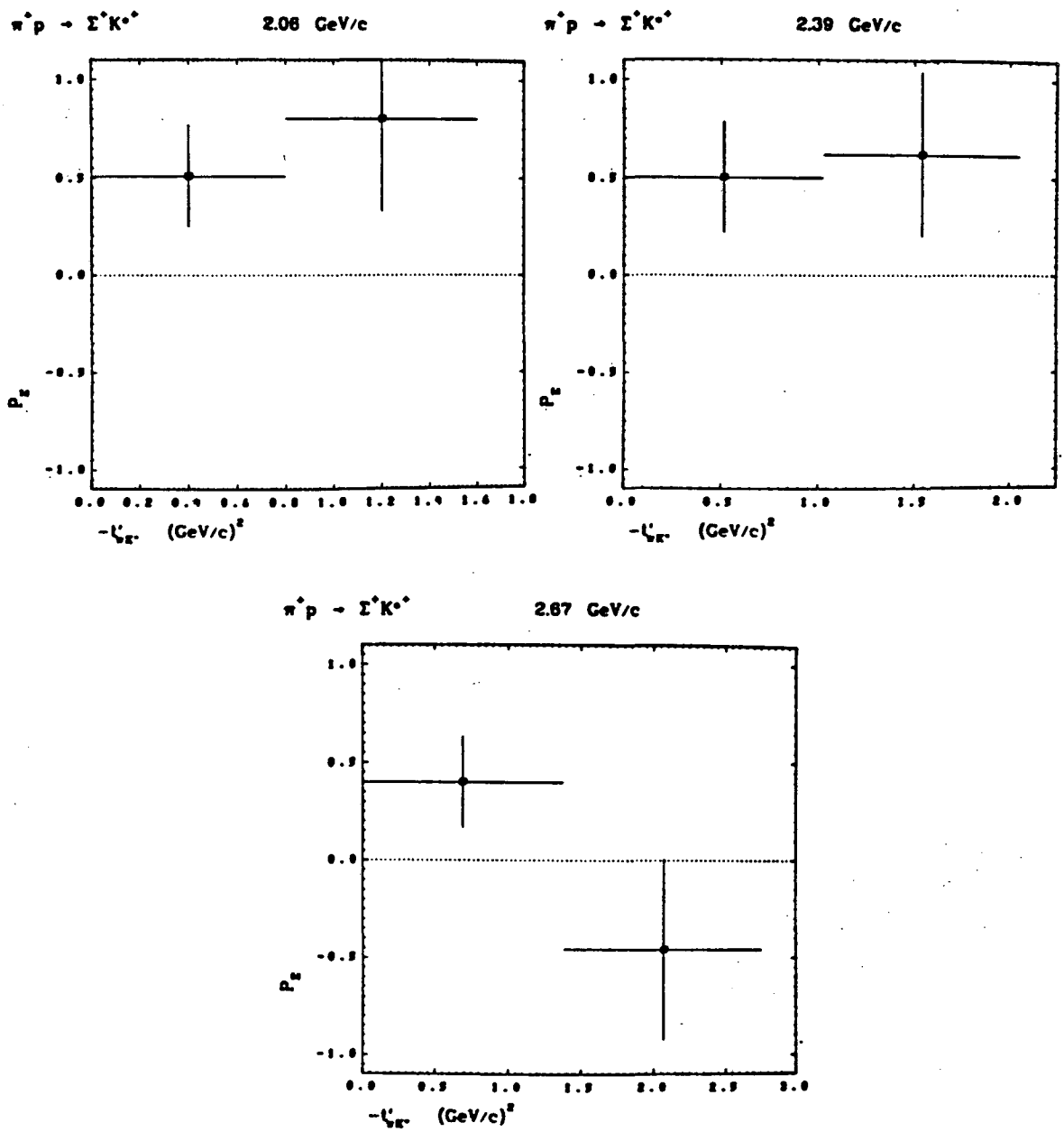

IV.17d

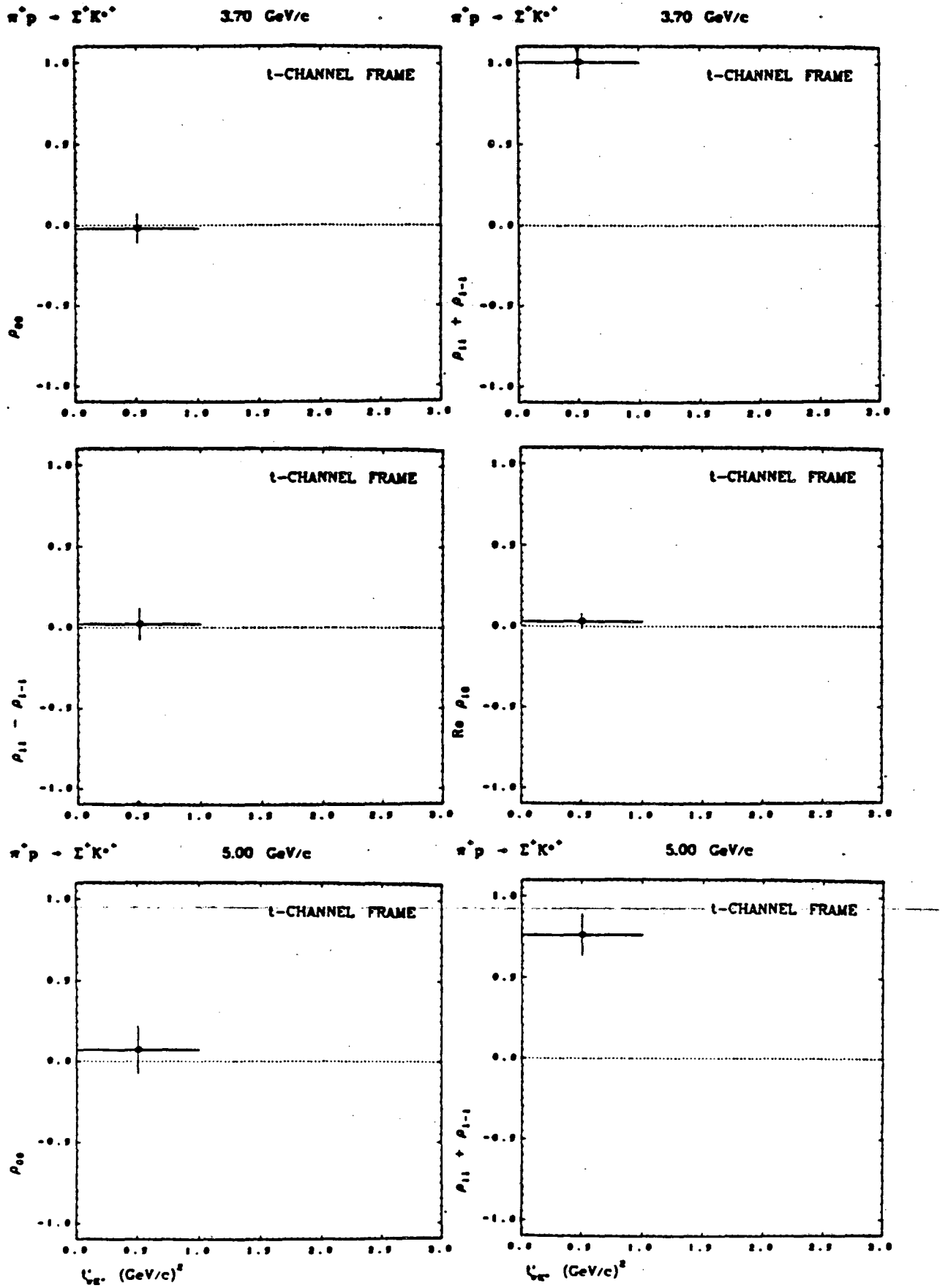
π⁺p → Σ⁺K*⁺
3.70 GeV/c
t-CHANNEL FRAME
ρ00
ρ11 + ρ1-1
ρ11 − ρ1-1
Re ρ10
5.00 GeV/c
t'K* (GeV/c)²

IV.18a

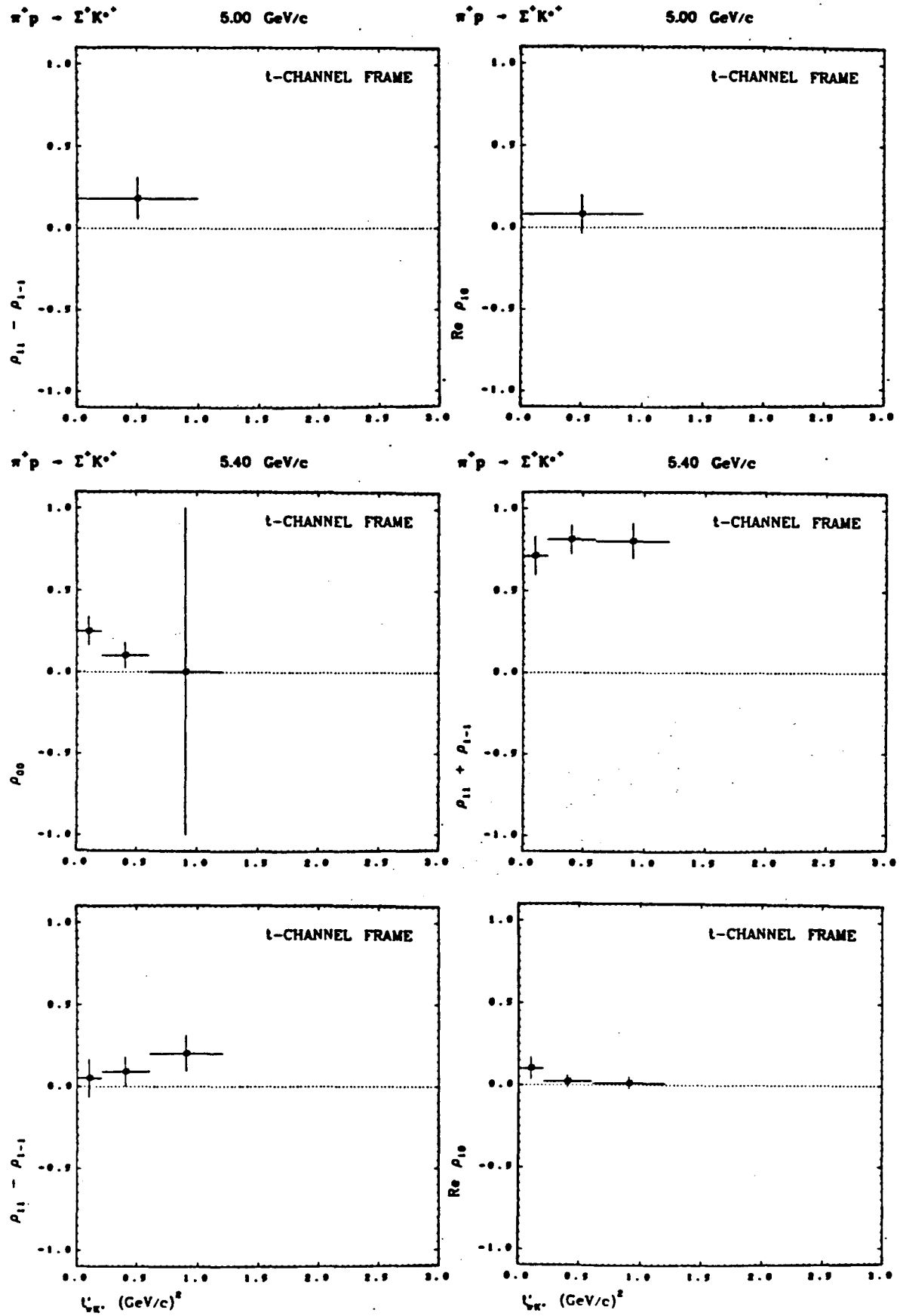
π⁺p → Σ⁺K*⁺
5.00 GeV/c
t-CHANNEL FRAME
ρ11 − ρ1-1
Re ρ10
5.40 GeV/c
ρ00
ρ11 + ρ1-1
t'K* (GeV/c)²

IV.18b

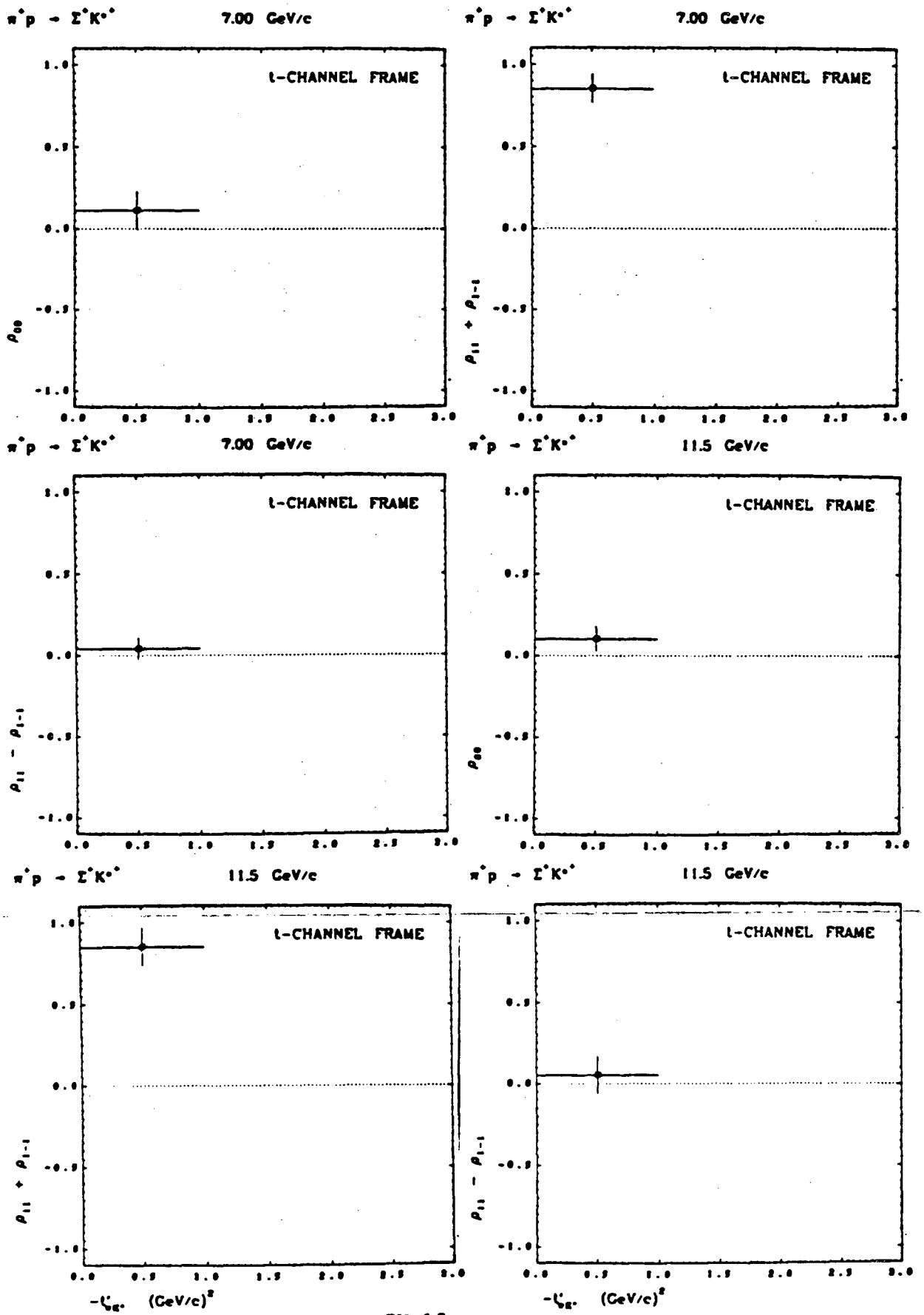
π⁺p → Σ⁺K*⁺
7.00 GeV/c
t-CHANNEL FRAME
ρ00
ρ11 + ρ1-1
ρ11 − ρ1-1
11.5 GeV/c
-t'K* (GeV/c)²

IV.18c

the 7, 11.5 SLAC data of ref. 52, $P_\Sigma = 0.5-0.7$ is observed in ΣK^* (see sections on WEXD and line reversal).

In Chapter II we observed that our K^* mass distribution is not sensitive to the $\Sigma^+K^+\pi^0 - \Sigma^+K^0\pi^+$ resolution; here we further note that for the parity conserving decay $K^* \to K\pi$ the observable ρ_{ij} of equations IV.B.6 are even functions of ϑ,φ under the interchange of the π and K identities, which in either the s- or t-channel helicity frames corresponds to the transformation

$$\vartheta \to \pi - \vartheta$$

$$\varphi \to \varphi + \pi .$$

This leaves the moment estimators of ρ_{00}, ρ_{1-1}, Re ρ_{10}, ρ_{11} unaltered. However, misidentification of $\pi-K$ ambiguous ΣK^* events may affect the $K^*\rho_{ij}$ because the $K^+\pi^0$ events have a larger background than $K^0\pi^+$, but this effect should be small, since the overlap events are ~ few percent, and the background is at most ~ $\frac{1}{3}$ of the overlap. We have also examined the ρ_{ij} estimators for the $K\pi$ system for $\Sigma K\pi$ events outside the K^* band, i.e., the phase space background; we find for these events for t' near 0, $\rho_{00} \approx 0.76\pm0.20$, $\rho_{11}+\rho_{1-1} \approx 0.57\pm0.20$, $\rho_{11}-\rho_{1-1} \approx -0.33\pm0.05$, which is unlike the $K^*\rho_{ij}$. Additionally, the ρ_{ij} for $K^{*+} \to K^+\pi^0$ events are basically the same as for the $K^0\pi^+$ data despite the greater background, i.e., $\rho_{11}+\rho_{1-1}$ is still dominant.

2. Additional Tests for Multiplicity/Naturality of Exchanges

Ringland and Thews (RT), ref. 29, noted that just as the presence or absence of polarization in processes like $\pi p \to \Sigma K$ tests the presence and relative phases of the contributing exchanges, so relations among the t-

channel helicity frame ρ_{ij} yield analogous information for ΣK^*. These relations follow from general quantum mechanical invariance principles (J^P conservation) applied to the t-channel amplitudes, and are *not* dependent upon particular dynamical assumptions (as, e.g., Regge theory or the quark model). We have already seen that the dominance of $\rho_{11}+\rho_{1-1}$ over $\rho_{00}, \rho_{11}-\rho_{1-1}$ indicates the importance of natural parity exchange even at our low momenta. Let $\sigma_E = +1(-1)$ for natural (unnatural) parity exchange. Then RT show first that if only $\sigma_E = +1$ exchanges contribute:

$$\rho_{00} = 0 \tag{IV.B.7a}$$

$$\mathrm{Re}\rho_{10} = 0\,. \tag{IV.B.7b}$$

(IV.B.7a) is the same as the result of ref. 49 already discussed, and at all p_{inc}, ρ_{00} is small. Clearly (IV.B.7b) agrees well with the data at all momenta (see also section IV.B.3 on Additive Quark Model predictions). RT also show that for $\sigma_E = +1$ exchanges only,

$$\rho_{1-1} = |\rho_{1-1}| \;\; or \;\; \rho_{1-1} > 0 \tag{IV.B.8}$$

which also agrees with the data. Further, RT observe that if a *single* $\sigma_E = +1$ exchange dominates, or if several $\sigma_E = +1$ exchanges occur but all have the *same phase*, then all helicity amplitudes have the same phase, and $\mathrm{Im}\rho_{ij} = 0$, all i,j in IV.B.2, and one has

$$2(Re\,\rho_{10})^2 = \rho_{00}(\rho_{11}-\rho_{1-1})\,. \tag{IV.B.9}$$

Figure IV.19 displays the ratio $\dfrac{2(\mathrm{Re}\rho_{10})^2}{\rho_{00}(\rho_{11}-\rho_{1-1})}$ versus t' for our data and also the 3.7, 5.0, 5.4, 7, 11.5 data (for which the RT relations have not been checked), and we see that generally it is far from unity. If K^*, K^{**} exchanges dominate, then although $\sigma_E = +1$ for both, WEXD implies for the amplitudes that $K^* \propto iK^{**}$ (see Appendix A), i.e., the exchanges are 90° out of phase, so

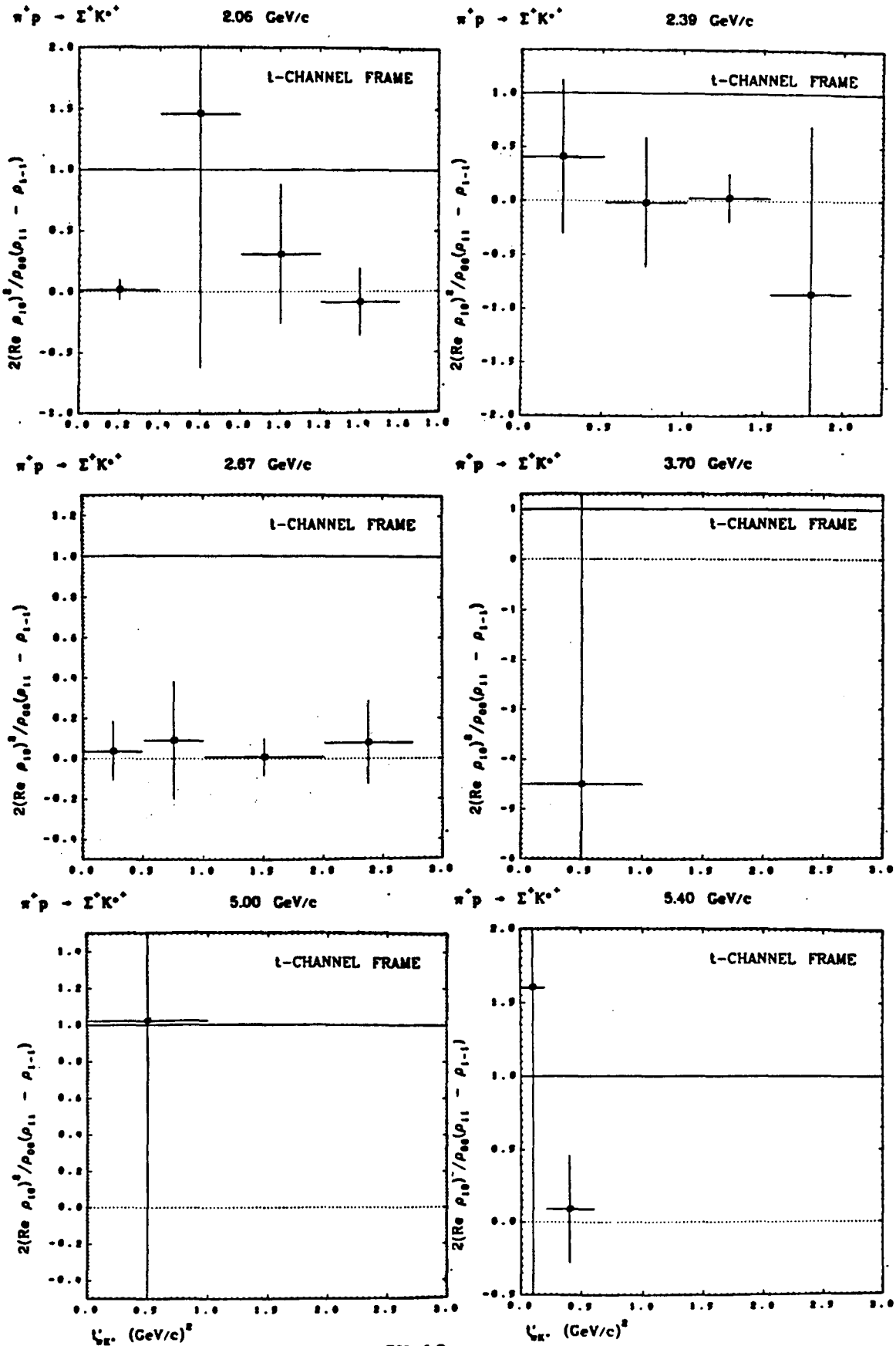
π⁺p → Σ⁺K*⁺
2.06 GeV/c
t-CHANNEL FRAME
π⁺p → Σ⁺K*⁺
2.39 GeV/c
t-CHANNEL FRAME
π⁺p → Σ⁺K*⁺
2.67 GeV/c
t-CHANNEL FRAME
π⁺p → Σ⁺K*⁺
3.70 GeV/c
t-CHANNEL FRAME
π⁺p → Σ⁺K*⁺
5.00 GeV/c
t-CHANNEL FRAME
π⁺p → Σ⁺K*⁺
5.40 GeV/c
t-CHANNEL FRAME
2(Re ρ10)s/ρ00(ρ11 − ρ1-1)
t'K* (GeV/c)²

IV.19

we expect (IV.B.9) to fail. In addition, $\mathrm{Im}\rho = 0$ (from which IV.B.9 follows) also implies $P_\Sigma = 0$, which we know does not hold.

Finally, RT show that if there are multiple exchanges and *all have the same* σ_E (but not necessarily identical phases), then:

$$\frac{z_t^2 - 1}{z_t^2 + 1} \leq \frac{|\rho_{1-1}|}{\rho_{11}} \leq 1 \qquad \text{(IV.B.10)}$$

where the upper bound follows merely from the positivity constraints on ρ and where z_t is the t-channel C.M. scattering angle cosine, given by (see Byckling and Kajantie, ref. 24):

$$z_t = \frac{t(s-u) + (m_\pi^2 - m_{K^*}^2)(m_p^2 - m_\Sigma^2)}{\lambda^{1/2}(t, m_\pi^2, m_{K^*}^2)\lambda^{1/2}(t, m_p^2, m_\Sigma^2)}$$

and $s+t+u = m_\pi^2 + m_{K^*}^2 + m_p^2 + m_\Sigma^2$, $\lambda(a,b,c) \equiv [a-(\sqrt{b}+\sqrt{c})^2][a-(\sqrt{b}-\sqrt{c})^2]$. In figure IV.20 is shown $|\rho_{1-1}|/\rho_{11}$ as a function of t' as well as the limits in (IV.B.10) above, and we see that at most momenta (IV.B.10) is either satisfied or consistent with the data as we expect for K^*, K^{**} dominance. We also note that as $s \to \infty$, $\frac{z_t^2 - 1}{z_t^2 + 1} \to 1$, so from (IV.B.10) for $\sigma_E = +1$, as $s \to \infty$, $\rho_{11} + \rho_{1-1} \to 2\rho_{11}$, $\rho_{11} - \rho_{1-1} \to 0$.

Also we note that for any spin 1 particle, the positivity conditions (which follow merely from the Hermiticity of ρ and parity conservation) on the density matrix elements ρ_{ij} are (see, e.g., R.D. Field et al., ref. 28, or Doncel et al., ref. 57):

$$2(Re\,\rho_{10})^2 \leq \rho_{00}(\rho_{11} - \rho_{1-1})$$

and

$$|\rho_{1-1}| \leq \rho_{11}$$

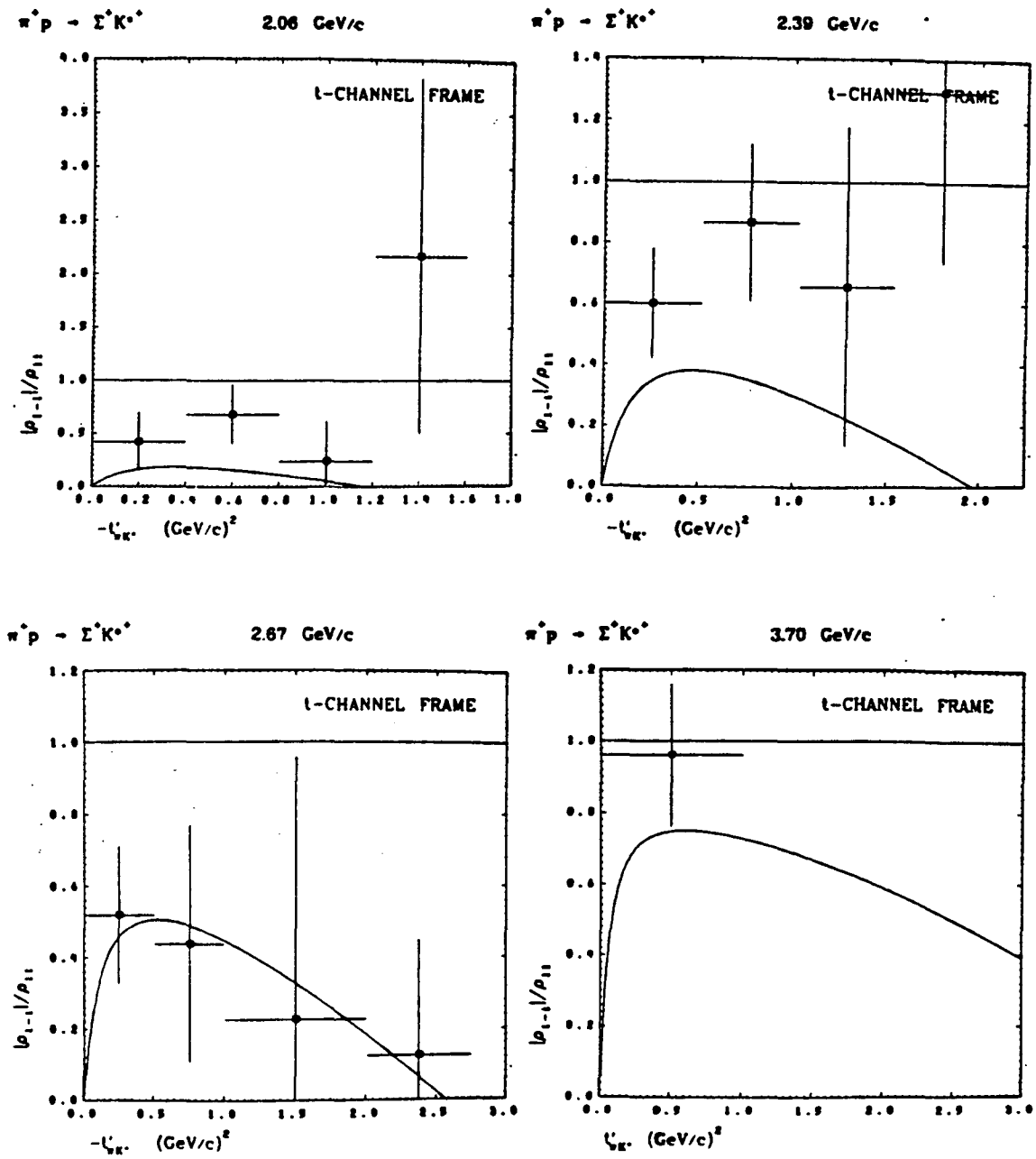
π⁺p → Σ⁺K*⁺
2.06 GeV/c
t-CHANNEL FRAME
|ρ1-1|/ρ11
-t'K* (GeV/c)²
π⁺p → Σ⁺K*⁺
2.39 GeV/c
t-CHANNEL FRAME
|ρ1-1|/ρ11
-t'K* (GeV/c)²
π⁺p → Σ⁺K*⁺
2.67 GeV/c
t-CHANNEL FRAME
|ρ1-1|/ρ11
-t'K* (GeV/c)²
π⁺p → Σ⁺K*⁺
3.70 GeV/c
t-CHANNEL FRAME
|ρ1-1|/ρ11
t'K* (GeV/c)²

IV.20a

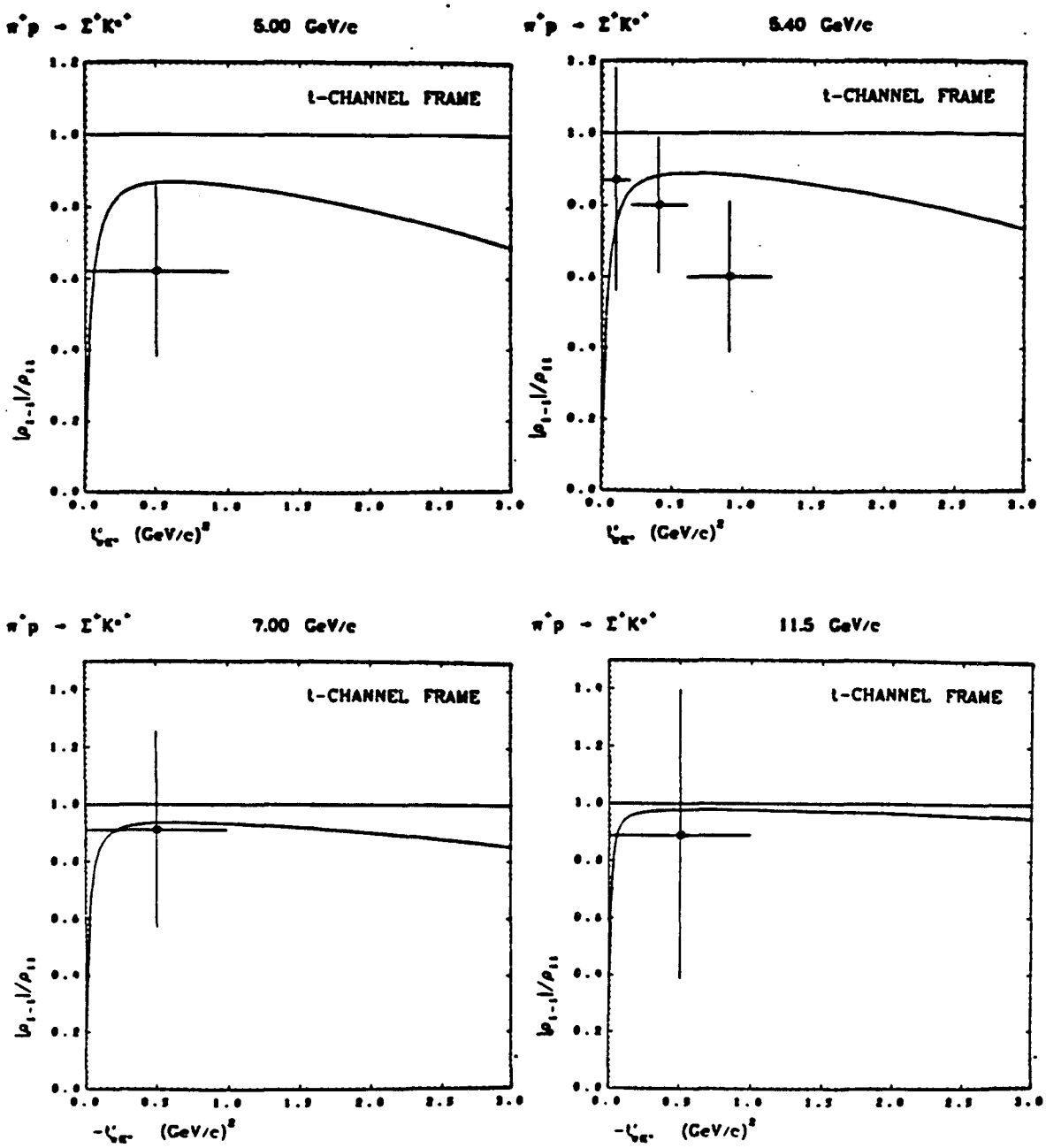
π⁺p → Σ⁺K*⁺
5.00 GeV/c
t-CHANNEL FRAME
π⁺p → Σ⁺K*⁺
5.40 GeV/c
t-CHANNEL FRAME
π⁺p → Σ⁺K*⁺
7.00 GeV/c
t-CHANNEL FRAME
π⁺p → Σ⁺K*⁺
11.5 GeV/c
t-CHANNEL FRAME
(GeV/c)²

IV.20b

and we note in figures IV.19 and IV.20 that most points satisfy these requirements, and the remainder are consistent with them; equality in the first constraint is just the RT test (IV.B.9), and the second condition is the right-hand half of (IV.B.10).

Because of the large experimental uncertainties and few data points in the world sample of Σ^+K^{*+}, we make no attempt to extract the α_{eff}'s for the various natural and unnatural parity contributions to $\frac{d\sigma}{dt'}$; instead we note again that the power law behavior of $\sigma(\Sigma K^*)$ in p_{inc} is consistent with that expected if K^*, K^{**} exchanges dominate.

3. Isospin of t-Channel Exchanges and Exchange Degeneracy for ΣK^*

Isotopic spin analysis in the t-channel yields for $\pi^+p \to K^{*+}\Sigma^+$ and $\pi^-p \to K^{*0}\Sigma^0$ a relation analogous to equation IV.A.9, provided we have only $I_t = \frac{1}{2}$exchange:

$$\frac{d\sigma}{dt}(\pi^+p \to K^{*+}\Sigma^+) = 2\,\frac{d\sigma}{dt}(\pi^-p \to K^{*0}\Sigma^0)\,. \qquad \text{(IV.B.11)}$$

We note that IV.B.11 should hold separately for the various naturality exchange components of $\frac{d\sigma}{dt}$discussed in section IV.B.1, and in particular:

$$(\rho_{11}+\rho_{1-1})\,\frac{d\sigma}{dt}(K^{*+}\Sigma^+) = 2(\rho_{11}+\rho_{1-1})\,\frac{d\sigma}{dt}(K^{*0}\Sigma^0)\,. \qquad \text{(IV.B.12)}$$

Relation IV.B.11 has in the past been tested only with integrated cross sections, and IV.B.12 has apparently not been examined experimentally. We test IV.B.11,12 using the only available data at the same momenta, the 3.7 $K^{*+}\Sigma^+$ data of Butler, ref. 21, and the new 3.95 GeV/c $K^{*0}\Sigma^0$ data of Aguilar-Benitez

et al., ref. 51. The ρ_{ij} of ref. 51 are in the s-channel helicity system, but $(\rho_{11}+\rho_{1-1})$ is invariant under rotation from the s- to the t-channel system (see, e.g., Field et al., ref. 28). Thus in figure IV.21 we display the 3.7 Σ^+K^{*+} data scaled to 3.95, with the Σ^0K^{*0} data multiplied by 2; clearly IV.B.11 is well satisfied, and IV.B.12 is consistent with the data within statistics. For both the $\Sigma^+K^{*+},\Sigma^0K^{*0}$ data there is presumably a background of at least 10% or so, so we conclude that to no better than that precision $I_t = \frac{3}{2}$ contributions to ΣK^* production are negligible.

$K^-p \to \rho^-\Sigma^+$ is related to $\pi^+p \to K^{*+}\Sigma^+$ (through $SU(3)$ and factorization) by generalized line reversal (see Appendix A), and just as with the ΣK channel, if the K^*,K^{**} Regge pole exchanges dominate $K^*\Sigma,\rho\Sigma$ (i.e., if cut and absorptive contributions are negligible) we expect the hierarchy of results (again, see Appendix A):

(a) *Line Reversal (LR)* only implies

$$\begin{aligned} &\mathrm{Im}\rho(K^*\Sigma)\,\mathrm{Im}\rho(\rho\Sigma) < 0 \\ \text{or}\quad &\mathrm{Im}\rho(K^*\Sigma)\,\frac{d\sigma}{dt} = -\mathrm{Im}\rho(\rho\Sigma)\,\frac{d\sigma}{dt} \end{aligned} \tag{IV.B.13}$$

for all density matrices and in particular

$$P_\Sigma(K^*\Sigma)P_\Sigma(\rho\Sigma) < 0 \tag{IV.B.14}$$

(b) *LR - WEXD* implies

$$\frac{d\sigma}{dt}(K^*\Sigma) = \frac{d\sigma}{dt}(\rho\Sigma) \tag{IV.B.15}$$

and

$$\rho(K^*\Sigma) = \rho^*(\rho\Sigma) \tag{IV.B.16}$$

for all density matrices, so in particular

3.95 GeV/c

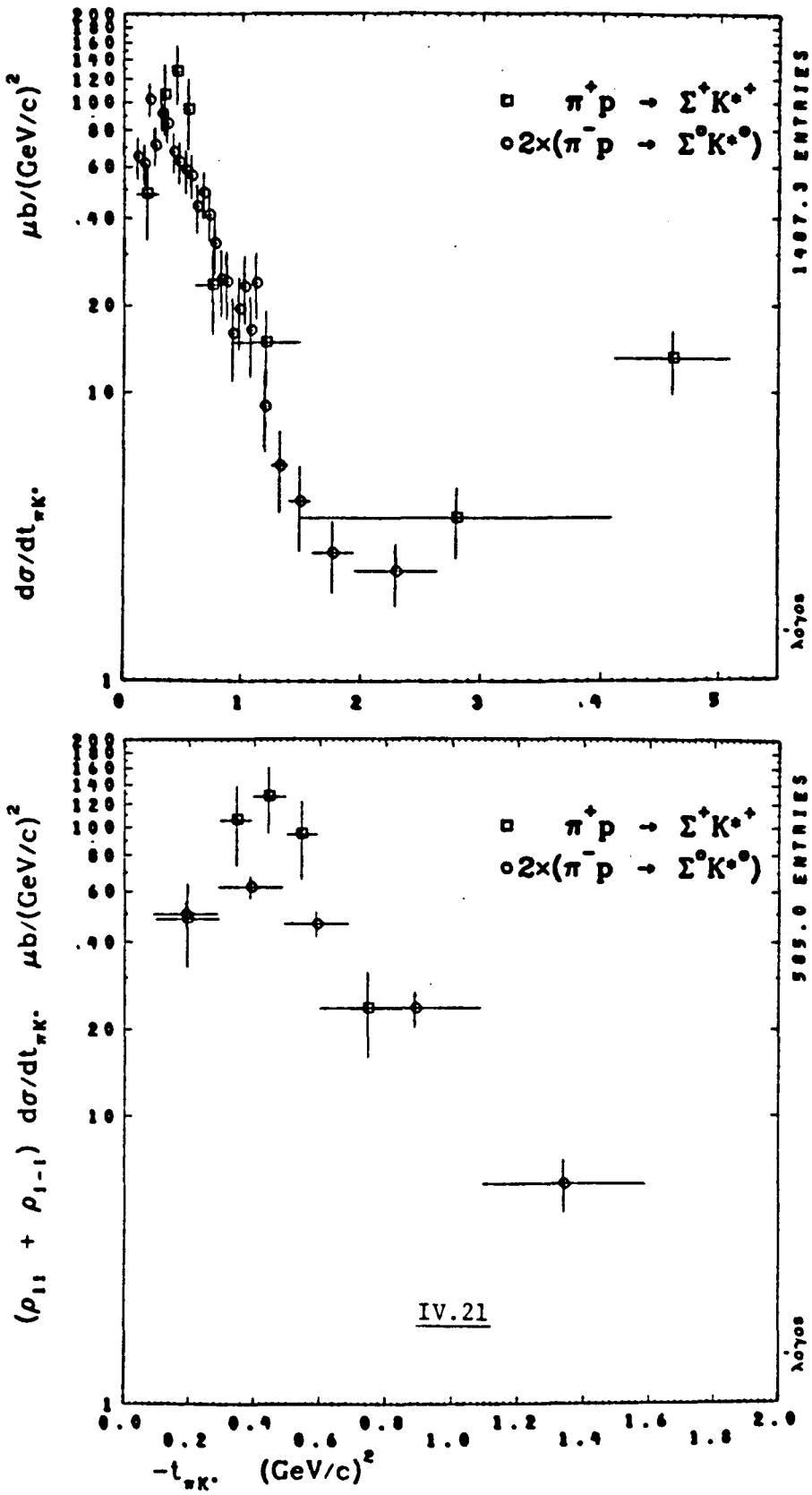

IV.21

$$P_\Sigma(K^*\Sigma) = -P_\Sigma(\rho\Sigma) \qquad \text{(IV.B.17)}$$

and equality is implied for the various naturality exchange cross section components, e.g.,

$$(\rho_{11}+\rho_{1-1})\ \frac{d\sigma}{dt}(K^*\Sigma) = (\rho_{11}+\rho_{1-1})\ \frac{d\sigma}{dt}(\rho\Sigma) \qquad \text{(IV.B.18)}$$

(c) *LR + EXD* implies IV.B.15,IV.B.16 and the additional result

$$\mathrm{Im}\rho(K^*\Sigma) = \mathrm{Im}\rho(\rho\Sigma) = 0 \qquad \text{(IV.B.19)}$$

for all density matrices, so

$$P_\Sigma(K^*\Sigma) = P_\Sigma(\rho\Sigma) = 0\ . \qquad \text{(IV.B.20)}$$

We first observe that at all momenta where $P_\Sigma(K^*\Sigma)$ is available, i.e., our 2.06, 2.38, 2.67 GeV/c and the 7, 11.5 GeV/c data, we have $P_\Sigma \neq 0$ so that EXD can immediately be ruled out. We test relations IV.B.13-IV.B.18 at lower momenta than ever before using the previously unanalyzed 3.7 GeV/c $K^{*+}\Sigma^+$ (ref. 21), 4.25 GeV/c $\rho^-\Sigma^+$ (de Groot et al., ref. 53) data shown in figure IV.22, which displays $\frac{d\sigma}{dt}$, $(\rho_{11}+\rho_{1-1})\ \frac{d\sigma}{dt}$, and the vector meson ρ_{ij} at 4.25 GeV/c (the 3.7 $K^*\Sigma$ $\frac{d\sigma}{dt}$ data has been scaled to 4.25).

We see that IV.B.15,IV.B.18 hold fairly well within the statistical precision; since we only have the real parts of the ρ's, we cannot from the 4.25 comparison alone distinguish IV.B.16 from IV.B.19, but the significantly nonzero P_Σ at the lower and higher momenta rule out IV.B.19, so we conclude that WEXD in equations IV.B.15-IV.B.18 holds fairly well for $K^{*+}\Sigma^+,\rho^-\Sigma^+$ as low as 4 GeV/c. The 7, 11.5 GeV/c $K^{*+}\Sigma^+,\rho^-\Sigma^+$ data of ref. 52 satisfy IV.B.15,IV.B.17 well; although the authors of ref. 52 do not point out that the general result IV.B.16 should apply to $K^*\Sigma,\rho\Sigma$ with WEXD, inspection of their

4.25 GeV/c

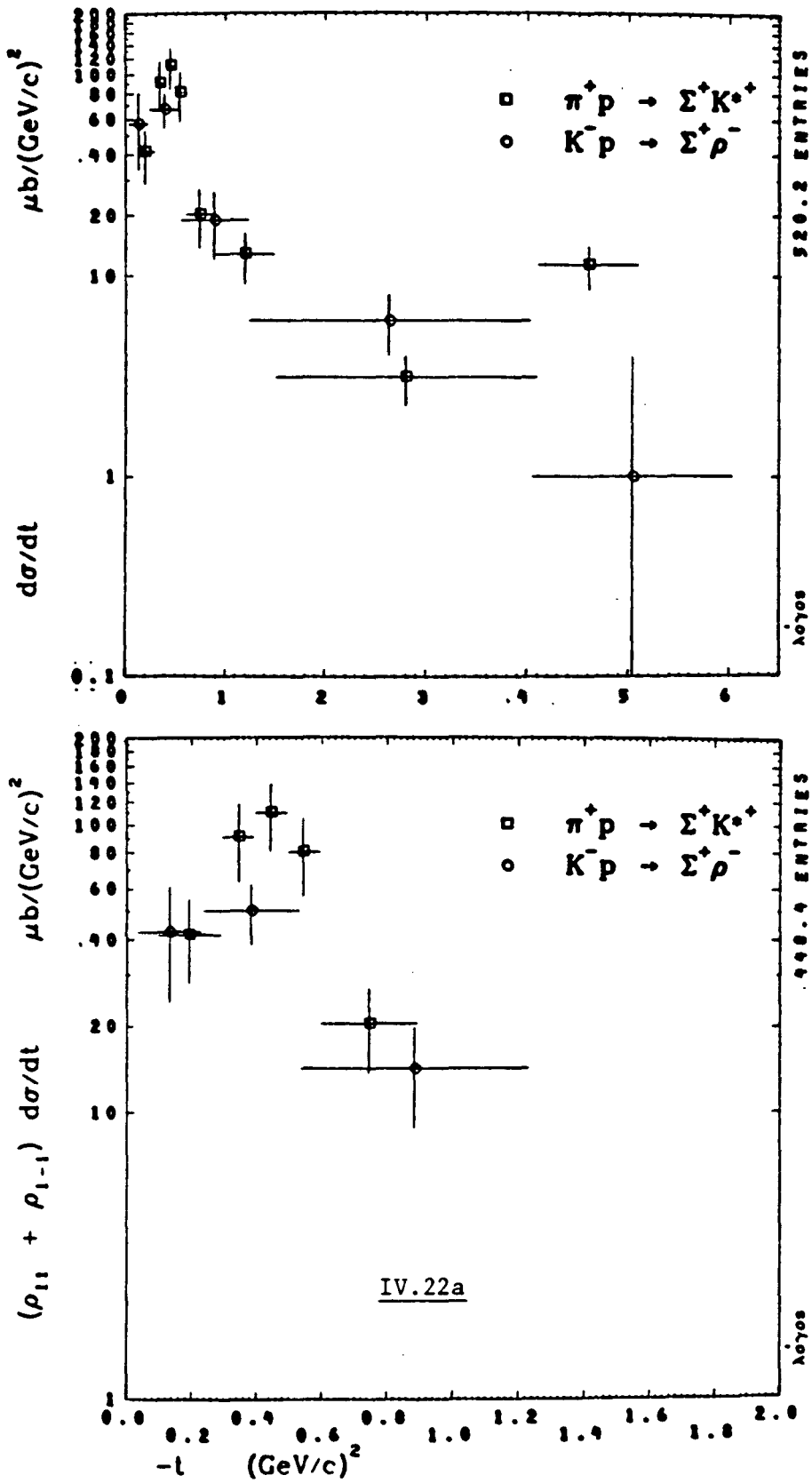
μb/(GeV/c)²
dσ/dt
π⁺p → Σ⁺K*⁺
K⁻p → Σ⁺ρ⁻
520.2 ENTRIES
(ρ₁₁ + ρ₁₋₁) dσ/dt
448.4 ENTRIES
IV.22a
−t (GeV/c)²

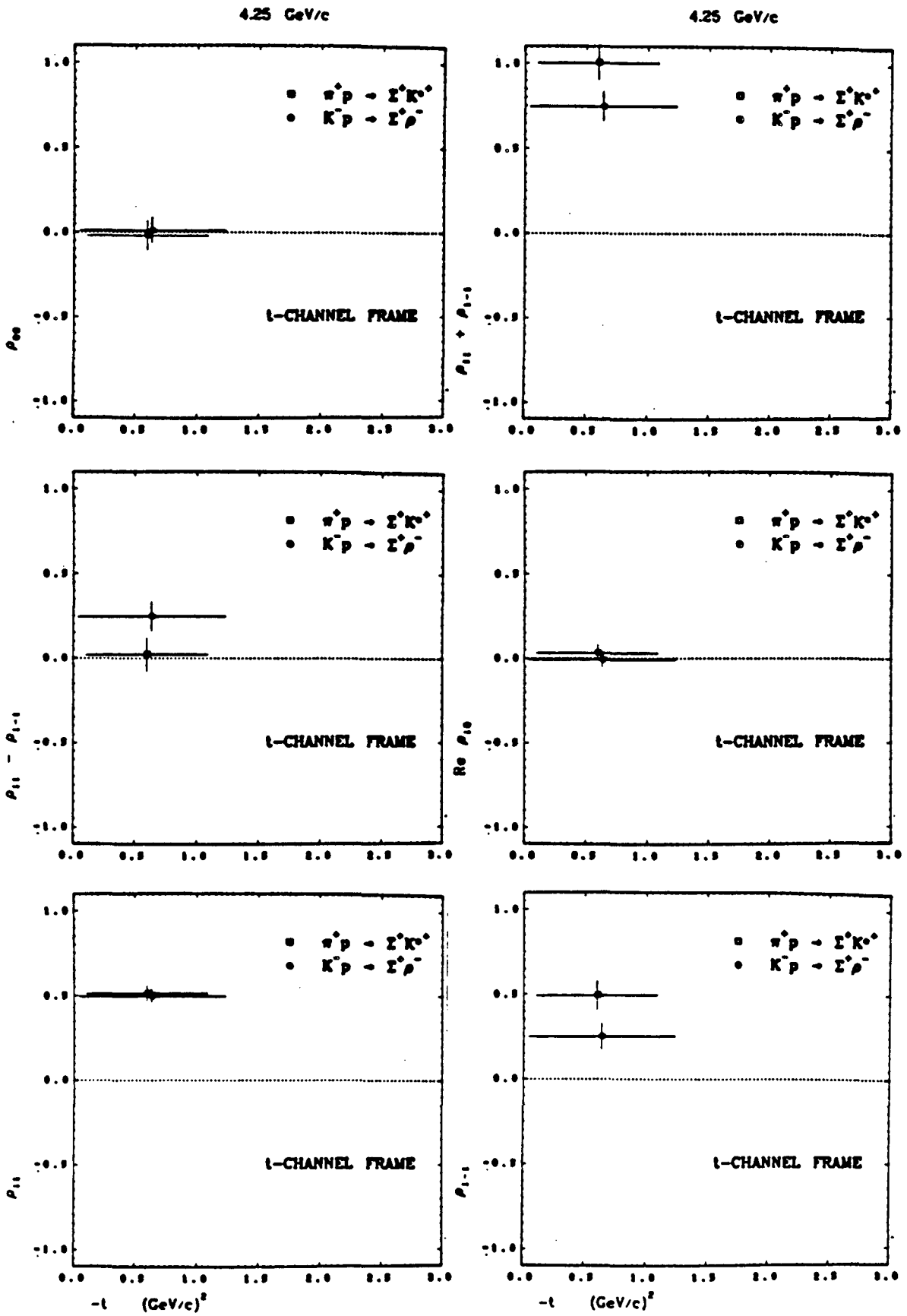
4.25 GeV/c
4.25 GeV/c
π⁺p → Σ⁺K⁰⁺
K⁻p → Σ⁺π⁻
t-CHANNEL FRAME
ρ00
ρ11 + ρ1-1
ρ11 − ρ1-1
Re ρ10
ρ11
ρ1-1
-t (GeV/c)²

IV.22b

data shows that $\rho(K^*\Sigma) = \rho^*(\rho\Sigma)$ is well satisfied at both 7 and 11.5 GeV/c.

We observe at all momenta that the $K^*\Sigma,\rho\Sigma$ data show pronounced forward turnovers, which as mentioned before, implies helicity flip amplitude dominance. As NS remark in ref. 41, the flip amplitudes for HYCEX are generally closer to pure Regge pole exchanges, so that the negligibility of cut and absorptive contributions required for the LR + WEXD results above to hold is provided by the flip dominance. In summary, if multiple exchange processes such as cut contributions are small (pole dominance), and if $SU(3)$ symmetry (for vertices) holds, then we expect IV.B.11 to be satisfied, as it seems to be; if in addition the dominant poles are WEXD, we expect IV.B.15-18 to hold as they apparently do.

4. Additive Quark Model Prediction

The Additive Quark Model (AQM) as developed by Bialas and Zalewski, ref. 54, describes the amplitude in the forward region for a process like $\pi p \to \Sigma K^*$, taking the hadrons as $SU(6)$ quark composites, as simply the sum of single quark-single quark scattering amplitudes, with no baryon number exchange or multiple quark scatterings; the constituent quarks are treated as essentially free particles in a spectator approximation. The no baryon number exchange approximation is slightly violated at our energies since there are backward peaks, but the additivity implication (since multiple quark scattering is ignored) that there are no exotic ($I > 1$) exchanges in the forward direction agrees with the data for Σ^+K^+, and with the tests of the previous section at 4 GeV/c for Σ^+K^{*+}. The consequences of these assumptions alone are called Class A Predictions. There are no Class A predictions

for ΣK^*, but with the further assumptions that the additive quark helicity amplitudes are charge-conjugation and time-reversal symmetric (Class C Predictions), ref. 54 predicts for $\pi p \to \Sigma K^*$:

$$\mathrm{Re}\rho_{10} = 0 . \qquad \text{(IV.B.21)}$$

Unfortunately (IV.B.21) is not independent of choice of helicity frame, and in ref. 55, Bialas, Kotanski, and Zalewski argue that the t-channel frame is the appropriate choice. For the ΣK^* (and $\rho\Sigma$) data (IV.B.21) is well obeyed in the forward region at all momenta in both the s- and t-channel frames. (IV.B.21) is also equivalent to the RT result (IV.B.7b); the RT condition of course follows from general invariance principles.

5. Quark Counting Rules and Large Angle Scattering

As we saw for ΣK, so for ΣK^* the quark composite picture for hadrons (again, see Sivers, Brodsky and Blankenbecler, ref. 46) leads to the expectation that at C.M. angles near 90°, $\frac{d\sigma}{dt}$ for $0^-\frac{1}{2}^+ \to 1^-\frac{1}{2}^+$ should be of form:

$$\frac{d\sigma}{dt}(\pi p \to \Sigma K^*) = \frac{1}{s^9} f(\cos\vartheta_{CM}) \qquad \text{(IV.B.22)}$$

where the extra power of $\frac{1}{s}$, as compared to (IV.A.20), comes from treating the vector spin of the K^* as an additional active field degree of freedom. Figure IV.23 shows $s^9 \frac{d\sigma}{dt}$ for the 2.38, 2.67, 3.7, and 5.4 GeV/c Σ^+K^+ data, and as in ΣK, we note a definite narrowing of the envelope of points for $\cos\vartheta_{CM} \approx 0$; the C.M. energies used cover a range in s^9 of a factor of 650. We conclude that the ΣK^* channel agrees qualitatively with quark-constituent hadron expectations. (Horizontal error bars have been suppressed in figure

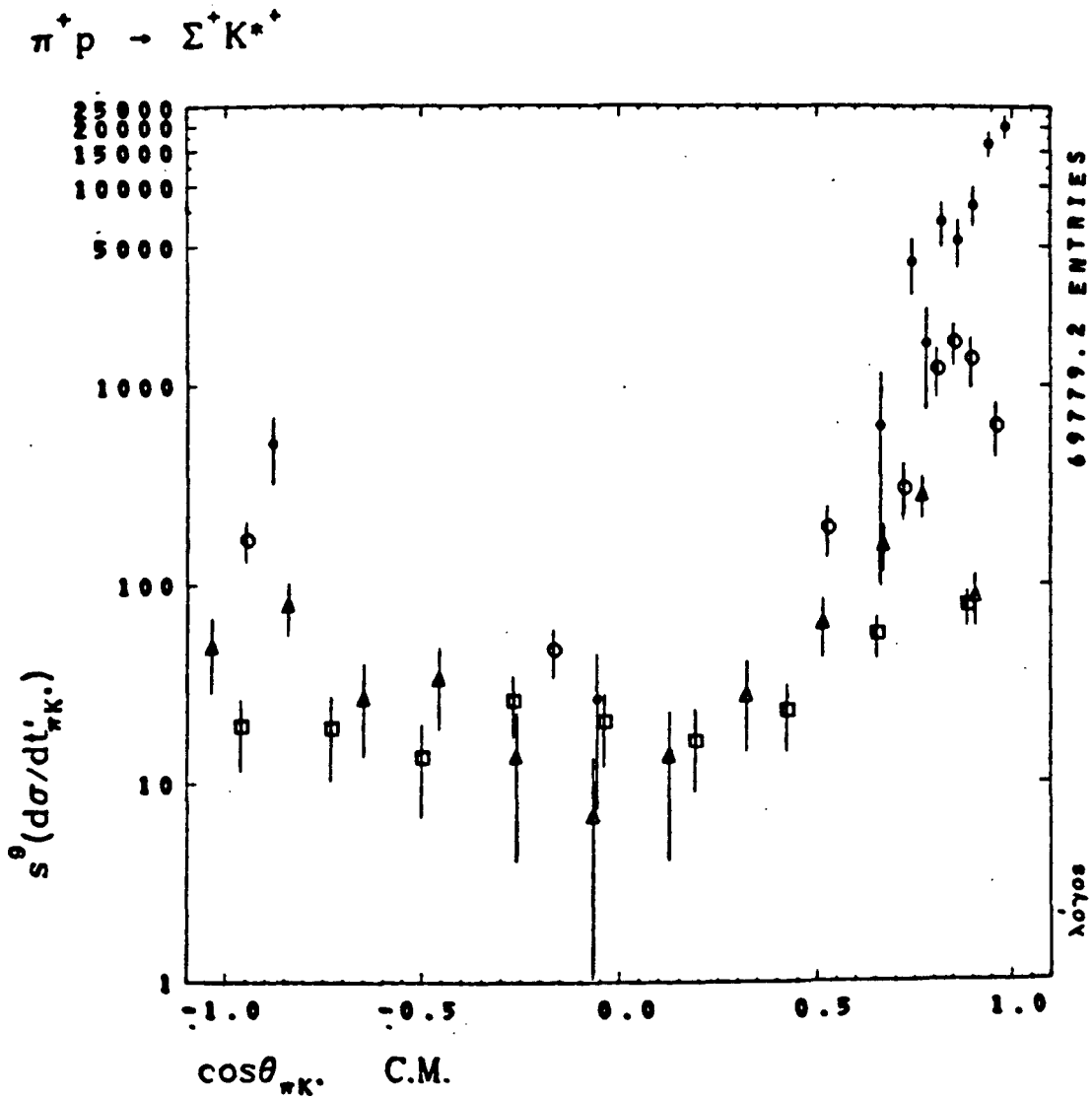
$\pi^+ p \rightarrow \Sigma^+ K^{*+}$
25000
20000
15000
10000
5000
1000
100
10
1
$s^{\theta}(d\sigma/dt'_{\pi K^*})$
-1.0
-0.5
0.0
0.5
1.0
$\cos\theta_{\pi K^*}$ C.M.
69779.2 ENTRIES
λόγος

IV.23

IV.23 for ease of interpretation; the points of the 3.7 and 5.4 GeV/c data at $\cos\vartheta_{CM} = 0$ unfortunately cover a fairly large fraction of the range of $\cos\vartheta_{CM}$.)

C. $\Sigma^* K$

1. $\frac{d\sigma}{dt}$, $\rho_{ij}(\Sigma^*)$

The process $\pi^+ p \to \Sigma^*(1385)^+ K^+$ has, after taking parity conservation into account, 4 independent invariant (s- or t-channel) helicity amplitudes (again, see, e.g., Doncel, Minnaert, and Michel, ref. 57): one non-flip $H_{\frac{1}{2}\frac{1}{2}}$, two single-flip $H_{\frac{1}{2}\frac{3}{2}}$, $H_{\frac{1}{2}-\frac{1}{2}}$, and one double-flip $H_{-\frac{1}{2}\frac{3}{2}}$. In terms of these H_{lm},

$$\frac{d\sigma}{dt} = \sum_{\text{helicities}} |H|^2 . \qquad \text{(IV.C.1)}$$

From here on, we will omit the denominators in the helicity subscripts so that, e.g., by H_{13} we mean $H_{\frac{1}{2}\frac{3}{2}}$.

The helicity state of the produced Σ^* is specified by the Σ^* density matrix elements ρ_{ij} where

$$\rho_{ij} = \frac{\sum_l H_{li} H_{lj}^*}{\sum_{m,n} |H_{mn}|^2} . \qquad \text{(IV.C.2)}$$

As usual, $t' \equiv t - t_{\min}$, $|t_{\min}| \equiv \textit{minimum}\,|t|$, and $t \equiv (p_k - p_\pi)^2$. For the purpose of data analysis, the $\Sigma^*(1385)K$ state is defined by a simple $m_{\Lambda\pi}$ cut on the $\Lambda\pi K$ final state:

$$m_{\Sigma^*} - 1.5\Gamma_0 \le m_{\Lambda\pi} \le m_{\Sigma^*} + 1.5\Gamma_0 .$$

With this cut there is approximately 12-14% 3-body background in the Σ^*

mass band for our 5 higher momenta.

Because of limited statistics, we combine the 1.41, 1.43, 1.55 GeV/c data samples which we label with the weighted average incident momentum 1.47 GeV/c; the 1.84 and 1.94 samples are combined as 1.89 GeV/c; the 2.15 and 2.30 samples are combined as 2.22 GeV/c; and the 2.46 and 2.67 samples are combined as 2.59 GeV/c. Figures IV.24 and IV.25 exhibit the $\Sigma^{*+}K^+$ $\frac{d\sigma}{dt'}$ and $\frac{dN}{d\cos\vartheta_{CM}}$ for our 7 incident momentum samples. We note a progressively stronger forward direction peaking as the incident momentum ascends, with a turnover at $t' = 0$, and in the 1.63, 1.89, 2.23, 2.59 samples, a suggestion of a secondary peak in the backward hemisphere. This backward hemisphere behavior is also apparent in the highest momentum $\pi^+p \to \Sigma^{*+}K^+$ data overlapping ours, that of Moore at 2.18 GeV/c and Davies at 2.24 GeV/c, both from π^+d experiments quoted in the PDG compilation, ref. 12. Data at incident momenta above 3 GeV/c do not extend far enough in t to observe whether the backward hemisphere features persist. The turnover at $t' = 0$, however, is a feature which does appear in the Σ^*K channel from near threshold on through the highest momenta yet obtained, such as that of Baker *et al.* and Cautis *et al.*, ref. 58, at 7.0 and 11.5 GeV/c, and that of May *et al.*, ref. 59, from FNAL at 35, 70, and 140 GeV/c.

To study the Σ^* helicity state, as for the K^* channel, two helicity-type quantization axis systems in the Σ^* rest frame are conventional: for reactions of type $0^-\frac{1}{2}^+ \to 0^-\frac{3}{2}^+$ (all unit vectors are in the Σ^* C.M.) we use

$$\begin{array}{ll} \text{t-channel} & \hat{y}_t \equiv \hat{n} \equiv \hat{p}_\pi \times \hat{p}_K = \hat{p}_p \times \hat{p}_{\Sigma^*} \\ \text{helicity frame} & \hat{z} \equiv \hat{p}_p \\ & \hat{x}_t \equiv \hat{y}_t \times \hat{z}_t \end{array} \qquad \text{(IV.C.3)}$$

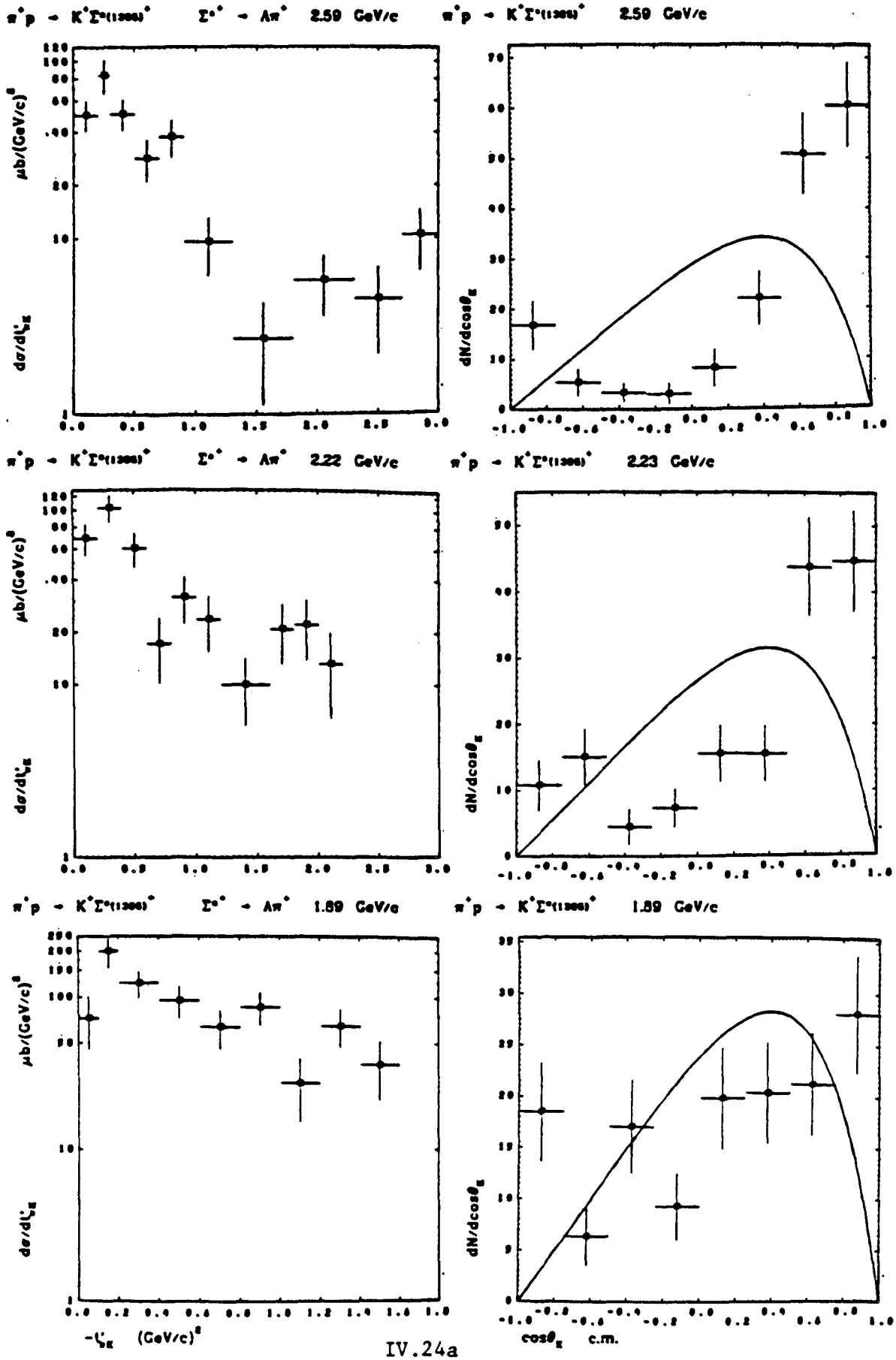
π⁺p → K⁺Σ*(1385)⁺ Σ*⁺ → Λπ⁺ 2.59 GeV/c
π⁺p → K⁺Σ*(1385)⁺ 2.59 GeV/c
π⁺p → K⁺Σ*(1385)⁺ Σ*⁺ → Λπ⁺ 2.22 GeV/c
π⁺p → K⁺Σ*(1385)⁺ 2.23 GeV/c
π⁺p → K⁺Σ*(1385)⁺ Σ*⁺ → Λπ⁺ 1.89 GeV/c
π⁺p → K⁺Σ*(1385)⁺ 1.89 GeV/c
μb/(GeV/c)²
dσ/dt'K
dN/dcosθK
-t'K (GeV/c)²
cosθK c.m.

IV.24a

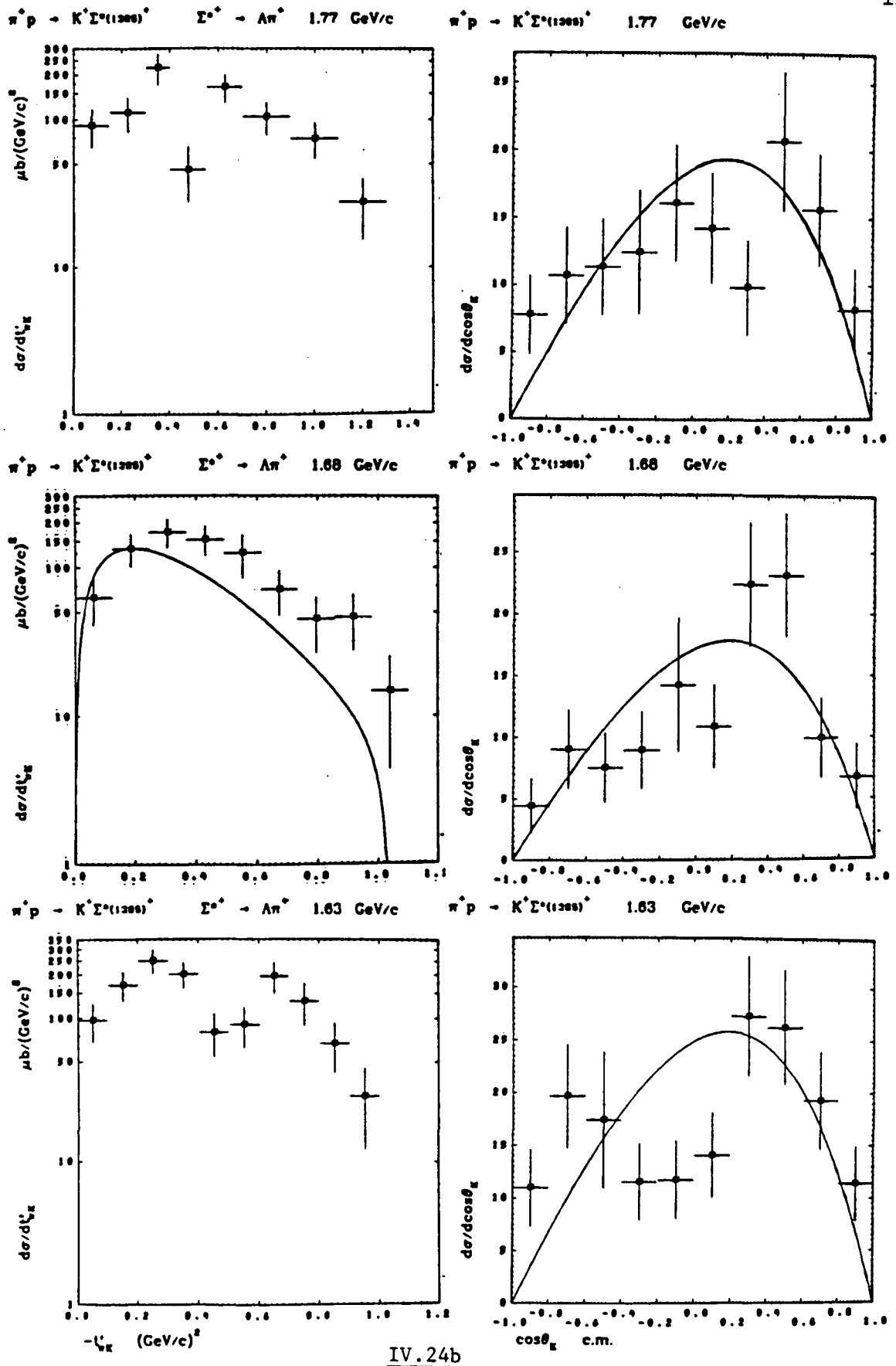
π⁺p → K⁺Σ*(1385)⁺ Σ*⁺ → Λπ⁺ 1.77 GeV/c
π⁺p → K⁺Σ*(1385)⁺ 1.77 GeV/c
π⁺p → K⁺Σ*(1385)⁺ Σ*⁺ → Λπ⁺ 1.68 GeV/c
π⁺p → K⁺Σ*(1385)⁺ 1.68 GeV/c
π⁺p → K⁺Σ*(1385)⁺ Σ*⁺ → Λπ⁺ 1.63 GeV/c
π⁺p → K⁺Σ*(1385)⁺ 1.63 GeV/c
μb/(GeV/c)²
dσ/dt'_K
dσ/dcosθ_K
-t'_K (GeV/c)²
cosθ_K c.m.

IV.24b

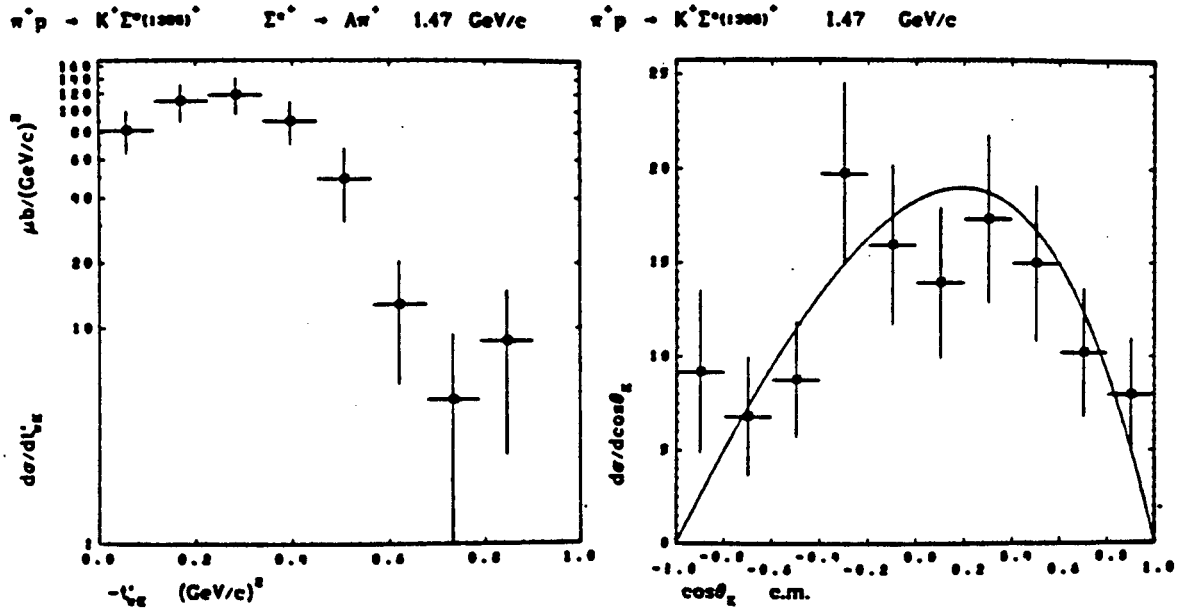
π⁺p → K⁺Σ*(1385)⁺ Σ*⁺ → Λπ⁺ 1.47 GeV/c
π⁺p → K⁺Σ*(1385)⁺ 1.47 GeV/c
μb/(GeV/c)²
dσ/dt'
-t' (GeV/c)²
dσ/dcosθ
cosθ c.m.

IV.25

$$\begin{array}{ll} \text{s-channel} & \hat{y}_s \equiv \hat{n} \equiv \hat{p}_p \times \hat{p}_{\Sigma^*} = \hat{y}_t \\ \text{helicity frame} & \hat{z}_s \equiv \hat{p}_{\Sigma^*} = -\hat{p}_K \\ & \hat{x}_s \equiv \hat{y}_s \times \hat{z}_s \end{array} \tag{IV.C.4}$$

(We observe again that the t-channel system of axes is invariant (unrotated) under a Lorentz transformation from the Σ^* rest frame to the t-channel center of mass ($p\bar{\Sigma}^*$) frame, and the s-channel axes are invariant under a Lorentz transformation from the Σ^* rest frame to the s-channel center of mass (πp) frame.) At very high energies near the forward direction the s- and t-channel frames asymptotically coincide.

With respect to either system the Σ^* decay angular distribution in terms of the ρ_{ij} of IV.C.2 is (again, see H.J. Schreiber, ref. 48):

$$W(\cos\vartheta,\varphi) = \frac{3}{4\pi}\left[\frac{1}{6}(1+4\rho_{33}) + \frac{1}{2}(1-4\rho_{33})\cos^2\vartheta \right. \tag{IV.C.5}$$

$$\left. - \frac{2}{\sqrt{3}}(\mathrm{Re}\rho_{3-1})\sin^2\vartheta\cos^2\varphi - \frac{2}{\sqrt{3}}(\mathrm{Re}\rho_{31})\sin 2\vartheta\cos\varphi \right]$$

and where $tr\rho = 1$ with $\rho_{-m-n} = (-1)^{m-n}\rho_{mn}$ implies $\rho_{11} = \frac{1}{2} - \rho_{33}$. Again because the background in the Σ^* region is only 12-14%, we use the method of moment estimators to determine the ρ_{ij} from the data (see ref. 48):

$$\rho_{33} = \frac{1}{8} < 7 - 15\cos^2\vartheta > \tag{IV.C.6a}$$

$$\mathrm{Re}\rho_{3-1} = -\frac{5\sqrt{3}}{8} < \sin^2\vartheta\cos 2\varphi > \tag{IV.C.6b}$$

$$\mathrm{Re}\rho_{31} = -\frac{5\sqrt{3}}{8} < \sin 2\vartheta\cos\varphi > \tag{IV.C.6c}$$

$$\rho_{11} = \frac{1}{8} < 15\cos^2\vartheta - 3 > . \tag{IV.C.6d}$$

The values of the $\Sigma^*\rho_{ij}$ for our 7 incident momentum samples are displayed in figures IV.26 through IV.31 as functions of t', as well as the Σ^* rest frame decay cosine with respect to the production normal $\hat{n}$.

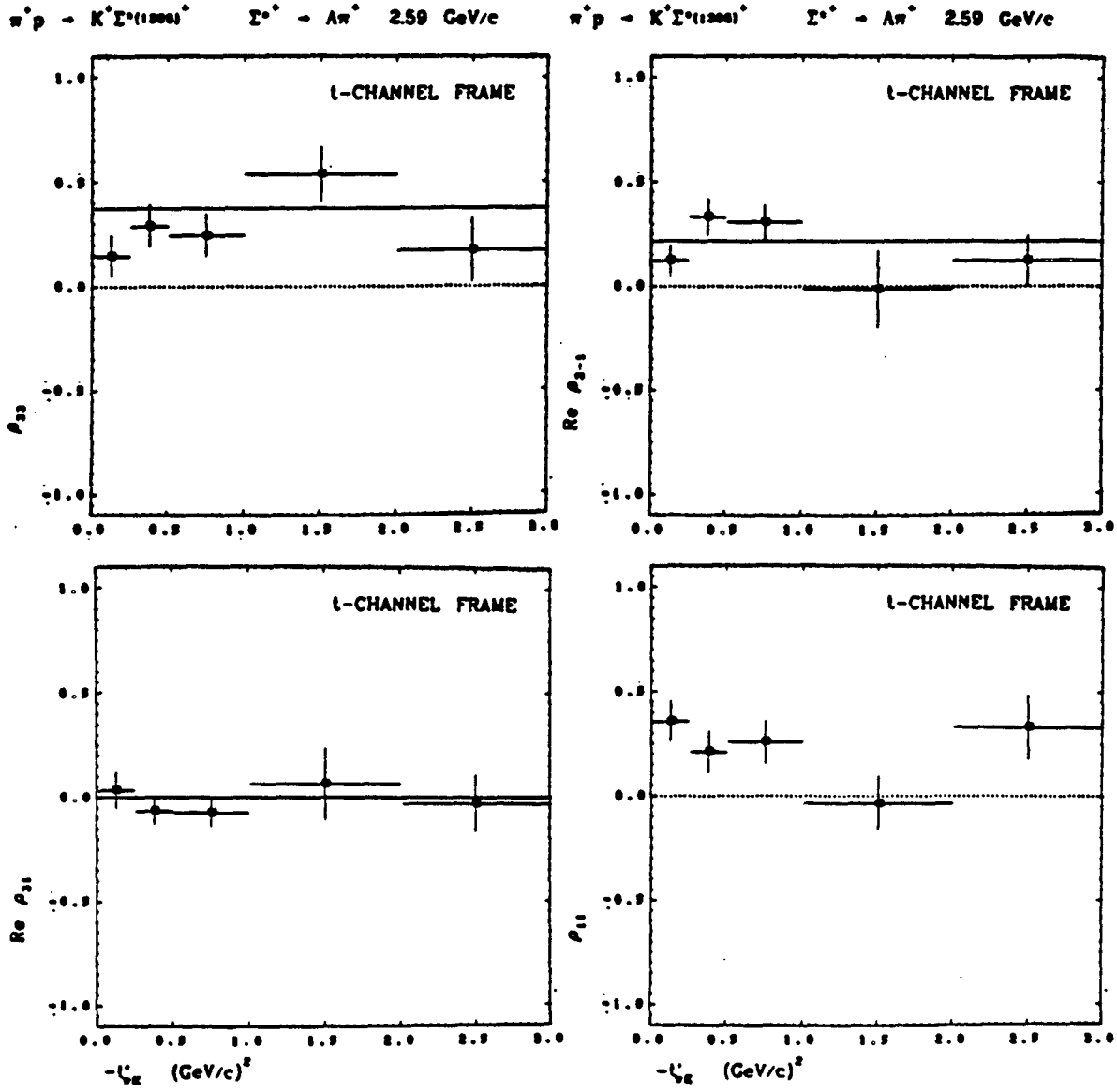
π⁺p → K⁺Σ*(1385)⁺ Σ*⁺ → Λπ⁺ 2.59 GeV/c
t-CHANNEL FRAME
ρ33
Re ρ3-1
Re ρ31
ρ11
-t'min (GeV/c)²

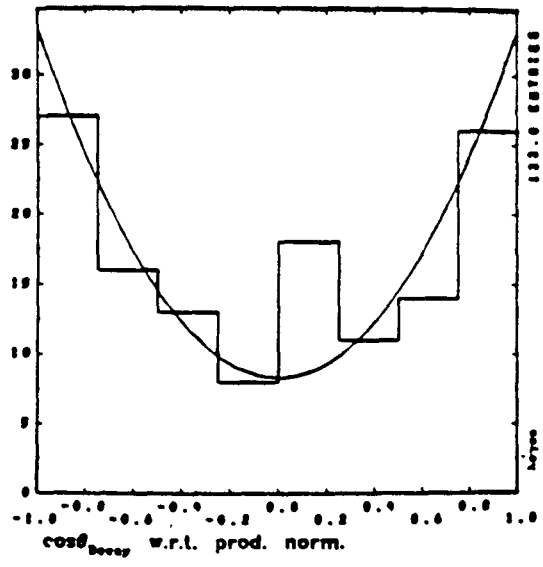
cosθdecay w.r.t. prod. norm.

IV.26a

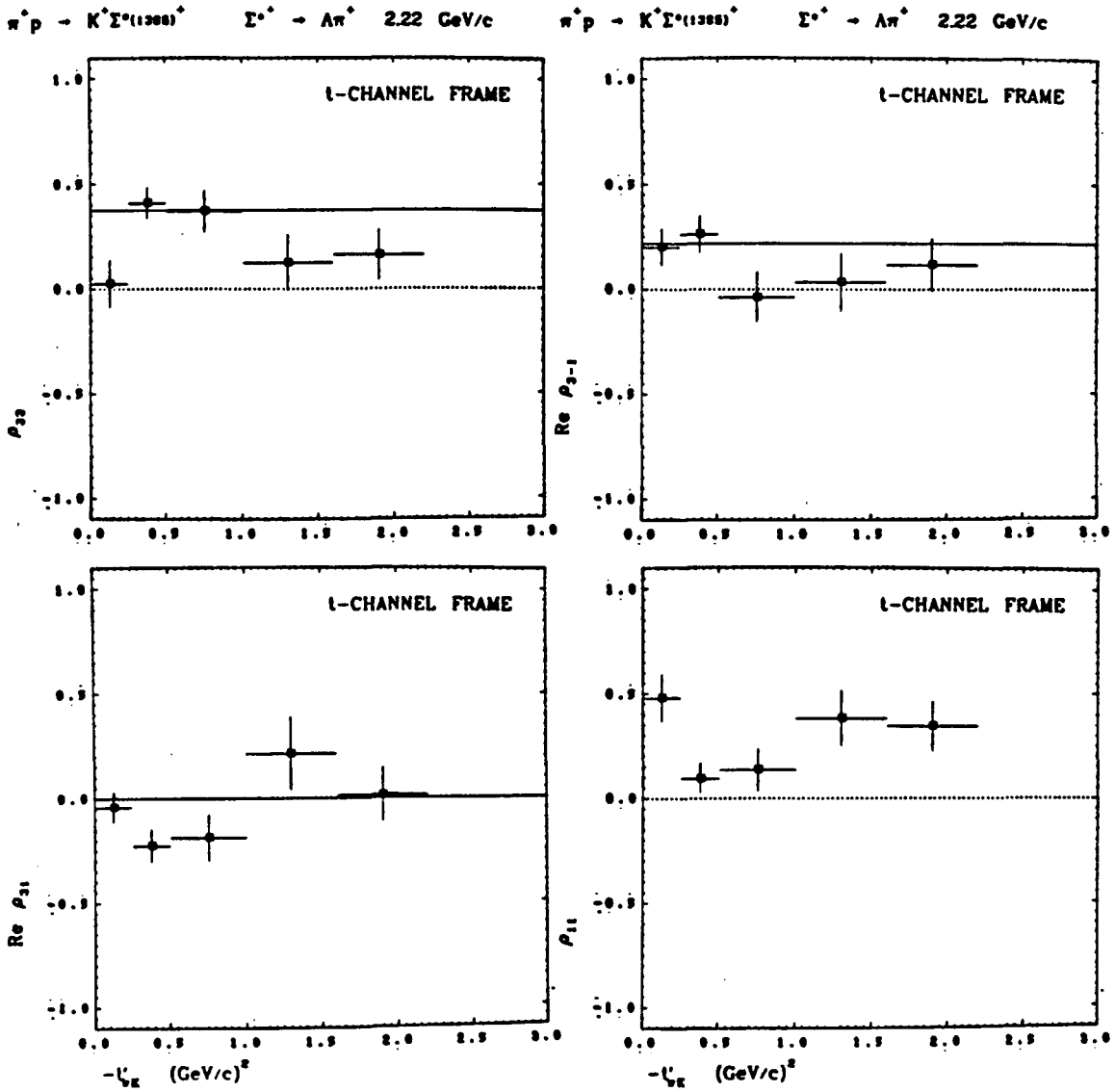
π⁺p → K⁺Σ*(1385)⁺ Σ*⁺ → Λπ⁺ 2.22 GeV/c
t-CHANNEL FRAME
ρ33
Re ρ3-1
Re ρ31
ρ11
-t'vK (GeV/c)²

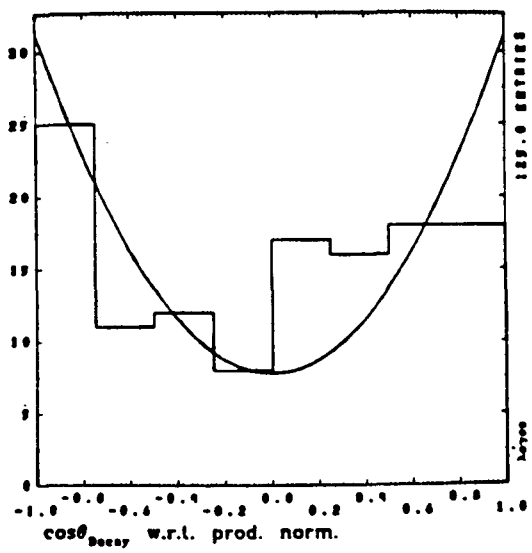
cosθDecay w.r.t. prod. norm.

IV.26b

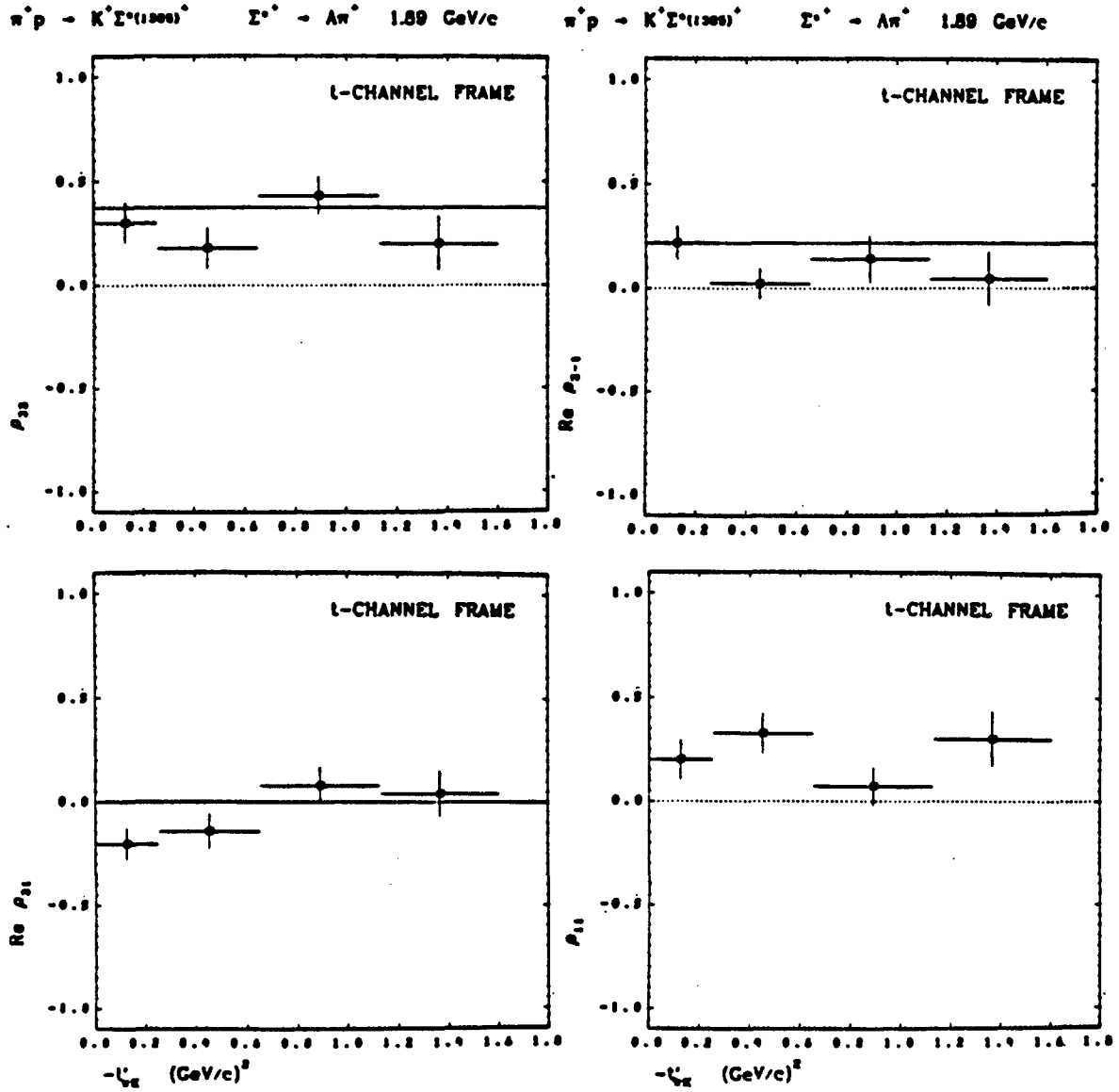
π⁺p → K⁺Σ*(1385)⁺ Σ*⁺ → Λπ⁺ 1.89 GeV/c
t-CHANNEL FRAME
ρ33
Re ρ3-1
Re ρ31
ρ11
-t'bc (GeV/c)²

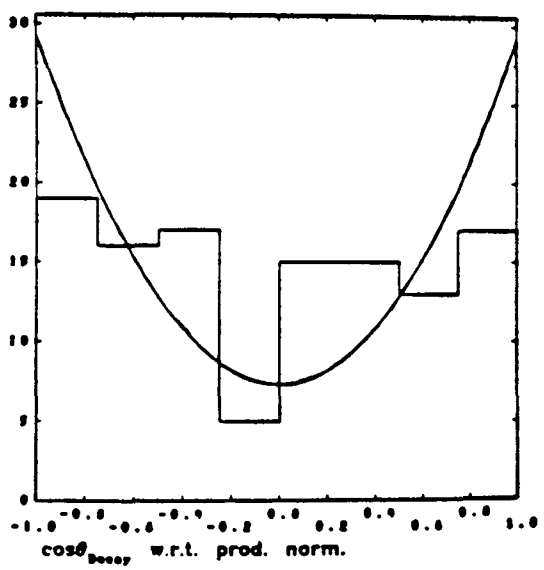
cosθDecay w.r.t. prod. norm.

IV.27

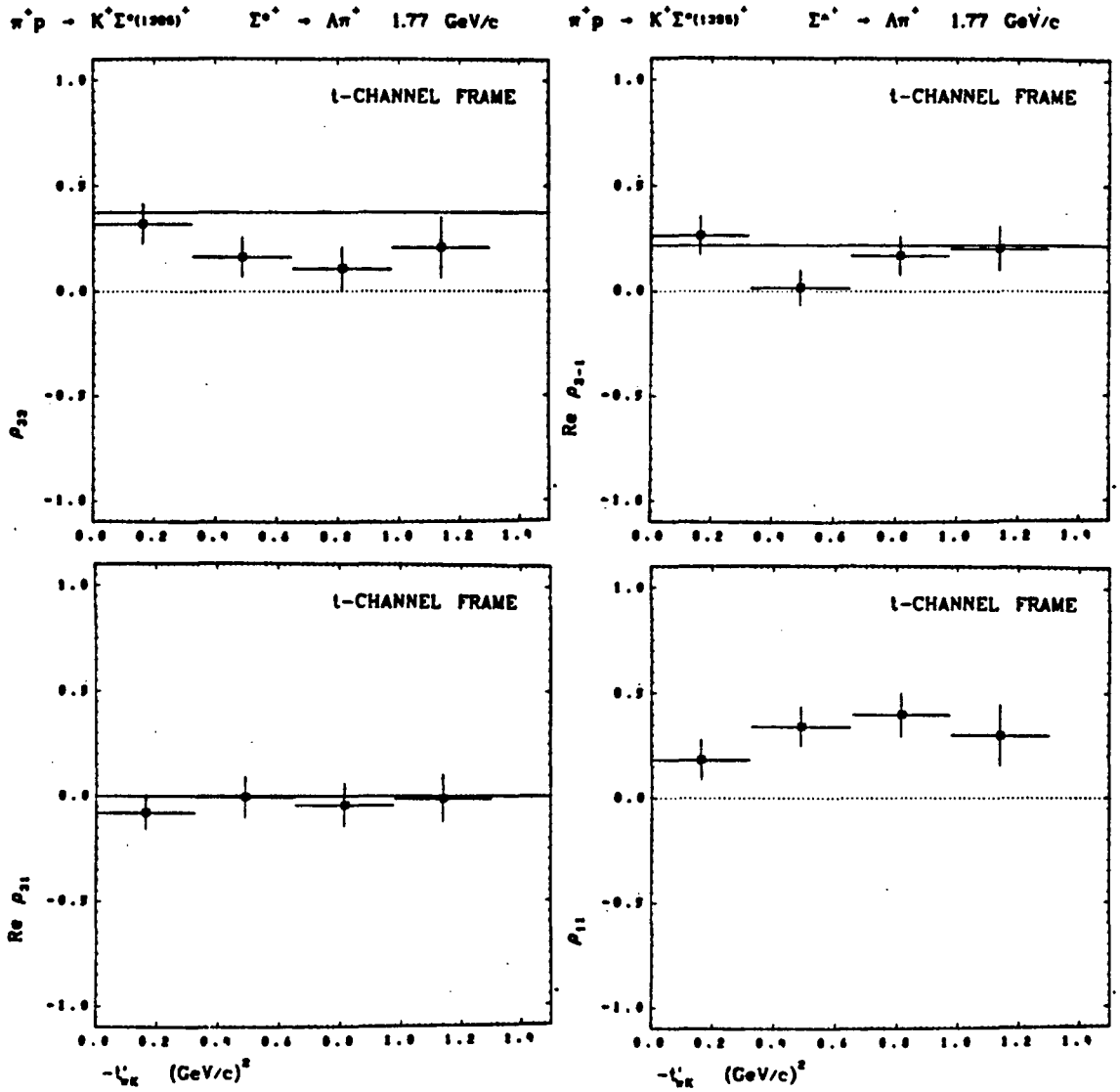
π⁺p → K⁺Σ*(1385)⁺ Σ*⁺ → Λπ⁺ 1.77 GeV/c
t-CHANNEL FRAME
ρ33
Re ρ3-1
Re ρ31
ρ11
-t'K (GeV/c)²

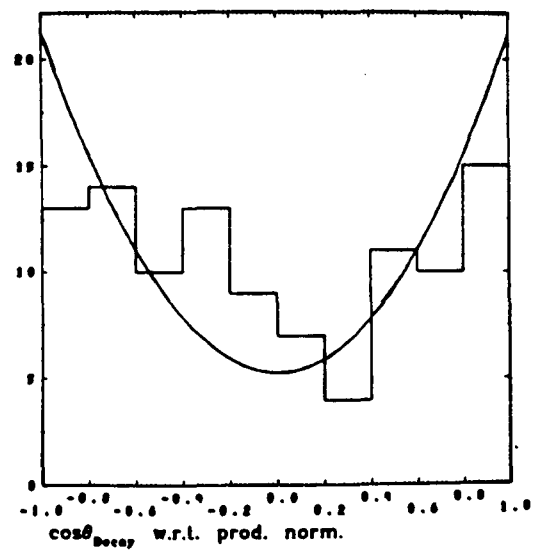
cosθDecay w.r.t. prod. norm.

IV.28

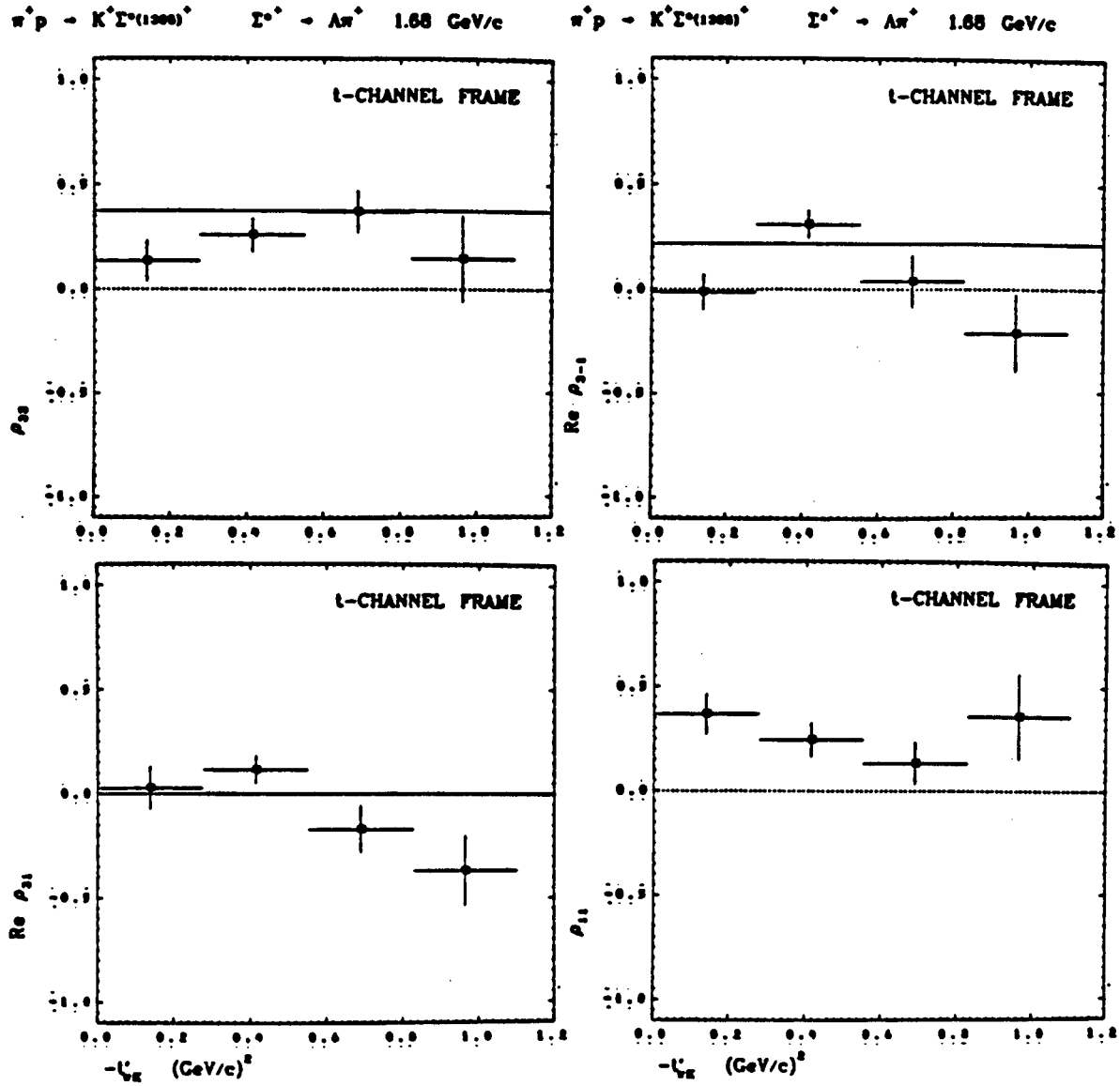
π⁺p → K⁺Σ*(1385)⁺ Σ*⁺ → Λπ⁺ 1.68 GeV/c
t-CHANNEL FRAME
ρ₃₃
Re ρ₃₋₁
Re ρ₃₁
ρ₁₁
-t'_K (GeV/c)²

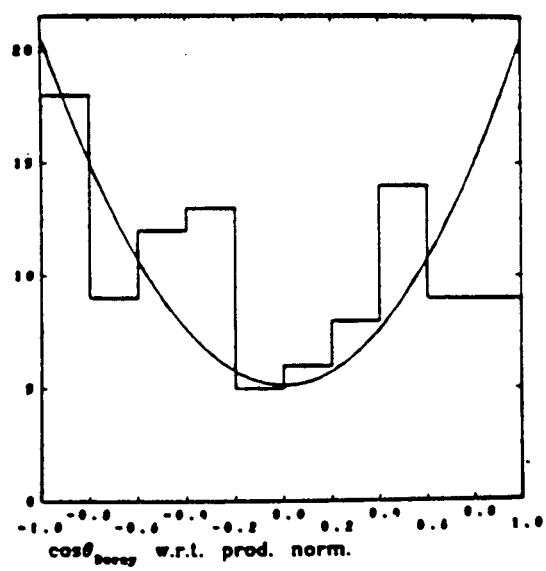
cosθ_Decay w.r.t. prod. norm.

IV.29

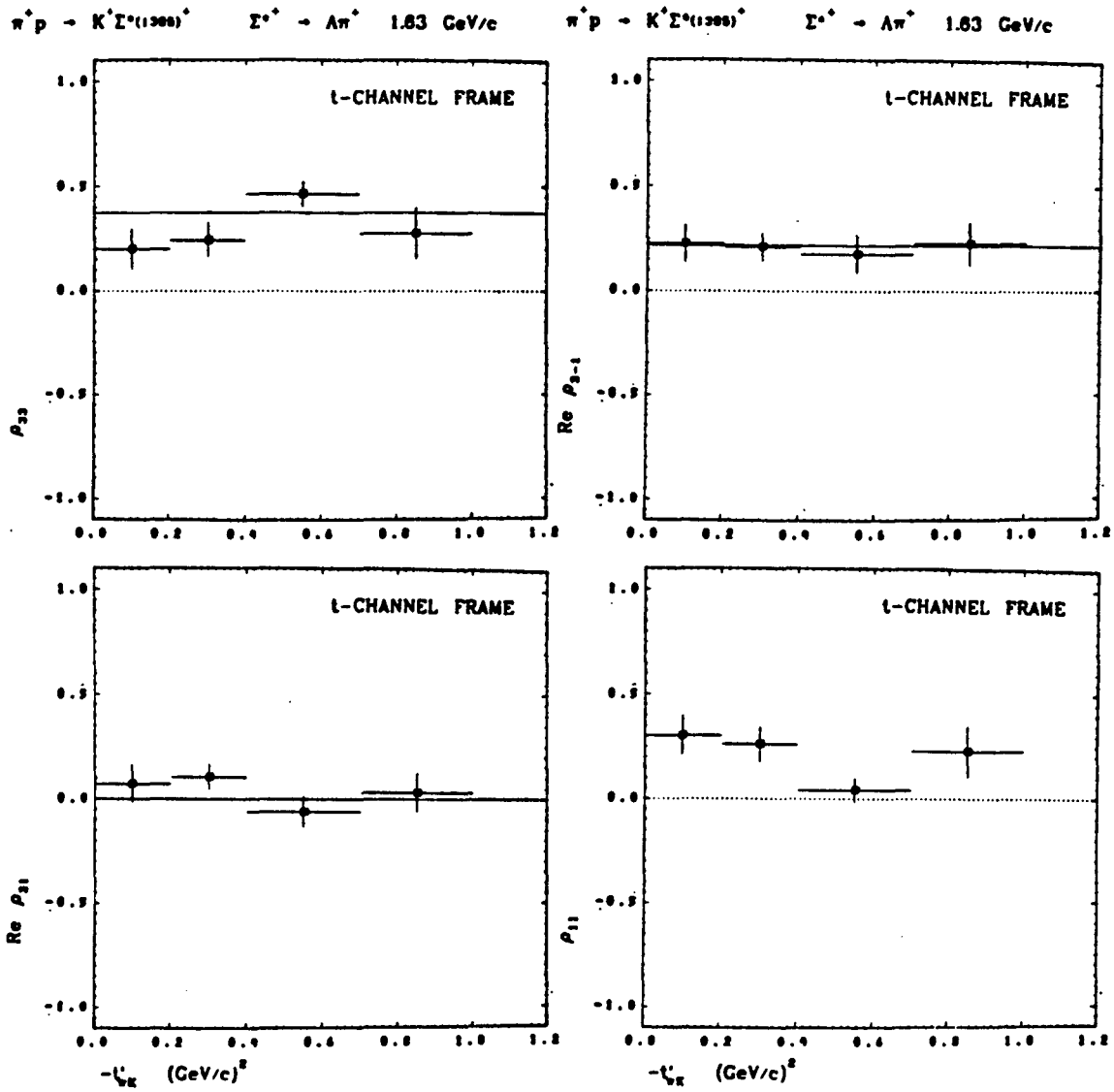
π⁺p → K⁺Σ*(1385)⁺ Σ*⁺ → Λπ⁺ 1.63 GeV/c
t-CHANNEL FRAME
ρ33
Re ρ3-1
Re ρ31
ρ11
-t'K (GeV/c)²

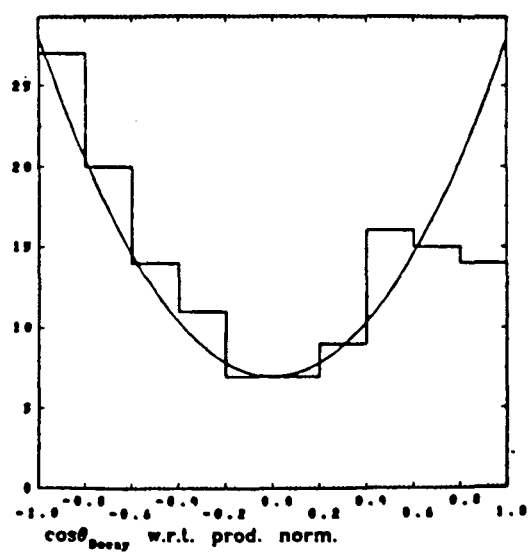
cosθDecay w.r.t. prod. norm.

IV.30

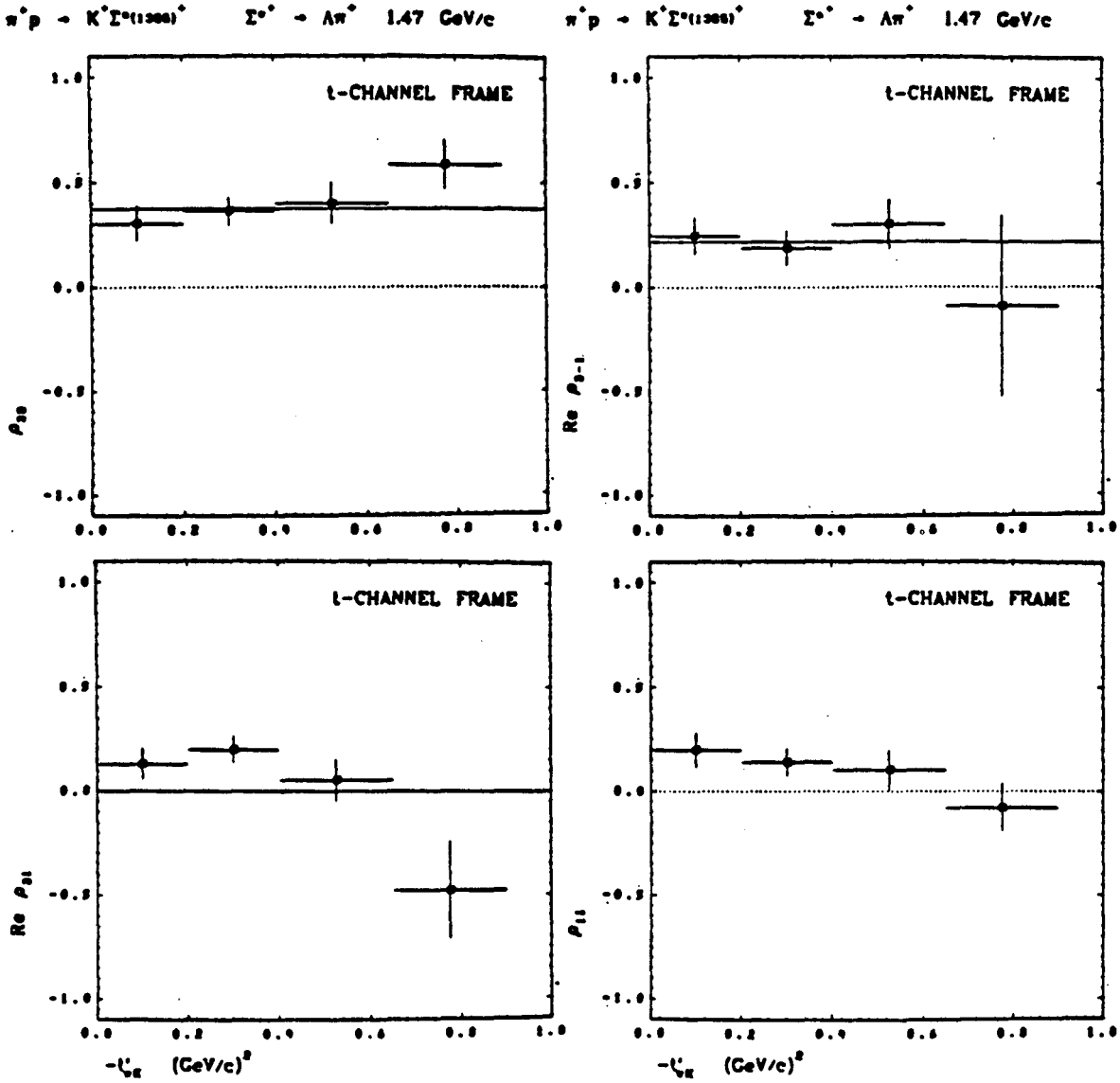
π⁺p → K⁺Σ*(1385)⁺ Σ*⁺ → Λπ⁺ 1.47 GeV/c
t-CHANNEL FRAME
ρ₁₁
-t'_K (GeV/c)²

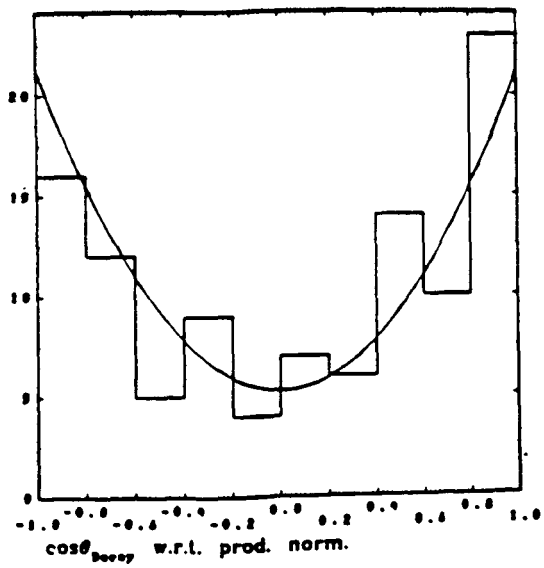
cosθ_Decay w.r.t. prod. norm.

IV.31

As in the ΣK^* case, with higher statistics it would be possible to use the polarization analyzing decay of the Λ jointly with the $\Sigma^* \to \Lambda\pi$ distribution to determine the 4 complete helicity amplitudes for $\pi p \to \Sigma^* K$ up to two phases.

2. Tests for the Nature of the Exchanges in $\pi p \to \Sigma^* K$

As with the ΣK^* channel, so for $\Sigma^* K$ general invariance principles (J^P conservation) applied to the t-channel amplitudes lead to simple relationships among the $\Sigma^* \rho_{ij}$ if certain conditions obtain among the exchanges contributing to the H_{lm} in the forward region. In particular, Ringland and Thews, ref. 29, have shown that if *only a single exchange* amplitude contributes to the H_{lm} or if multiple exchanges occur but *all have the same phase*, then the H_{lm} will all have the same phase, and in the t-channel helicity system all ρ_{ij} are real with:

$$(\mathrm{Re}\rho_{31})^2 + (\mathrm{Re}\rho_{3-1})^2 = \rho_{33}\rho_{11} \,. \qquad \text{(IV.C.7)}$$

We observe that the general constraint on these ρ_{ij} for a $\frac{3}{2}^+$ decay is (see ref. 57):

$$(\mathrm{Re}\rho_{31})^2 + (\mathrm{Re}\rho_{3-1})^2 \leq \rho_{33}\rho_{11} \,. \qquad \text{(IV.C.8)}$$

Thus if a single exchange or multiple in-phase exchanges dominate the H_{lm}, the left-hand side of IV.C.8 is at its upper bound, i.e., IV.C.7 holds. We emphasize again that IV.C.7 follows from general quantum mechanical principles and is *not* dependent on any model or dynamical assumptions.

In figures IV.32, IV.33 we show the quantities $(\mathrm{Re}\rho_{31})^2 + (\mathrm{Re}\rho_{3-1})^2$ and $\rho_{33}\rho_{11}$ in the t-channel helicity frame for our 7 momenta as well as for the available world data on $\Sigma^* K$ at higher momenta, because relation IV.C.7 has

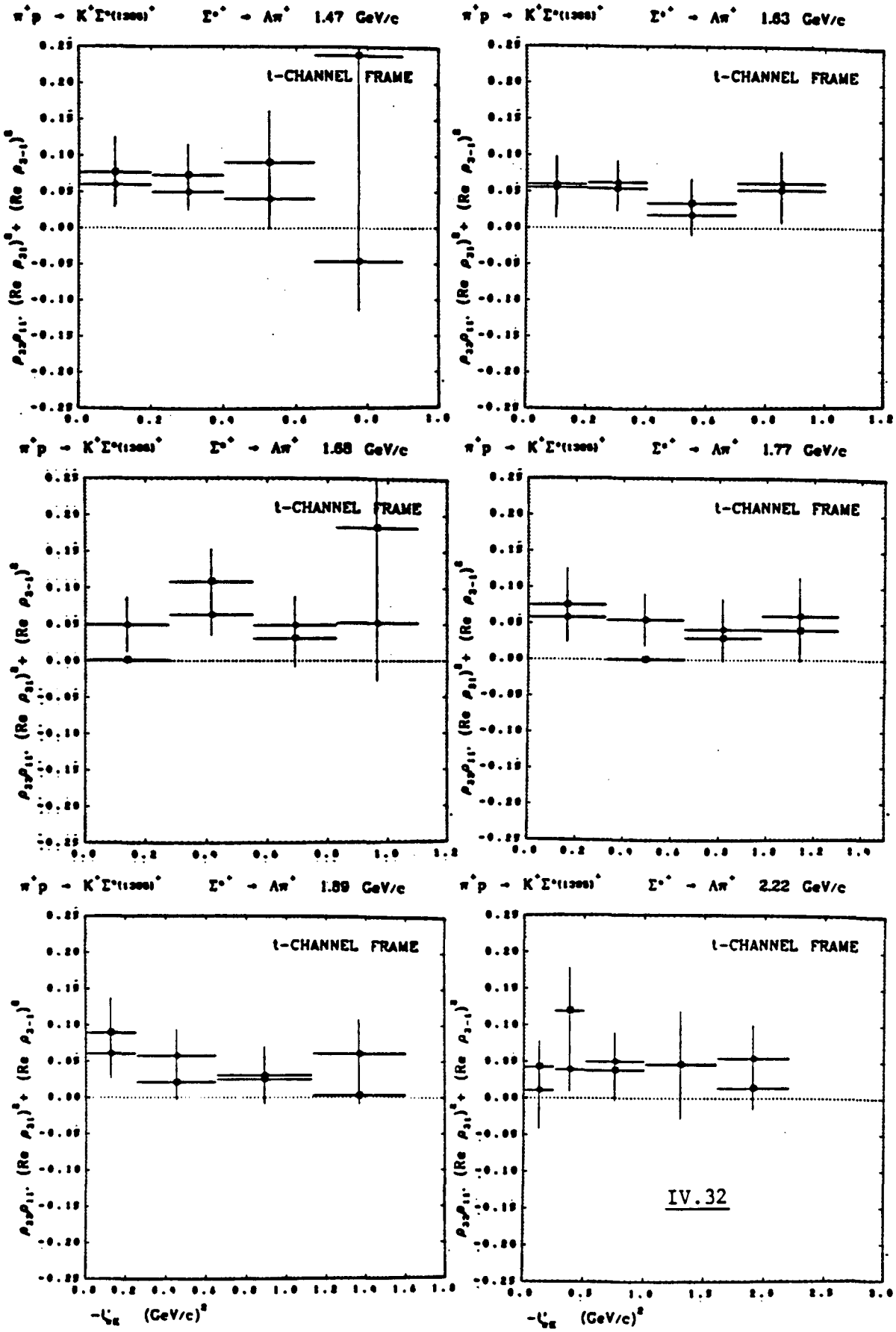
π⁺p → K⁺Σ*(1385)⁺ Σ*⁺ → Λπ⁺ 1.47 GeV/c
π⁺p → K⁺Σ*(1385)⁺ Σ*⁺ → Λπ⁺ 1.63 GeV/c
π⁺p → K⁺Σ*(1385)⁺ Σ*⁺ → Λπ⁺ 1.68 GeV/c
π⁺p → K⁺Σ*(1385)⁺ Σ*⁺ → Λπ⁺ 1.77 GeV/c
π⁺p → K⁺Σ*(1385)⁺ Σ*⁺ → Λπ⁺ 1.89 GeV/c
π⁺p → K⁺Σ*(1385)⁺ Σ*⁺ → Λπ⁺ 2.22 GeV/c
t-CHANNEL FRAME
$\rho_{33}\rho_{11}$, (Re ρ_{31})^2+ (Re ρ_{3-1})^2
$-t'_{K}$ (GeV/c)^2

IV.32

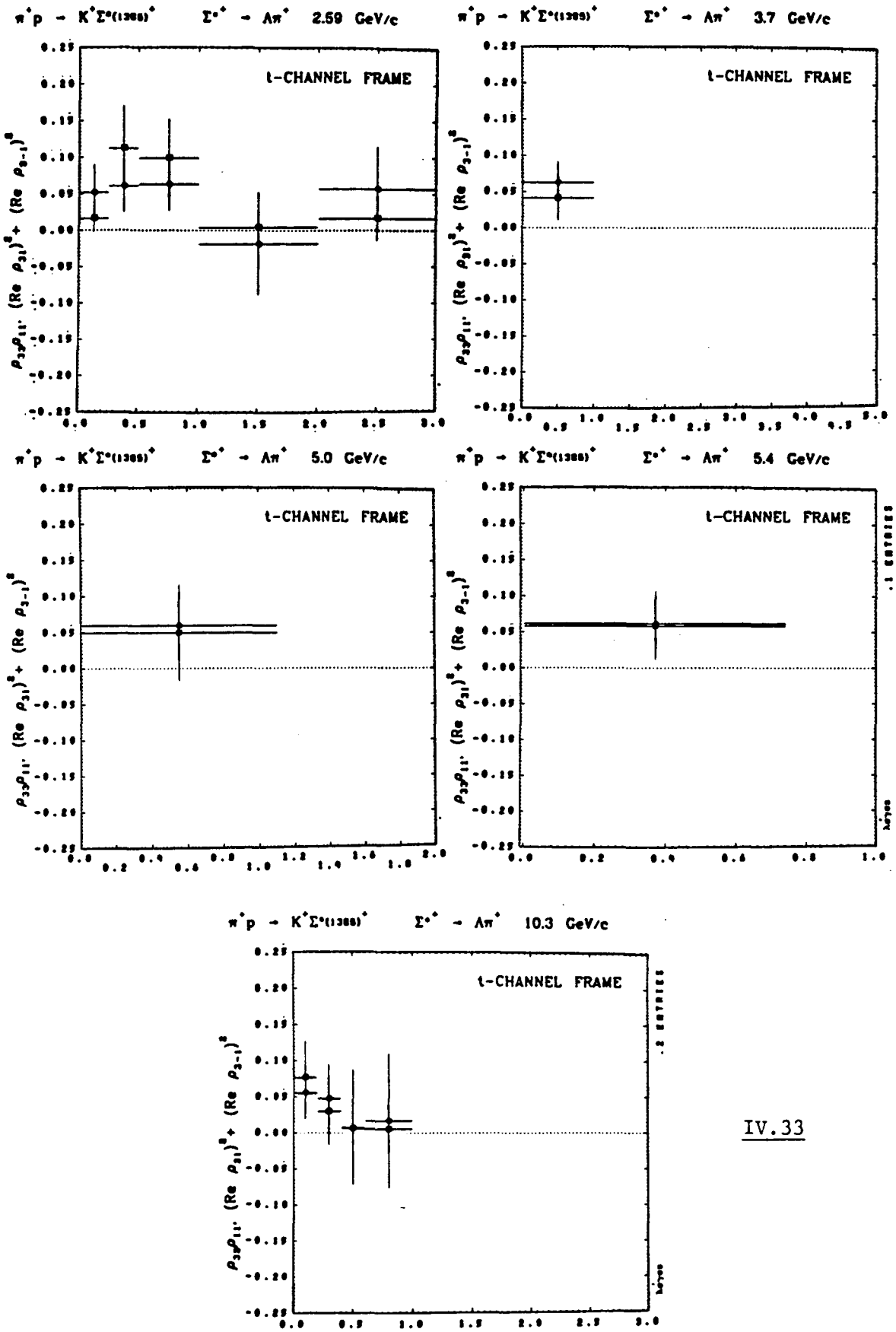
π⁺p → K⁺Σ*(1385)⁺ Σ*⁺ → Λπ⁺ 2.59 GeV/c
t-CHANNEL FRAME
π⁺p → K⁺Σ*(1385)⁺ Σ*⁺ → Λπ⁺ 3.7 GeV/c
t-CHANNEL FRAME
π⁺p → K⁺Σ*(1385)⁺ Σ*⁺ → Λπ⁺ 5.0 GeV/c
t-CHANNEL FRAME
π⁺p → K⁺Σ*(1385)⁺ Σ*⁺ → Λπ⁺ 5.4 GeV/c
t-CHANNEL FRAME
π⁺p → K⁺Σ*(1385)⁺ Σ*⁺ → Λπ⁺ 10.3 GeV/c
t-CHANNEL FRAME

IV.33

never been examined for HYCEX. We observe that IV.C.7 is consistent with the data in the forward region ($-t' < 1(\mathrm{GeV}/c)^2$) at all p_{inc}, but seems to be better satisfied at higher momenta.

What does IV.C.7 tell one in the context of particular pictures for $\pi p \to \Sigma^* K$? More will be said in the next section on the Additive Quark and Stodolsky-Sakurai Models, but in the Regge picture of forward HYCEX scattering, we expect that this process will be dominated by K^* and K^{**} exchange since unnatural J^P exchange is forbidden as it is for $\pi p \to \Sigma K$. Indeed the general $p_{inc}^{-1.45}$ dependence of the channel cross section $\sigma(\Sigma^* K)$ in the previous chapter is consistent with a Regge description of the data from p_{inc} of 1.6 to 16 GeV/c. Now *if*, as appears also to be the case with $\pi p \to \Sigma K$, the vector $K^*(V)$ and tensor $K^{**}(T)$ contributions to the H_{lm} are approximately Weak Exchange Degenerate (WEXD) (i.e., $\alpha_V(t) = \alpha_T(t)$ but the residues are unequal), then $V_{lm}(t) \propto iT_{lm}(t)$, that is, V_{lm} and T_{lm} are 90° out of phase (see Appendix A), and the H_{lm} in general will *not* all have the same phase, so that IV.C.7 should be violated as in fact it seems to be. If Strong Exchange Degeneracy (EXD) holds (i.e., the residues have $\gamma_{lm}^V = \gamma_{lm}^T$, as well as $\alpha_V = \alpha_T$) then all H_{lm} *do* have the same phase and IV.C.7 will be satisfied. Of course, all the foregoing ignores absorptive and cut contributions which will presumably affect the flip and non-flip H_{lm} differently. In summary, assuming absorptive and cut effects are small (pole dominance), we expect IV.C.7 to be satisfied if, for example, (a) there is only one exchange, or (b) all exchanges have the same phase, or (c) EXD holds. If there are multiple exchanges not all in phase, as, e.g., in WEXD, IV.C.7 is expected to fail.

3. The Additive Quark and Stodolsky-Sakurai Predictions

The Additive Quark Model (AQM) using only the simple additivity assumption (Class A predictions) as discussed in the section on ΣK^* (again, see ref. 54) makes the following predictions for the H_{lm} of $\pi p \to \Sigma^* K$ in the forward region at high energy:

$$H_{11} = 0 \tag{IV.C.9a}$$

$$H_{-13} = 0 \tag{IV.C.9b}$$

$$H_{13} = \sqrt{3} H_{1-1} \, . \tag{IV.C.9c}$$

Thus the AQM predicts no non-flip and no double-flip contributions to $\frac{d\sigma}{dt}$ or ρ_{ij}; in particular, since angular momentum conservation in the forward direction requires all flip $H_{lm} \to 0$ as $t' \to 0$, IV.C.9 implies that $\frac{d\sigma}{dt}$ should have a dip or turnover in the forward direction, as is observed in the data at all incident momenta. The beautiful simplicity of the AQM allows one to see that IV.C.9a,b hold without any explicit calculation for the process $0^- \frac{1}{2}^+ \to 0^- \frac{3}{2}^+$: since the initial and final state particles are all $l = 0$ $q\bar{q}$ or qqq systems, and only single quark-single quark interactions are allowed in AQM, to transform the $\frac{1}{2}^+ qqq$ state at the baryon vertex to a $\frac{3}{2}^+ qqq$ state, while retaining the $0^- q\bar{q}$ at the meson vertex, requires one and only one quark to flip its helicity, yielding a net helicity flip of ± 1. All $|net\ helicity\ change| \neq 1$ amplitudes are zero. To get the $\sqrt{3}$ proportionality in IV.C.9c we have to invoke the Clebsch-Gordan coefficients of the explicit SU(6) quark wave functions. Equations (IV.C.9) should apply to any process where initial and final state particles have the same J^P structure as $\pi p \to K\Sigma^*$.

Putting equations IV.C.9 into IV.C.2 (and using the parity symmetries of the H_{lm} where necessary), we get the AQM predictions of ref. 54 for the ρ_{ij} in either the s- or t-channel helicity systems:

$$\begin{aligned} \rho_{33} &= \frac{3}{8} \\ \mathrm{Re}\rho_{3-1} &= \frac{\sqrt{3}}{8} \\ \mathrm{Re}\rho_{31} &= 0 \\ \rho_{11} &= \frac{1}{8} \\ \rho_{3-3} &= 0 = \rho_{1-1} \,. \end{aligned} \tag{IV.C.10}$$

With $tr\rho = 1$, $\rho = \rho^{+}$, and $\rho_{-m-n} = (-1)^{m-n}\rho_{mn}$, this completely specifies ρ; we note the AQM gives $\mathrm{Im}\rho_{ij} = 0$, all ij (see Appendix A), which of course means that the Σ^{*} polarization is zero.

We observe immediately that the ρ_{ij} values of IV.C.10 satisfy the Ringland and Thews condition IV.C.7 exactly since all H_{lm} have the same phase in IV.C.9; the AQM prediction that $\mathrm{Im}\rho = 0$ can also be obtained using $SU(3)$ for the forward direction exchange plus EXD, which as we have already noted, will automatically satisfy IV.C.7. Wagner, ref. 60, has observed that in the *extreme* forward direction, double quark scattering can contribute significantly to the H_{lm} and thus to violations of the simple AQM very near $t' = 0$.

The Stodolsky-Sakurai vector meson-photon analogy (ref. 61), which argues that (in analogy to $\gamma N \to P_{3/2}$ isobar) the $K^{*}p \to \Sigma^{*}$ vertex for $\pi p \to K\Sigma^{*}$ by HYCEX should be an $M1$ transition, makes the same predictions for the Σ^{*} decay as the AQM, i.e., that the Σ^{*} rest frame decay distribution with respect to $\hat{n}$ be of form

$$\frac{dN}{d(\hat{p}_\Lambda \cdot \hat{n})} = 1 + 3(\hat{p}_\Lambda \cdot \hat{n})^2$$

which gives the ρ_{ij} of the AQM. Further, the Stodolsky-Sakurai model predicts that the overall center of mass Σ^* production cosine have distribution

$$\frac{dN}{d\cos\vartheta_{CM}} = \frac{1-\cos^2\vartheta_{CM}}{(t_{\pi K} - m_{K^*}^2)^2}.$$

In figures IV.24,IV.25 the Σ^* production cosine distributions have the Stodolsky-Sakurai prediction superimposed; clearly the agreement is good up through incident momentum of 1.77 GeV/c, above which the model fails to describe the greater concentration of events near $t' = 0$, which is not unexpected since the model uses only a fixed spin exchange parameterization. An early Reggeized Stodolsky-Sakurai model (ref. 62) fitted to high energy data gives a good (absolute) description of $\frac{d\sigma}{dt}$ when extrapolated down to our momenta; the 1.68 GeV/c $\frac{d\sigma}{dt}$ figure for our data has this prediction displayed.

The $\Sigma^*\rho_{ij}$ in figures IV.26-IV.31 have the AQM predictions displayed as solid lines, and we note that the agreement is generally fair to good for $t' < 1(\mathrm{GeV/c})^2$, even at the lowest incident momentum which is less than 100 MeV above the channel threshold. The Σ^* decay distribution with respect to $\hat{n}$ implied by the AQM ρ_{ij} values is likewise exhibited on the experimental distribution in figures IV.26-IV-31, and at all momenta there is at least qualitative agreement. The AQM predictions have been studied at higher energies with again qualitative agreement in the data of Butler at 3.7 GeV/c (ref. 21) and Toet at 5.0 GeV/c (ref. 19), and excellent agreement in the data of Goddard at 10.3 (ref. 22) and the SLAC 40" SHF data at 7 and 11.5 GeV/c (ref.

58). See also ref. 26. In ref. 1 we demonstrated that for our lower energy $K\Sigma^*$ data, s-channel models based on formation of a high spin Δ resonance are in disagreement with the Σ^* production and decay distributions.

We thus conclude that the AQM picture affords a good qualitative description of $\pi^+p \to K^+\Sigma^{*+}$ down to nearly the channel threshold, where such high energy descriptions might not be expected to work at all, and we further note that for incident momenta above ~1.7 GeV/c the production dynamics $\left(\frac{d\sigma}{dt}\right)$ appear to be Regge-like with helicity-flip amplitudes dominant, features which are reported by May et al., ref. 59, to persist to the highest energies yet studied for this channel.

4. Isospin of t-Channel Exchanges and Exchange Degeneracy for $\pi^+p \to K^+\Sigma^{*+}$

Since there is no $\pi^-p \to K^0\Sigma^*(1385)^0$, $K^-p \to \pi^-\Sigma^*(1385)^+$ data available at energies overlapping ours, for completeness here we merely summarize the world data results on t-channel isospin analysis and EXD,WEXD for the $K\Sigma^*$ channel. The CERN-College de France-Madrid-Stockholm (CCMS) Collaboration, ref. 63, has compared their 3.95 GeV/c $\pi^-p \to K^0\Sigma^{*0}$ with the 3.7 and 4.0 GeV/c data on $\pi^+p \to K^+\Sigma^{*+}$ of Butler (ref. 21) and Ying (ref. 64), and found a significant $I_t = 3/2$ contribution at very small t'; this is the only such comparison which has yet been performed. Further, forward peaks have long been observed in the reactions $\pi^-p \to K^+\Sigma^{*-}$, $K^-p \to \pi^+\Sigma^{*-}$, most recently in the 3.95 GeV/c data of ref. 63, the 4-5 GeV/c data of Aleshin et al., ref. 65, and the 4.2 GeV/c data of Holmgren et al., ref. 66; such peaks must be a consequence of some double charge exchange mechanism (at higher

energies), which apparently is more important for $\pi p \to K\Sigma^*$ than for $\pi p \to K\Sigma, K^*\Sigma$, for which channels we have seen that $I_t = \frac{3}{2}$ contributions are very small.

The Weak and Strong Exchange Degeneracy expectation that

$$\frac{d\sigma}{dt}(\pi p \to K\Sigma^*) = \frac{d\sigma}{dt}(\bar{K}p \to \pi\Sigma^*) \qquad \text{(IV.C.11)}$$

has been examined for the 4.2 GeV/c data of the Amsterdam-CERN-Nijmegen-Oxford (ACNO) group, ref. 66, the 7.0,10.1 GeV/c data of Berglund et al., ref. 67, and the 7.0,11.5 GeV/c data of Baker et al., Cautis et al., ref. 58. At all these momenta, it is found that

$$\frac{d\sigma}{dt}(\pi p \to K\Sigma^*) \approx \frac{2}{3}\frac{d\sigma}{dt}(\bar{K}p \to \pi\Sigma^*) ,$$

i.e., both EXD and WEXD appear to be violated. This is the same pattern of breaking as in $K\Sigma, \pi\Sigma$ production at low energies; as we have previously noted, for $p_{inc} \geq 4$ GeV/c, WEXD is reasonably satisfied for both $\Sigma K, \Sigma K^*$.

In addition, the 7,11.5 GeV/c SLAC data of ref. 58 has the (helicity quantization) ρ_{ij} of the Σ^*; these authors do not mention that WEXD implies the general result (see Appendix A)

$$\rho_{lm}(\pi p \to K\Sigma^*) = \rho^*_{lm}(\bar{K}p \to \pi\Sigma^*) . \qquad \text{(IV.C.12)}$$

Of course, EXD implies the stronger constraint (a restriction of IV.C.12):

$$\begin{aligned} \mathrm{Re}\rho_{lm}(\pi p \to K\Sigma^*) &= \mathrm{Re}\rho_{lm}(\bar{K}p \to \pi\Sigma^*) \\ \mathrm{Im}\rho_{lm}(\pi p \to K\Sigma^*) &= \mathrm{Im}\rho_{lm}(\bar{K}p \to \pi\Sigma^*) = 0 . \end{aligned} \qquad \text{(IV.C.13)}$$

However, if both $\pi p \to K\Sigma^*$ and $\bar{K}p \to \pi\Sigma^*$ separately obey the AQM predictions of the previous section, then IV.C.13 will hold automatically, independently of EXD and IV.C.11. The data of ref. 58 show that IV.C.11 is violated, but IV.C.12

holds fairly well, i.e., $\rho_{lm}(K\Sigma^*)$ and $\rho_{lm}(\pi\Sigma^*)$ exhibit a nice mirror symmetry; this is not too surprising, since double exchange processes (such as multiple quark interactions) can lead to effective $I_t = 3/2$ contributions and to violations of WEXD and the AQM as well, but the AQM and WEXD predictions for ρ_{lm} depend only on ratios of amplitudes, while the WEXD predictions for $\frac{d\sigma}{dt}$ are sensitive to overall magnitudes. Wagner, ref. 60, and the CCMS collaboration, ref. 63, observe that the amount of $I_t = \frac{3}{2}$ in $\pi p \to K\Sigma^*$ from comparison of $K^0\Sigma^{*0}$ with $K^+\Sigma^{*+}$ is consistent with the amount inferred from AQM violations in the CCMS and ACNO data.

5. t-Channel $SU(3)$ and Flavor Independence for $\Sigma^* K$

Following Martin, Michael, and Phillips (MMP), ref. 45, and Girardi and Navelet (GN), ref. 68, in analogy to the treatment of ΣK in section A4 of this chapter, the helicity amplitudes for forward scattering in $\pi^+ p \to K^+\Sigma^{*+}$ and $K^- n \to \bar{K}^0\Delta^-$, using $SU(3)$ for the t-channel exchanges, are

$$\begin{aligned} H(\pi^+ p \to K^+\Sigma^{*+}) &= \lambda(T+V) \\ H(K^- n \to \bar{K}^0\Delta^-) &= \sqrt{3}(T+V) \\ &(\textit{helicities suppressed}) \end{aligned} \tag{IV.C.14}$$

where as before T, V are the K^*, K^{**} or ρ, A_2 exchanges. Here again, exact $SU(3)$ for vertices is assumed, and if overall exact $SU(3)$ held as well, we would have $|\lambda| = 1$; again, one knows empirically that $|\lambda|$ is very different from unity, so we follow MMP and make the simple ansatz that the $SU(3)$ breaking dynamics are of Regge form and entirely attributable to the non-strange/strange mass splitting:

$$|\lambda| = \left(\frac{s}{s_0}\right)^{-\Delta\alpha} \qquad \text{(IV.C.15)}$$

where $\Delta\alpha = \alpha(\rho, A_2) - \alpha(K^*, K^{**}) \approx m_{K^*}^2 - m_\rho^2 = 0.2$, and s_0 is a scale parameter on the order of unity.

We note that IV.C.14 makes the very limited EXD assumption that λ is the same for T, V. Thus again except for the non-strange/strange mass splitting, light quark flavor independence of the strong interactions as embodied in IV.C.14 leads one to expect that HYCEX and CEX processes are basically the same.

Since for decuplet production there is no complication of symmetric/antisymmetric coupling of the exchanges to the baryon vertex, one immediately gets the simple broken $SU(3)$ equality of ref. 68:

$$\frac{d\sigma}{dt}(K^+\Sigma^{*+}) = \frac{|\lambda|^2}{3}\frac{d\sigma}{dt}(\bar{K}^0\Delta^-) \,. \qquad \text{(IV.C.16)}$$

Also, one immediately gets from IV.C.14, as GN observe, a relation for the baryon decay density matrices:

$$\rho_{ij}(\bar{K}^0\Delta^-) = \rho_{ij}(K^+\Sigma^{*+}) \qquad \text{(IV.C.17)}$$

which of course also follows from the AQM/$SU(6)$ picture discussed in section C3 of this chapter. The value of s_0 has been determined by GN by fitting a similar relation between $K^+p \to K^0\Delta^{++}$ and $K^-p \to \pi^-\Sigma^{*+}$ to data at 4.25 and 4.6 GeV/c; they find $s_0 = 0.6$.

Equation IV.C.16 has been tested at 4 GeV/c by Irving and Worden, ref. 69, on counter data, and by GN at 6 GeV/c also on counter data, and both found good agreement. The only other (and the highest momentum) test of IV.C.16 is that of Damerall et al., ref. 70, using 10.1 GeV/c $K^+\Sigma^{*+}$ data scaled in incident momentum for comparison to 6 GeV/c $\bar{K}^0\Delta^-$. They also find good

agreement, but this author feels that comparisons involving scaling cross sections by more than 20% in incident momentum constitutes as much a test of the scaling used as of any symmetry relation involved, since the scale factors for typical power laws over this range are on the order of two. Equation IV.C.17 has not been tested.

We have examined relations IV.C.16 and IV.C.17 using our own 2.59 GeV/c $K^+\Sigma^{*+}$ data (scaled) and the published 3 GeV/c $\bar{K}^0\Delta^-$ bubble chamber data of Scheuer et al., ref. 71, and we have done the same tests using the 3.7 GeV/c $K^+\Sigma^{*+}$ bubble chamber data of Butler, ref. 21, scaled to the 4.5 $\bar{K}^0\Delta^-$ bubble chamber data of Carmony et al., ref. 72. Figures IV.34 and IV.35 display the $K\Sigma^* \frac{d\sigma}{dt}$ and $\bar{K}\Delta \frac{|\lambda|^2}{3}\left(\frac{d\sigma}{dt}\right)$ data, as well as the ρ_{ij}, where we have used the GN value of $s_0 = 0.6$ to compute λ. We observe that IV.C.16 works well even as low as 3 GeV/c, and that IV.C.17 is reasonably satisfied, within statistics, for $-t < 1$ (GeV/c)^2. The AQM predictions of section C3 of this chapter for the ρ_{lm} (same for HYCEX,CEX) are again shown as solid lines. We have also tested IV.C.16 at higher momenta than ever before, using the 7,11.5 GeV/c $K\Sigma^*$ SLAC SHF data of Baker and Cautis, ref. 58, scaled to the 8.36,12.8 GeV/c, respectively, $\bar{K}^0\Delta^-$ counter data of Gilchriese et al., ref. 73; these are displayed in figure IV.36, and we note excellent agreement with IV.C.16 at 8.36 GeV/c, but poor agreement (by a factor of 2) at 12.8 GeV/c. However, the disagreement at 12.8 may well reflect an overall normalization problem, first, since for both the 7,11.5 $K^+\Sigma^{*+}$ data, and the 8.36,12.8 $\bar{K}^0\Delta^-$, the authors give only statistical errors for $\frac{d\sigma}{dt}$, and there are additional typical systematic uncertainties of 10-20%. Secondly, the integrated $\bar{K}^0\Delta^-$ cross section of ref. 73 is 32 μb at 12.8, which is much smaller than the value of 51 μb expected from the cross section of 97 μb at 8.36 if the CEX process follows a

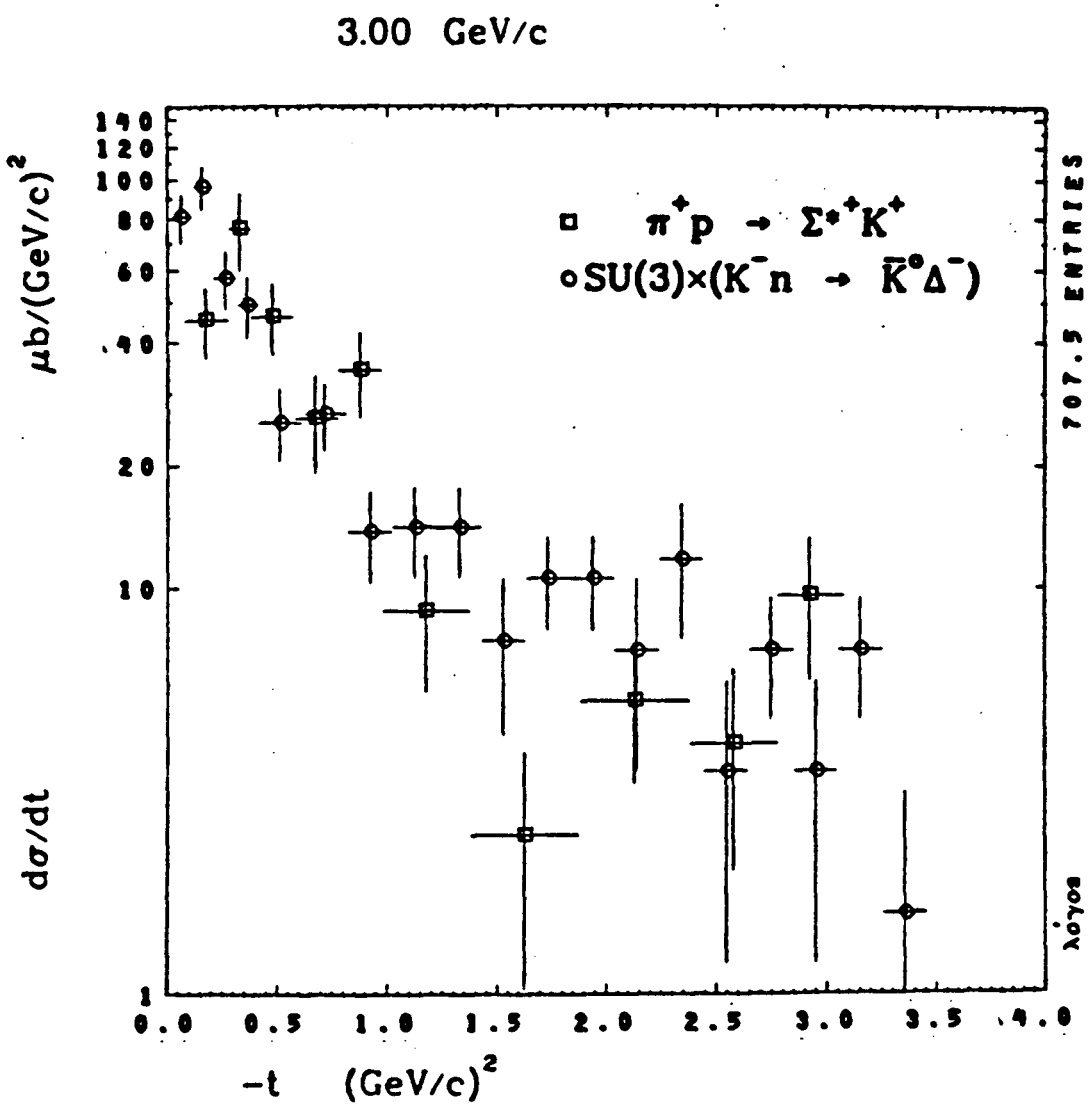
3.00 GeV/c
□ π⁺p → Σ*⁺K⁺
○ SU(3)×(K⁻n → K̄⁰Δ⁻)
dσ/dt
μb/(GeV/c)²
140
120
100
80
60
40
20
10
1
0.0
0.5
1.0
1.5
2.0
2.5
3.0
3.5
4.0
−t (GeV/c)²
707.5 ENTRIES
λόγος

IV.34a

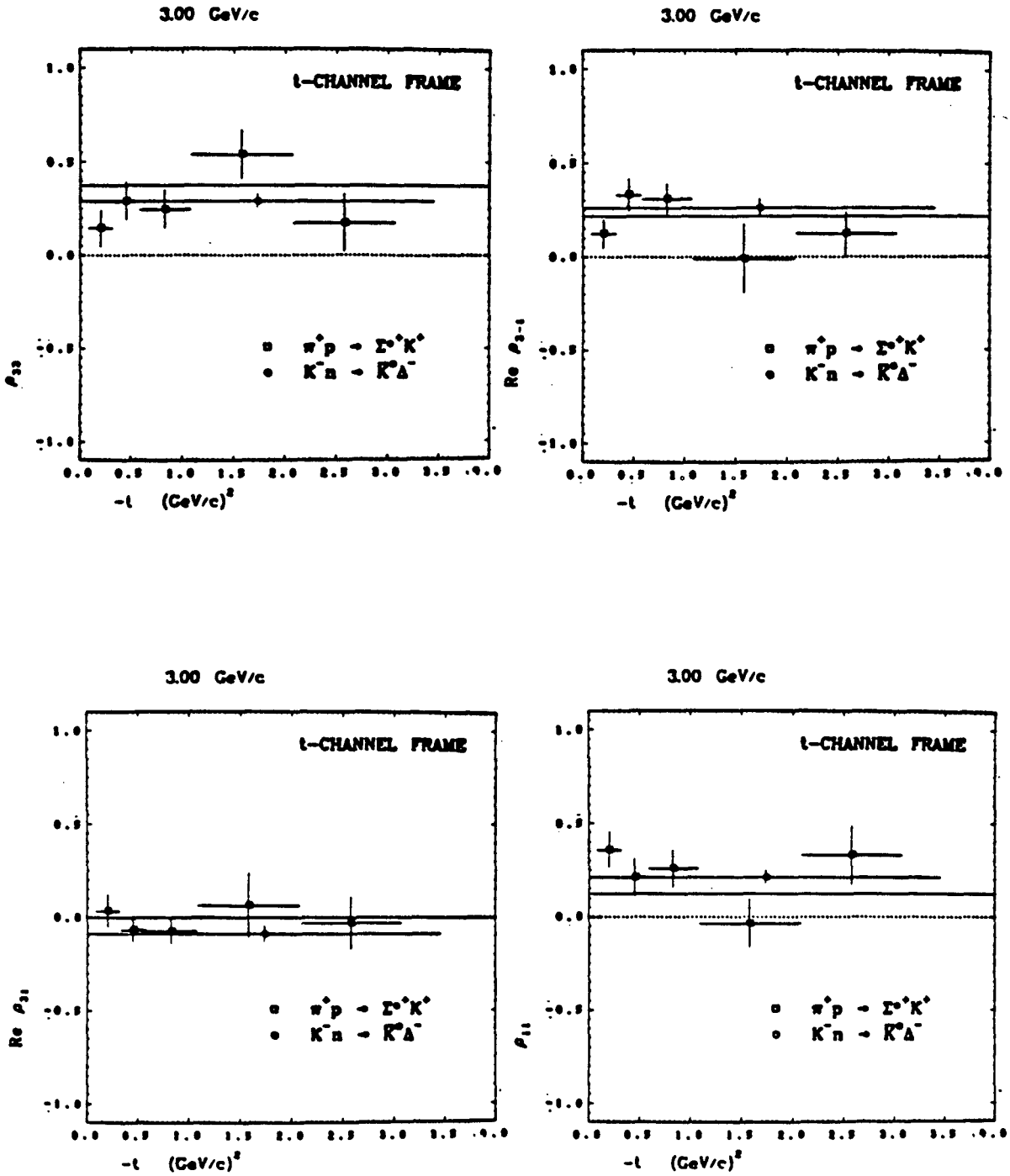
3.00 GeV/c
t-CHANNEL FRAME
$\pi^+p \to \Sigma^{*+}K^+$
$K^-n \to \bar{K}^0\Delta^-$
ρ_{33}
$-t$ (GeV/c)^2
3.00 GeV/c
t-CHANNEL FRAME
$\pi^+p \to \Sigma^{*+}K^+$
$K^-n \to \bar{K}^0\Delta^-$
Re ρ_{3-1}
$-t$ (GeV/c)^2
3.00 GeV/c
t-CHANNEL FRAME
$\pi^+p \to \Sigma^{*+}K^+$
$K^-n \to \bar{K}^0\Delta^-$
Re ρ_{31}
$-t$ (GeV/c)^2
3.00 GeV/c
t-CHANNEL FRAME
$\pi^+p \to \Sigma^{*+}K^+$
$K^-n \to \bar{K}^0\Delta^-$
ρ_{11}
$-t$ (GeV/c)^2

IV.34b

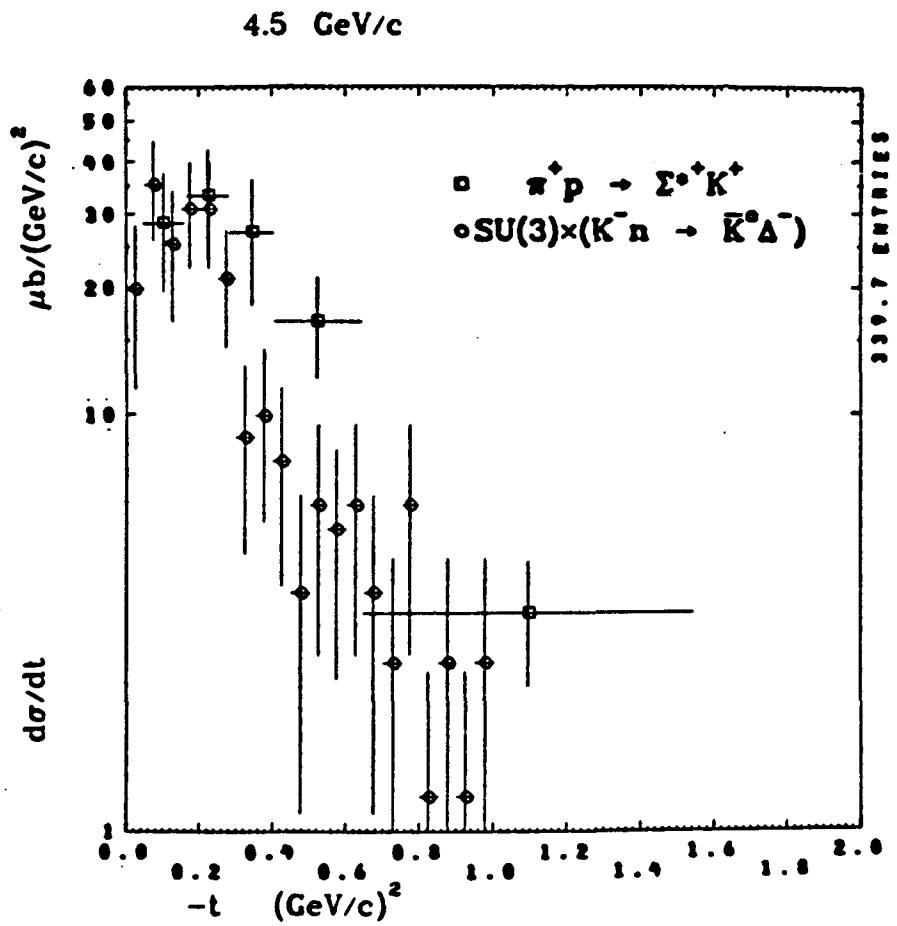
4.5 GeV/c
□ $\pi^+p \to \Sigma^{*+}K^+$
○ SU(3)×($K^-n \to \bar{K}^0\Delta^-$)
dσ/dt
μb/(GeV/c)²
−t (GeV/c)²
0.0
0.2
0.4
0.6
0.8
1.0
1.2
1.4
1.6
1.8
2.0
1
10
20
30
40
50
60

IV.35a

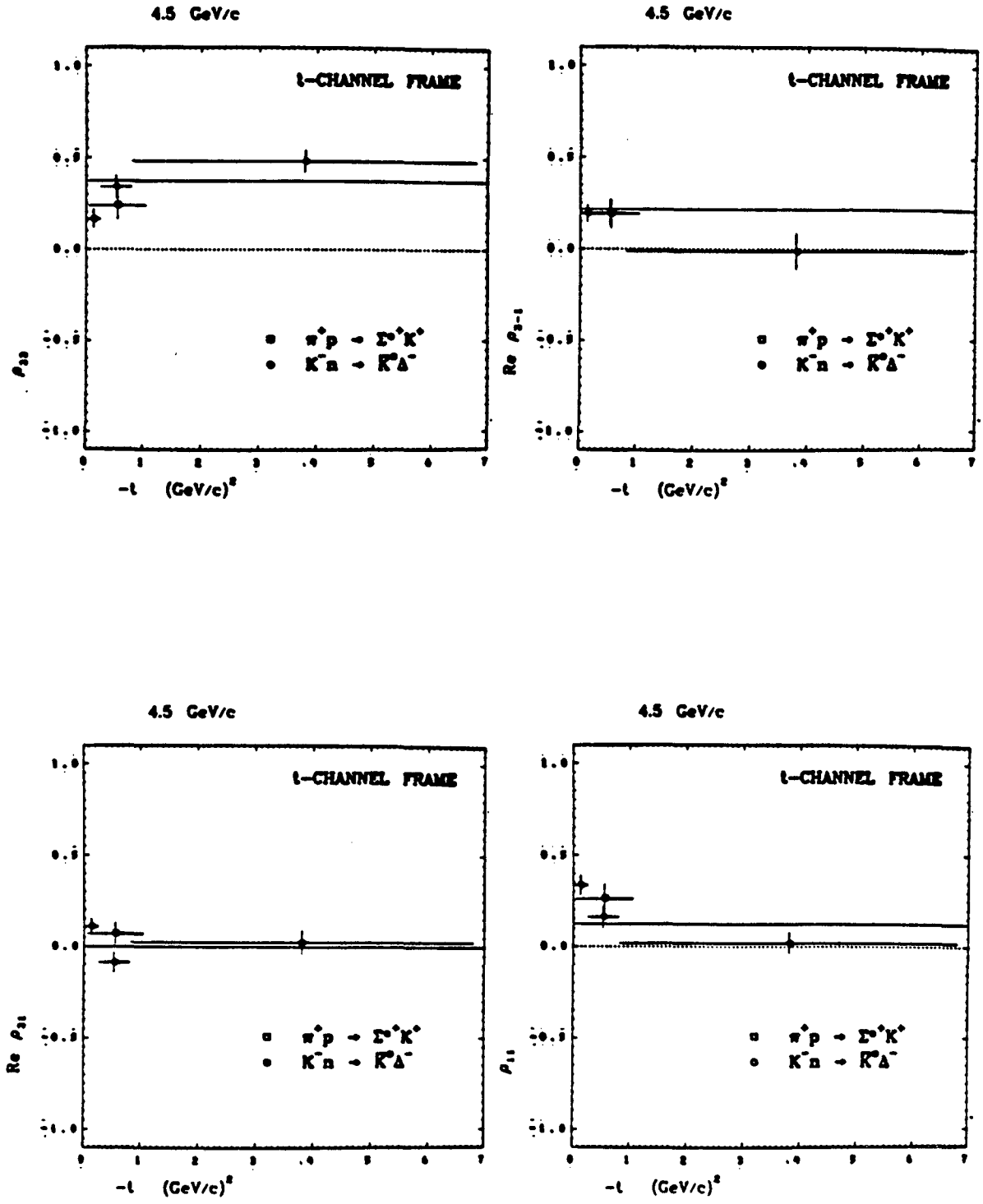
4.5 GeV/c
t-CHANNEL FRAME
$\pi^+p \to \Sigma^{*+}K^+$
$K^-n \to \bar{K}^0\Delta^-$
ρ_{33}
Re ρ_{3-1}
Re ρ_{31}
ρ_{11}
-t (GeV/c)^2

IV.35b

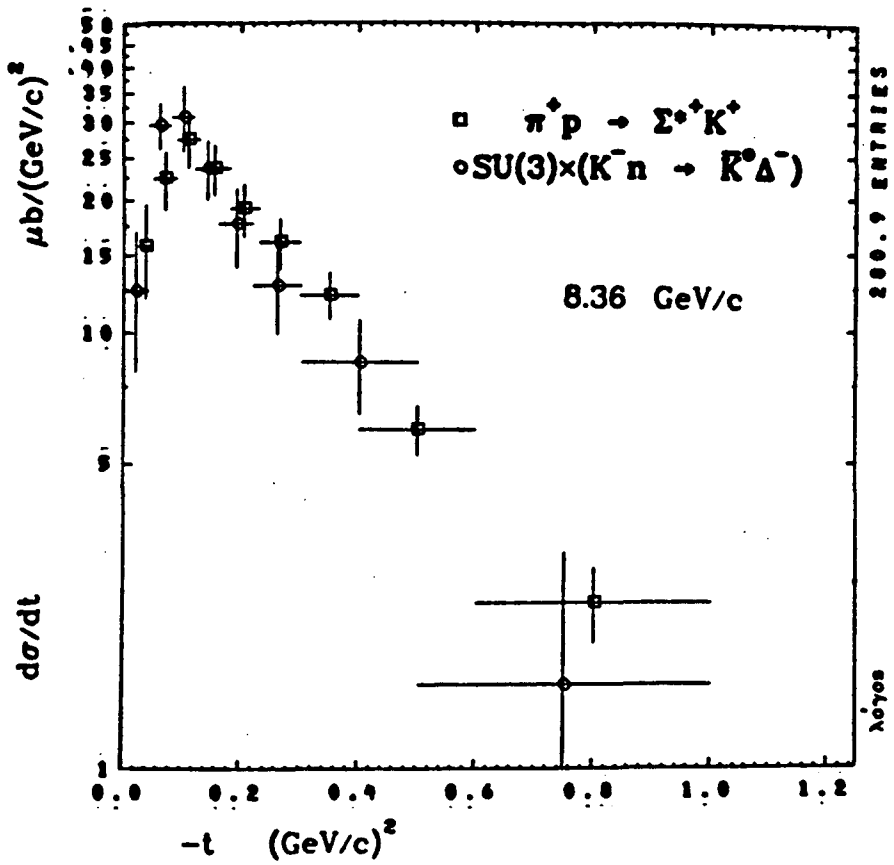
μb/(GeV/c)²
dσ/dt
□ π⁺p → Σ*⁺K⁺
○SU(3)×(K⁻n → K̄*Δ⁻)
8.36 GeV/c
280.9 ENTRIES
λ0708
−t (GeV/c)²

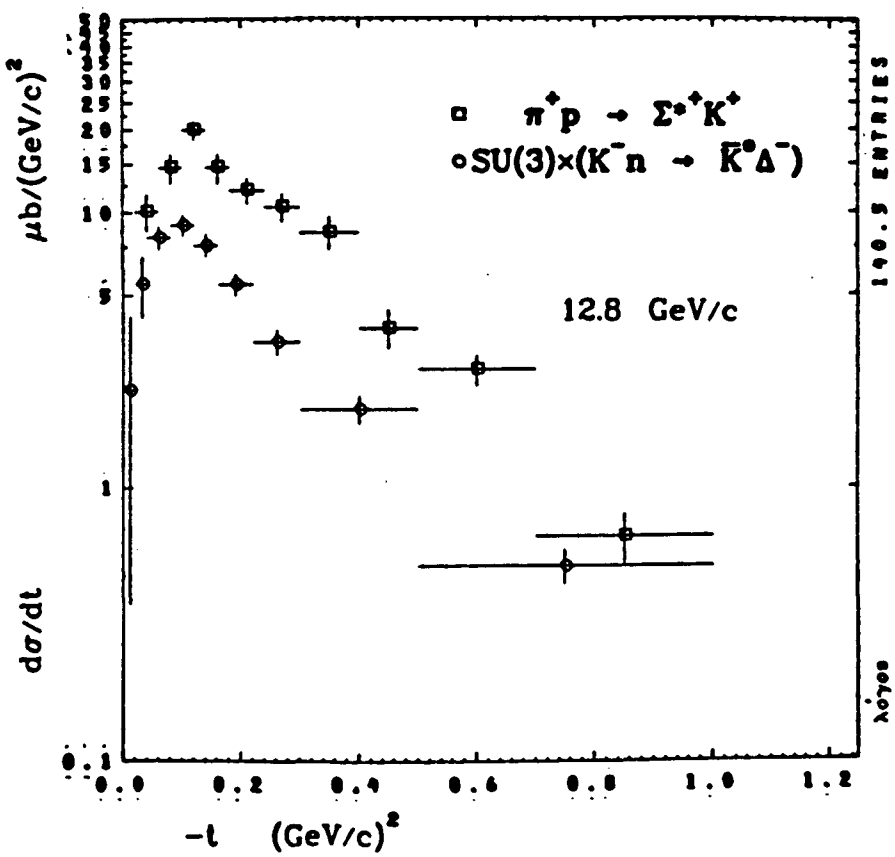
μb/(GeV/c)²
dσ/dt
□ π⁺p → Σ*⁺K⁺
○SU(3)×(K⁻n → K̄*Δ⁻)
12.8 GeV/c
140.5 ENTRIES
λ0708
−t (GeV/c)²

IV.36

Regge-like power law of $p_{inc}^{-1.5}$.

At all momenta, we note that the *shapes* of $\frac{d\sigma}{dt}$ are the same (forward turnover) for both the CEX and HYCEX processes, and that IV.C.16 is observed at all (but the highest) momenta, in agreement with flavor-independence expectations as embodied in the Regge $+SU(3)$ picture and/or AQM/$SU(6)$; we also note in the ρ_{ij} data that the pattern of disagreement with the AQM in the forward direction is the same for HYCEX and CEX. We remark that IV.C.16 is a nontrivial test of the $SU(3)$-breaking parametrization in IV.C.15, since at the momenta where we test IV.C.16, $|\lambda|^2$ reconciles HYCEX cross sections with CEX cross sections which are typically greater by a factor of 3.

D. $\Sigma^* K^*$

Although our highest momentum is barely above channel threshold for $\pi^+ p \to K^*(892)^+ \Sigma^*(1385)^+$, there exists published but incompletely analyzed $K^{*+}\Sigma^{*+}$ data at 3.7, 5 GeV/c (refs. 19,21), which have not been examined, e.g., for $I_t = \frac{3}{2}$ exchange, AQM predictions, or WEXD expectations, and which allow us to consider $\Sigma^* K^*$ in parallel with the preceding $\Sigma K, \Sigma K^*, \Sigma^* K$ analysis.

First we examine the $\rho_{ij}(K^*)$ in $\pi p \to K^* \Sigma^*$, which should obey the Ringland and Thews condition (ref. 29) in equation IV.B.10 *if* exchanges of only one naturality (presumably the natural J^P of K^*, K^{**}) dominate as in $K^*\Sigma$ production. At 3.7, 5, 7, 10.3, 11.5 GeV/c there is $\Sigma^{*+}K^{*+}$ data (refs. 19,21,22,52) on which IV.B.10 has not been tested. At all these momenta ρ_{00} is generally substantially different from zero, so we expect IV.B.10 not to be

satisfied, and in figure IV.37, we see that the data are inconsistent with the RT condition. Thus we conclude that $\Sigma^* K^*$ has a significant effective mixed J^P exchange, in agreement with the published values of $\rho_{00}, \rho_{11}-\rho_{1-1}$ relative to $\rho_{11}+\rho_{1-1}$ at the 5 momenta tested. However, we note that at most momenta in the forward direction $\Sigma^* K^*$ is, like $\Sigma^* K$ and ΣK^*, helicity flip dominated since there is a dip or turnover near $t' = 0$, but not as pronounced or as consistent as in those other channels.

In analogy to equations IV.A.9,IV.B.11, if *only* $I_t = \frac{1}{2}$ exchange contributes to forward $\pi p \to K^* \Sigma^*$ we expect:

$$\frac{d\sigma}{dt}(\pi^+ p \to K^{*+}\Sigma^{*+}) = 2\,\frac{d\sigma}{dt}(\pi^- p \to K^{*0}\Sigma^{*0})\,. \qquad \text{(IV.D.1)}$$

IV.D.1 has never been tested, so in figure IV.38 we compare the 3.7 $\Sigma^{*+}K^{*+}$ data of ref. 21 with the 3.95 $\Sigma^{*0}K^{*0}$ data of the CCMS collaboration, ref. 51, where we have scaled the 3.7 data to 3.95 using the power law fit to $\Sigma^{*+}K^{*+}$. We see that

$$\frac{d\sigma}{dt}(K^{*+}\Sigma^{*+}) < 2\,\frac{d\sigma}{dt}(K^{*0}\Sigma^{*0})$$

which is exactly the same pattern of violation of $I_t = \frac{1}{2}$ – only which the CCMS collaboration sees in its comparison of $K^+\Sigma^{*+}$ with $K^0\Sigma^{*0}$ in ref. 63, and which contrasts with the success of $I_t = \frac{1}{2}$ – only for $\Sigma K, \Sigma K^*$ production. We also observe in figure IV.38 that for the natural J^P exchange part of the cross sections we have

$$(\rho_{11}+\rho_{1-1})\,\frac{d\sigma}{dt}(K^{*+}\Sigma^{*+}) < 2(\rho_{11}+\rho_{1-1})\,\frac{d\sigma}{dt}(K^{*0}\Sigma^{*0})$$

so that we cannot attribute the disagreement with IV.D.1 entirely to the unnatural J^P contribution. We further observe that $\Sigma^{*0}K^{*0}$ has no forward

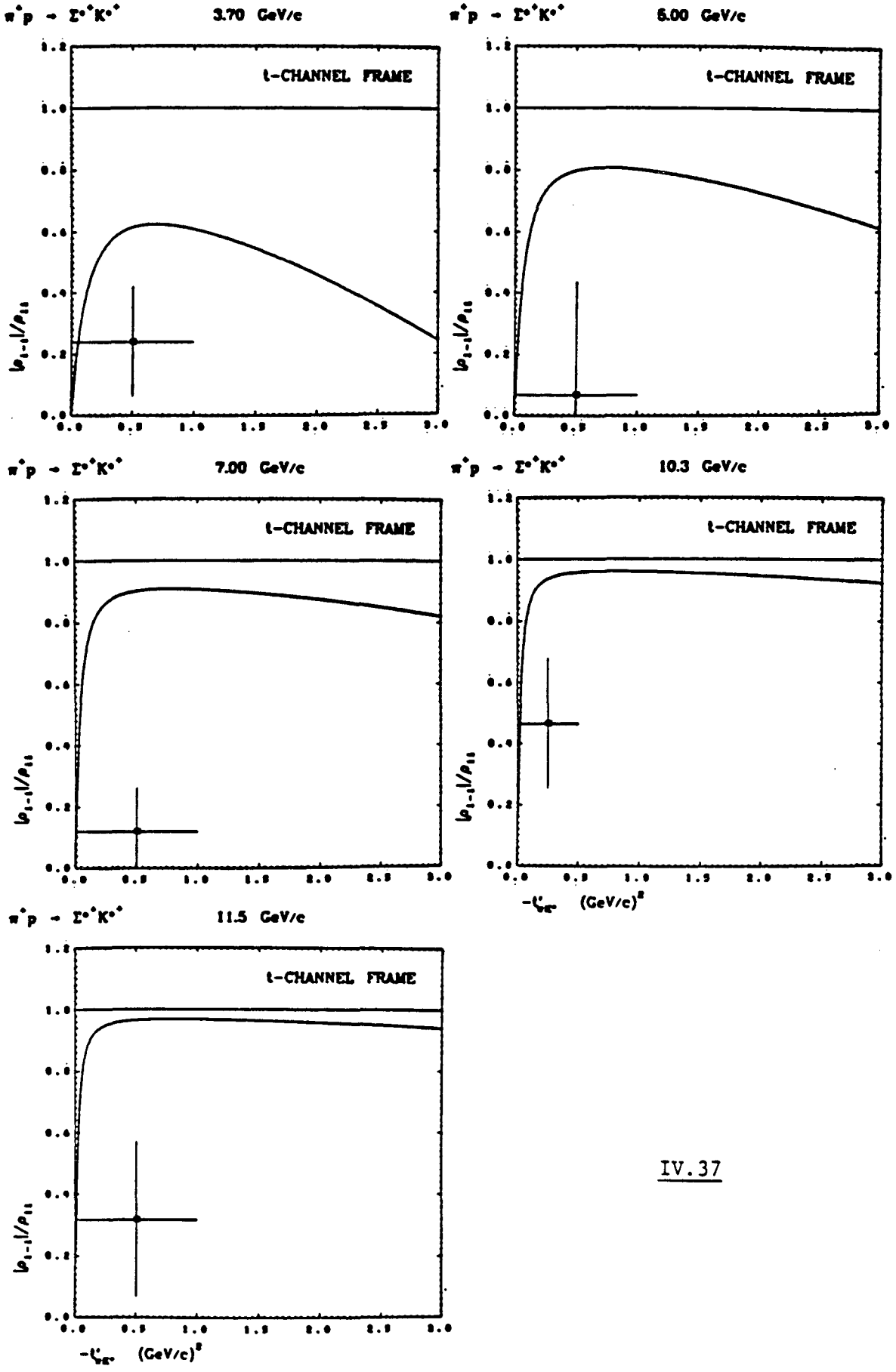
π⁺p → Σ°⁺K°⁺
3.70 GeV/c
t-CHANNEL FRAME
π⁺p → Σ°⁺K°⁺
5.00 GeV/c
t-CHANNEL FRAME
π⁺p → Σ°⁺K°⁺
7.00 GeV/c
t-CHANNEL FRAME
π⁺p → Σ°⁺K°⁺
10.3 GeV/c
t-CHANNEL FRAME
π⁺p → Σ°⁺K°⁺
11.5 GeV/c
t-CHANNEL FRAME
(GeV/c)²

IV.37

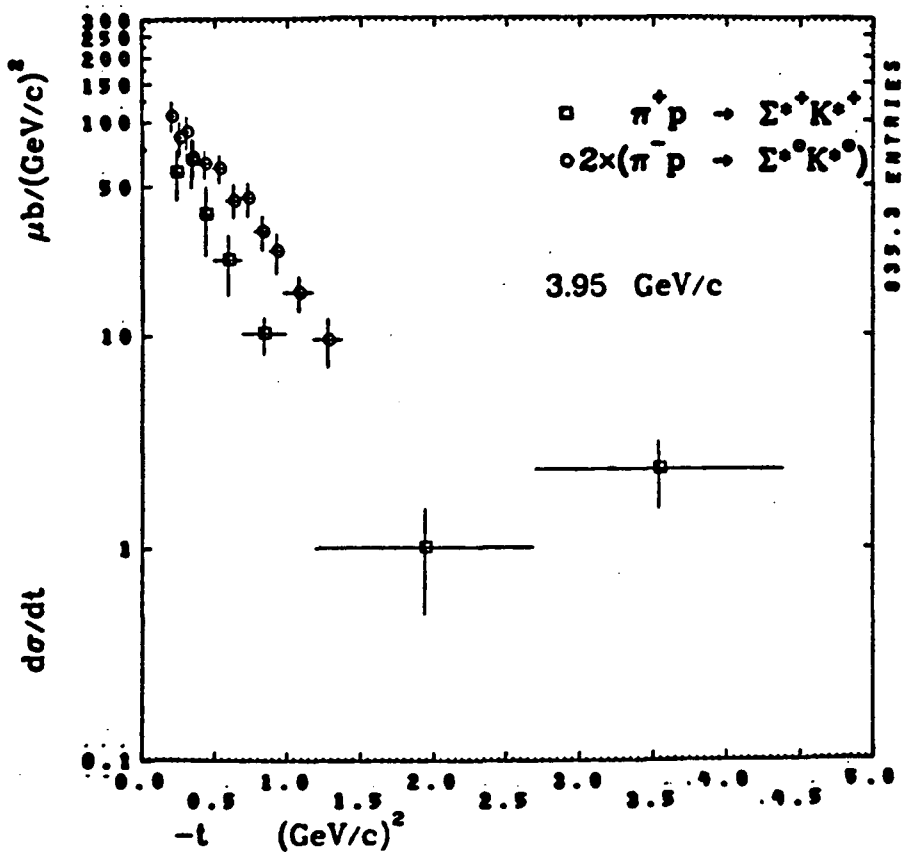
μb/(GeV/c)²
dσ/dt
□ π⁺p → Σ*⁺K*⁺
○ 2×(π⁻p → Σ*⁰K*⁰)
3.95 GeV/c
−t (GeV/c)²

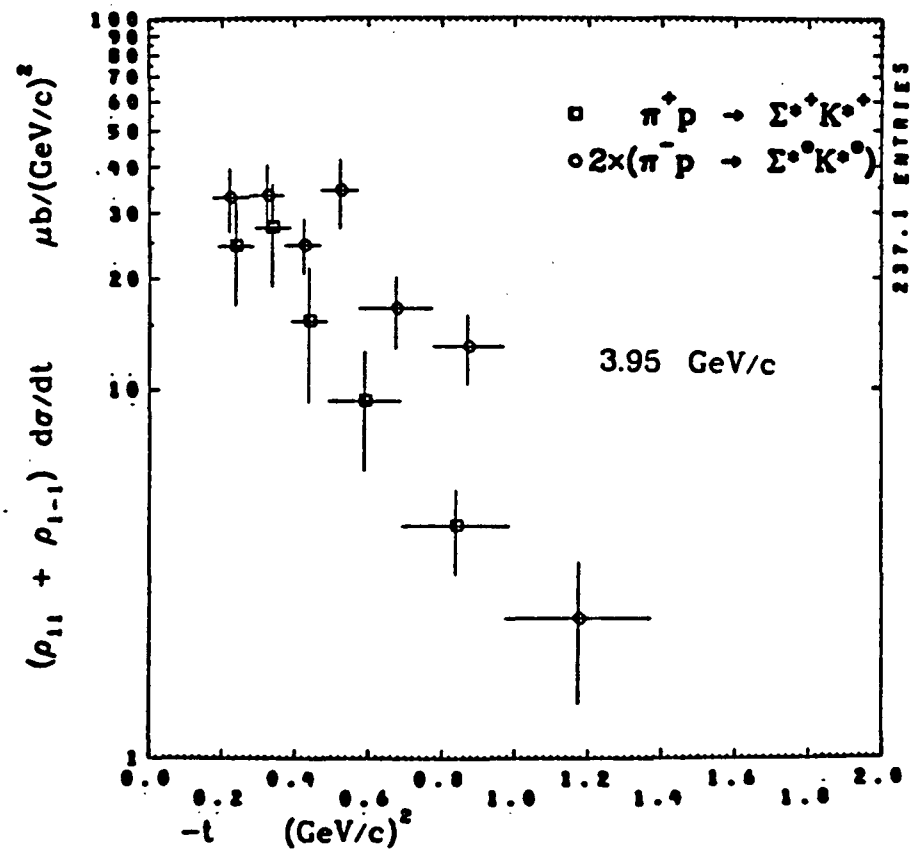
μb/(GeV/c)²
(ρ11 + ρ1-1) dσ/dt
□ π⁺p → Σ*⁺K*⁺
○ 2×(π⁻p → Σ*⁰K*⁰)
3.95 GeV/c
−t (GeV/c)²

IV.38

dip or turnover, unlike $\Sigma^{*+}K^{*+}$.

Next, we examine the WEXD implication for $\pi^+p \to K^{*+}\Sigma^{*+}$ and the line reversed process $K^-p \to \rho^-\Sigma^{*+}$ (see Appendix A) that:

$$\frac{d\sigma}{dt}(K^{*+}\Sigma^{*+}) = \frac{d\sigma}{dt}(\rho^-\Sigma^{*+}) \qquad \text{(IV.D.2)}$$

and

$$\rho(K^{*+}\Sigma^{*+}) = \rho^*(\rho^-\Sigma^{*+}) \qquad \text{(IV.D.3)}$$

where IV.D.3 holds for both the joint and single K^*,Σ^* and ρ,Σ^* density matrices in helicity quantization. (Again, the WEXD implication IV.D.3 is apparently not well-known; it is not mentioned, e.g., in ref. 52.) We scale the 3.7 $K^*\Sigma^*$ data of ref. 21 to the 4.2 GeV/c $\rho\Sigma^*$ data of the CCMS/ACNO groups published in ref. 51. Unfortunately all available $\Sigma^{*+}K^{*+},\Sigma^{*+}\rho^-$ data have no Imρ, so we can check only the Reρ part of IV.D.3. Also, the 4.2 $\rho^-\rho_{ij}$ are in the s-channel helicity system, while the 3.7 $K^*\rho_{ij}$ are in the t-channel system, so without rotating one of the data sets, we can compare only $\rho_{11}+\rho_{1-1}$ which is invariant under $s \to t$ helicity system. In figure IV.39, we see that at 4.2 GeV/c, both IV.D.2,IV.D.3 are violated, with:

$$\text{(a)} \qquad \frac{d\sigma}{dt}(K^*\Sigma^*) < \frac{d\sigma}{dt}(\rho\Sigma^*)$$

and

$$\text{(b)} \qquad \rho_{11}+\rho_{1-1}(K^*) > \rho_{11}+\rho_{1-1}(\rho)$$

(Additionally, the $\rho\Sigma^*$ data at 4.2 has no forward turnover, while $K^*\Sigma^*$ does.)

However, we see in figure IV.39 that the discrepancies (a),(b) to some extent compensate one another so that for the natural J^P exchange part of the cross sections, we have, within the fairly large errors,

$$\text{(c)} \qquad (\rho_{11}+\rho_{1-1})\ \frac{d\sigma}{dt}(K^*\Sigma^*) \approx (\rho_{11}+\rho_{1-1})\ \frac{d\sigma}{dt}(\rho\Sigma^*)\ .$$

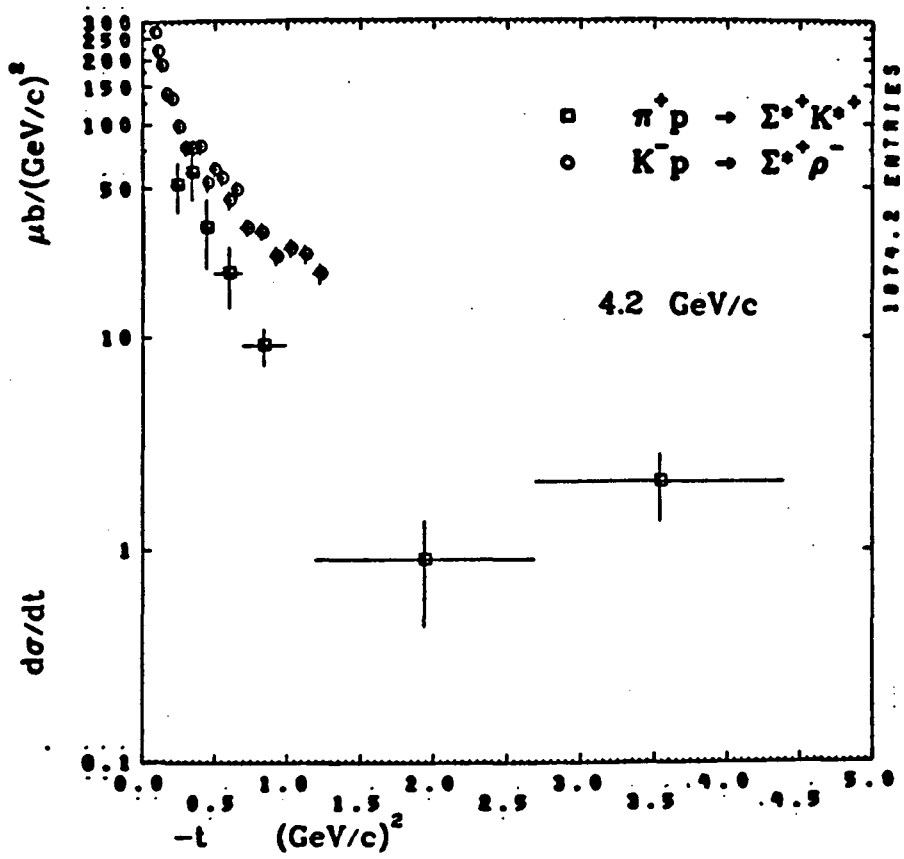
μb/(GeV/c)²
dσ/dt
π⁺p → Σ*⁺K*⁺
K⁻p → Σ*⁺ρ⁻
4.2 GeV/c
1874.2 ENTRIES
−t (GeV/c)²

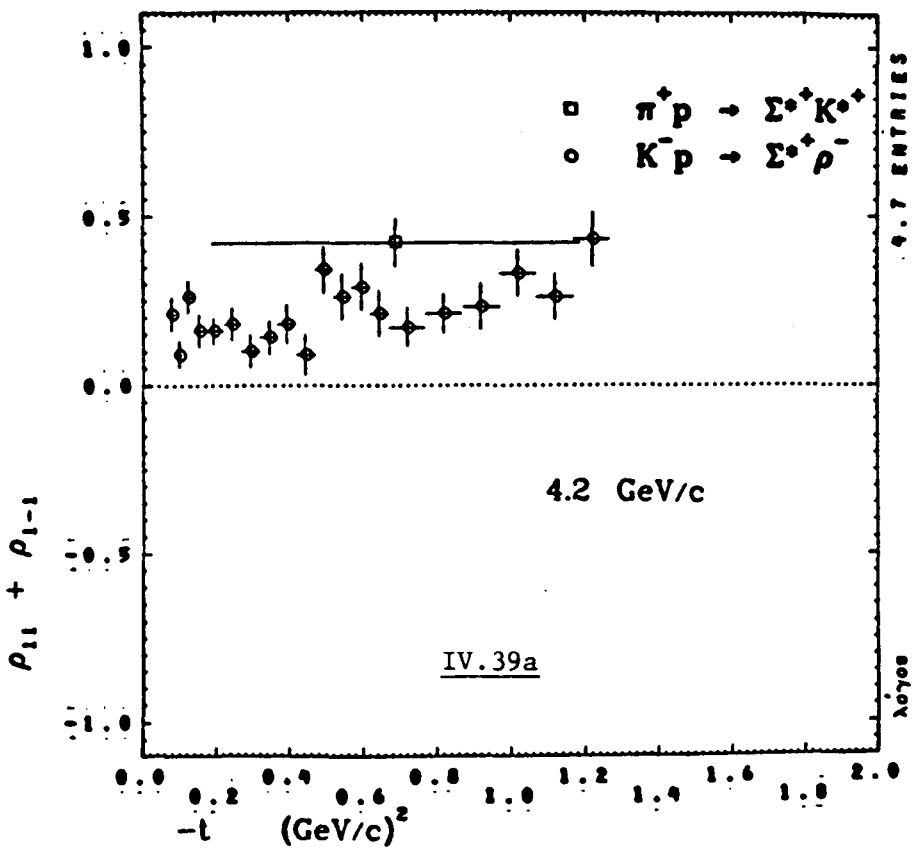
ρ11 + ρ1-1
π⁺p → Σ*⁺K*⁺
K⁻p → Σ*⁺ρ⁻
4.2 GeV/c
4.7 ENTRIES
−t (GeV/c)²

IV.39a

4.2 GeV/c

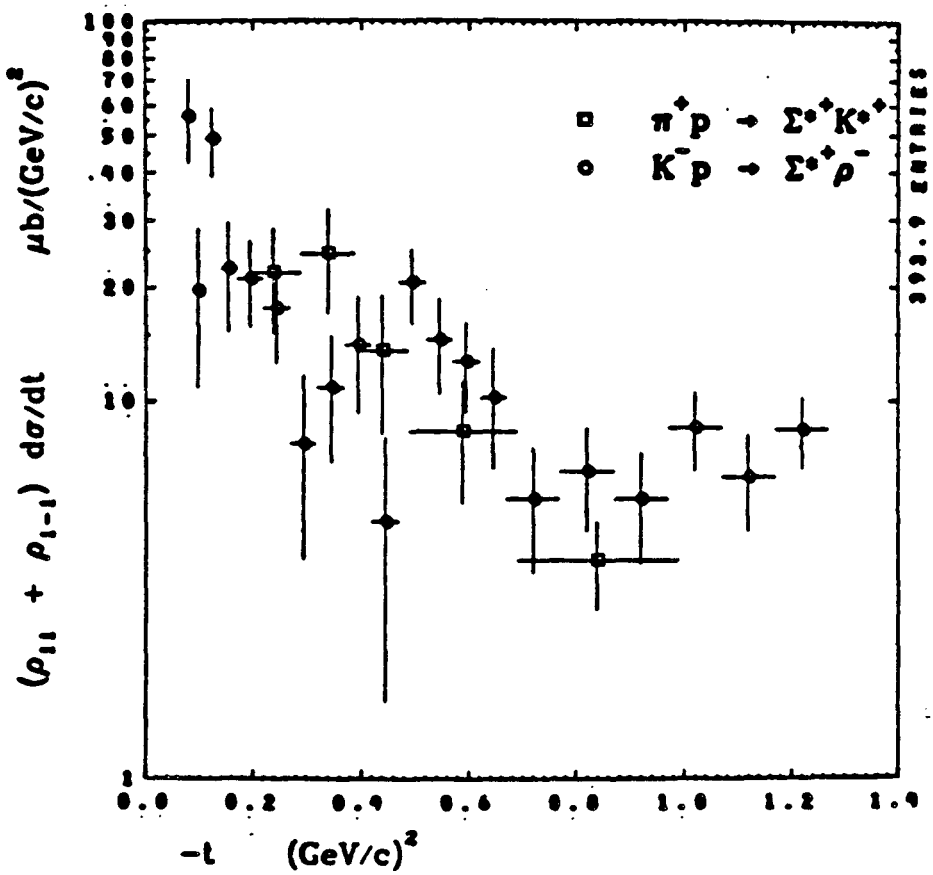

IV.39b

We see precisely the same violations (a),(b) of IV.D.2,3 in the 7, 11.5 GeV/c $K^*\Sigma^*,\rho\Sigma^*$ data of Ballam et al. (ref. 52) from the SLAC SHF. In addition, feature (a) is also the pattern of WEXD breaking seen in $\Sigma^*K,\Sigma^*\pi$ production comparisons discussed previously. The authors of ref. 51 compare their 4.2 $K^-p \to \rho^-\Sigma^{*+}$ $\frac{d\sigma}{dt}$ with 2 $\frac{d\sigma}{dt}$ for their 3.95 $\pi^-p \to K^{*0}\Sigma^{*0}$ data and find good equality; we note that the violations of IV.D.1 and IV.D.2 are of comparable magnitude.

Thus we conclude that $I_t = \frac{1}{2}$-- only and WEXD expectations in equations IV.D.1-3 above are violated in Σ^*K^* production at 4 GeV/c, and moreover the pattern of violation is the same as at the only other available momenta of 7, 11.5 GeV/c. Further, the pattern of disagreement with IV.D.2 for Σ^*K^* over this energy span is of the same sign and of comparable magnitude as in Σ^*K production, and in contrast to the good agreement of $\Sigma K,\Sigma K^*$ with $I_t = \frac{1}{2}$ and WEXD expectations in the same range.

Finally, we examine the 3.7, 5 GeV/c data for AQM predictions which also have not been tested for $\Sigma^{*+}K^{*+}$ at these low momenta. The AQM of ref. 54 as discussed in sections B.4,C.3 of this chapter gives for $\pi p \to K^*\Sigma^*$ the Class A (additivity alone) prediction:

$$\rho_{11} + \rho_{1-1} = \frac{4}{3}\rho_{33} + \frac{4}{\sqrt{3}}\mathrm{Re}\,\rho_{3-1} \qquad \text{(IV.D.4)}$$

where the left-hand side quantities are vector meson, right-hand side decuplet baryon. At 3.7 we find from ref. 21 for the left/right hand sides of IV.D.4 for $-t < 1$ (GeV/ c)^2:

$$0.42 \pm .07 \;/\; 0.18 \pm .16$$

and at 5 GeV/c (ref. 19) for $-t < 1$ (GeV/ c)^2:

$$0.32\pm0.12 \;/\; 0.44\pm0.27\,.$$

The Class B AQM relations are:

$$\rho_{11} = \frac{4}{3}\rho_{33} \qquad \text{(IV.D.5a)}$$

$$\rho_{1-1} = \frac{4}{\sqrt{3}}\mathrm{Re}\,\rho_{3-1} \qquad \text{(IV.D.5b)}$$

$$\rho_{10} = \frac{4}{\sqrt{6}}\rho_{31} \qquad \text{(IV.D.5c)}$$

and at 3.7 we find:

$$\begin{array}{l} 0.34\pm.04 \;/\; 0.27\pm.08 \\ 0.08\pm.06 \;/\; -.09\pm.14 \\ -.09\pm.05 \;/\; -.20\pm.11 \end{array}$$

and at 5:

$$\begin{array}{l} 0.30\pm.04 \;/\; 0.21\pm.13 \\ 0.02\pm.11 \;/\; 0.23\pm.23 \\ 0.02\pm.08 \;/\; 0.26\pm.18 \end{array}$$

The Class C AQM expectations are:

$$\mathrm{Re}\,\rho_{10} = 0 = \mathrm{Re}\,\rho_{31}\,. \qquad \text{(IV.D.6)}$$

We find at 3.7:

$$-.12\pm.07 \;/\; -.09\pm.05$$

and at 5:

$$0.02\pm.08 \;/\; 0.01\pm.11$$

Thus IV.D.4 is satisfied within statistics at 5 but not at 3.7 GeV/c; IV.D.5a,b,c are consistent with the data at 3.7 and 5; IV.D.6 is satisfied at 5 GeV/c. The only other test of the AQM for $\Sigma^{*+}K^{*+}$ is that of Goddard (ref. 22) at 10.3 GeV/c who finds a very similar pattern of agreement: IV.D.4,5a,6 are fairly well obeyed, but IV.D.5b,c are only consistent with the data. Thus we conclude that by 5 GeV/c the AQM relations IV.D.4,5a,6 are satisfied by

$\Sigma^{*+}K^{*+}$, which is the case at 10 GeV/c. The 7,11.5 data of ref. 52 have no ρ_{ij} for the Σ^* so we cannot test the AQM there.

V. Summary, Conclusions, Perspective

We have seen in our phenomenological examination of Σ^+K^+, Σ^+K^{*+}, $\Sigma^{*+}K^+$, $\Sigma^{*+}K^{*+}$ production in π^+p HYCEX that first, and most strikingly, the high energy behavior of the 10-20 GeV/c (where available, ~100 GeV/c) world data persist down into the low and intermediate energy region of our own 1-3 GeV/c data, which region is, indeed, the interval spanned by the four channel thresholds. Thus for example we note the early onset of fixed $-t$ or $-u$ features (as opposed to fixed $\cos\vartheta_{CM}$), that is to say, the early dominance of exchange over formation features. Secondly, or perhaps merely restated, one observes that over a span of an order of magnitude (in some cases two orders) in incident momentum, the dominant features in πp production of $\Sigma K, \Sigma K^*, \Sigma^* K, \Sigma^* K^*$ are generally well described by a remarkably small and simple set of phenomenological tools, to wit:

(A) Regge s, t dependence of amplitude moduli; and

(B) Regge-WEXD description of amplitude phase behavior; and

(C) the AQM/$SU(6)$ spectator quark picture of composite hadron scattering, coupled with the apparent light quark flavor independence of the strong interaction, which lead to the $SU(2)_{flavor}, SU(3)_{flavor}$ unitary symmetries of the amplitudes.

Thus (A) gives the typical power law behavior of channel cross sections as functions of incident momentum, as well as the $\frac{d\sigma}{dt} \sim s^{-2}$ behavior in the forward region and the $\frac{d\sigma}{dt} \sim s^{-4}$ behavior in the backward region. For ~90° scattering, (C) in the form of the hard-scattering quark constituent picture gives the typical $\frac{d\sigma}{dt} \sim s^{-8}$ behavior. While (A) generally gives the *energy and*

angle dependence of channels whose initial, final state (respectively) particles are *similar* (e.g., ΣK and $\Sigma^* K^*$), (B) and/or (C) generally associate *different* channels at the *same energy and angle*. We have noted, for example, that Regge amplitudes fitted at much higher energies describe well the $\Sigma K, \Sigma^* K$ data in the ~2 GeV/c region out to fairly large *C.M.* scattering angles. We have also seen that *LR* related HYCEX channels are reasonably described by WEXD (especially at higher energies), that is, they display an absence of signature effects, e.g., in the form of small or zero interference terms in cross sections, etc. The $SU(2)_{flavor}, SU(3)_{flavor}$ symmetries, which may be regarded as originating in the $SU(6)$ quark-composite picture of hadrons in conjunction with flavor independence of the strong interaction, lead to remarkably well obeyed sum rules or equalities between HYCEX and CEX processes over nearly an order of magnitude in incident momentum, once the non-degeneracy of the (p,n) and λ quark masses (as reflected in $\rho - K^*$ splitting) is taken into account. The simple AQM expectations are also fairly well satisfied.

It has become increasingly clear (we summarize here ideas most recently treated, e.g., in the reviews of H. Harari, ref. 75, and E. Bloom, ref. 76, in the 1981 SLAC Summer Institute Proceedings) that (A),(B),(C) are not unrelated, nor are they in themselves in any sense theoretically fundamental to the emerging view of the strong interactions, but rather can be regarded as deriving from (probably) the Standard Model of elementary particle strong and electroweak interactions, i.e., from a renormalizable non-Abelian gauge field theory of quarks and leptons, with their gauge vector bosons, the (8) gluons and $W^{\pm}, Z$ photon. The Standard Model's fundamental local gauge symmetry is $SU(3)_{color} \times SU(2) \times U(1)$, which is spontaneously broken to $SU(3)_{color} \times U(1)_{EM}$. In the spontaneous breakdown of the weak isospin

($SU(2)\times U(1)$) portion of the overall symmetry, two doublets of Higgs scalar bosons emerge, which serve to give non-zero masses to the $W^{\pm}, Z$ (but unfortunately, or perhaps fortunately, leave us with one uneaten Higgs). (We ignore here the question of whether the $SU(3)_{color}\times SU(2)\times U(1)$ symmetry is merely a component of, e.g., some Grand Unified symmetry like $SU(5)$, or a supersymmetry group.) By 'accident' the (p,n) weak isospin doublet quark masses are almost exactly degenerate, and the λ quark is only ~1.4 times as massive; this leads, if the strong interaction is at least p,n,λ flavor-independent (in addition to the fundamental QCD $SU(3)_{color}$ symmetry), to the $SU(2)_{flavor}, SU(3)_{flavor}$ symmetries which seem to work so well, as well as to the $SU(6)_{flavor,spin}$ descriptions of the light hadrons; thus we have (C) above. Further, the color confinement aspect (which may or may not be absolute) of QCD portrays the light quarks in a hadron as confined, but relatively free within their hadronic 'bags' (which are consequences of the complicated QCD hadronic vacuum around quarks); this makes the otherwise somewhat paradoxical spectator-quark approximation of the AQM intuitively plausible. (Paradoxical in the old pre-QCD view of hadrons: since quarks were demonstrably difficult to remove from hadrons, they must be very deeply bound. The masses of the light hadrons are relatively small; the constituent quarks must be very massive if they are in non-relativistic bound states: this is not the kind of system where one would expect a spectator approximation to work.)

That (A) can be related to a quantum field theory description of interactions (*without* assuming analyticity in J) has been long known. Thus Van Hove, Durand (ref. 77) noted that Regge behavior in s,t can arise from an infinite series of fixed spin exchanges in a field theory; Collins and Squires (ref. 78) observed that sums of ladder diagrams also give rise to Regge

behavior in field theories of fixed spin particles. It is thus not hard to imagine that the quark-quark scattering dynamics of QCD will lead to Regge-like quark amplitudes, and thus by additivity to Regge-like hadron amplitudes. For the way in which Regge behavior is related to constituent scattering of hadrons and 90° cross sections, see the review of Sivers et al. (ref. 46).

Finally, the (at least qualitative) success of WEXD for HYCEX amplitudes can also be motivated by a quark field theoretic picture for hadron scattering. Again, this has been known for some time; the treatment we outline here is that of Collins and Squires, ref. 78. One considers hadron interactions in the spectator limit of, say, the AQM, so that we ignore the non-interacting quarks. Thus for meson-meson scattering, the forward region amplitude (t-channel exchange or 'direct force' in the language of potential scattering) has diagram:

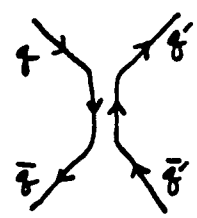

$$= H(q\bar{q} \to q'\bar{q}') \tag{V.1}$$

where the exchanged quantum numbers are of a $q\bar{q}'$ state. The backward region (u-channel exchange or 'exchange force' in the language of potential scattering) has diagram:

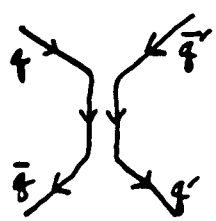

$$= H(q\bar{q} \to \bar{q}'q') \tag{V.2}$$

But in V.2 the exchanged quantum numbers are those of a qq' state. Under the old $SU(3)_{flavor}$/eightfold-way view, such exchanges would be highly suppressed, since they possess and would produce non-octet quantum numbers; from the QCD/$SU(3)_{color}$ color-confinement point of view, V.2 is non-color-singlet exchange and production, and is suppressed. One can of course always add a third quark line to V.2, but then it becomes baryon exchange in meson-baryon scattering:

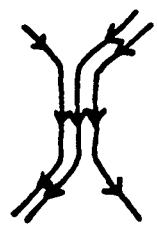

(V.3)

which is energetically suppressed relative to V.1 simply because the qqq states are usually much more massive than the $q\bar{q}$ states. The only significant contribution will be the 'direct force' V.1; but the effective lack of an 'exchange force' (V.2) leads precisely, as ref. 78 observes, to overlapping trajectories of opposite signature, i.e., to WEXD, and thus to (B) above.

Thus the fair success of (A),(B),(C) above in describing HYCEX processes over the energy ranges considered may be regarded as most probably originating in an underlying QCD + Electroweak quark dynamics.

APPENDIX A

PROPERTIES OF DENSITY MATRICES UNDER LINE REVERSAL, WEAK, AND STRONG EXCHANGE DEGENERACY

We examine the formal properties of the single meson, single baryon, and joint meson-baryon decay density matrices in helicity quantization for reactions of type $MB \to M^*B^*$, assuming pole dominance, under generalized line reversal (LR), and with weak and strong exchange degeneracy (WEXD,EXD). By helicity quantization, we mean the description of the M^* or B^* decay in an axis system in which $\hat{y} = \hat{n}$ = production normal, and $\hat{z}$ = initial or final state particle direction. Some of these properties (particularly the behavior of ρ under WEXD), which follow easily from standard Regge phenomenology, have apparently not been pointed out in the literature, especially as they apply to recent high statistics studies of LR in HYCEX reactions (see refs. 58,63,66). This simple general treatment will apply to such HYCEX reaction pairs as:

direct reactions	$\pi p \to$	$K\Sigma$	$\bar{K}p \to$	$\pi\Sigma$	**line reversed reactions**
		$K\Sigma^*$		$\pi\Sigma^*$	
		$K^*\Sigma$		$\rho\Sigma$	
		$K^*\Sigma^*$		$\rho\Sigma^*$	
		$K^{**}\Sigma$		$A_2\Sigma$	
		$K^{**}\Sigma^*$		$A_2\Sigma^*$	

I. General Predictions of Line Reversal

In what follows the helicity amplitudes for the direct (or 'rotating') reactions will be written as H^n_{lm} with

$$\frac{d\sigma}{dt} = \sum_{nlm} |H^n_{lm}|^2 \tag{A.1}$$

where the upper index refers to the produced meson helicity, and the lower indices to the initial and final baryon helicities, respectively. The reversed (or 'real') reaction has amplitudes H^{nr}_{lm} with

$$\frac{d\sigma^r}{dt} = \sum_{nlm} |H^{nr}_{lm}|^2 . \tag{A.2}$$

The two reactions have exchange diagrams

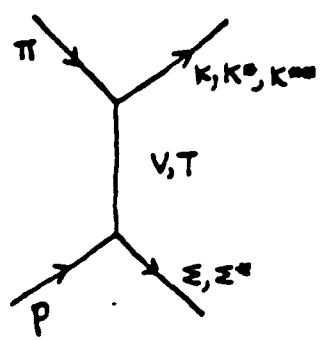

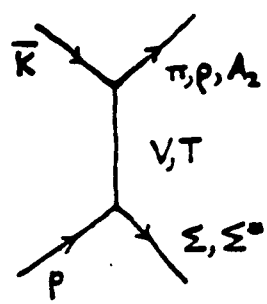

We will make the simple approximation that absorptive and cut effects are negligible (pole dominance), i.e., no terms such as (see ref. 27):

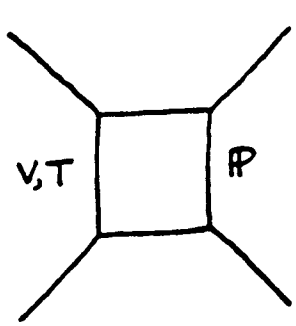

or

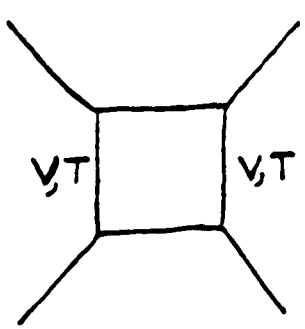

etc.

This is a reasonable approximation for HYCEX in $\pi N, \bar{K}N$ Σ production. We will further assume that only exchanges of a single J^P naturality dominate, i.e., we will consider only natural J^P exchange for HYCEX. With such approximations, helicity quantization is convenient (as opposed to transversity quantization, $\hat{z} = \hat{n}$) for studying the density matrices because of the simple behavior of the helicity amplitudes under line reversal.

Using $SU(3)$ for the exchange vertices plus factorization, the vector V contribution to the direct reaction changes sign when we go to the line reversed channel, while the tensor T does not (see any standard text or review paper on Regge phenomenology, such as Irving and Worden, ref. 69). By line reversal for HYCEX here, we mean merely the crossing of K-like internal quantum numbers (strange isospinor) from final to initial state, and crossing of π-like internal quantum numbers (non-strange isovector) from initial to final. Since we do not also transfer any vector or tensor spin of the final meson, we do not acquire any additional phase factors from line reversal of non-zero spin. (Note also that for $\frac{1}{2}^+\Sigma$ production in particular, no assumptions are made about F/D ratios for V and T exchanges, since both πp and $\bar{K}p$ Σ production couple the K^*, K^{**} exchange to $p\bar{\Sigma}$ as $2F-1 = F-D$; see ref. 69 or ref. 23.)

Thus in obvious notation, with pole dominance:

direct channel:

$$H^n_{lm} = V^n_{lm} + T^n_{lm} = v^n_{lm}(t)[-1+e^{-i\pi\alpha_V}]g(s,t) + \tau^n_{lm}(t)[1+e^{-i\pi\alpha_T}]h(s,t) \quad \text{(A3)}$$

Here all the signature dependent phase information is in the Regge phase $\pm 1 + e^{-i\pi\alpha}$ (same for all V^n_{lm}, respectively, T^n_{lm}), and the effective residues $v^n_{lm}(t), \tau^n_{lm}(t)$ in this approximation are real functions of t; $g(s,t), h(s,t)$ (which may have additional multiplicative phases) contain the energy

dependences as functions of α_V, α_T respectively. In a strict Regge model, g, h would be of asymptotic form $\left(\frac{s-u}{2}\right)^{\alpha}$, but we make no such assumption here: we merely assume that g, h have the same functional form (so that if $\alpha_V = \alpha_T$, then $g = h$).

Under *LR with no further assumptions* (we do not yet assume $\alpha_V = \alpha_T$):

line reversed reaction:

$$H^{mr}_{lm} = -V^{n}_{lm} + T^{n}_{lm} = -v^{n}_{lm}(-1+e^{-i\pi\alpha_V})g + \tau^{n}_{lm}(1+e^{-i\pi\alpha_T})h \ . \tag{A4}$$

The cross sections are

$$\frac{d\sigma}{dt} = \sum_{nlm} |H^{n}_{lm}|^2 = \sum_{nlm} |V^{n}_{lm} + T^{n}_{lm}|^2 \tag{A5}$$

$$\frac{d\sigma^r}{dt} = \sum_{nlm} |H^{mr}_{lm}|^2 = \sum_{nlm} |-V^{n}_{lm} + T^{n}_{lm}|^2 \tag{A6}$$

so that with pole dominance, *under LR alone* $\frac{d\sigma}{dt}$ *is not necessarily equal to* $\frac{d\sigma^r}{dt}$.

The joint decay density matrix, with the standard definition (see, e.g., Pilkuhn, ref. 23) is, in terms of the helicity amplitudes:

$$\rho^{mj}_{kn} = \frac{\sum_l H^{m}_{lk} H^{j*}_{ln}}{\Sigma |H|^2} \tag{A7}$$

and

$$\rho^{mjr}_{kn} = \frac{\sum_l H^{mr}_{lk} H^{jr*}_{ln}}{\Sigma |H^r|^2} \tag{A8}$$

where $\sum |H|^2 \equiv \sum_{nlm} |H^{n}_{lm}|^2$, etc., and where upper indices on ρ refer to the final meson, lower to the final baryon. Thus with pole dominance and *LR* alone,

$$\rho_{kn}^{mj} = \frac{\sum_l \left[V_{lk}^m V_{ln}^{j*} + T_{lk}^m V_{ln}^{j*} + V_{lk}^m T_{ln}^{j*} + T_{lk}^m T_{ln}^{j*} \right]}{\sum |H|^2} \tag{A9}$$

and

$$\rho_{kn}^{mjr} = \frac{\sum_l \left[V_{lk}^m V_{ln}^{j*} - T_{lk}^m V_{ln}^{j*} - V_{lk}^m T_{ln}^{j*} + T_{lk}^m T_{ln}^{j*} \right]}{\sum |H^r|^2} . \tag{A10}$$

Now all V's have the same phase, and all T's have the same phase so terms of form $VV^* + TT^*$ are *real*, and we see

$$(\mathrm{Im}\,\rho_{kn}^{mj})(\mathrm{Im}\,\rho_{kn}^{mjr}) < 0 \quad \text{or} \quad \mathrm{Im}\,\rho_{kn}^{mj}\left(\frac{d\sigma}{dt}\right) = -\mathrm{Im}\,\rho_{kn}^{mjr}\left(\frac{d\sigma^r}{dt}\right) \tag{A11}$$

i.e., ρ and ρ^r have imaginary parts of opposite sign. The meson single density matrix is

$$\rho^{kj} = \frac{\sum_{ml} H_{lm}^k H_{lm}^{j*}}{\sum |H|^2} = \sum_m \rho_{mm}^{kj} \tag{A12}$$

and the hyperon matrix is

$$\rho_{mk} = \frac{\sum_{jl} H_{lm}^j H_{lk}^{j*}}{\sum |H|^2} = \sum_j \rho_{mk}^{jj} \tag{A13}$$

with similar expressions for ρ^{kjr}, ρ_{mk}^r in terms of H_{lm}^{mr}. Thus we see also that under LR alone,

$$\begin{aligned} (\mathrm{Im}\,\rho^{kj})(\mathrm{Im}\,\rho^{kjr}) &< 0 \\ (\mathrm{Im}\,\rho_{mk})(\mathrm{Im}\,\rho_{mk}^r) &< 0 . \end{aligned} \tag{A14}$$

For a $\frac{1}{2}^+$ hyperon like Σ, the polarization with respect to the production normal $\hat{n} = \hat{y}$ is (again, see Pilkuhn):

$$P = -2\mathrm{Im}\,\rho_{\frac{1}{2}-\frac{1}{2}} = -2\,\mathrm{Im}\,\frac{\sum_{nl} H^n_{l\frac{1}{2}} H^{n*}_{l-\frac{1}{2}}}{\sum |H|^2} \tag{A15}$$

and similarly for P^r, so we see that as a special case of (A14) we get the well-known result first discussed by Gilman, ref. 74, that

$$PP^r < 0 \tag{A16}$$

i.e., the direct and line reversed channels have polarizations of opposite signs (but not necessarily equal magnitudes). In summary, LR alone implies $\mathrm{Im}\,\rho\,\mathrm{Im}\,\rho^r < 0$ only.

II. Line Reversal with WEXD

Weak Exchange Degeneracy is expressed in (A3),(A4) as

$$\alpha_V(t) = \alpha_T(t) = \alpha(t) \tag{A17}$$

so that in equations (A3),(A4), $g(s,t) = h(s,t)$, and we have with LR under WEXD:

$$\begin{aligned} H^n_{lm} &= V^n_{lm} + T^n_{lm} = v^n_{lm}(-1+e^{-i\pi\alpha})g + \tau^n_{lm}(1+e^{-i\pi\alpha})g \\ H^{nr}_{lm} &= -V^n_{lm} + T^n_{lm} = -v^n_{lm}(-1+e^{-i\pi\alpha})g + \tau^n_{lm}(1+e^{-i\pi\alpha})g \end{aligned} \tag{A18}$$

Thus

$$\begin{aligned} V^n_{lm}(s,t) &= -i\left[\frac{v^n_{lm}(t)}{\tau^n_{lm}(t)}\right]\tan\left(\frac{\pi\alpha}{2}\right) T^n_{lm}(s,t) \\ &\equiv i\, f^n_{lm}(t)\, T^n_{lm}(s,t) \end{aligned} \tag{A19}$$

where f^n_{lm} is a *real* function of t: f^n_{lm} is the ratio of odd to even signature. Thus $V^n_{lm} \propto i\, T^n_{lm}$. Thus (A18) becomes

$$H^n_{lm} = (i f^n_{lm} + 1)\, T^n_{lm} = e^{\frac{i}{2}\varphi^n_{lm}} a^n_{lm}\, T^n_{lm} \tag{A20}$$

$$H^{nr}_{lm} = (-if^n_{lm} + 1)T^n_{lm} = (i\,f^n_{lm} + 1)^* T^n_{lm}$$
$$= e^{-\frac{i}{2}\varphi^n_{lm}} a^n_{lm} T^n_{lm} \tag{A21}$$

where we define a^n_{lm}, φ^n_{lm} by $(if^n_{lm} + 1) \equiv a^n_{lm} e^{\frac{i}{2}\varphi^n_{lm}}$ and a^n_{lm}, φ^n_{lm} are *real* functions of t. Thus LR plus WEXD has

$$H^{nr}_{lm} = e^{-i\varphi^n_{lm}} H^n_{lm} \tag{A22}$$

with

$$e^{i\varphi^n_{lm}} = \frac{(if^n_{lm} + 1)}{(if^n_{lm} + 1)^*}$$

so that under LR, the WEXD amplitudes transform by a *helicity dependent phase*. (The f^n_{lm} are not completely arbitrary since parity conservation for the H^n_{lm} implies (see Pilkuhn):

$$H^{-n}_{-l-m} = P_A P_B P_C P_D (-1)^{S_B - S_C - S_D} (-1)^{n-m+l} H^n_{lm}$$

where for $AB \to CD$ with spin zero A, P_A, P_B, P_C, P_D are the intrinsic parities, and S_B, S_C, S_D the spins.) Thus LR + WEXD means $f^n_{lm} \to -f^n_{lm}$ or $\varphi^n_{lm} \to -\varphi^n_{lm}$.

We immediately get the well-known prediction of LR + WEXD for cross sections:

$$\frac{d\sigma}{dt} = \sum_{nlm} |\mathrm{i}f^n_{lm} + 1|^2 |T^n_{lm}|^2 = \frac{d\sigma^r}{dt} \,. \tag{A23}$$

For the joint decay density matrix we get a similarly simple result which is apparently not as well known; (A7) and (A8) become:

$$\rho^{mj}_{kn} = \frac{1}{\Sigma|H|^2} \sum_l [f^m_{lk} f^j_{ln} - \mathrm{i}f^j_{ln} + \mathrm{i}f^m_{lk} + 1] T^m_{lk} T^{j*}_{ln} \tag{A24}$$

$$\rho^{mjr}_{kn} = \frac{1}{\Sigma|H|^2} \sum_l [f^m_{lk} f^j_{ln} - \mathrm{i}f^j_{ln} + \mathrm{i}f^m_{lk} + 1]^* T^m_{lk} T^{j*}_{ln} \tag{A25}$$

but $T^m_{lk} T^{j*}_{ln}$ is real, so we see LR + WEXD gives the result

$$\rho^r = \rho^* \tag{A26}$$

or

$$\mathrm{Re}\,\rho^{mj}_{km} = \mathrm{Re}\,\rho^{mjr}_{km} \quad , \quad \mathrm{Im}\,\rho^{mj}_{km} = -\mathrm{Im}\,\rho^{mjr}_{km} \,. \tag{A27}$$

Thus we have general reflection symmetry in ρ, ρ^r. For the meson and hyperon single density matrices, similarly, LR + WEXD gives

$$\rho^{kjr} = \rho^{kj*} \tag{A28}$$

$$\rho^r_{mk} = \rho^*_{mk} \,. \tag{A29}$$

Since $\rho = \rho^+$, we have $\rho^{kjr} = \rho^{jk}$, $\rho^r_{mk} = \rho_{km}$. For a $\frac{1}{2}^+$ hyperon, the specific prediction of LR + WEXD is, using (A15) and (A29), the well-known special case:

$$P = -P^r \tag{A30}$$

i.e., mirror symmetric polarization.

If the f^n_{lm} in (A19) are almost but not quite all equal, then the imaginary parts of the ρ's will be small but non-zero (see next section); conversely, if in (A24),(A25) we have $\sum_l f^j_{ln} \approx -\sum_l f^m_{lk}$, the imaginary part of ρ^{mj}_{km} will be maximized.

Thus in summary, LR + WEXD gives $\frac{d\sigma^r}{dt} = \frac{d\sigma}{dt}$ and $\rho^r = \rho^*$.

III. Line Reversal with EXD

Strong Exchange Degeneracy is expressed in equations (A3),(A4) as:

$$\alpha_V(t) = \alpha_T(t) = \alpha(t) \tag{A31}$$

and

$$v^n_{lm}(t) = \tau^n_{lm}(t) \tag{A32}$$

so in (A19) we have $f^n_{lm} = -\tan\left(\frac{\pi\alpha}{2}\right)$. We get immediately from (A18),(A20):

$$H^{nr}_{lm} = e^{i\pi\alpha} H^n_{lm} = e^{-i\varphi} H^n_{lm} \tag{A33}$$

and $H^n_{lm} = (2\tau^n_{lm} g)e^{-i\pi\alpha}$, $H^{nr}_{lm} = (2\tau^n_{lm} g)$. (This is why the direct channel is sometimes called 'rotating' and the line reversed channel 'real', terms which are meaningful in the limit of strict Regge behavior with Strong Exchange Degeneracy, or strict duality.) Thus under *LR* + EXD, all helicity amplitudes transform under *LR* with the same *helicity independent phase;* cf. the case for WEXD, equation (A22). The result $H^r = e^{-i\varphi} H$ in A33 will *also* follow from the looser condition that all f^n_{lm} *be the same* (independent of helicity) under WEXD in A20,A21 (but not necessarily equal to $-\tan\left(\frac{\pi\alpha}{2}\right)$).

Under *LR* + EXD, *all* observables for the direct and line reversed channels will be equal, and we have the well-known results

$$\frac{d\sigma^r}{dt} = \frac{d\sigma}{dt} \ , \ \rho^r = \rho \ , \ \mathrm{Im}\rho^r = \mathrm{Im}\rho = 0 \ . \tag{A34}$$

In particular, hyperon polarizations must vanish.

We emphasize that A34 will *also* follow from WEXD with the condition that the ratio of odd to even signature (f^n_{lm} in A19) be the same for all helicity amplitudes; this will imply that all H^n_{lm} have the same phase, yielding A34.

IV. Summary of Results and Application to Specific Reactions

With pole dominance of the direct and *LR* reactions, we get the simple hierarchy of results in helicity quantization:

(1) *LR* alone implies $\mathrm{Im}\,\rho\,\mathrm{Im}\,\rho^r < 0$; this is the only prediction;

(2) *LR* + WEXD implies $\frac{d\sigma^r}{dt} = \frac{d\sigma}{dt}$ and $\rho^r = \rho^*$ for all density matrices;

(3) *LR* + EXD imply $\frac{d\sigma^r}{dt} = \frac{d\sigma}{dt}$ and $\rho^r = \rho$ with $\mathrm{Im}\,\rho^r = \mathrm{Im}\,\rho = 0$ for all density matrices. (If conditions (3) are observed to hold empirically, we really can only conclude that the *ratios* of even and odd signature residues are equal for all helicity amplitudes, but not necessarily unity as in EXD.)

Thus for $\pi^+p \to K^+\Sigma^+, K^-p \to \pi^-\Sigma^+$, *LR* + WEXD gives:

$$\frac{d\sigma}{dt}(K^+\Sigma^+) = \frac{d\sigma}{dt}(\pi^-\Sigma^+) \quad \text{and} \quad P_\Sigma = -P_\Sigma^r \,.$$

For $\pi^+p \to K^{*+}\Sigma^+, K^-p \to \rho^-\Sigma^+$, we have for the observables (without using decay correlations) with *LR* + WEXD:

$$\frac{d\sigma}{dt}(K^{*+}\Sigma^+) = \frac{d\sigma}{dt}(\rho^-\Sigma^+) \;,\; P_\Sigma = -P_\Sigma^r \;,\; \rho^{00} = \rho^{00r} \;,\; \rho^{11} = \rho^{11r} \;,$$
$$\rho^{1-1} = \rho^{1-1r} \;,\; \mathrm{Re}\,\rho^{10} = \mathrm{Re}\,\rho^{10r} \,.$$

For $\pi^+p \to K^+\Sigma^{*+}, K^-p \to \pi^-\Sigma^{*+}$, we have for the observables (without using decay correlations) with *LR* + WEXD:

$$\frac{d\sigma}{dt}(K^+\Sigma^{*+}) = \frac{d\sigma}{dt}(\pi^-\Sigma^{*+}) \;,\; \rho_{33} = \rho_{33}^r \;,\; \rho_{11} = \rho_{11}^r \;,$$
$$\mathrm{Re}\,\rho_{3-1} = \mathrm{Re}\,\rho_{3-1}^r \;,\; \mathrm{Re}\,\rho_{31} = \mathrm{Re}\,\rho_{31}^r \,.$$

For $\pi^+p \to K^{*+}\Sigma^{*+}, K^-p \to \rho^-\Sigma^{*+}$, the vector meson and decuplet hyperon relations above hold simultaneously under LR + WEXD. We have here also used those properties of the ρ's which follow from general quantum mechanical principles (again, see Pilkuhn) independently of any dynamical assumptions:

$$\rho = \rho^+ \qquad \textit{(hermiticity)}$$

$$\rho_{-l-m} = (-1)^{l-m}\rho_{lm} \qquad \textit{(symmetry property from parity constraints on the helicity amplitudes)}$$

so that *integer* l: $\rho^{-ll} = \rho^{l-l} = \rho^{l-l*}$ and so ρ^{l-l} is *real*, ρ^{ll} is *real*, and *half odd integer* l: $\rho_{-ll} = \rho^*_{l-l} = -\rho_{l-l}$ and so ρ_{l-l} is *imaginary*, ρ_{ll} is *real*.

V. General Comments on WEXD, EXD and the AQM

Cast in the form of equations (A33), we note that EXD predictions are not really dependent on details of Regge phenomenology except the phase behavior of the amplitudes; any dynamics which transform the direct and line reversed amplitudes according to (A33) (simple phase transformation) will yield EXD-like expectations, as for example in the case of the well-known $SU(3)$ + factorization (or $AQM/SU(6)$) prediction for $K^-p \to \varphi\Sigma^0$, $\pi^-p \to K^{*0}\Sigma^0$ that $H^n_{lm}(\varphi\Sigma^0) = -H^n_{lm}(K^{*0}\Sigma^0)$.

We note that the AQM relations predicted among the elements of the ρ's for a given direct channel will also in general be separately predicted for the LR channel, since such AQM predictions usually depend only on the J^P properties of the initial and final particles, and generally relate Reρ and Imρ separately. If the LR related channels obey WEXD or EXD, we see that they can simultaneously be consistent with the AQM, since $\rho^r = \rho^*$. In most cases,

$SU(3)$ + factorization + WEXD/EXD is equivalent to $AQM/SU(6)$.

REFERENCES

1. P. Hanson, G.E. Kalmus, and J. Louie, Phys. Rev. **D4**, 1296 (1971).

2. G.E. Kalmus, G. Borreani, and J. Louie, Phys. Rev. **D4**, 1824 (1970).

3. G.E. Kalmus, G. Borreani, and J. Louie, Phys. Rev. **D4**, 916 (1971).

4. W. Ko, Omega Production in π^+p Interactions at 2.67 and 2.30 BeV/c, Dissertation, Department of Physics, University of Pennsylvania (unpublished) (1971).

5. G. Kalmus, W. Michael, R. Birge, π^+p Elastic Scattering Data, UCRL-19775 (unpublished) (1970).

6. H.C. Albrecht, E.P. Binnall, R.W. Birge, M.H. Myers, P.W. Weber, The Cobweb Data Reduction System, UCRL-18528 Rev. (1968).

7. H. White, The Fog, Cloudy, and Fair Program for Bubble Chamber Data Reduction, UCRL-9457 (1960).

8. R.L. Kelly et al., Rev. Mod. Phys. **52** (1980).

9. C.P. Horne et al., An Indexed Compilation of Experimental High Energy Physics Literature, LBL-90 (1978).

10. Particle Data Group Compilation, πN Two-Body Scattering Data, LBL-63 (1973).

11. Aderholz et al., Nucl. Phys. **B11**, 259 (1969).

12. D.M. Chew et al., π^+p, π^+n, and π^+d Interactions – A Compilation, LBL-53 (1973).

13. H.W.J. Foelshe et al., Paper submitted to XIIth International Conference on High Energy Physics, Dubna (unpublished) (1964).

14. S. Dagan et al., Phys. Rev. **161**, 1384 (1967).

15. M. Winnik et al., Nucl. Phys. **B128**, 66 (1977).

16. P.A. Baker et al., Nucl. Phys. **B166**, 207 (1980)
J. Ballam et al., Phys. Rev. Lett. **41**, 676 (1978).

17. D.W. Davies et al., Phys. Rev. **D2**, 506 (1970).

18. M.J. Emms et al., Nucl. Phys. **B145**, 285 (1978).

19. D.Z. Toet et al., Nucl. Phys. **B63**, 248 (1973).

20. P. Girtler et al., Nucl. Phys. **B159**, 397 (1979).
P. Bosetti et al., Nucl. Phys. **B128**, 205 (1977).

21. W. Butler et al., Phys. Rev. **D7**, 3177 (1973).

22. M.C. Goddard et al., Phys. Rev. **D19**, 1350 (1979).

23. H. Pilkuhn, *The Interactions of Hadrons*, North-Holland Publishing Co., Amsterdam, 1967.

24. E. Byckling and K. Kajantie, *Particle Kinematics*, John Wiley and Sons, New York (1973).

25. J.D. Jackson, Nuovo Cimento **XXXIV**, 1644 (1964).

26. J.V. Beaupre et al., Nucl. Phys. **B49**, 405 (1972).

27. G. Girardi, Nucl. Phys. **3**, 1031 (1977).

28. R.D. Field et al., Phys. Rev. **D6**, 1863 (1972).

29. G.A. Ringland and R.L. Thews, Phys. Rev. **170**, 1569 (1968).
R.L. Thews, Phys. Rev. **188**, 2264 (1969).

30. D.R.O. Morrison, Phys. Lett. **22**, 528 (1966).

31. V. Barger and D. Cline, *Phenomenological Theories of High Energy Scattering*, W.A. Benjamin, Inc., New York, 1969.

32. P.F. Loverre et al., Z. Physik **C6**, 283 (1980).

33. S. Gasiorowicz, *Elementary Particle Physics*, John Wiley and Sons, New York, 1966.

34. F.T. Solmitz, Ann. Rev. Nucl. Sci. **14**, 375 (1964).

35. R. Kofler et al., Phys. Rev. **163**, 1479 (1967).

36. R.O. Bangerter, Nonleptonic Decay of Sigma Hyperons (Ph.D. Thesis), UCRL-19244 (1969).

37. F. Bradamante et al., Phys. Lett. **44B**, 202 (1973).

38. A. Bashian et al., Phys. Rev. **D4**, 2680 (1971).
C.W. Akerlof et al., Phys. Rev. Lett. **27**, 539 (1971).

C.W. Akerlof et al., Phys. Rev. Lett. **33**, 119 (1974).

39. O.I. Dahl et al., Phys. Rev. **163**, 1430 (1967).

40. K.J. Foley et al., Phys. Rev. **D8**, 27 (1973).
K.J. Foley et al., Phys. Rev. **D9**, 42 (1974).
I. Ambats et al., Nucl. Phys. **B77**, 269 (1974).
C.E.W. Ward et al., Phys. Rev. Lett. **31**, 1149 (1973).
A. Lesnik, ANL/HEP-7364 (1973).
J.C. Hart et al., Nucl. Phys. **B166**, 73 (1980).
D.H. Saxon et al., Nucl. Phys. **B162**, 522 (1980).

41. H. Navelet and P.R. Stevens, Nucl. Phys. **B104**, 171 (1976).

42. B.F.L. Ward, Phys. Rev. **D20**, 683 (1979).

43. A. de Bellefon et al., Nuovo Cimento **37A**, 175 (1977).
A. Berthon et al., Nucl. Phys. **24B**, 417 (1970).

44. A. Bashian et al., Phys. Rev. **D4**, 2667 (1971).
P. Kalbaci et al., Phys. Rev. Lett. **27**, 74 (1971).
S.M. Pruss et al., Phys. Rev. Lett. **23**, 189 (1969).

45. A.D. Martin, C. Michael, R.J.N. Phillips, Nucl. Phys. **B43**, 13 (1972).

46. D. Sivers, S.J. Brodsky, R. Blankenbecler, Physics Reports, **23**, 1 (1976).

47. W.A. Cooper et al., Phys. Rev. Lett. **20**, 472 (1968).
W.A. Cooper et al., Nucl. Phys. **B23**, 605 (1970).

48. H.J. Schreiber, Density Matrix Elements Determined by the Method of Moments, Institut für Hochenergiephysik, PHE 73-7 (1973).

49. J.P. Ader et al., Nuovo Cimento **56A**, 952 (1968).
K. Gottfried and J.D. Jackson, Nuovo Cimento, **33**, 309 (1964).

50. D.J. Crenell et al., Phys. Rev. **D6**, 1220 (1972).

51. M. Aguilar-Benitez et al., Z. Physik **C6**, 195 (1980).

52. J. Ballam et al., Nucl. Phys. **B166**, 189 (1980).

53. A.J. deGroot et al., Nucl. Phys. **B74**, 77 (1974).

54. A. Bialas and K. Zalewski, Nucl. Phys. **B6**, 449 (1968).
A. Bialas and K. Zalewski, Nucl. Phys. **B6**, 465 (1968).
A. Bialas and K. Zalewski, Nucl. Phys. **B6**, 478 (1968).

55. A. Bialas, A. Kotanski, and K. Zalewski, Nucl. Phys. **B28**, 1 (1971).

56. G.W. Brandenburg et al., Phys. Lett. **44B**, 305 (1973).

57. M.G. Doncel, P. Minnaert, and L. Michel, Amplitude Reconstruction for Usual Quasi Two Body Reactions with Unpolarized or Polarized Target – CERN/D.Ph.II/PHYS 74-7 (1974).

58. C.V. Cautis et al., Nucl. Phys. **B156**, 507 (1979).

59. E.N. May et al., Proc. of XXth Int. Conf. on High Energy Physics, 60 (1980).

60. F. Wagner, 11th Rencontre de Moriond, 217 (1976).

61. L. Stodolsky and J.J. Sakurai, Phys. Rev. Lett. **11**, 90 (1963).
L. Stodolsky, Phys. Rev. **134**, 1099 (1964).

62. G.H. Renninger and K.V.L. Sarma, Phys. Rev. **D2**, 1281 (1970).
G.H. Renninger and K.V.L. Sarma, Phys. Rev. **178**, **2201 (1969)**.

63. M. Aguilar-Benitez et al., Z. Physik **C6**, 109 (1980).

64. S.P. Ying et al., Phys. Lett. **30B**, 289 (1969).

65. Yu.D. Aleshin et al., Sov. J. Nucl. Phys. **24**, 519 (1976).

66. S.O. Holmgren et al., Nucl. Phys. **B119**, 261 (1977).

67. A. Berglund et al., Nucl. Phys. **B166**, 25 (1980).

68. G. Girardi and H. Navelet, Nucl. Phys. **B116**, 168 (1976).

69. A.C. Irving and R.P. Worden, Phys. Rep. **34**, 117 (1977).

70. C.J.S. Damerell et al., Phys. Lett. **60B**, 121 (1975).

71. J.C. Scheurer et al., Nucl. Phys. **B33**, 61 (1971).

72. D.D. Carmony et al., Phys. Rev. **D2**, 30 (1970).

73. M.G.D. Gilchriese et al., Phys. Rev. Lett. **40**, 6 (1978).

74. F.J. Gilman, Phys. Lett. **29B**, 673 (1969).

75. H. Harari, Proc. of Summer Institute on Particle Physics, SLAC Report No-245, 685 (1982).

76. E.D. Bloom, Proc. of Summer Institute on Particle Physics, SLAC Report No-245, 1 (1982).

77. L. Van Hove, Phys. Lett. **24B**, 183 (1967).

L. Durand III, Phys. Rev. **161**, 1610 (1967).

78. P.D.B. Collins and E.J. Squires, *Regge Poles in Particle Physics*, Springer-Verlag, Berlin, 1968.

TABLE I

Incident Momentum GeV/c	No. of Pictures 1000's	μb /Event Σ^+ Events	μb / Event Λ Events
2.67	340	.30	.26
2.46	179	.59	.54
2.30	172	.70	.59
2.15	272	.68	.46
1.94	123	.91	.95
1.84	119	.95*†	1.00†
1.77	122	.74*†	.72†
1.68	47	.63*†	.59†
1.63	164	.59*†	.52†
1.55	121	.90*†	.85†
1.43	41	.64*†	.62†
1.41	125	.77*†	.70†
1.34	52	.51*†	.46†
1.28	127	.77*†	.73†

*From refs. 2 and 3.

†From ref. 1 and this work.

TABLE IIa

Numbers of Events

Incident Momentum GeV/c	Σ^+K^+ $\Sigma^+\to\pi^+n$ UNWTD/WTD	Σ^+K^+ $\Sigma^+\to p\pi^0$ UNWTD	$\Sigma^+K^+\pi^0$ $\Sigma^+\to\pi^+n$ UNWTD/WTD	$\Sigma^+K^+\pi^0$ $\Sigma^+\to p\pi^0$ UNWTD/WTD
2.67	198/286±21	146	172/234±19	130/
2.46	137/185±16	94	79/105±12	68/
2.30	96/132±14	85	89/114±12	49/
2.15	150/200±17	106	71/ 92±11	49/
1.94	158/204±16	101	41/ 55± 9	36/
1.84	158/201*	102*	20/ 26†	27/36†
1.77	209/265*	129*	25/ 32†	14/18†
1.68	299/377*	197*	15/ 19†	13/19†
1.63	299/375*	255*	18/ 23†	15/19†
1.55	219/279*	142*	9/ 11†	8/11†
1.43	293/374*	222*	3/ 3.8†	5/ 6.7†
1.41	238/301*	150*	1/ 1.3†	3/ 3.9†
1.34	290/367*	249*	0/†	0/†
1.28	165/208*	118*	--	--

*From refs. 2 and 3.

†From this work and ref. 1.

TABLE IIb

Numbers of Events

Incident Momentum GeV/c	$\Sigma^+\pi^+K^0$ $\Sigma^+\to\pi^+n$ $K_s^0\to\pi^0\pi^0$ or K_L^0 UNWTD/WTD	$\Sigma^+\pi^+K^0$ $\Sigma^+\to p\pi^0$ $K_s^0\to\pi^0\pi^0$ or K_L^0 UNWTD/WTD	$K^+\pi^+\Lambda$ $\Lambda\to p\pi^-$ UNWTD/WTD
2.67	112/147±14	79/	169/231±18
2.46	51/ 66± 9	42/	103/136±14
2.30	61/ 82±11	33/	108/142±14
2.15	50/ 64± 9	39/	149/198±17
1.94	32/ 41± 7	20/	78/102±12
1.84	16/ 21*	16/22*	80/109*
1.77	17/ 22*	11/14*	115/157*
1.68	10/ 12*	9/12*	113/145*
1.55	3/ 3.8*	5/ 6.3*	58/ 83*
1.43	1/ 1.2*	1/ 1.3*	34/ 45*
1.41	0/*	0/*	18/ 24*
1.34	2/ 2.5*	1/ 1.4*	0/*
1.28	–	–	3/ 3.8*

*From this work and ref. 1.

TABLE III

Channel Cross Sections

Incident Momentum GeV/c	$\pi^+p \to \Sigma^+K^+$ (μb)	$\pi^+p \to \Sigma^+K^+\pi^0$ (μb)	$\pi^+p \to \Sigma^+\pi^+K^0$ (μb)	$\pi^+p \to K^+\pi^+\Lambda$ (μb)
2.67	178±18	146±15	139±16	94 ± 9
2.46	226±25	128±17	122±19	114 ±13
2.30	190±25	164±22	180±28	130 ±15
2.15	281±33	140±20	147±24	141 ±14
1.94	385±39	104±18	117±22	152 ±20
1.84	395±50*	70±15†	72±16†	162 ±18†
1.77	405±50*	40±15†	42±14†	170 ±17†
1.68	490±40*	30± 6†	24± 6†	128 ±13†
1.63	458±40*	25± 6†	25± 7†	163 ±16†
1.55	517±50*	21± 6†	14± 6†	107 ±16†
1.43	497±40*	6± 3†	2± 1.4†	42 ±12†
1.41	390±35*	4± 2.2†	0†	25 ± 6†
1.34	476±45*	0†	3± 2.2†	0†
1.28	331±35*	0†	0†	4.5± 3.3†

*Calculated from data of refs. 2 and 3 using the value of $r \equiv \frac{\Sigma^+ \to \pi^+ n}{\Sigma^+ \to p\,\pi^0}$ from Particle Data Group Compilation, ref. 8.

†From ref. 1 and this work.

TABLE IV

Fractions of Resonance Production in 3-Body Final States

Incident Momentum GeV/c	$\Sigma^+K^*(892)^+/\Sigma^+\pi^+K^0$	$\Sigma^+K^*(892)^+/\Sigma^+K^+\pi^0$	$\Sigma^*(1385)^+K^+/\Lambda\pi^+K^+$
2.67	.76±.07	.44±.05	.55±.05
2.46	.68±.12	.35±.09	.51±.08
2.30	.67±.10	.47±.08	.47±.07
2.15	.79±.11	.40±.09	.64±.07
1.94	.84±.15	.50±.12	.73±.09

TABLE V

Resonance Production Cross Sections

Incident Momentum GeV/c	$\pi^+p \to \Sigma^*(1385)^+K^+$ $\Sigma^* \to \Lambda\pi$ $\sigma(\mu b)$	$\pi^+p \to \Sigma^+K^*(892)^+$ $K^* \to K^+\pi^0$ $\sigma(\mu b)$	$\pi^+p \to \Sigma^+K^*(892)^+$ $K^* \to K^0\pi^+$ $\sigma(\mu b)$	$\pi^+p \to \Sigma^+K^*(892)^+$ $\sigma(\mu b)$	$R = \frac{(K^* \to K^0\pi^+)}{(K^* \to K^+\pi^0)}$
2.67	52± 7	64±10	106±16	170±19	1.7±0.4
2.46	58±11	45±13	83±20	128±24	1.8±0.7
2.30	61±11	77±17	121±26	198±31	1.6±0.5
2.15	90±13	56±15	116±25	172±29	2.1±0.7
1.94	111±20	52±15	98±25	150±29	1.9±0.7
1.84	140±25*			47±14	
1.77	125±25*				
1.68	100±20*				
1.63	130±20*				
1.55	95±20*				
1.43	42±12*				
1.41	25± 6*				

*From ref. 1 and this work

TABLE VI

Fits to Channel Cross Sections of Form $\sigma = Ap_{\pi}^{q}$

Channel	q
$\pi^+p \to \Sigma^+K^+$	-1.77±.04
$\pi^+p \to \Sigma^+K^+\pi^0$	-1.10±.09
$\pi^+p \to \Sigma^+\pi^+K^0$	-1.21±.11
$\pi^+p \to K^+\pi^+\Lambda$	-0.91±.04
$\pi^+p \to \Sigma^+K^*(892)^+$	-2.07±.12
$\pi^+p \to \Sigma^*(1385)^+K^+$	-1.45±.04
$\pi^+p \to \Sigma^*(1385)^+K^*(892)^+$	-1.81±.24

This report was done with support from the Department of Energy. Any conclusions or opinions expressed in this report represent solely those of the author(s) and not necessarily those of The Regents of the University of California, the Lawrence Berkeley Laboratory or the Department of Energy.

Reference to a company or product name does not imply approval or recommendation of the product by the University of California or the U.S. Department of Energy to the exclusion of others that may be suitable.

TECHNICAL INFORMATION DEPARTMENT
LAWRENCE BERKELEY LABORATORY
UNIVERSITY OF CALIFORNIA
BERKELEY, CALIFORNIA 94720